Molecular characterisation of autophagy deficits in a LRRK2-BAC transgenic rat model of Parkinson's disease

A thesis submitted for the degree of Doctor of Philosophy



Rebecca Wallings

Christ Church college

Department of Physiology, Anatomy and Genetics

University of Oxford

Trinity Term 2018

Abstract

Parkinson's disease (PD) is the second most common neurodegenerative disorder worldwide. PD is characterised by the preferential loss of dopaminergic neurons in the *Substantia Nigra pars compacta* in the midbrain accompanied by progressive motor dysfunction. The precise aetiology of PD is unknown, however a causative role of Leucine-rich repeat kinase 2 (LRRK2) has been proposed. Mutations in the *LRRK2* gene are the most frequent cause of familial PD and are also an independent risk factor for sporadic PD. Although the function of LRRK2 is not well characterised, a role of LRRK2 in the autophagy pathway has been suggested. The disruption of the autophagy pathway by LRRK2 pathogenic mutations has been described. However, the literature is often contradictory and the exact underlying mechanisms remain unknown. In this study, primary cortical cultures were generated from three bacterial artificial chromosome (BAC) transgenic (TG) rat models of PD harbouring either the whole human wild-type *LRRK2* gene, the G2019S mutant (the most common *LRRK2* mutation) or the R1441C mutant (the *LRRK2* mutation leading to a more aggressive pathology). After characterising the autophagy pathway it was observed that the presence of either hWT-LRRK2 or LRRK2-G2019S inhibits autophagosome biogenesis in primary cortical cultures. hWT-LRRK2 and LRRK2-G2019S each localise to the Golgi apparatus where autophagy signalling complexes are situated, which may underlie the inhibitory effect on autophagosome biogenesis. The presence of LRRK2-R1441C, however, induces a lysosomal deficit that causes an accumulation in autophagosomes and decreased autolysosome maturation and lysosomal protein degradation. LRRK2-R1441C also increases lysosomal pH levels and causes lysosomal Ca^{2+} release deficits. Furthermore, hWT-LRRK2 and LRRK2-G2019S were found to

bind to the a1 subunit of the v-type ATPase pump (vATPase a1) which is responsible for modulating lysosomal pH. Whereas LRRK2-R1441C showed a loss of binding capacity to this subunit, which was associated with a decrease in a1 subunit protein expression and cellular mislocalisation. Lastly, the Zn^{2+} ionophore, clioquinol, was able to rescue the LRRK2-R1441C-mediated lysosomal phenotypes through modulating lysosomal zinc levels and increased vATPase a1 expression which re-acidified lysosomes, corrected localised calcium release and increased autolysosome maturation. These data describe a novel functional link between LRRK2 and vATPase a1, and define critical mechanisms underlying the inhibition of autophagy by different pathogenic *LRRK2* mutations. These findings demonstrate a novel mode of action by which drugs may rescue lysosomal dysfunction and alleviate blockage in autophagic flux. These results demonstrate the importance of LRRK2 in lysosomal biology, as well as the critical role of the lysosome in PD and the potential of lysosome-targeting compounds as a novel therapeutic for the disease.

Declaration

I confirm that the work presented in this thesis is my own and performed by the author at the University of Oxford. Where information has been derived from other sources, I confirm that this has been indicated in the thesis. This work has not been submitted for any other degree in this or any other University

Acknowledgements

Completing this DPhil has been hard work and would have been impossible without those that supported, encouraged and challenged me to develop as both an individual and a scientist.

To my supervisor Prof Richard Wade-Martins. Thank you for offering me the opportunity to join the Wade-Martins lab and carry out such a stimulating project. Thank you so much for four years of support, guidance and continuing encouragement that has allowed me to evolve as a scientist. I hope in the future our relationship can move from student-supervisor to collaborators! To my supervisor and friend, Dr Natalie Connor-Robson. I thank you from the bottom of my heart for being my close friend and mentor from start to finish, both in and out of lab. You have taught me how to be a better scientist and you have shown me how to break through that glass ceiling.

The Wade-Martins lab has been a phenomenal place to complete my DPhil, and I have loved working with every member of the group, all of which have no doubt influenced and helped me in some way or another. However, some special thanks need to be made. Thank you to Max for doing the leg work before my arrival in the lab by characterising this animal model before passing the baton on to me. The biggest of thanks to Milena who has been a phenomenal amount of help to me for the last four years by managing my animal colonies and being a pillar for this lab to stand on. A huge thank you to Brent for his advice on autophagy and science in general. He taught me how to be more critical of my own work and, far more importantly, kept me entertained with his humour that is often as inappropriate as my own. Thank you to Nora for her advice and support and for showing me the kind of post-doc I aspire to be. Thank you to Dayne for his endless amount of both scientific and personal advice (quite often over a drink). Thank you to Heather for many conversations about LRRK2, advice and sharing my love-hate relationship for LRRK2. Thank you to Siv and Pip for showing me how strong females can succeed in science whilst still retaining their effortless creativity. To Federico, Mang Ching & Alastair for paving the way and providing me with endless

amounts of laughter. Sar Bear – we did it! I am so happy I got to share my entire time here with you, start to finish. You have taught me to be calm and patient and see everything in a positive light. Gabi cita, thank you so much for being the ray of sunshine in the lab that never fails to brighten my day. Deepak, my brother! Thank you for letting me rant and cry to you on our long runs around uni parks; you brightened the darkest of days. Thank you to Chazza, Irene and Pete for keeping things spicy and never failing to have so many words of encouragement. And the rest of the lab; Hugo, Gabriele, Mel, Tara, Saba, Ben, Kathie, Marta, Bryan, Matt, Helle, Mindaugas, Janine, Uroosa and Dana, thank you all so much for making the lab so vibrant a place to have spent four years.

Thank you to Nicholas and the Pitts-Tucker family trust for funding my DPhil and for providing me the opportunity to become a better scientist. Thank you to my college, Christ Church, for supporting me financially and providing the setting for many happy memories.

I want to thank my boo, Anna, immensely for being my closest friend and for supporting me in literally everything I do. And the same goes for her wonderful fiancé James White; thank you for being an amazing friend and letting me third wheel your relationship with Boo! Marie, my princess, for sharing many, many, many bottles of wine and even more laughs with me. Georgia and Bug for continuing to make home feel like home, no matter how long it has been. Becki (with an I) for appreciating that life can keep us busy and always making the time for me to have those long overdue catch ups. And Sam, for showing me that a couple of nobodies from Halstead, Essex, can one day go on to become a couple of very impressive somebodies.

To my mum and dad, Margaret and Steve, thank you for providing me the love and support to pursue my dreams. I can never begin to repay you for all you have done for me. I love and appreciate you beyond words. To my sister, Gemma, and brother, Doody, thank you for always showing me support and encouragement no matter what I do. My nephews and niece, Sam, Phoebe, Max, Jack and Will. I hope one day you'll

be able to read this thesis. Even if science isn't the path for you, I hope it inspires you to work hard and follow your passions. There is a big wide world out there just waiting for you to explore it and I hope I have shown you that you can do anything and go anywhere if you put your mind to it.

And finally, to my Grandad Frank and Grandma Mo. I dedicate this thesis to you. It breaks my heart knowing you aren't here to see me become Dr. Boo, but I hope I can continue to make you proud, where ever you may be.

Publications and conference presentations

Sloan, M., Alegre-Abarrategui, J., Potgeiter, D., Kaufmann, A., Exley, R., Deltheil, T., Threlfell, S., Connor-Robson, N., Brimblecombe, K., **Wallings, R.,** Cioroch, M., Bannerman, D., Bolam, P., Magill, P., Cragg, S., & Wade-Martins. R. (2016). LRRK2 BAC transgenic rats develop progressive, L-DOPA-responsive motor impairment, and deficits in dopamine circuit function. Human Molecular Genetics, 25(5). 951-963.

Wallings, R., Manzoni, C., & Bandopadhyay, R. (2015). Cellular processes associated with LRRK2 function and dysfunction. FEBS, 282(15). 2806-2826.

Wallings, R., Connor, N., & Wade-Martins, R. Modulating zinc transport corrects lysosomal dysfunction and rescues autophagy deficits in LRRK2 mutant neurons. (Selected poster presentation). Biennial International LRRK2 meeting, Padua, Italy, 2018

Wallings, R., Connor-Robson, N., & Wade-Martins, R. Molecular characterisation of the autophagy pathway in LRRK2-BAC transgenic rodent model of Parksinson's disease. (Selected poster presentation). OPDC research day, Oxford. March 2017.

Wallings, R. The role of animal models in Parkinson's disease. (Invited guest speaker). Institute of animal technicians, Department of Pharmacology, Oxford University, Oxford. December, 2015.

Contents

Abstract 1

Declaration 3

Acknowledgements 4

Publications and conference presentations 7

Abbreviations 12

List of figures 17

List of tables 19

Chapter 1: Introduction 20

1.1 Parkinson's disease 20

1.1.1 Introduction 20

1.1.2 Clinical features 21

1.1.3 Parkinson's disease pathology 22

1.1.4 Aetiology of Parkinson's disease 27

(i) The genetic bases of Parkinson's disease 27

(ii) Environmental risk factors of Parkinson's disease 33

1.1.5 Current and future treatments for Parkinson's disease 34

1.2 Autophagy in Parkinson's disease 38

1.2.1 Mitophagy defects 39

1.2.2 Trafficking defects 41

1.2.3 Lysosomal defects 42

1.3 LRRK2 44

1.3.1 LRRK2 mutations and Parkinson's disease 44

1.3.2 LRRK2 structure and function 46

1.3.3 Enzymatic activity and mutations 49

1.3.4 Cellular functions of LRRK2 51

(i) LRRK2 and Autophagy 51

(ii) LRRK2 at the synapse 59

(iii) LRRK2 and mitochondria 60

(iv) LRRK2 and Vesicle trafficking 61

1.4 Rodent models of Parkinson's Disease 64

1.4.1 Toxin induced models 64

(i) 6-Hydroxydopamine 65

(ii) 1-methyl-4-phenyl-1,2,3,6-tetrahydropyridine (MPTP) 66

(iii) Paraquat 68

(iv) Rotenone ... 69
1.4.2 Genetic rodent models of Parkinson's disease ... 70
(i) Viral models ... 70
(ii) Use of genetic constructs ... 71
1.4.3 Rodent models of LRRK2 ... 73
1.5 Aims of this thesis ... 83
Chapter 2: Methods and Materials ... 84
2.1 Animal husbandry ... 84
2.2 Genotyping ... 84
2.2.1 DNA extraction from tissue clip ... 84
2.2.2 Polymerase chain reaction for genotyping ... 84
2.3 Generation of primary cortical cultures ... 86
2.4 Generation of primary astrocytic cultures ... 87
2.5 Generation of primary neuronal cultures ... 88
2.6 Antibodies ... 89
2.7 Fixation of cells and Immunocytochemistry ... 91
2.8 Immunohistochemistry ... 91
2.8.1 Transcardial perfusion ... 91
2.8.2 Tissue embedding ... 92
2.8.3 Tissue rehydration and staining ... 92
2.9 Protein biochemistry ... 93
2.9.1 Cellular lysis ... 93
2.9.2 Tissue homogenization ... 93
2.9.3 Protein quantification and sample preparation ... 94
2.9.4 Western Blotting ... 94
2.9.5 Co-immunoprecipitation ... 95
2.10 Lysosensor imaging and quantification of lysosome pH ... 95
2.11 RNA extraction and QPCR ... 96
2.12 C^{14}-valine pulse-chase protein degradation assay ... 97
2.13 ^{3}H-Glutamate uptake assay ... 98
2.14 Calcium imaging ... 99
2.15 Zinc imaging ... 99
2.16 DQ™ BSA assay ... 99
2.17 Deglycosylation assay ... 100
2.18 Cell profiler image analysis ... 100
Chapter 3: Exploring the involvement of LRRK2 in the autophagy pathway ... 102

3.1 Introduction and aims ... 102
3.2 Results ... 106
3.2.1 Establishing primary cortical culture cell populations ... 106
3.2.2 Generating pure astrocytic cultures ... 107
3.2.3 Generating enriched neuronal cultures ... 108
3.2.4 Assessing endogenous Lrrk2 and transgene protein expression in primary cortical cultures ... 110
3.2.5 Assessing astrocytic glutamate uptake ... 114
3.2.6 Quantifying basal autophagy protein levels ... 114
3.2.7 Autophagosome, autolysosome and lysosome quantification in neurons of primary cortical cultures ... 117
3.2.8 Investigating LC3 changes in cortical and midbrain tissue of aged animals 119
3.2.9 Autophagy modulating compound treatments to probe autophagic flux ... 121
3.2.10 Lysosome size and localisation ... 124
3.2.11 LRRK2 localisation to autophagy-related proteins ... 125
3.2.12 Effects of human LRRK2 on trans-Golgi fragmentation ... 127
3.2.13 Analysing lysosomal protein degradation ... 127
3.2.14 The ubiquitin proteasome system ... 128
3.2.15 UPS protein expression and proteasome degradation ... 129
3.3 Discussion ... 132
Chapter 4: Identifying mechanisms underlying lysosomal deficits in mutant LRRK2 cortical cultures ... 137
4.1 Introduction and aims ... 137
4.2 Results ... 142
4.2.1 Characterising the effect of Lrrk2-knock out on the autophagy pathway ... 142
4.2.2 The role of LRRK2 kinase activity in autophagy ... 144
4.2.3 Quantifying lysosomal pH ... 147
4.2.4 Assessing lysosomal pH pump expression ... 148
4.2.5 The effects of LRRK2 on intracellular calcium stores ... 149
4.2.6 Changes in SNARE protein and RNA levels in primary cortical cultures ... 153
4.2.7 Characterising LRRK2-vATPase a1 binding ... 155
4.2.8 Monitoring vATPase a1 cellular localization ... 156
4.2.9 Observing vATPase a1 glycosylation ... 159
4.3 Discussion ... 160
Chapter 5: Using tool compounds to correct lysosomal deficits in mutant LRRK2 cortical cultures ... 169
5.1 Introduction and aims ... 169

5.2 Results 172

5.2.1 Monitoring the effect of Nilotinib on autophagy 172

5.2.2 Assessing clioquinol treatment on autophagy in LRRK2-R1441C primary cortical cultures 173

5.2.3 The role of zinc in clioquinol treatment 176

5.2.4 The effect of primaquine and its derivatives on autolysosome maturation and protein degradation in LRRK2-R1441C cultures 180

5.3 Discussion 185

Chapter 6: General discussion 192

6.1 Discussion 192

6.2 Future directions 199

References 202

Abbreviations

-/- = knock out (also KO)

6-OHDA = 6-Hydroxydopamine

AADC = aromatic l-amino acid decarboxylase

AD = Alzheimer's disease

AMPK = 5' adenosine monophosphate-activated protein kinase

AP = adaptor protein AP

AR = autosomal recessive

AraC = Cytosine-1-β-D-arabinofuranoside

Arp2/3 = actin related protein 2/3

ATG = autophagy related proteins

ATP = adenosine triphosphate

AV = anterograde adenoviral

BAC = bacterial artificial chromosome

BAPTA = 1,2-bis(2-aminophenoxy) ethane-N,N,N′,N′-tetraacetic acid

BBB = blood-brain barrier

BCA = Bicinchonic acid

BG = basal ganglia

BSA = bovine serum albumin

CCCP = Carbonyl cyanide m-chlorophenyl hydrazine

CMA = chaperone mediated autophagy

CMAP = Connectivity Map

COMT = catechol-O-methyltransferase

COR = carboxy-terminal of ROC

CPA = Cyclopiazonic acid

CPM = counts per minute

DA = dopamine

DAn = dopaminergic neurons

DAPI = 4′,6-diamidino-2-phenylindole

DAT = dopamine transporter

DBS = deep brain stimulation

dH2O = distilled H2O

di-22:6-BMP = di-docosahexaenoyl (22:6) bis(monoacylglycerol) phosphate

DJ-1 = Daisuke-Junko-1

DMEM = dulbecco's modified eagle medium

DMV = dorsal motor nucleus of the vagus

DNA = Deoxyribonucleic acid

DNAse = Deoxyribonuclease

DOPAC = dopamine forming forming 3,4-dihydroxyphenylacetic acid

DPBS = dulbecco's phosphate buffered saline

DRP1 = Dynamin-1-like protein

EDTA = ethylenediaminetetraacetic acid

EDTA = ethylenediaminetetraacetic acid

eGP = external globus pallidus

EndoA1 = endophilin A1

ERT = enzyme replacement therapy

ESCs = embryonic stem cells

FBS = foetal bovine serum

FCCP = Carbonyl cyanide-p-trifluoromethoxyphenylhydrazone

GBA = Glucocerebrosidase

GDI = Guanosine nucleotide dissociation inhibitor

GDP = Guanosine diphosphate

GFAP = glial fibrillary acidic protein

GFP = green fluorescent protein

GPN = Gly-Phe-β-naphthylamide

GTP = Guanosine triphosphate

GWAS = Genome wide association studies

HD = Huntington's disease

HEK293 = Human embryonic kidney cells (also HEKs)

HEKs = Human embryonic kidney cells (also HEK293)

hLRRK2 = human LRRK2

HRP = horseradish peroxidase

HSC70 = heat shock-cognate protein of 70 kDa

HVA = Homovanillic acid

IBA1 = ionized calcium-binding adapter molecule 1

ICD = Impulse Control Disorder

iGP = internal globus pallidus

iPSCs = induced pluripotent stem cells

kDa = kilodalton

KI = knock in

KO = knock out (also -/-)

KRS = Kufor-Rakeb Syndrome

LAMP2a = lysosomal associated membrane protein 2a

LBs = lewy bodies

LC = locus coeruleus

LC3 = Microtubule associated protein 1 light chain

LD = lipid droplet

L-DOPA = L-3,4-dihydroxyphenylalanine

LID = L-DOPA induced dyskinesia

LIMP2 = Lysosome membrane protein 2

LNs = lewy neurites

LPS = lipopolysaccharide

LRR = leucine rich repeat

LRRK2 = Leucine rich repeat kinase 2

LSDs = lysosomal storage disorders

MAO-B = monoamine oxidase B

MAP2 = microtubule associated protein 2

MDR1 = multidrug resistance protein 1

MEFs = mouse embryonic fibroblasts

MHC-II = major histocompatibility complex II

MIRO1 = Mitochondrial Rho GTPase 1

ML-IV = Mucolipidosis type IV disease

MPAC = metal protein attenuating compound

MPP+ = 1-methyl-4-phenylpyridinium (MPP+)

MPR = mannose-6-phosplate receptor

MPTP = 1-methyl-4-phenyl-1,2,3,6-tetrahydropyridine

mRNA = messenger RNA

mtDNA = mitochondrial DNA

MTOC = microtubule-organizing centre

mTOR = mechanistic target of rapamycin

NAADP = Nicotinic acid adenine dinucleotide phosphate

NeuN = neuronal nuclei

OST = oligosaccharyltransferase

p62 = ubiquitin binding protein p62/sequesosome

PAC = bacterial P1 artificial chromosome

PB = phosphate buffer

PBMCs = peripheral blood mononuclear cells

PBS = phosphate buffered saline

PCR = Polymerase chain reaction

PD = Parkinson's Disease

PFA = paraformaldehyde

PI(3)P = Phosphatidylinositol 3-phosphate

PI3K = Phosphoinositide 3-kinase

PINK1 = phosphate and tensin homolog-induced putative kinase 1

PKA = cyclic-AMP-dependent kinase

PLA = proximity ligation assay

PLAN = PLA2G6 associated neurodegeneration

Ppt1 = palmitoyl-protein thioesterase 1

PVDF = polyvinylidene difluoride

RBD = REM sleep behaviour disorder

REM = rapid eye movement

RN = raphe nuclei

RNA = ribonucleic acid

RNase = ribonuclease

ROC = ras of complex

ROCO = roco domain containing

ROS = reactive oxygen species

Rpm = rotations per minute

RRF = retrorubal field

SCA = spinocerebellar ataxia

SD = Sprague dawley

SNARE = Soluble N-ethylmaleimide-sensitive factor attachment protein receptors

SNpc = substantia nigra pars compacta

SNpr = substantia nigra pars reticulata

SNPs = single nucleotide polymorphisms

STAT1 = signal transducer activators of transcription type 1

STN = subthalamic nucleus

TBE = Tris/Borate/ethylenediaminetetraacetic acid

TCA = trichloroacetic acid

TFEB = Transcription factor EB

TG = transgenic

TH = tyrosine hydroxylase

TMEM175 = Transmembrane protein 175

TPC2 = Two-Pore calcium channel 2 TPC2

TPEN = N,N,N',N'-tetrakis(2-pyridylmethyl)ethane-1,2-diamine

TRPML1 = transient receptor potential cation channel 1

ULK1 = Unc-51 like autophagy activating kinase 1

UPDRS = Unified Parkinsons Disease Rating Scale

UPR = unfolded protein response

UPS = ubiquitin proteasome system

vmDAn = ventral midbrain dopaminergic neurons

VPS34 = vacuolar protein sorting 34

VTA = ventral tegmental area

WASH = Wiskott-Aldrich syndrome and SCAR homology

WIPI = WD-repeat protein interacting with phosphoinositides

YAC = yeast-artificial chromosome

ZnT2 = Zn2+ transporter 2

List of figures

Figure 1.1 Parkinson's disease pathology *23*

Figure 1.2 Substantia Nigra pars compact compacta neuronal loss and basal ganglia circuitry.. ..... *25*

Figure 1.3 Parkinson's disease and the autophagy and endolysosomal system. *37*

Figure 1.4 Schematic of MitoQC. *39*

Figure 1.5 LRRK2 structure, mutations and phosphorylation sites. *46*

Figure 1.6 Macroautophagy. *52*

Figure 1.7 Chaperone mediated autophagy. *57*

Figure 1.8 Chemical structure of neurotoxins used in animal models of Parkinson's disease *64*

Figure. 2.1. Genotyping PCR conditions *83*

Figure. 2.2. Schematic diagram of the pulse chase assay calculation. *98*

Figure. 2.3. Schematic diagram of cellprofiler image analysis pipeline. *99*

Figure 3.1. Establishing primary cortical cultures *107*

Figure 3.2. Assessing LRRK2 protein expression. *109*

Figure 3.3. Establishing astrocyte and neuronal cultures. *111*

Figure 3.4. Assessing basal autophagy protein levels. *114*

Figure 3.5. Assessing basal autophagy levels by immunofluorescence *116*

Figure 3.6. Assessing LC3 in aged tissue *118*

Figure 3.7. Autophagy modulating compound treatments *120*

Figure 3.8. Lysosome size and localisation. *122*

Figure 3.9. LRRK2 localisation to autophagy proteins. *125*

Figure 3.10. Lysosomal protein degradation. *126*

Figure 3.11. Ubiquitin proteasome system. *129*

Figure 4.1. Structure of the v-type proton ATPase. 136

Figure 4.2. Lrrk2-/- neurons have increased autophagic activity 142

Figure 4.3. LRRK2 kinase inhibition and autophagy 144

Figure 4.4. R1441C neuronal cultures exhibit increased lysosomal pH 145

Figure 4.5. R1441C cortical cultures exhibit decreased vATPase a1 expression. 147

Figure 4.6. R1441C neurons have impaired lysosome Ca2+ dynamics....149

Figure 4.7. Ca2+ channel mRNA expression. 151

Figure 4.8. SNARE protein and mRNA levels.....152

Figure 4.9. LRRK2 and vATPase a1 co-immunoprecipitation 153

Figure 4.10 vATPase a1 cellular localisation 155

Figure 4.11. vATPase a1 glycosylation 157

Figure 5.1. Nilotinib treatment and autophagy. 170

Figure 5.2. Clioquinol increases autolysosome maturation in LRRK2-R1441C neurons 171

Figure 5.3. Clioquinol rescues lysosomal deficits in LRRK2-R1441C neuronal cultures. 172

Figure 5.4. Clioquinol modulates lysosomal zinc levels and upregulates pH regulating pumps.....174

Figure 5.5. Clioquinol modulates lysosomal zinc levels corrects lysosomal pH in LRRK2-R1441C cultures 175

Figure 5.6. Molecular structure of clioquinol and Primaquine and its derivatives ..177

Figure 5.7. The effect of primaquine derivatives on autolysosome count in primary cortical cultures 179

Figure 5.8. The effect of primaquine derivatives on DQTM-BSA fluorescence 181

Figure 6.1 Schematic diagram of the effect of LRRK2 pathogenic mutations on the autophagy pathway....190

List of tables

Table 1.1. List of genes and proteins proposed to be associated with Parkinson's disease……28

Table 1.2 single nucleotide polymorphisms (SNPs) identified as risk factors for PD…32

Table 1.3 An overview of previously generated LRRK2 transgenic rodent models……72

Table 2.1 Genotyping PCR components……84

Table. 2.2. Genotyping PCR primers……84

Table. 2.3. Cell densities……85

Table. 2.4. Compound treatment concentrations and times……86

Table. 2.5. Antibodies for immunostaining……87

Table. 2.6. Antibodies for western blotting……88

Table 3.1 An overview of reports of LRRK2 and autophagy in in vitro models……101

Table 3.2 An overview of reports of LRRK2 and autophagy in animal models and human post mortem……103

Chapter 1: Introduction

1.1 Parkinson's disease

1.1.1 Introduction

Parkinson's disease (PD) is the second most common neurodegenerative disorder worldwide (Pringsheim et al., 2014). The first detailed description of PD was made over two centuries ago by James Parkinson in 1817 in his essay entitled 'An essay in the shaking palsy', where he described the characteristic involuntary tremors of the limbs and bradykinesia with no apparent loss of sense and intellect (Parkinson, 1817). The risk of PD is known to increase with age, with risk increasing nearly exponentially over time, peaking after 80 years of age; affecting 156 per 100,000 in the 4th decade and 2,500 per 100,000 in those over the age of 80 (Pringsheim et al., 2014). With longevity increasing globally, the number of cases in the USA alone is expected to increase to ~700,000 by the year 2040 (Rossi et al., 2018), with a global number of 6.2 million estimated back in 2015 (The Global Burden of Diseases, Injuries and Risk Factors study, 2015). A recently completed study commissioned by Parkinson's UK on the economic cost of PD in the UK has shown enormous financial burden on those who have been diagnosed and their families, with costs amounting to over £16,500 per household per year (Gumber et al., 2017). The annual cost of treatment to the NHS was £2,118 per patient. With an estimated 145,000 PD patients in the UK, the total financial burden on the NHS is therefore estimated to total over £300 million per annum. Despite being described two centuries ago, treatments remain palliative in nature, with no treatment currently able to halt or reverse disease progression. Furthermore, a reliable biomarker for PD is yet to be identified leading to delayed diagnosis, which is

exacerbated by the fact that the onset of symptoms is often misdiagnosed as the early stages of normal ageing (Lees et al., 2009). PD is a debilitating and costly pathology and it is therefore crucial to understand the early pathological mechanisms that cause its onset to develop neuroprotective treatments.

1.1.2 Clinical features

The most common clinical symptom of PD is motor dysfunction, which is classically characterised by a tetrad of motor deficits including resting tremor, postural instability and rigidity of the neck, trunk and limbs. Bradykinesia (slowness of movement) and impairments in gait are also often observed in patients (Kalia & Lang, 2015). These motor symptoms are heterogeneous in patients which has led to attempts to identify subtypes of the disease, including tremor-dominant (with absence of other motor symptoms) and non-tremor dominant. Non-tremor dominant can be further divided into akinetic-rigid syndrome and postural instability gait disorder (Marras & Lang, 2013).

Although primarily considered a motor related disorder, PD is known to affect multiple systems and patients often present with accompanying non-motor symptoms. These include pain, fatigue, mild-cognitive impairment and urinary symptoms (Kalia & Lang, 2015). These particular non-motor symptoms are often observed in the early stages of disease in the first 8 years post-diagnosis (Khoo et al., 2013). Non-motor symptoms also often precede the onset of motor symptoms by as much as 4 decades (Postuma et al., 2012). This prodromal stage of the disease includes impairments in olfaction and gastrointestinal function, and depression. In fact, mood disorders and constipation have been shown to double an individual's risk of subsequently developing PD (Noyce et

al., 2012). It has been observed that patients diagnosed with postural instability gait difficulty report increased number of non-motor symptoms than those diagnosed with tremor-dominant PD, or an intermediate form of the disease (Khoo et al., 2013). The occurrence of rapid eye movement (REM) sleep behaviour disorder (RBD) has been associated with the subsequent development of neurodegenerative disease characterized by the deposition of α-synuclein (Berg et al., 2012). RBD is thought to be the prodromal stage of the disease and these patients are important for early intervention or disease modifying strategies, especially for PD (Iranzo et al., 2014; Dos Santos et al., 2014). Dementia is also particularly prevalent in PD, occurring in 83% of patients who have had 20 years disease duration (Hely et al., 2008). Overall, a clinical diagnosis is generally made after the onset of disease, when 50-70% of the effected neurons are already lost (Kordower et al., 2013) and can only be confirmed by *post-mortem* examination.

1.1.3 Parkinson's disease pathology

The crucial pathological feature of PD is loss of dopaminergic neurons (DAn) within the *Substania Nigra pars compatca* (SNpc). Around 75% of DAn in the brain are found in the midbrain where three different types are present; A8, A9 and A10. A8 DAn reside in the retrorubal field (RRF), A9 in the SNpc, and A10 in the ventral tegmental area (VTA). It is the preferential loss of A9 ventral midbrain DAn (vmDAn) in the SNpc which lead to the emergence of motor symptoms in PD (Figure 1.1a; Kordower et al., 2013). The loss of these neurons results in decreased innervation of the caudate putamen (dorsal striatum) and a reduction in striatal dopamine (DA) content (Ehringer & Hornykiewicz, 1960). The SNpc and striatum form part of a larger circuit of

subcortical nuclei, the basal ganglia (BG), which are involved in voluntary motor function (Albin et al., 1989). The BG are comprised of both inhibitory and excitatory connections between the major nuclei, which include the internal and external globus pallidus (iGP and eGP), the subthalamic nucleus (STN), striatum, substantia nigra and the thalamus (Albin et al., 1989). The BG receives inputs from cortical regions and also sends outputs to the cortex via the thalamus. Loss of neurons from the SNpc leads to a decrease in excitatory signals to the cortex via the thalamus (Figure 1.2 illustrates this, in a simplified form).

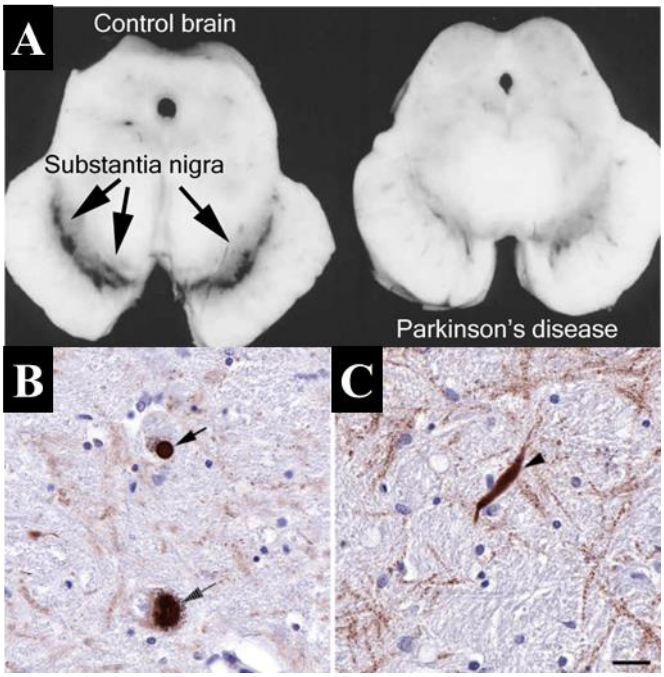


Figure 1.1 Parkinson's disease pathology *(**A**) Horizontal human brain sections from a healthy control and PD patient (Mackenzie, 2001). Arrows indicate the pigmented cells of the SNpc. α-synuclein immunostaining shows LBs (**B**) and LNs (**C**) in the SNpc of PD patient. Scale bar: 25 µm (figure adapted from Vermilyea & Emborg, 2015).*

It is important to note that other areas of the brain outside of the SNpc also degenerate in PD, but to a much lesser extent. It is not yet understood what makes the DAn of the SNpc more susceptible to degeneration in PD compared to other areas of the midbrain and BG. These areas include neurons in the VTA and RRF as well as those in the dorsal motor nucleus of the vagus (DMV), locus coeruleus (LC) and the raphe nuclei (RN; Sulzer & Surmeier, 2013). DAn of the SNpc have highly branched, long, unmyelinated axons that put a high energetic burden on the cell (Pissadaki & Bolam, 2013) which may lead them to become more susceptible to cellular stress. As well, SNpc neurons use L-type calcium channels for pacemaking activity (Surmeier et al., 2010) and it has been proposed that maintenance of calcium gradients will place high energy demands on the cell, therefore exacerbating the already increased burden on these DAn.

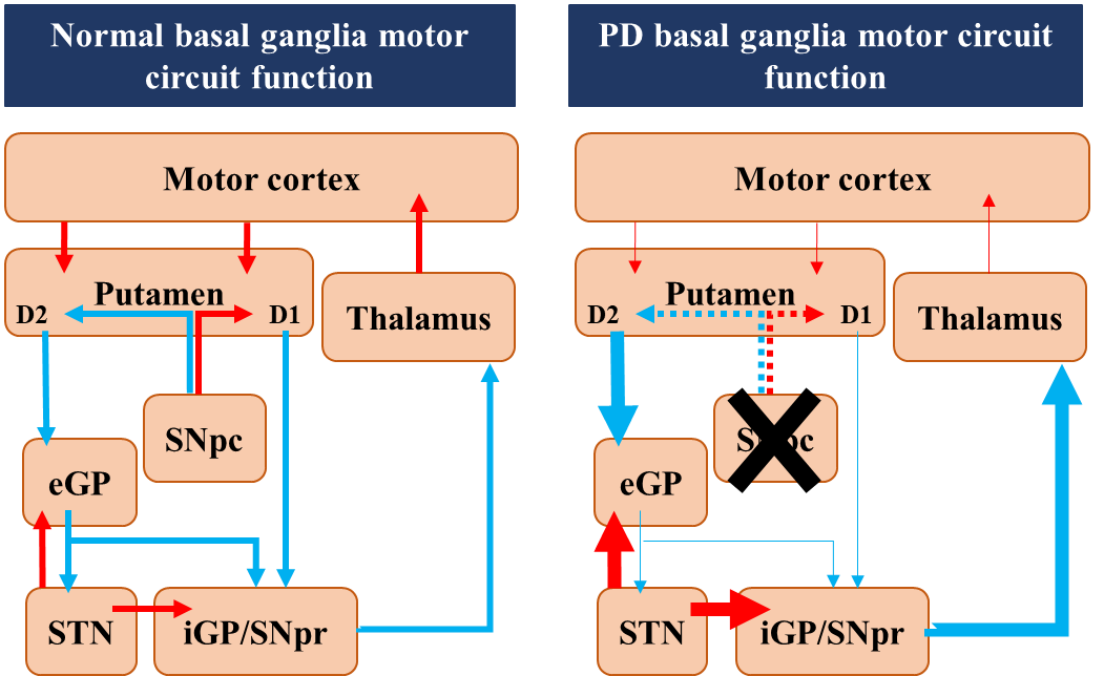


Figure 1.2 Substantia Nigra pars compact compacta neuronal loss and basal ganglia circuitry. *The left panel indicates the circuits in the 'normal' state, and the right shows the overall changes in activity that have been associated with Parkinsonism. Blue and red arrows indicate inhibitory and excitatory connections, respectively. The thickness of the arrows corresponds to their presumed activity. Abbreviations: D1 and D2, dopamine receptor subtypes; eGP, external segment of the globus pallidus; iPG, internal segment of the globus pallidus; SNpc, substantia nigra pars compacta; SNpr, substantia nigra pars reticulate; STN, subthalamic nucleus (figure adapted from Galvan et al., 2015).*

Another pathological hallmark of PD is the presence of Lewy bodies (LBs) which were first described by Frederich Heinrich Lewy in 1912 who observed neuronal inclusions in the brains of patients with what we now know as PD. These are spherical and eosinophilic protein aggregates that are found in all PD affected brain regions and are mostly composed of the protein α-synuclein (Figure 1.1b; Spillantini et al., 1997; Spillantini et al., 1998). Post mortem studies have reported that, in addition to LBs, susceptible neurons also exhibit 'pale bodies', which are considered precursors to LBs. Furthermore, α-synuclein aggregates in neuronal processes, known as Lewy neurites (LNs) have also been described (Figure 1.1c; Forno, 1987; Dickson et al., 2009). These LBs can be found in virtually the whole brain, especially in the later stages of disease (Braak et al., 2003). The spread of this pathology over the disease course led to the development of the Braak hypothesis of PD pathology. The Braak hypothesis suggests that pathology begins in the olfactory bulb and brain stem in the prodromal stages of disease (stages 1 and 2), followed by the BG when motor-symptoms will become apparent (stages 3 and 4) and finally in the cortical and limbic areas in the later stages of disease (stages 5 and 6). Using a Proximity Ligation Assay (PLA) that allows the discrimination of different α-synuclein conformations, it has been observed that areas of the brain originally thought to be unaffected by PD also demonstrate early stage oligomeric α-synuclein pathology (Roberts et al., 2015).

It is not yet completely understood why LBs form or what their role in disease is. Not all familial PD brains of have revealed LBs at post mortem examination (Doherty & Hardy, 2013; Gaig et al., 2007) and LBs have even been observed in neurologically normal post mortem brains (Markesbery et al., 2009). LB load in patients also correlates poorly with the severity of symptoms (Colosimo et al., 2003; Parkinnen et

al., 2008). Collectively, these data suggest that LBs may not be toxic. It is known that the oligomeric form of α-synuclein, which is a precursor to the fibrillary α-synuclein found in LBs, is highly neurotoxic (Winner et al., 2011; Nasstrom et al., 2011) and α-synuclein oligomers have been observed in post mortem brains (Tofaris et al., 2003; Roberts et al., 2015). It has therefore been hypothesised that oligomeric species of α-synuclein are the culprits for neuronal degeneration in PD (Helwig et al., 2016; Winner et al., 2011; Bengo-Vergniory et al., 2017). Other proteins have also been found in LBs including ubiquitin (Spillantini et al., 1997), 14-3-3 proteins (Kawamoto et al., 2002), heat shock cogntate 71 kDa protein (HSC70; Leverenz et al., 2007) and tau (Ishizawa et al., 2003).

1.1.4 Aetiology of Parkinson's disease

Several environmental and genetic risk factors conferring an increased risk of PD have been identified in recent years. Mutations in a number of genes have been found to cause autosomal dominant (AD) or autosomal recessive (AR) monogenic forms of PD, as well as genetic variants that modulate the risk of sporadic forms of the disease. It is widely believed that an interaction between genetic and environmental factors influences the susceptibility (Dardiotis et al., 2013).

(i) The genetic bases of Parkinson's disease

Until twenty years ago, it was largely assumed that PD was purely sporadic in nature. However, the first PD associated mutation was identified in the *SNCA* gene which encodes for the α-synuclein protein (Polymeropoulos et al., 1997) and bought the role

of genetics in PD to the forefront of research. To date, monogenic mutations in 20 different genes have been found to contribute the genetic aetiology of PD or other disorders where Parkinsonism is the primary clinical feature (Table 1.1; Ferreira & Massano, 2017). It is estimated that approximately 30% of familial cases and 3-5% of sporadic cases are accounted for by these monogenic mutations (Kumar et al., 2011).

Gene	Locus	PARK	Inheritance	Pathology
SNCA	4q22-1	1/4	AD	Early onset PD
Parkin	6q25.2-q27	2	AR	Early onset PD
Unknown	2p13	3		
UCHL1	4p13	5	AD	PD
PINK1	1p36.12	6	AR	Early onset PD
DJ-1	1p36.23	7	AR	Early onset PD
LRRK2	12q12	8	AD	PD
ATP13A2	1p36.13	9	AR	KRS
Unknown	1p32	10		
GIGYF2	2q36-27	11	AD	PD
Unknown	Xq21-q25	12	X-linked	
HTRA2	2p12	13	AD	PD
PLA2G6	22q13.1	14	AR	PLAN
FBXO7	22q12.3	15	AR	Early onset PD
Unknown	1q32	16		
VPS35	16q11.2	17	AD	PD
EIF4G1	3q27.1	18	AD	PD
DNAJC16	1p31.3	19	AR	Early onset PD
SYNJ1	21q22	20	AR	Early onset PD
RAB39B	Xq28	-	X-linked	Early onset PD

Table 1.1. List of genes and proteins proposed to be associated with Parkinson's disease. *Annotations: AD = Autosomal dominant, AR = Autosomal recessive, PLAN = PLA2G6 associated neurodegeneration, KRS = Kufor-Rakeb Syndrome*

The most common autosomal dominant genes associated with PD are *SNCA* and *LRRK2* (a detailed overview of *LRRK2* and its PD associated mutations is found in section 1.3). To date, five different missense mutations in *SNCA* have been identified as a cause of PD. Patients carrying the A53T, A30P or E46K mutations present with severe parkinsonism at an early age of onset, with a good response to L-3,4-dihydroxyphenylalanine (L-DOPA), rapid disease progression and the onset of cognitive decline and hallucinations in the later stages of disease (Zarranz et al., 2004; Sheerin et al., 2014; Houlden et al., 2012). Those carrying the H50Q mutation typically develop a form of PD that is characterised by late-onset, responsiveness to L-DOPA as well as the presentation of cognitive impairment (Proukakis et al., 2013; Appel-Cresswell et al., 2013). Finally, those with the G51D mutation have been reported to develop parkinsonian-pyramidal syndrome with an early-onset and rapid disease progression (Lesage et al,, 2013). As well, duplications and triplications of the *SNCA* locus are also a cause of PD, being more frequent than point mutations and providing a pathogenic overexpression of the wild-type (WT) α-synuclein (Singleton et al., 2003; Nishioka et al., 2004).

Of the 7 identified autosomal recessive (AR) genes associated with PD, *PARKIN*, phosphate and tensin homolog-induced putative kinase 1 *(PINK1)* and Daisuke-Junko-1 (*DJ-1)* are the most well studied and characterised. Mutations in the *PARKIN* gene were first identified to cause AR juvenile parkinsonism (Kitada et al., 1998), a rare syndrome characterised by dystonia, osteotendinous hyperreflexia and a relatively slow motor progression. To date, 79 different *PARKIN* mutations have been reported in both familial and sporadic forms of PD, and are the most common cause of AR early-onset PD (Ferreira & Massano, 2017). The second most common cause of AR early-onset

PD are mutations in the *PINK1* gene (Kumazawa et al., 2010), which are typically missense mutations however copy nunmber mutations and exonic rearrangements have also been described (Samaranch et al., 2010). Clinically, *PINK1*-related PD is similar to that seen in *PARKIN* patients, displaying slowly progressive L-DOPA responsive disease (Samaranch et al., 2010). However, atypical features such as prominent dystonia, cognitive and psychiatric problems can also be present (Nuytemans et al., 2010). Finally, rare missense mutations in the *DJ-1* have been identified in around 1% of early-onset PD cases (Abou-Sleiman et al., 2003). The clinical phenotype of *DJ-1* patients is identical to *PARKIN* and *PINK1*-related parkinsonism with a good response to L-DOPA and slow disease progession (Abou-Sleiman et al., 2003).

The majority of PD cases have unknown cause, therefore genome-wide association studies (GWAS) have been conducted in sporadic PD patients in an effort to identify rare variants that increase risk of disease (Satake et al., 2009; Simon-Sanchez et al., 2009; Pankratz et al. 2009; Hamza et al. 2010; Nalls et al. 2014; Chang et al., 2017). To date, 43 genetic loci have been identified as risk factors for the development of PD (Table 1.2).

SNP	Candidate gene	Effect allele/alternate allele	Odds Ratio
rs35749011	*GBA*	G/A	0.58
rs823118	*NUCKS1*, *SLC41A1*	C/T	0.89
rs10797576	*SIPA1L2*	T/C	1.12
rs6430538	*TMEM163*,*CCNT2*	T/C	0.89
rs1474055	*STK39*	C/T	0.83
rs115185635	*CHMP2B*	C/G	1.21
rs12637471	*MCCC1*	A/G	0.85
rs34311866	*TMEM175*,*DGKQ*	C/T	1.23
rs11724635	*FAM200B*, *CD38*	C/A	0.90
rs6812193	*FAM47E*	T/C	0.92
rs356182	*SNCA*	G/A	1.33
rs9275326	*HLA-DRB6*, *HLA-DQA1*	T/C	0.85
rs199347	*KLHL7*, *NUPL2*, *GPNMB*	G/A	0.91
rs591323	*MICU3*	A/G	0.91
rs117896735	*BAG3*	A/G	1.65
rs3793947	*DLG2*	A/G	0.93
rs329648	*MIR4697*	T/C	1.09
rs76904798	*LRRK2*	T/C	1.15
rs11060180	*OGFOD2*	G/A	0.90
rs11158026	*GCH1*	T/C	0.91
rs1555399	*TMEM229B*	T/A	1.09
rs2414739	*VPS13C*	G/A	0.91
rs14235	*ZNF646*, *KAT8*	A/G	1.08

SNP	Candidate gene	Effect allele/alternate allele	Odds Ratio
rs12456492	*SYT4*	G/A	1.10
rs62120679	*LSM7*	T/*C*	1.08
rs8118008	*DDRGK1*	A/*G*	1.07
rs4653767	*ITPKB*	C/T	0.92
rs34043159	*IL1R2*	C/T	1.08
rs353116	*SCN3A*	T/C	0.94
rs4073221	*SATB1*	G/T	1.10
rs12497850	*NCKIPSD*, *CDC71*	G/T	0.93
rs143918452	*ALAS1*, *TLR9*, *DNAH1*, *B AP1*, *PHF7*, *NISCH*, *STA B1*, *ITIH3*, *ITIH4*	G/A	0.68
rs78738012	*ANK2*, *CAMK2D*	C/T	1.13
rs2694528	*ELOVL7*	C/A	1.15
rs9468199	*ZNF184*	A/G	1.11
rs2740594	*CTSB*	A/G	1.09
rs2280104	*SORBS3*, *PDLIM2*, *C8orf 58*, *BIN3*	T/C	1.07
rs13294100	*SH3GL2*	T/G	0.92
rs10906923	*FAM171A1*	C/A	0.93
rs8005172	*GALC*	T/C	1.08
rs11343	*COQ7*	T/G	1.07
rs4784227	*TOX3*	T/C	1.09
rs601999	*ATP6V0A1*, *PSMC3IP*, *T UBG2*	C/T	NA

Table 1.2 single nucleotide polymorphisms (SNPs) identified as risk factors for PD, *along with details of their candidate genes, possible alleles and odds ratio (Table adapted from Chang et al., 2017).*

(ii) Environmental risk factors of Parkinson's disease

Setting aside the monogenic cases, it is likely that sporadic PD onset is a result of a complex interaction between the exposure to environmental agents and a predisposition at the genetic level. Several studies have shown an association between professional pesticide exposure and late-onset PD, mostly with insecticides (Elbaz et al., 2009). Some polymorphisms in the multidrug resistance protein 1 gene (*MDR1*), a G protein involved in epuration of xenobiotic/drugs from the blood brain barrier (BBB), are associated with a specific vulnerability for PD in individuals exposed to pesticides (Dutheil et al., 2010). This is a compelling illustration of gene-environment interaction in PD pathogenesis. The mechanisms underlying the effects of pesticides and how they lead to neurodegeneration will be discussed in more detail in section 1.4.1 in the context of animal models of PD. PD is more frequent in men than in women (Wooten et al., 2004), which has led to the hypothesis that oestrogen may be protective against PD. However, disparate results from multiple studies suggest that this is currently undetermined (Miller & Cronin-Golomb, 2010; Liu & Dluzen, 2007). For instance, oophorectomy increases the risk for PD, with a stronger risk in women who have a younger age at oophorectomy (Rocca et al., 2008). A meta-analysis has also demonstrated that PD patients have lower plasma uric levels than healthy subjects (Shen & Ji, 2013). Urate acts as a reactive oxygen species (ROS) and peroxynitrite scavenger, which may underlie why decreases in its levels may increase PD risk.

Other environmental factors that have been identified include cigarette smoking (Ritz et al., 2007) and coffee drinking (Costa et al., 2010), which both reduce risk of PD development and are therefore thought of as neuroprotective. As well, in a meta-analysis, ibuprofen was shown to reduce PD risk (Samii et al., 2009) and this is

hypothesised to be due to its anti-inflammatory and anti-oxidative effects (Charurvedi & Beal, 2008).

1.1.5 Current and future treatments for Parkinson's disease

So far, the only available treatments for PD are symptomatic in nature, with no treatment currently able to halt or reverse disease progression. Most currently approved pharmacological therapies for the treatment of PD aim to increase striatal DA levels to ameliorate associated motor deficits. The most commonly prescribed are dopamine precursors, most frequently L-DOPA. DA itself is unable to cross the BBB, therefore in order for an orally administered pharmaceutical approach to dopamine replacement, a dopamine precursor is required. L-DOPA is converted to dopamine via aromatic l-amino acid decarboxylase (AADC). However various side effects have been reported surrounding fluctuation in motor response. The most debilitating class of motor fluctuation is involuntary movements known as L-DOPA induced dyskinesia (LID), with 80-90% of patients suffering from LID after 10 years of treatment (Ahlskog & Muenter et al., 2001; Hauser et al., 2007). Carbidopa is often given in combination to reduce systemic metabolism of L-DOPA and increase central exposure, allowing lower doses of L-DOPA to maintain efficacy whilst reducing side-effects (Ellis & Fell, 2017). Monoamine oxidase B (MAO-B) inhibitors have also been employed in pharmacological approaches. MAO-B is an enzyme involved in the metabolism of dopamine forming 3,4-dihydroxyphenylacetic acid (DOPAC) which is eventually transformed by catechol-O-methyltransferase (COMT) into homovanillic acid (HVA; Edmondson et al., 2007). MAO-B inhibitors are used to treat PD to decrease DA metabolism and increase DA concentrations in the brain to alleviate motor symptoms.

Approved MAO-B inhibitors include selegiline and rasagiline, which are used both on their own and in conjunction with L-DOPA therapy (Fernandez & Chen, 2007). DA agonists are another safe and effective alternative to L-DOPA, especially in younger patients, and is associated with a lower incidence of motor complications at the 5-year mark (Alonso Cánovas et al., 2014). A 2010 meta-analysis of all the controlled trials performed with DA agonists found a significant reduction in 'off' time, Unified Parkinson's Disease Rating Scale (UPDRS) score and incidence of dyskinesia (Stowe et al., 2010). However, it is has been demonstrated that DA agonists play a role in the pathogenesis of Impulse Control Disorder (ICD); particularly pathological gambling, hypersexuality and compulsive shopping and eating (Alonso Cánovas et al., 2014).

Deep brain stimulation (DBS) is an established therapy in patients with early or uncontrollable motor fluctuations (Schuepbach et al., 2013). DBS works by the implantation of a stimulating electrode in the iGP or STN with the aim to disrupt the unbalanced neuronal activity that underlies motor symptoms. STN surgeries are carried out more frequently than iGP targeting surgeries, illustrating the preference for this anatomical structure for surgery (Krack et al., 2017). DBS allows for a lower dosage of L-DOPA and also reduces the rate of dyskinesia (Breit et al., 2004). However, DBS is not without its limitations. There is a risk of infection at the surgery site which increases with the number of battery changes (Pepper et al., 2013) and despite DBS decreasing PD symptoms, it still does not halt progressive degeneration of neurons (Shulman et al., 2011). Furthermore, in recent years it has been shown that the removal of the impulse generator can lead to a life-threatening DBS withdrawal syndrome, characterised by a severe akinetic state, dysphagia and the need for constant intensive

medical care (Reuter et al., 2015). Early re-implantation has been shown to improve this syndrome (Reuter et al., 2018).

Increasing effort is being put into the improvement of stem cell transplantation therapies to reverse the damage that is done by PD. Techniques and studies concerning the grafting of DAn from human embryonic brains started to become popular towards the end of the twentieth century (Lindvall et al., 1989). Although some clinical trials have shown a positive effect of these grafts (Lindvall et al., 1992), others have shown graft-induced dyskinesia (Barker et al., 2013), and there are ethical dilemmas around using embryonic stem cells (ESCs) as well as the issue of tissue-rejection by the host. Recent developments in stem cell research have shown that it is possible to retrieve the pluripotent state in somatic cells by expressing specific reprogramming factors (Takashi & Yamanaka, 2006). These induced pluripotent stem cells (iPSCs) can subsequently be directed to differentiation into neurons *in vitro* and potentially provide an autologous and easily accessible source of neurons for cell transplantation. Following optimisation of the protocol for the patterning towards ventral midbrain neurons, human iPSC-derived DAn have been successfully transplanted in the striatum of adult rats (Kirkeby et al., 2012). Autologous iPSC-derived DAn have also been successfully transplanted into non-human primate and were shown to survive for 12 months without immune-suppression (Sundberg et al., 2013). However, the use of these cells come with a number of issues, mainly on the account of safety. The biggest safety concern surrounding the use of iPSCs in transplantation is the risk of tumour development; prolonged culturing of iPSCs will introduce similar mutations as seen in tumour development (Pen & Jensen, 2016) and iPSCs express proto-oncogenes possibly involved in dedifferentiation towards cancer stem cells (Kumar et al., 2012).

There is also a risk for post-differentiation loss of cell-phenotype (Pen & Jensen, 2016). Obtaining cells with high fidelity is required for a long-lasting effect of the transplantation and will have to be guaranteed before using reprogrammed cells in patients. Lastly, it has been demonstrated in the grafting of ESCs that pathology is found in the donor-graft at long-term follow ups (Kordower et al., 2008; Li et al., 2008), leading to the hypothesis that α-synuclein pathology could spread from host-to-graft in a prion-like fashion and eventually lead to disease in the implanted cells (Luk et al., 2009; Masuda et al., 2013).

1.2 Autophagy in Parkinson's disease

Defects of the autophagy pathways and the resulting accumulation of protein aggregates represent a common pathobiological feature in PD across different PD-associated genes (see figure 1.3). LRRK2 has been implicated in these pathways, and will be discussed in detail in section 1.3.

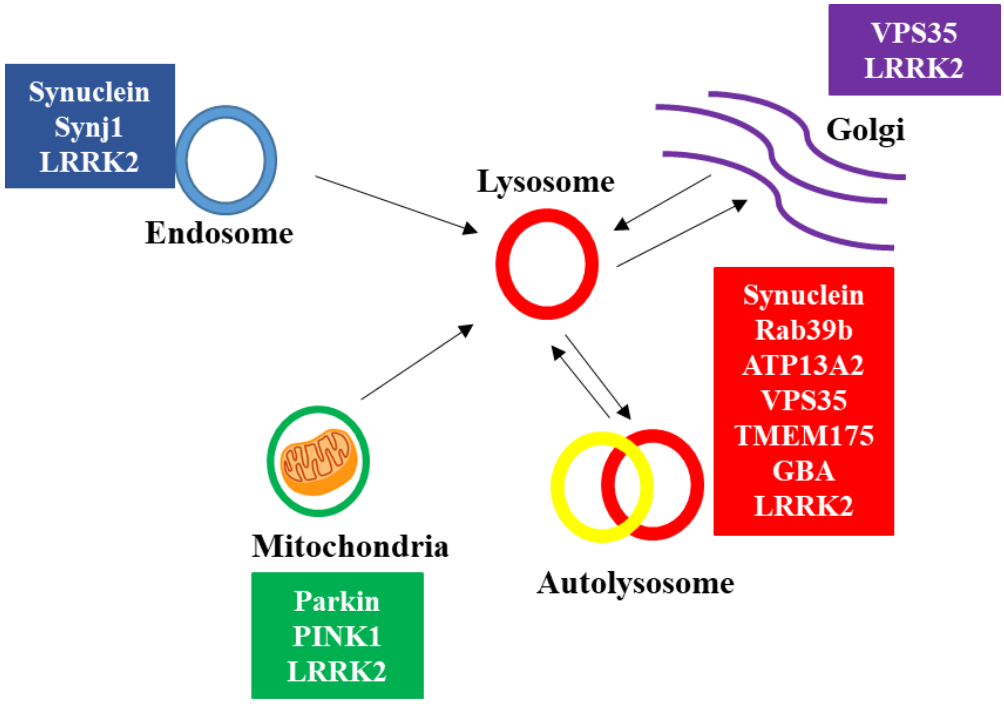


Figure 1.3 Parkinson's disease and the autophagy and endolysosomal system.
PD genes and their involvement in autophagy and the endolysosomal pathways

1.2.1 Mitophagy defects

PD-related genes have been linked to mitophagy, and mitochondrial deficiency has been suggested as responsible for neurodegeneration in PD (Gao et al., 2017). Mutations in *PINK1* and *PRKN* which lead to autosomal recessive forms of PD were discussed in section 1.1.4 (i). PINK1-dependent activation of parkin is recognized as a major pathway of mitophagy (Grenier et al., 2013). Parkin is an E3 ubiquitin ligase which is phosphorylated by PINK1 to trigger mitophagy. Whilst WT PINK1 can successfully recruit parkin to mitochondria for their degradation, pathogenic mutant-PINK1 is unable to do so, leading to a decrease in perinuclear (an area associated with autophagy) mitochondrial clusters in HeLa cells (Vives-Bauza et al., 2010). Interestingly, knock-down of PINK1 via RNAi in SR2+ cells (*Drosophila* cell line) prevents parkin recruitment to mitochondria and the accumulation of Mfn, a mitochondrial profusion factor (Ziviani et al., 2010). PINK1$^{-/-}$ mice expressing the mito-QC transgene, a fluorescence based reporter which enables the subcellular visualization of mitophagy in tissues (Figure 1.4), have recently been characterised by McWilliams et al., (2018). In both the midbrain and the striatum in TH+ neurons and microglia, mitophagy levels were unaffected by the knock-out of Pink1. Rather than concluding that Pink1 is dispensable for mitophagy, however, it was hypothesised that distinct basal and stress-evoked pathways exist to coordinate mitochondrial clearance in a context-dependent fashion. Indeed, MEFs from PINK1$^{-/-}$ animals displayed no alterations in mitophagy levels relative to WT controls at basal levels, however a decrease in mitophagy upon Carbonyl cyanide m-chlorophenyl hydrazone (CCCP) treatment was observed in the absence of PINK1, suggesting a role of PINK1 in mitophagy that is context-dependent. In PD patient-derived fibroblasts, mutations in *PINK1* and *PRKN* impair the ubiquitination of mitofusins (Rakovic et al., 2011). Although bi-allelic mutations in *PRKN* typically have a high penetrance rate (Hedrich et al., 2004), an unusual case of a homozygous *PRKN* mutation carrier who remains asymptomatic in her eighth decade of life has been identified (Koentjoro et al., 2012). The putative mechanism that protects this asymptomatic patient from PD has recently been identified. In contrast to *PRKN*-related PD patient-derived

fibroblasts who exhibited decreased mitophagy levels, the asymptomatic carrier cells showed preserved mitophagy which was mediated by the mitochondrial receptor Nip3-like protein X (Nix; Koentjoro et al., 2017). Nix has previously been shown to mediate mitochondrial clearance in primary MEFs (Novak et al., 2010), highlighting the importance of mitophagy in PD as well as a promising target for neuroprotective treatment.

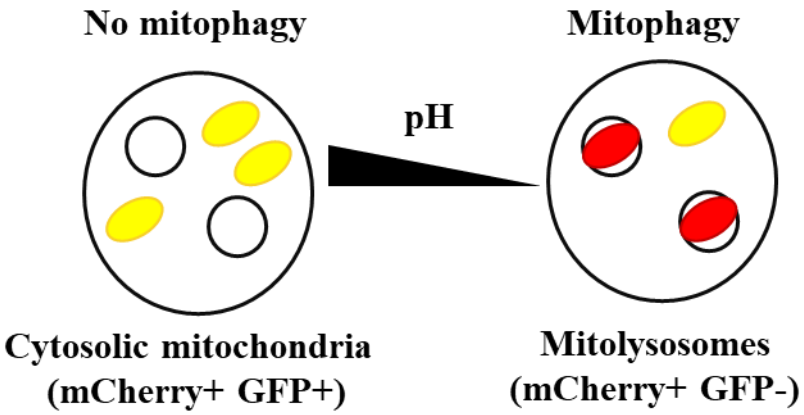


Figure 1.4 Schematic of MitoQC. *mCherry and GFP labelled Mitochondria fission protein 1 protein is used to visualise mitophagy. In increased pH levels in cytoplasm, mitochondria will visualised as yellow. In acidic lysosomes during mitophagy, GFP will be quenched and mitochondria will be identified with mCherry only. Figure adapted from McWilliams et al., (2018).*

1.2.2 Trafficking defects

Genetic discoveries are beginning to illuminate cellular pathways and functions that are involved in the development of PD, and the impairment of intracellular trafficking is emerging as a mechanistic link between many PD-associated genes. Studies in model systems that range from yeast cells to transgenic (TG) mice have shown that elevated levels of α-synuclein disrupt numerous essential intracellular trafficking steps, including those at the endoplasmic reticulum (Cooper et al., 2006), the early and late endosome (Outeiro et al., 2003) and the lysosome (Chung et al., 2013; Mazzulli et al., 2011). In iPSC-derived midbrain DAn from a healthy control that were infected with lentiviral particles to overexpress human WT α-synuclein, α-synuclein was shown to disrupt hydrolase trafficking at the cis-Golgi through aberrant association with fusion machinery (Mazzulli et al., 2015). α-synuclein is also shown to function as a chaperone that facilitates the maintenance of SNARE complexes at the synapse, and *Snca/Sncb/Sncg* triple-KO mice exhibit neurological impairments and deficits in SNARE-complex assembly (Burré et al., 2010).

The retromer protein complex controls recycling of transmembrane proteins from the endosome and lysosome back to the trans-Golgi network (TGN). Mutations in *VPS35* have been shown to cause autosomal dominant, late-onset PD (Zimprich et al., 2011) and encodes for a component of the retromer. VPS35-deficient mice or mice expressing the D620N mutant have been shown to accumulate α-synuclein in SNpc-DAn, as well as impaired endosome-to-Golgi retrieval of LAMP2a and accelerated LAMP2a degradation (Tang et al., 2015). The D620N mutation leads to decreased binding affinity of VPS35 to family with sequence similarity 21 (FAM21), an important component of the Wiskott-Aldrich syndrome and SCAR homology (WASH) complex, in HeLa cells (McGough et al., 2014). The WASH complex is an actin related protein 2/3 (Arp2/3) activating protein that localises to the surface of endososmes and induces the formation of branched actin networks (Derivery & Gautreau, 2010). This decrease in WASH binding by mutant VPS35 has been observed to impair

macroautophagy in HeLa cells via the abnormal sorting of the autophagy protein ATG9a which decreased autophagosome formation (Zavodsky et al., 2014).

Synaptojanin-1 and auxilin, which are both implicated in clathrin mediated endocytosis, have been identified as LRRK2 substrates (Islam et al., 2016; Nguyen and Krainc, 2018). Loss-of-function mutations in the gene encoding for Rab39B, which localizes to early endosomes, have also been described in familial forms of parkinsonism with cognitive impairment and α-synuclein pathology (Wilson et al., 2014). How disruption of clathrin-mediated endocytosis causes neurodegeneration is unknown, but it has been suggested that it likely has unspecified effects on lipid signalling, synaptic proteins and/or extra-vesicular DA accumulation (Kett & Dauer, 2017).

1.2.3 Lysosomal defects

Many of the pathways implicated in PD converge on the lysosome. Furthermore, lysosomal function decreases with age, with a rise in lysosomal pH (Cuervo & Dice, 2000) highlighting an association between age-related disease and lysosomal enzymatic activity. Mutations in *ATP13A2*, a lysosomal ATPase, have been shown to induce impaired lysosomal acidification and a reduction in the degradation of lysosomal substrates (Dehay et al., 2012) in PD patient-derived fibroblasts. VPS35 deficiency has also been observed to perturb the maturation of cathepsin D by increasing mannose-6-phosplate receptor (MPR) turnover, leading to the accumulation of α-synuclein in lysosomes of *Drosophila* (Miura et al., 2014). The expression of A53T α-synuclein has been observed to decrease lysosomal acidification in rat PC12 cells (Stefanis et al., 2001) and reduce lysosomal protein turnover (Cuervo et al., 2004). Transmembrane protein 175 (TMEM175), the late endosome and lysosomal K^+ channel, has been identified as a candidate gene residing in a highly significant risk loci on chromosome 4

via a PD GWAS meta-analysis (Nalls et al., 2014). TMEM175 deficiency in rat primary neurons results in an instability in lysosomal pH, decreased lysosomal catalytic activity and impaired autophagosome clearance (Jinn et al., 2017).

Lysosomal Ca^{2+} has also been highlighted as potentially dysregulated in the presence of PD-associated genetic mutations. Local calcium release from lysosomes is required for late endosome-lysosome fusion (Pryor et al., 2000). As well as lysosomal Ca^{2+} being seen to be dysregulated in the presence of pathogenic *LRRK2* mutations (Gomez-Suaga et al., 2012), it has been observed that the N370S mutation in the glucocerebrosidase (*GBA*) gene induces a reduction in lysosomal Ca^{2+} in PD patient-derived fibroblasts (Kilpatrick et al., 2016). Interestingly, a cofactor required for the import of glucocerebrosidase into the lysosome, lysosome membrane protein 2 (LIMP2), which is encoded by the gene *SCARB2*, has also been linked by GWAS to the risk of developing PD (Do et al., 2011). A deficiency in LIMP2 leads to the defective transport of glucocerebrosidase, as well as lysosomal dysfunction and α-synuclein accumulation (Nalls et al., 2014; Rothaug et al., 2014). Furthermore, in a recent meta-analysis of genome-wide association studies the a1 subunit of v-ATPase, otherwise known as ATP6V0A1, was identified as a novel PD risk loci (Chang et al., 2017).

A mouse model of Parkinson's disease resulting from the exposure to MPTP shows accumulation of autophagosomes and an early decrease in lysosome number in DAn as a result of lysosomal membrane destabilization and cytosolic release of cathepsins (Dehay et al., 2010). A tetracycline-regulated inducible TG mouse model that overexpressed A53T α-synuclein under the control of the promotor Pitx3 in DAn develops profound motor disabilities, midbrain neuronal loss and impaired lysosomal degradation as evident by the accumulation of autophagy-related proteins in midbrain (Lin et al., 2012). Furthermore, a significant burden of rare lysosomal storage disorder gene variants associated with PD risk has been discovered

(Robak et al., 2017). Taken together, these studies highlight the crucial role of the lysosome in PD.

1.3 LRRK2

1.3.1 LRRK2 mutations and Parkinson's disease

As discussed in section 1.1.4, a minority of PD cases arise from genetic mutation inherited in an autosomal dominant or recessive manner. Mutations in the gene encoding for Leucine-Rich repeat Kinase 2 (LRRK2) are the most frequent cause of familial PD (Singleton et al., 2013). The *LRRK2* gene was identified in 2004 as the gene residing in the PARK8 locus (Paisán-Ruíz et al., 2004; Zimprich et al., 2004). In these first studies, the Y1699C and R1441G and C mutations were identified. Subsequently, the G2019S mutations was identified in multiple kindreds across North America and Europe (Hernandez et al., 2005; Kachergus et al., 2005) and the R1441H mutation was identified in a patient of European ancestry (Zabetian et al., 2005). Furthermore, I2020T mutation has been identified in the Japanese family in which the PARK8 locus was first described as associated with PD (Funayama et al., 2002). The I2012T mutation has also been identified in a PD family in Taiwan (Deng et al., 2006). Finally, the N1437H mutation was identified in a large Norwegian family (Aasly et al., 2010).

In addition to the known monogenic mutations there are number of associated risk variants within the *LRRK2* gene which are extremely rare and some are also present in controls (Paisán-Ruíz et al., 2013). The R1628P (Ross et al., 2008) and G2385R (Di

Fonzo et al., 2006) risk factors both confer a two-fold increased risk for the development of PD.

Mutations in *LRRK2* lead to the development of PD with incomplete penetrance (Healy et al., 2008). Of the confirmed mutations the G2019S mutation is widely recognised as the most frequent (Dachsel and Farrer, 2010) and its penetrance has been the most well studied. It was initially estimated that G2019S mutation had a penetrance of 80-100% (Paisán-Ruíz et al., 2004). However, as more families carrying the G2019S mutation have been identified this number is now considered to be between 25-43% (Goldwurm et al., 2011; Lee et al., 2017).

Clinically, mutant LRRK2 PD patients are often considered indistinguishable from sporadic patients. Mutant LRRK2 PD patients show a similar age of onset to sporadic cases, as well as cell loss within the SNpc, the presence of LBs (although a significant minority of cases have been reported without LBs [Kalia et al., 2014]) and responsiveness to DA replacement therapy (Singleton et al., 2013). Healy et al. (2008) in a large case-controlled study of over 350 patients found that with this similar age of onset and motor and non-motor symptoms, *LRRK2* mutant carriers exhibited reduced incidences of cognitive impairment and sleep disturbances. Importantly, however, while all known mutations were studied, due to the infrequence of some of the mutations (R1441C/G/H, I2020T), it was not clear if their clinical presentation significantly differed from the more common G2019S mutation. It has more recently been shown that R1441C carriers have a clinically similar presentation of PD to

G2019S carriers and PD patients without mutations in the *LRRK2* gene (Pchelina et al., 2011; Cilia et al., 2014).

Furthermore, the *LRRK2* gene has been identified as an independent risk factor for sporadic PD (Ross et al., 2008). Furthremore, the LRRK2 locus and it's risk association has been fine-mapped in over 5000 PD patients, and a common variant PD association located outside of the LRRK2 protein coding region has been identified (Trabzuni et al., 2013). Di Maio and colleagues recently demonstrated that there is an increase in LRRK2 activation in the brains of idiopathic PD patients, with increases in LRRK2 autophosphorylation observed (Di Maio et al., 2018). Taken together, this has fuelled the hypothesis that LRRK2 might also play a role in the pathogenesis of sporadic PD and will provide understanding of the disease process that may be occurring in a broader population of patients.

1.3.2 LRRK2 structure and function

The *LRRK2* gene is located on chromosome 12 and consists of 51 exons; it codes for a 286 kDa, 2527 amino acid, multidomain protein encompassing two enzymatic functions at its core (Figure. 1.5). The catalytic core consists of the Ras of complex (ROC) and the carboxy-terminal of ROC (COR), which collectively forms the GTPase domain of the protein, and the serine/threonine kinase domain. This enzymatic core is surrounded by protein-protein interaction domains. The N-terminal harbours the armadillo, the ankyrin and the leucine rich repeat (LRR) domains. At the C-terminal there is the WD40 domain, which has been demonstrated to be crucial for protein folding (Rudenko et al., 2012).

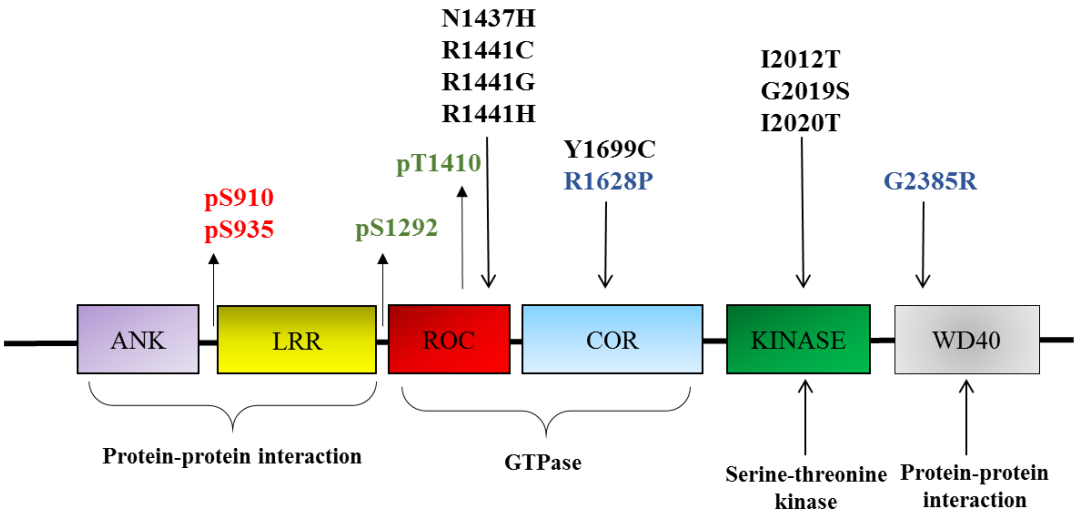


Figure 1.5 LRRK2 structure, mutations and phosphorylation sites. *Schematic showing the domains of LRRK2 and their functions, including locations of PD monogenic mutations (black), risk variants (blue) and sites of phosphorylation (red) and autophosphorylation (green). Abbreviations: ANK, ankyrin repeat; LRR, leucine-rich repeat; ROC, ras of complex; COR, C-terminal of ROC.*

The kinase domain of LRRK2 has been of particular interest to pharmacologists as kinases are typical targets for pharmaceuticals. The LRRK2 kinase domain is thought to assume a typical kinase fold, where an N-terminal and a C-terminal sub-domain can be identified, with the active site sitting in the cleft between these two sub-domains. The activation loops, which is thought to be situated in the C-terminal of the kinase domain (Hudkins et al., 2008), possesses a DYG motif which may undergo conformational changes that may regulate kinase activity (Jura et al., 2011).

The Roc-COR tandem domain classifies LRRK2 as a member of the Roco domain containing (ROCO) protein superfamily which represents a unique multi-domain family of Ras-like G proteins. LRRK2 is known to possess GTPase activity, at least when measured in *in vitro* assays using recombinant protein. LRRK2 can selectively bind to guanine nucleotides (GDP and GTP) with similar affinity via phosphate-binding 'P-loop' motif (^{1341}GNTGSGKT^{1348}) within its GTPase domain (Nguyen & Moore, 2018). LRRK2 exhibits a low rate of GTP hydrolysis activity *in vitro* (Ito et al., 2007; Li et al., 2007). A number of key residues within the LRRK2 Roc domain have been identified to influence GTPase activity; P-loop null mutants, K1347A and T1348N, are useful tools that disrupt GTP binding as well as impairing dimerization and protein stability (Ito et al., 2007; West et al., 2007; Biosa et al., 2013).

The presence of a double enzymatic core within the LRRK2 protein suggests these two functions could influence each other's activity. Autophosphorylation of specific residues (Figure 1.5) within the ROC domain have been found to modulate GTP binding (Webber et al., 2011) and it has therefore been suggested that LRRK2 GTPase activity is regulated by its kinase activity. However, familial mutations located in the kinase domain such as G2019S have no discernible effects on GTP binding or hydrolysis (Xiong et al., 2010). The physiological relevance of autophosphorylation sites is still not clear and some of them have failed to be detected *in vivo;* in the cellular context, autophosphorylation has been observed at Thr1410 (Pungaliya et al., 2010) and at Ser1292 and this was proposed as a potential measure of LRRK2 kinase activity (Sheng et al., 2012). However, Kluss and colleagues have recently optimised a method of observing LRRK2 autophosphorylation at Ser1292 in mice (Kluss et al., 2018). It was demonstrated that the fractionation of microsomes from mice brain tissue leads to

the enrichment of endogenous Lrrk2 phosphorylated at this residue. Mutations in these residues lead to decreased enzymatic activity of the protein (Webber et al., 2011). The role of the GTPase domain on kinase activity regulation is inconsistent (Nguyen and Moore, 2018) as various reports have seen increases (Covy & Giasson, 2009; Smith et al 2006; West et al., 2007), decreases (Lewis et al., 2007) and no changes (Anand et al., 2009; West et al., 2005) in kinase activity with altered GTP binding. Furthermore, LRRK2 is capable of forming a dimer and this dimerization has been shown to be dependent on the proteins capacity for kinase activity and GTP binding, but not GTP hydrolysis (Biosa et al., 2013). LRRK2 dimers demonstrate increased kinase and GTPase activity in comparison to monomers, and are thought to be enriched at cell membranes (Berger et al., 2010).

1.3.3 Enzymatic activity and mutations

All seven of the pathogenic *LRRK2* mutations identified so far cluster around the catalytic domains of the protein (Figure 1.5). The G2019S and I2020T reside in the kinase domain and the R1441C/G/G, Y1699C and N1437H reside in the ROCO supradomain. The G2019S mutation causes a consistent increase in kinase activity that has been reported in multiple models (Covy et al., 2008; Luzon-Toro et al., 2007; West et al., 2005; Anand et al., 2009; Smith et al., 2006). This is not the case for the I2020T mutation which has had both increases (West et al., 2007) and decreases (Jaleel et al., 2007) in kinase activity reported. As previously mentioned, mutations residing in the GTPase domain of LRRK2 also lead to inconsistent changes in LRRK2 kinase activity. Interestingly, the coding variant G2385R, residing in the WD40 domain, results in a 50% loss of kinase activity (Rudenko et al., 2012) and the coexpression of both G2019S

and G2385R leads to kinase activity similar to that seen in WT LRRK2 (Rudenko et al., 2012) suggesting opposing mechanisms in these disease associated mutations.

With regards to the effects of *LRRK2* mutations on GTPase activity, familial mutations in the Roc-COR domain have been shown to reduce GTPase activity to varying degrees. R1441C/G/H and Y1699C variants all exhibit decreased GTP hydrolysis compared to WT LRRK (Ito et al., 2007; Li et al., 2007; Daniels et al., 2011; Liao et al., 2014). As mentioned previously, the G2019S mutation in the kinase domain has no discernible effect on GTPase activity. Interestingly, the familial mutation N1437H mutation, located in the Roc domain, simultaneously increased both GTP binding and kinase activity (Aasly et al., 2010).

Phosphorylation of LRRK2 at Ser910/935 (Figure 1.5) is required for its binding with the 14-3-3 protein (Muda et al., 2014), which is able to regulate its association to membranes (Schapansky et al., 2014; Mamais et al., 2014) and downstream signalling. It has been suggested that this phosphorylation and binding regulates kinase activity negatively by preventing dimerization of its Roc domain (Muda et al., 2014; Mamais et al., 2014). Take together this is suggestive of a complex interplay of intramolecular interactions within the LRRK2 molecule that is likely to reflect on cellular functions of LRRK2.

1.3.4 Cellular functions of LRRK2

(i) LRRK2 and Autophagy

Autophagy is a self-degradative, highly regulated process that is crucial for maintaining cellular homeostasis via the digestion of selected cellular substrates. There are a number of autophagy sub-types, including macroautophagy, chaperone mediated autophagy (CMA) and mitophagy.

Macroautophagy arises from the formation of a phagophore, engulfing cargo for degradation, enclosing to become the autophagosome which will fuse with a lysosome to form a mature autolysosome and contents can be degraded. Macroautophagy can be envisioned as a cycle (Figure 1.6) which is, in the canonical pathway, initiated by the changes in phosphorylation status of the Unc-51 like autophagy activating kinase 1 (ULK1) complex via the mechanistic target of rapamycin (mTOR) or 5' adenosine monophosphate-activated protein kinase (AMPK) signalling (Kim et al., 2013). This subsequently triggers the translocation of the vacuolar protein sorting associated 34 (VPS34) from the cytoskeleton (Bartolomeo et al., 2010) to the phosphoinositide 3-kinase (PI3K) complex at the pre-autophagosomal structure (Suzuki et al., 2007) leading to the enrichment of phosphatidylinositol 3-phosphate (PI(3)P) and the recruitment of WD-repeat proteins interacting with phosphoinositides (WIPIs) and autophagy related proteins (ATGs) to mediate the elongation of the phagophore (Vergne et al., 2009; Axe et al., 2008) to form the autophagosomal membrane around the autophagy substrate. Microtubule associated protein 1 light chain 3 (LC3) is conjugated to phosphatidylethanolamine by ATG7 and ATG3 in an ubiquitin-like manner, resulting in autophagosome associated LC3-II (Kabeya et al., 2004). To

complete the digestion process, autohagosomes depend on retrograde transport to the microtubule organization centre (MTOC) of the cell where lysosomes are most abundant (Johnson et al., 2016). Soluble *N*-ethylmaleimide-sensitive factor attachment protein receptors (SNAREs) situated on lysosomes and autophagosomes form complexes to facilitate fusion of the two vesicles to form autolysosomes (Minton, 2013) and the contents is degraded and digestion products are released.

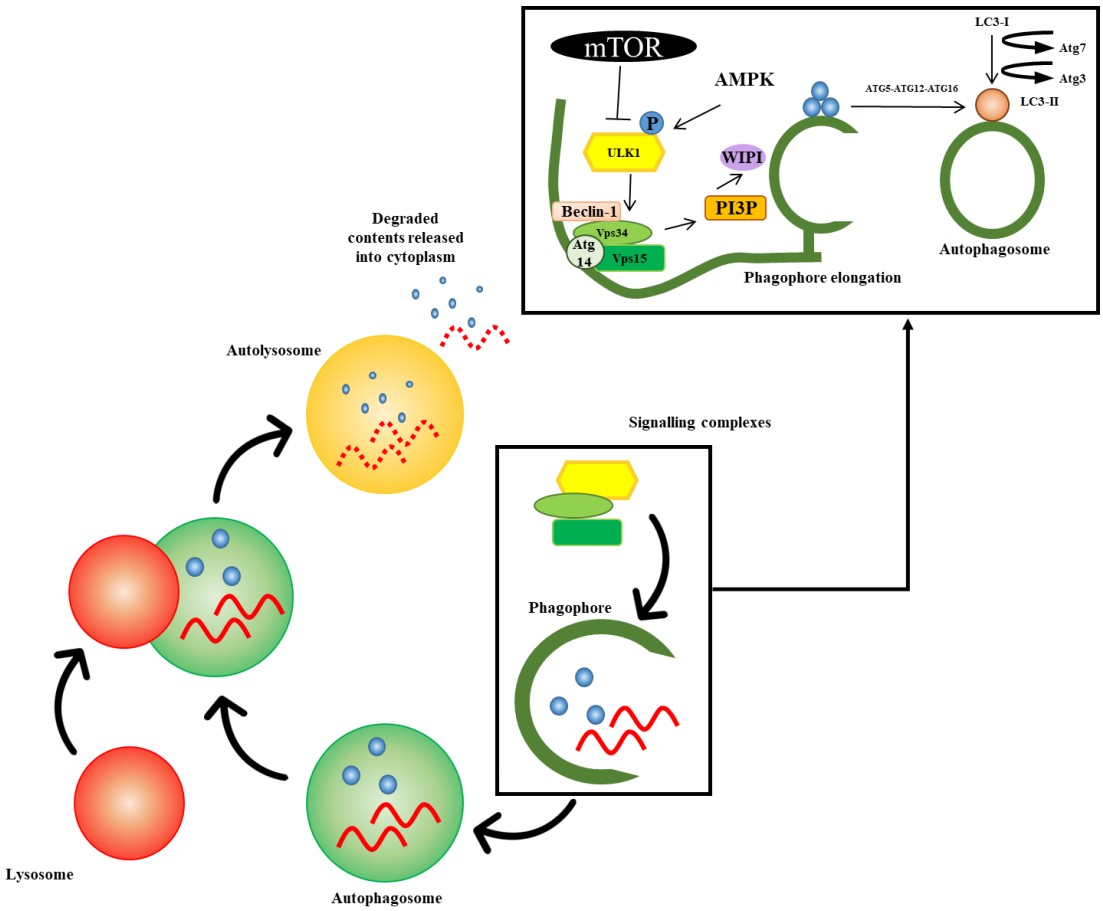


Figure 1.6 Macroautophagy. *Schematic showing the fundamental stages of macroautophagy. The principle stages of macroautophagy include the highly regulated production of a phagophore under direction of multiple signalling and protein modification assemblies; elongation of the phagophore around a region of cytoplasm; closure of the phagophore to form a autophagosome; fusion of the autophagosome with a lysosome; and digestion of the autophagosome contents by hydrolytic enzymes, yielding basic metabolites that are released into the cytoplasm for new synthesis or sources for energy. Figure adapted from Nixon (2013)*

LRRK2 was first implicated in macroautophagy (hereby referred to as autophagy) in 2008 where the knock-down of ATG7 and ATG8 attenuated LC3-II accumulation and neurite shortening in SH-SY5Y cells overexpressing G2019S-LRRK2 (Plowey et al., 2008). Similarly, the expression of an R1441C-LRRK2 bacterial artificial chromosome (BAC) construct in human embryonic kidney cells (HEKs) increased autophagic vacuoles (Alegre-Abarrategui et al., 2009) and G2019S-LRRK2 (Gomez-Suaga et al., 2012) in HEK293s lead to an increase in both autophagosomes and autolysosomes. It would seem from these findings that PD-linked mutations lead to an up-regulation of autophagy. However, inconsistencies and conflicting data reported in the literature have become more apparent in the last five years.

Decreased autophagic vacuoles and decreases in LC3-II levels in the presence of *G2019S-LRRK2* mutations have been reported (Sanchez-Danes et al., 20102, Bravo-San Pedro et al., 2013) as well as inhibited LC3-II responses to starvation, a commonly used tool to assess flux through the autophagy pathway (Manzoni et al., 2013). Similarly, in animal models of LRRK2-PD, G2019S and R1441C-TG mice have been reported to have enlarged and increased autophagic vacuoles in striatum and cortex (Ramonet et al., 2011) as well as increased reliance on macroautophagy compared to other sub-types. However other models have failed to replicate this phenotype (Tsika et al., 2014; Tsika et al., 2015).

The picture is complicated further with the addition of Lrrk2 knock-out ($Lrrk2^{-/-}$) research; biphasic, age-dependent, changes in LC3-II and ubiquitin binding protein p62/sequesosome (p62) levels have been reported in the kidneys of $Lrrk2^{-/-}$ mice (Tong

et al., 2012) as well as increased lysosome numbers in Lrrk2$^{-/-}$ rat kidneys (Baptista et al., 2013). These rats also exhibited elevated lipofuscin, a lipid-based by-product indicative of poor lysosomal turnover. By extension, such Lrrk2$^{-/-}$ data collectively would imply that Lrrk2 normally functions to enhance flux throughout the autophagy pathway. However, no overt neurodegeneration has been observed in Lrrk2$^{-/-}$ rodents, most likely explained by the relatively low levels of Lrrk2 in the brain compared to other areas as well as the presence of the Lrrk2 homologue, Lrrk1, in the brain to compensate for the loss of Lrrk2 activity (Roosen and Cookson, 2016).

The use of LRRK2 kinase inhibitors has informed researchers on the specific role of this enzymatic domain of the protein on the autophagy pathway. Whilst some of the earlier inhibitors had rather limited use because of their non-selective effects in cells (Ramsden et al., 2011), the development of LRRK2-IN-1 (Deng et al., 2011) provided the first step towards a pharmacological tool to define the biological role of LRRK2. LRRK2-IN-1 treatment was shown to increase LC3-II levels and p62, an ubiquitin-binding scaffold protein, in both SH-SY5Y and HEK cells (Manzoni et al., 2013) and the combined treatment of bafilomycin, to block lysosomal acidification and protein clearance, and LRRK2-IN-1 lead to an increase in LC3-II accumulation. This suggests that LRRK2 normally functions through inhibiting autophagosome formation. However, more recently it has become apparent that LRRK2-IN-1 off-target effects could considerably complicate interpretation. LRRK2-IN-1 is able to increase neurite outgrowth in Lrrk2$^{-/-}$ neurons (Luerman et al., 2013) and prevent LPS-induced ROS generation (Schapansky et al., 2015); both perceived pathways of LRRK2 pathology. More recently compounds with much higher selectivity for LRRK2 kinase inhibition have been developed (Reith et al., 2012; Fell et al., 2015; Estrada et al., 2014). An

increase in LC3-II and p62 have been reported in SH-SY5Y in response to the compound GSK257815A (Saez-Atienzar et al., 2014) and GNE-7915/0877 treated non-human primates had decreased di-docosahexaenoyl (22:6) bis(monoacylglycerol) phosphate (di-22:6-BMP) in their urine, a marker for lysosomal dysregulation, suggesting an inhibitory role of Lrrk2 kinase activity in autophagy regulation (Fuji et al., 2015).

It is clear that LRRK2 may play a role at various points in the autophagy pathway, however it is still unclear whether LRRK2 possesses a positive or negative regulatory role in the control of macroautophagy and if the role of LRRK2 resides within the initiation or the clearance steps. Furthermore the details of the molecular mechanisms underlying the role of LRRK2 in autophagy remain ambiguous, however some potential mechanisms have been described. It has been suggested that LRRK2 affects autophagosome formation via an mTOR-independent, Beclin-1 mediated pathway (Manzoni et al., 2016). Other studies have found that LRRK2 interacts with the lysosome via the Nicotinic acid adenine dinucleotide phosphate (NAADP) receptor, Two-Pore calcium channel 2 (TPC2), and that LRRK2 mediated changes in lysosome number and protein levels could be reversed using TPC2 inhibitors (Gomez-Suaga et al., 2012; Hockey et al., 2015). It has also been demonstrated that p62, which binds to ubiquitin-tagged proteins and targets them to the autophagosome, binds LRRK2 to regulate its stability (Park et al., 2016). As well, the presence of LRRK2 reduces phosphorylation of p62, decreasing its affinity for ubiquitin-tagged proteins, which results in decreased protein degradation via macroautophagy (Park et al., 2016).

CMA is a multi-step process that involves substrate recognition, substrate binding to the lysosome, translocation into the lysosome and digestion (Figure 1.7). Substrate recognition occurs in the cytosol via the binding of hsc70 to a pentapeptide motif present in the amino acid sequences (KEFRQ). Once bound, substrates are targeted to the lysosome where it interacts with the cytosolic tail of the single-span membrane protein lysosome-associated membrane protein type 2a (LAMP2a). A proportion of WT LRRK2 is degraded via this mechanism, however, the G2019S and R1441C mutations have been found to result in a low efficiency of chaperoning, and blockage at the lysosome (Orenstein et al., 2013). This was shown to be caused by the inhibition of LAMP2a oligomerization and subsequent formation of the CMA translocation complex and lead to impaired degradation of α-synuclein and increased α-synuclein oligomers. It was also suggested that, whilst the degradation of WT LRRK2 was dependent on CMA, mutant LRRK2 degradation is more dependent on ubiquitin proteasome system and autophagy degradation (Yue and Yang, 2013).

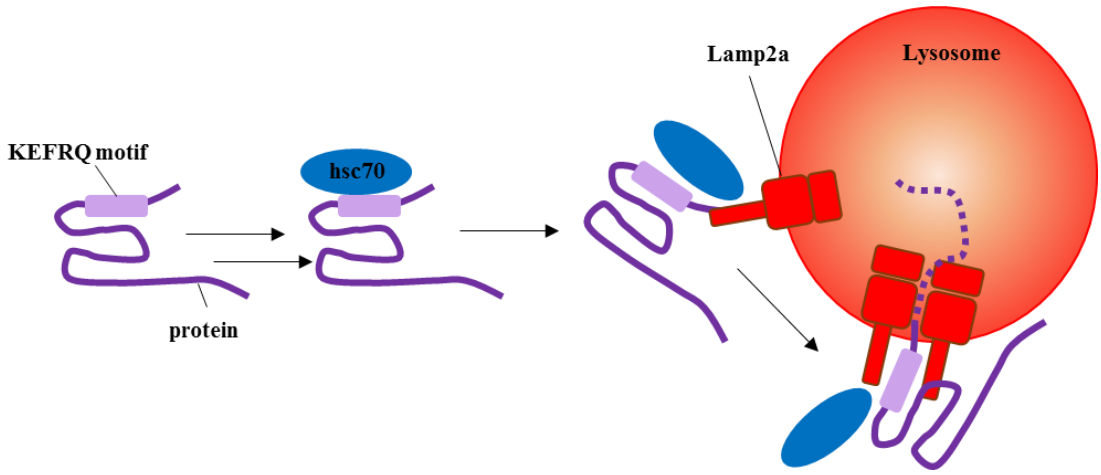


Figure 1.7 Chaperone mediated autophagy. *Schematic showing the fundamental stages of CMA. The Hsc70 chaperone complex delivers cytosolic proteins containing a KFERQ motif to the lysosomal lumen for degradation through the binding to a LAMP2-containing protein complex located on the lysosomal membrane. Figure adapted from Nixon (2013).*

Mitophagy is a form of macroautophagy that selectively degrades damaged mitochondria. It has been demonstrated in PD patient fibroblasts and iPSC-derived DAn that the inhibition of LRRK2 kinase activity was able to mediate the removal of mitochondrial Rho GTPase 1 (MIRO1) from the surface of mitochondria (Hsieh et al., 2016). MIRO1 anchors mitochondria to microtubules, and its removal is necessary for mitophagy to occur. In this same study, PINK1 mutations and cells from sporadic patients also exhibited the same impairment, suggesting a potential common pathogenic mechanism in PD. However, heightened and excessive mitophagy has also been reported in G2019S and R1441C expressing cortical neurons (Cherra, et al., 2013), G2019S transfected HeLa cell lines (Su et al., 2015) and patient fibroblasts (Smith et al., 2016).

(ii) LRRK2 at the synapse

In depth investigation of genes linked to PD has bought attention to the role of synaptic dysfunction to disease, such as mutations in *DNAJC6* (auxilin) and *SYNJ-1* (synaptojanin-1) which both encode proteins involved in clathrin-dependent synaptic vesicle endocytosis (Edvardson et al., 2012; Olgiati et al., 2014; Oligiati et al., 2016). LRRK2 kinase activity has been identified as crucial for synaptic vesicle endocytosis, specifically clathrin-mediated endocytosis, by phosphorylating endophilin A1 (EndoA1) (Arranz et al., 2015). Synaptojanin1, another endocytosis-associated protein, has also been identified as a LRRK2 substrate (Islam et al., 2016). The R1441C mutation has been shown to increase phosphorylation of auxilin and increasing clathrin binding, subsequently reducing synaptic vesicle density by ~40% and increasing oxidized DA (Nguyen and Krainc, 2018).

Knock-out of *Lrrk2* has been shown to disrupt action potential firing rates, implicating Lrrk2 in normal synaptic function. The knock-out of *Lrrk2* decreases inter-event intervals (Piccoli et al., 2011; Beccano-Kelly et al., 2014) and increase amplitude (Parisiadou et al., 2014). The expression of G2019S- and R1441C-*Lrrk2* mutations leads to an increase excitatory synaptic activity in mouse primary cortical (Plowey et al., 2014; Beccano-Kelly et al., 2014) and hippocampal (Maas et al., 2017) neurons. DA phenotypes have also been demonstrated in animal models of PD; G2019S-knock in (KI) mice (Yue et al., 2015), R1441G-BAC TG mice (Li et al., 2009) and G2019S- and R1441C BAC TG rats (Sloan et al., 2016) all develop age dependent decrease in striatal DA release. Taken together these findings suggest that LRRK2 plays a critical role at the synapse and can modulate synaptic machinery and function.

(iii) LRRK2 and mitochondria

As described in section 1.3.4 (i), LRRK2 has been implicated in mitophagy. Furthermore, LRRK2 has also been described to have a role in mitochondrial fission/fusion. Mitochondria are dynamic organelles that constantly fuse and divide. These mitochondrial dynamics are crucial for mitochondrial inheritance and maintenance of mitochondrial functions. The process of fission and fusion is regulated by molecular machinery that includes dynamin-related GTPases and WD40 repeat-containing proteins. As LRRK2 contains these domains it could potentially serve as a scaffolding protein during mitochondrial dynamics. WT LRRK2 interacts with dynamin-1-like protein (DRP1) and increases its phosphorylation and, subsequently, mitochondrial fission (Wang et al., 2012; Niu et al., 2012). Pathogenic mutations have been associated with arrested fission (Yue et al., 2015; Mortiboys et al., 2010) as well as increased fragmentation (Grunewald et al., 2014; Smith et al., 2016) that can be attenuated with LRRK2 kinase inhibition (Smith et al., 2016). Recently, a novel LRRK2 variant, E139K, was found to alter LRRK2 binding to DRP1 and prevented mitochondrial fission (Perez carrion et al., 2018).

Mitochondria generate ROS is a by-product of oxidative phosphorylation by the respiratory chain complex. Oxidative stress is a result of disequilibrium between excessive production of ROS and limited antioxidant defences. Superoxide anion, which is produced mainly by mitochondrial complexes I and III of the electron transport chain, is highly reactive and can easily cross the inner mitochondrial membrane, where it can be reduced to H_2O_2. Multiple studies have demonstrated increased susceptibility to oxidative stress with pathogenic *LRRK2* mutations

(Mendivil-Perez et al., 2016; Smith et al., 2016; Nguyen et al., 2011) as well as increased mitochondrial DNA (mtDNA) damage (Sanders et al., 2014; Mendivil-Perez et al., 2016).

In many cases where *LRRK2* mutations have been found to alter mitochondrial fission (Su and Qi, 2013), membrane potential (Cherra et al., 2013), mitochondrial content (Zhu et al., 2013), mitochondria transport (Hsieh et al., 2016) and increased ROS production (Grunewald et al., 2014) there has also been perturbed autophagy. Autophagic dysfunction may result in increased ROS production (Jia et al., 2011) which in turn can lead to mitochondrial dysfunction and dysfunctional mitophagy. Intriguingly, the lysosomal Rab7 has recently been implicated in mitochondrial fission (Wong et al., 2018) and Rab7 GTP hydrolysis can regulate mitochondrial fission. Rab7 has been identified has one of the substrates of LRRK2 (Gomez-Suaga, et al., 2014) and therefore lends a potential overlapping mechanism between mitochondrial and autophagic dysfunction.

(iv) LRRK2 and Vesicle trafficking

It is becoming increasingly apparent, with the identification of more potential LRRK2 interactors, that the study of LRRK2 in the aforementioned cellular functions be considered from a much wider perspective, taking into account a possible involvement of LRRK2 in vesicle dynamics in general. This could potentially be via indirect mechanisms, such as effects on metabolism and signalling pathways that indirectly affect autophagy and mitochondria. However, it has been speculated that the multiple protein interaction domains of LRRK2 are likely important effectors of its function

(Roosen and Cookson, 2016) and therefore direct protein-protein interactions have been mainly researched.

There is mounting evidence for the role of LRRK2 in the regulation of Rab GTPases which are instrumental in membrane trafficking. Using two distinct and unbiased phosphoproteomics approaches, it has been demonstrated that Rab10 is a bonafide substrate of Lrrk2 in mouse embryonic fibroblasts (MEFs) (Steger et al, 2016). Rab10 was found to be phosphorylated at thre73; this residue is located in the switch-II domain of the protein, which is essential for Rab GTPases protein-protein interaction (Pfeffer et al., 2005). Pathogenic mutations were demonstrated to result in the increased phosphorylation of Rabs (Rab8a and Rab10) and disrupted Rab-GDI1/2 association. Guanosine nucleotide dissociation inhibitor (GDIs) extract inactive, prenylated Rabs from the membranes and bind them with high affinity in the cytosol (Pylypenko et al., 2003). Furthermore it has been observed in HEK293 and SH-SY5Y cells transfected with plasmids expressing WT or pathogenic mutant LRRK2 that in order for Rab7L1 to be phosphorylated by LRRK2 at the switch-II domain, that Rab7L1 needs to be membrane and GTP-bound (Liu et al., 2018). It was also demonstrated that *LRRK2* mutations increase Rab7L1 phosphorylation and decreases GTP-bound Rab10 protein interaction with As160, which is a critical GTPase activating protein (GAP) for Rab10. Interestingly, *RAB7L1* is one of the five candidate genes within the PARK16 non-familial PD risk-associated locus (Tan et al., 2010; Macleod et al., 2013). Furthermore, dysregulation of the LRRK2 phosphorylation site on Rab GTPases induces neuronal toxicity in primary cortical cultures (Jeong et al., 2018). Rab10 and Rab12 have also been identified as LRRK2 kinase substrates in human peripheral blood mononuclear cells (PBMCs; Thirstup et al., 2017). Interestingly, risk variants on Rab7L1 have now

been identified in PD (Perrett et al., 2015) highlighting the potential common mechanism of dysregulated membrane trafficking in PD.

Mutations in the gene encoding for VPS35 have also been shown to segregate with PD (Perrett et al., 2015). Intriguingly, LRRK2 has been shown to interact with VPS35 (Macleod et al., 2013), and the overexpression of VPS35 can rescue lysosomal and retromer complex sorting deficits in mutant Lrrk2 *Drosophila* (Macleod et al., 2013; Linhart et al., 2014). Subsequently, Rab7 was found in complex with LRRK2 to co-operatively promote clearance of Golgi derived vesicles through the autophagy-lysosomal system. The pathogenic mutations, G2019S, R1441C and Y1699C enhanced Golgi clearance but the hypothesis-testing mutations that decrease GTP binding, the T1348N, or the kinase-inactive K1906M, did not sustain Golgi clearance, suggesting that both kinase and GTPase activities are required for maintaining this cellular process (Beilina et al., 2014).

Collectively, together with evidence for the role of LRRK2 at the synapse, autophagy pathway and mitochondria dynamics, it is evident that LRRK2 can interact with multiple proteins associated with vesicles. It is unclear how these different results are to be collated from different models to draw a clear picture of the precise molecular mechanisms underlying LRRK2's role in vesicle dynamics. However one hypothesis that has been discussed is that the synergism of all of these membrane dynamics may be controlled by LRRK2 and may be at the molecular base of PD neurodegeneration (Wallings et al., 2015) and holds exciting potential for future research.

1.4 Rodent models of Parkinson's Disease

Dawson et al. (2010) described a number of essential features of PD an animal model of the disease should recapitulate. Firstly, there should be an age-dependent, progressive degeneration of DAn of the SNpc, accompanied by motor dysfunction resembling the PD tetrad that is responsive to DA replacement therapy. As well, LBs which are positive for α-synuclein should be observed. Finally, neurodegeneration elsewhere in the brain should be less severe to that seen in the DAn in the midbrain. Current animal models of PD can be broadly divided into two categories: neurotoxic and genetic models, with each recapitulating some, but not all, of these features.

1.4.1 Toxin induced models

Traditionally, rodent models of PD have relied on the rapid chemical ablation of the DA nigrostriatal pathway, resulting in severe striatal DA depletion that mirrors an advanced stage of the disease (Jenner, 2008). Such approaches have the advantage of not having to rely on the ageing process in order to observe cell death in the DA system and therefore allows for the rapid study of the consequences and mechanisms of DA dysfunction. Neurotoxic models have primarily relied on the use of one of four chemical toxins; 6-Hydroxydopamine (6-OHDA), 1-methyl-4-phenyl-1,2,3,6-tetrahydropyridine (MPTP), paraquat and rotenone (Figure 1.8).

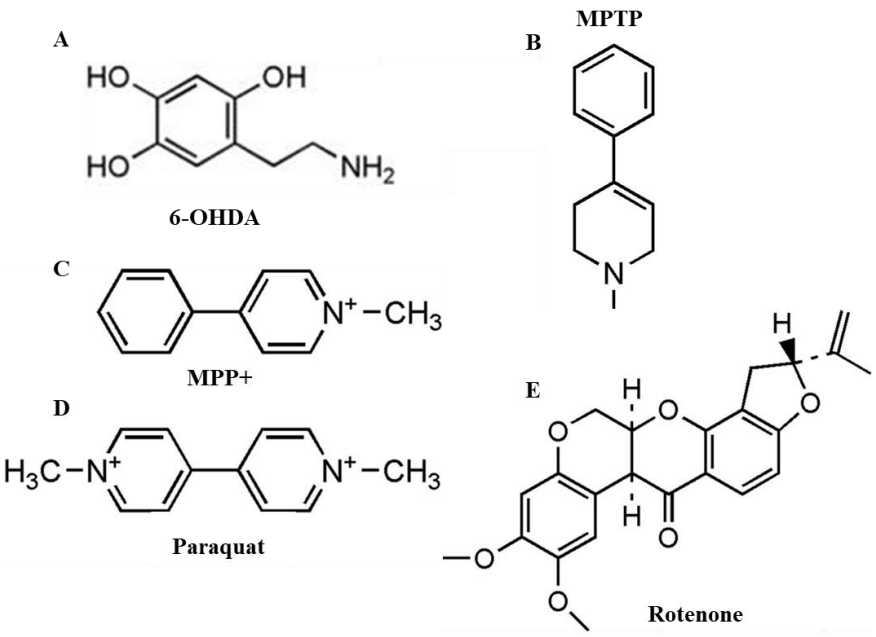


Figure 1.8 Chemical structure of neurotoxins used in animal models of Parkinson's disease*. (**A**) 6-OHDA, (**B**) MPTP, (**C**) the MPTP metabolite MPP+, (**D**) Paraquat, (**E**) Rotenone*

(i) 6-Hydroxydopamine

6-OHDA is a hydroxylated analogue of DA, and was first identified almost 60 years ago (Senoh & Witkop, 1959). In the brain, 6-OHDA is capable of inducing degeneration of both DA and noradrenergic neurons as DA and noradrenergic transporters have high affinity for 6-OHDA (Luthman et al., 1989). Once taken up into neurons, 6-OHDA accumulates in the cytosol where it is oxidized, generating ROS and promoting cell death. In order to target specific neurons and by-pass the BBB, 6-OHDA is typically injected stereotactically in to the brain region of interest. When injected into the nigra, degeneration of DAn takes place within 12 hours preceding the loss of striatal terminal 2-3 days later (Jeon et al., 1995). However, when delivered into the striatum, 6-OHDA induces slow, progressive, and partial damage to the nigrostriatal structure in a retrograde fashion over a 3 week period (Przedborski et al., 1995). This

latter route is advantageous as not only is this progressive lesion more relevant to PD, but it has also been shown to produce non-motor symptoms of PD such as cognitive and psychiatric dysfunction (Branchi et al., 2008). Typically, unilateral injection into one hemisphere is performed allowing for an internal control in the unlesioned hemisphere. Unilateral 6-OHDA treatment leads to rotational behaviour in the animal following the administration of DA receptor agonists, L-DOPA or DA releasing compounds such as amphetamine (Bové & Perier, 2011). Although the unilateral 6-OHDA rat model has been used to assess the neuroprotection of cell transplantation (Bjorklund et al., 2002), it lacks the progressive, age dependent effects of PD. This model also fails to take into account pathological processes elsewhere in the brain and may reinforce the perception of PD being a disease of the DA system alone. Furthermore, LBs are not present in this model (Tieu, 2011).

(ii) 1-methyl-4-phenyl-1,2,3,6-tetrahydropyridine (MPTP)

In 1977, a previously healthy 23-year-old man was presented to the National Institute of Mental Health for evaluation of persistent parkinsonian syndrome. An enquiry from the National Insititue of Health revealed that the patient had been self-administering a mixture of MPPP and its elimination product MPTP (Davis et al., 1979). Then, in the 1980s, a number of intravenous drug users in California were admitted to hospital showing severe symptoms similar to PD. Further investigations revealed that these patients had self-administered a synthetic meperidine, a narcotic analgesic, contaminated with MPTP (Langston et al., 1983). Humans who have received MPTP demonstrate a loss of nigrostriatal structures and are L-DOPA responsive, suggesting

a similar underlying neuropathological and biochemical feature to PD (Langston et al., 1999).

MPTP is lipophilic and therefore can cross the BBB. MPTP is metabolized to its toxic metabolite, 1-methyl-4-phenylpyridinium (MPP^+) by MAO-B in astrocytes. MPP^+ is released from nigral and striatal astrocytes into the extracellular space via the organic cation transporter 3 (Rappold & Tieu, 2010) where it is taken up by the DA transporter (DAT) and induces toxicity in DAn by inhibition complex I of the mitochondrial electron transport chain and increasing ROS production (Nicklas et al., 1985).

MPTP is typically used in primates and mice but not rats due to drug resistance from high levels of MAO in the rat BBB. This converts MPTP to MPP^+ which is not lipophilic and therefore cannot permeate the brain (Riachi et al., 1988). MPTP-treated mice and primates develop motor dysfunctions as well as intraneuronal inclusions reminiscent of LBs (Fornai et al., 2005). Such abnormal phenotypes in mice are reversible by L-DOPA, confirming a connection between these symptoms and damage in the nigrostriatal system (Rozas et al., 1998). With the caveat of its acute toxic property seen with other neurotoxic PD models, MPTP is firmly established and will continue to play a role as an *in vivo* model in PD research. As well, the observation that MPTP could induce so many of the features of PD led to the environmental hypothesis of PD and the idea that PD could have environmental as well as genetic causes.

(iii) Paraquat

A large number of studies have shown exposure to the herbicide, paraquat, is a risk factor for PD (Tanner, 2010). The toxic metabolite of MPTP, MPP^+ has a strikingly similar chemical structure to the herbicide paraquat (differing only by one methyl group; see figure 1.5) However, unlike MPP^+, paraquat is able to cross the BBB. Interestingly, the amount of paraquat that is able to accumulate in the brain is age dependent, with the highest levels detected in 2 week old or 12+ month old rats (Corasanti et al., 1991). It is known that the BBB is most permeable in young and old animals, suggesting this age-dependent effect is due to this BBB permeability. Once inside mitochondria, paraquat does not act as a complex I inhibitor (Richardson et al., 2005) although it is presumed that this is the site where it is reduced to form superoxide (Cocheme & Murphy, 2008). Whilst paraquat causes oxidative stress, it has been shown that recruitment of microglia is required for the degeneration of DAn, suggesting an inflammatory response to be crucial in the degenerative process (Bové & Perier, 2011). When injected into mice, paraquat was reported to induce motor deficits and loss of nigral DAn in a dose and age dependent manner (McCormack et al., 2002; Thiruchelvam et al., 2003). However, the effect of paraquat on the nigrostriatal system is not consistently observed (Thiruchelvam et al., 2000; Cicchetti et al., 2005). Paraquat however has been observed to increase α-synuclein aggregates reminiscent of LBs (Fernagut et al., 2007; Mak et al., 2010). Yet, paraquat does not have an effect on striatal DA levels (McCormacke et al., 2002) so its use in assessing neuroprotective therapies and modelling PD may be limited.

(iv) Rotenone

Rotenone is a pesticide that is highly lipophilic and can therefore readily permeate the BBB and induces toxicity via its inhibition on complex I (Tieu, 2011). When infused continuously into rats via osmotic pump subcutaneously, rotenone produces selective nigrostriatal neurodegeneration and α-synuclein-positive inclusions (Betarbet et al., 2000). Although the rotenone model reinforces the theory that environmental agents may play a role in the pathogenesis of sporadic PD, the model has not been widely adopted due to high levels of variability in animal sensitivity and inability of other reports to reproduce neuropathology and phenotype (Hoglinger et al., 2003; Fleming et al., 2004; Lapointe et al., 2004; Zhu et al., 2004). Daily intraperitoneal injection of rotenone using medium chain fatty acid as a specialised vesicle, however, produces more consistent nigrostriatal pathology (Cannon et al., 2009) which is reproducible (Drolet et al., 2009).

Toxin induced models of PD lead to severe striatal DA depletion that mirrors an advanced stage of the disease. These models have allowed for the study of the consequences and mechanisms of DA dysfunction and have been invaluable in assessing the neuroprotection of new pharmacological therapies. However, these models fail to recapitulate the progressive, age dependent effects of PD. Furthermore, they fail to take into account pathological processes elsewhere in the brain, LBs are not commonly observed and results have been shown to be inconsistent.

1.4.2 Genetic rodent models of Parkinson's disease

Transgenic (TG) rodent models have been created which overexpress, modify or suppress PD-associated genes in an attempt to recapitulate PD pathology and motor deficits. The expression of foreign genes in animals can be achieved via a number of methods, all of which possess certain advantages and disadvantages.

(i) Viral models

Viruses are efficient vehicles to infect cells to introduce genetic material and force the cell to replicate the viral genome in order to produce new virus particles. Viruses can be engineered to non-replicating viral vectors that retain their ability of entering cells and introducing genes. By deleting parts of the viral genome and replacing them by the genes of interest, application of the vector will result in a single-round infection without replication in the host cell. The choice of vector system depends on the size of the gene of interest, the required duration of gene expression and the target cells. For stable gene transfer in the brain lentiviral vectors and adeno-association viral vectors are the vector systems of choice since they lead to efficient and long-term gene expression in the rodent brain. In the case of PD models, this administration tends to be delivered to either the striatum or the SNpc via stereotaxic injection (Lee et al., 2010; Dusonchet et al., 2011; Daher et al., 2014). Viral models have been successfully applied to the expression of human WT or mutant α-synuclein. Such injections cause rapidly progressive neurodegeneration phenotype, (Klein et al., 2002; Yamada et al., 2004; Oliveras-Salvá et al., 2013) and reductions in motor function (Kirik et al., 2002). However, the rapid progression in viral models makes the causal progression of pathology difficult to determine. And the injection site has the effect of biasing the

investigation towards pre-defined brain regions. Pathology is also seen in other areas of the brain and therefore it is important to keep this selectivity in mind.

Recently, a unique model has arisen to study the role of α-synuclein in the pathogenesis of PD. This model involved the conversion of recombinant monomeric α-synuclein protein to a fibrillar form (known as pre-formed fibrils [PFF]) which is then injected into the brain of animals to model disease. Intracerebral injection of α-synuclein PFFs into the dorsal striatum results in the dysregulation of striatal DA release, neurodegeneration in the SNpc, and behavioural deficits in rodents overexpressing disease-related proteins or non-transgenic rodents (Luk et al., 2012; Volpicelli-Daley et al., 2014; Abdelmotilib et al., 2017). Similar to toxin- and viral vector based models of PD, the α-synuclein PFF model of PD is an inducible model that allows for spatiotemporal control of the α-synuclein PFF introduction. This enables baseline measurements of behaviour prior to induction of PD symptoms. Although the introduction of α-synuclein PFF induces a model using supra-physiological levels of α-synuclein, the levels are much closer to that of the human condition as compared to viral vector-based (Pollinski et al., 2018). However, it still remains unclear if the recombinant α-synuclein PFFs are identical to the species of α-synuclein present in the pathology of the human condition (Pollinksi et al., 2018).

(ii) Use of genetic constructs

An alternative approach to transgene expression is the expression of genetic constructs integrated permanently into the genome of the model animal. This can be achieved via pronuclear injection of the desired genetic material into fertilised cells at an early stage

of embryonic development and the subsequent introduction of the developing embryo into a recipient female. Largely because of vector capacity restrictions, generated models have utilised cDNA driven by foreign promoters (Ramonet et al., 2011; Chen et al., 2012; Tsika et al., 2014). The development of tools such as yeast-, bacterial P1- and bacterial-artificial chromosome technology (YACs, PACs and BACs) which possess a high cloning capacity, have allowed for the introduction of entire genes with endogenous regulatory sequences, including promoters (Cannon et al., 2013; Janezic et al., 2013; Sloan et al., 2016). This approach allows for the expression of a transgene in the cell types and at the stage of development in which they would typically be expressed, causing a more unbiased, physiologically relevant spatial and temporal expression pattern and proper gene splicing. However, such technologies are not without their drawbacks such as the fact that the random integration method is employed and there is no control over copy number. Gene targeting strategies overcome these by using genomic DNA to construct targeting vectors to alter endogenous genes by either rendering genes non-functional by deleting essential sequences (KO), having sequences replaced or added (KI) or made into a conditional mutants (e.g. floxed allele).

1.4.3 Rodent models of LRRK2

Many transgene and gene targeting strategies have been utilised to model LRRK2-associated PD (Table. 1.3). These models vary widely with regards to the species and strain of the animal used, the promoters used for transgene expression, the choice of *LRRK2* mutations, the use of human or endogenous genes, use of cDNA or complete human genetic sequence and the specifics of their characterisation of the models. Unsurprisingly, therefore, the reported phenotypes from these models vary greatly.

Table 1.3 An overview of previously generated LRRK2 transgenic rodent models. *↑ = increased, ↓ = decreased. For the purposes of clarity, double-transgenics (LRRK2 and α-synuclein) and kinase dead-mutants have been excluded from this table. Abbreviations: RC, R1441C; GS, G2019S; end., endogenous; PI, perinuclear injection; pTau, phosphorylated tau; m, months; w, weeks; OFE, open field experiment; RR, rota rod; AV, anterograde adenovirus.*

Author /year	Species	Gene	Promotor	Max. age	LRRK2 expression	Genetic Design	Pathology	DA alterations	Behaviour
Tong et al, 2009	Mouse	Whole mLrrk2 (RC)	mLrrk2	22 m	RC (1 x end. LRRK2)	KI	No changes	Impaired D2 receptor function (RC)	No changes
Li et al, 2009	Mouse	Whole hLRRK2 (RG or WT)	hLRRK2	10 m	R1441G, WT (5-10 x end. LRRK2)	BAC	No SNpc neurodegeneration, no α-synuclein pathology, pTau pathology (R1441G)	R1441G ↓ striatal DA release	↓ rearing and immobility at 12 m (RC)
Andres-Mateos et al., 2009	Mouse	Lrrk2 KO	-	22 m	-	KO	-	No changes	↑ grooming, viability 7-10% of KO animals
Gillardon et al., 2009	Mouse	Lrrk2 KO	-	10 w	-	KO	pTau declined (KO)	-	-
Li et al.,2010	Mouse	Whole mLrrk2 (GS or WT)	mLrrk2	18 m	GS, WT (6 x end. LRRK2)	BAC	No changes	↓ striatal DA release and reuptake (GS). ↑ striatal DA release (WT)	↑ rearing, motor activity, longer strides and ↑ balance beam activity (WT)
Winner., 2010	Mouse	Whole hLRRK2 (GS) (same as Melrose et al, 2010)	hLRRK2	4 m	G20192 (2.5 x end. LRRK2), WT (3.5 end. LRRK2)	BAC	-	-	-
Melrose et al.,2010	Mouse	Whole hLRRK2 (GS or WT)	hLRRK2	24 m	G20192 (2.5 x end. LRRK2), WT (3.5 end. LRRK2)	BAC	-	↓ striatal DA release (GS, WT). ↑ D1 receptor levels (WT)	↑ exploration and wall hugging in OFE (GS)

Author/ year	Species	Gene	Promotor	Max. age	LRRK2 expression	Genetic Design	Pathology	DA alterations	Behaviour
Tonget al., 2010	Mouse	Lrrk2 KO	-	24 m	-	KO	Age-dependent reduction in kidney size and weight (KO). No changes in brain	No changes	-
Lee et al, 2010	Mouse	hLRRK2 cDNA (WT, GS)	CMV	3 m	Similar for all genotypes	Striatal injection of HSV	SNpc neurodegeneration following transduction (GS)	-	-
Herzig et al, 2011	Mouse	Lrrk2 KO + Whole mLrrk2 (GS)	mLrrk2	26 m	GS (1 x end. LRRK2)	KO or KI	No changes in brain (GS, D1994S). ↑ kidney weight and lipofuscin-like substance (KO)	No changes	No changes
Ramonet et al, 2011	Mouse	hLRRK2 cDNA (GS, RC, WT)	CMV-ePDGFβ	24 m	GS, RC, WT (3-5x end. LRRK2)	PI of cDNA	SNpc neurodegeneration at 21 m (GS), no pTau/ αsynuclein pathology	↓ DOPAC and HVA in OB (GS), ↓ DA in CTX (RC)	↓ locomotor activity at 15 m (RC)
Zhou et al, 2011	Rat	hLRRK2 cDNA (GS)	Tre promoter	18 m	Similar expression between genotypes	Conditional Tre-tTa expression	No changes	↑ striatal DA release (GS temporal)	↑ locomotor activity (GS temporal)
Dusonchet et al., 2011	Rat	hLRRK2 cDNA (GS, WT)	Synapsin-1 Promoter	42 days	GS, WT (2 x end. LRRK2)	Striatal injection of AV	SNpc neurodegeneration following transduction, pTau pathology (GS, WT), no α-synuclein pathology	-	-
Hinkle et al., 2012	Mouse	Lrrk2 KO	-	20 m	-	KO	No changes in pTau or α-synuclein. ↑ size and inflammation in kidneys (KO)	No changes	↑ wall hugging in OFE, ↑ latency to fall in RR (KO)
Tong et al., 2012	Mouse	Lrrk2 KO	-	20 m	-	KO	↑ lipofuscin granules in kidney (KO)	-	-
Maekawa et al., 2012	Mouse	hLRRK2 cDNA (I2020T)	CMV	18 m	I2020T (1.5 x end. LRRK2)	PI of cDNA	No changes (SNpc neuronal morphology changes) (I2020T)	↓ striatal DA (I2020T)	↑ slipping in BB, ↑ latency to fall in RR and ↑ rearing (I2020T)

Author/ year	Species	Gene	Promotor	Max. age	LRRK2 expression	Genetic Design	Pathology	DA alterations	Behaviour
Daher et al., 2012	Mouse	Lrrk2 KO, Whole hLRRK2 (GS)	CMV-ePDGFβ	14 m	GS (2-4 x end. LRRK2)	KO or PI of cDNA	No changes	-	No changes
Herzig et al., 2012	Mouse	hLRRK2 cDNA (GS, WT)	Mouse Thy1	28 m	GS, WT (3-5 x end. LRRK2)	PI of cDNA	No changes	-	↑ latency to fall on RR and ↑ locomotion (young GS)
Chen et al., 2012	Mouse	hLRRK2 cDNA (GS, WT)	CMV-ePDGFβ	16 m	GS, WT (10 x end. LRRK2)	PI of cDNA	No SNpc neurodegeneration at 12 and 16 m, pTau pathology (GS), no α-synuclein pathology	↓ striatal DA reuptake (GS)	↓ locomotion and impaired pole test (GS)
Gillardon et al., 2012	Mouse	Whole hLRRK2 (RG) (same as Li et al, 2009)	hLRRK2	8 m	GS (3 x end. LRRK2)	BAC	-	-	-
Bichler et al., 2013	Mouse	Whole hLRRK2 (RG) (same as Li et al, 2009)	hLRRK2	21 m	R1441G (5-10 x end. LRRK2)	BAC	-	-	↓ rearing (RC)
Dranka et al., 2013	Mouse	Whole hLRRK2 (RG) (same as Li et al, 2009)	hLRRK2	16 m	R1441G (5-10 x end. LRRK2)	BAC	No changes	-	↓ latency to fall on RR and impaired pole test (RC)
Baptista et al., 2013	Rat	Lrrk2 KO	-	12m	-	KO	↑ lipofuscin granules in kidney (KO)	-	-
Ness et al., 2013	Rat	Lrrk2 KO	-	4 m	-	KO	↑ kidney size and immune markers (KO)	-	No behaviour changes. ↓ GI tract and kideny weight (KO)
Longo et al., 2014	Mouse	Whole mLrrk2 (GS) (same as Herzig et al., 2011)	mLrrk2	19 m	GS (1 x end. LRRK2)	KI	-	-	↑ activity in OFE (GS), ↑ stepping activity in drag test (GS), ↑ latency to fall in RR (WT)

Author/ year	Species	Gene	Promotor	Max. age	LRRK2 expression	Genetic Design	Pathology	DA alterations	Behaviour
Sancheze t al., 2014	Mouse	Whole hLRRK2 (RG) (same as Li et al, 2009)	hLRRK2	6-8 w	R1441G, WT (5-10 x end. LRRK2)	BAC	-	No changes	-
Chou et al., 2014	Mouse	hLRRK2 cDNA (GS, WT) (Same as Chen et al., 2012)	CMV-ePDGFβ	9 m	GS, WT (10 x end. LRRK2)	PI of cDNA	No changes	↓ neuronal firing rate and striatal DA release (GS)	Hypokinesia (GS
Walker et al., 2014	Rat	Whole hLRRK2 (GS) (same as Melrose et al., 2011)	hLRRK2	12 m	GS (2 x end. LRRK2)	BAC	No changes	No changes	L-Dopa resistant ↓ in latency to fall in RR (GS)
Lee et al., 2014	Rat	Whole hLRRK2 (GS)	hLRRK2	12 m	GS (5-8 x end. LRRK2)	BAC	No changes (SNpc neuronal morphology changes) (GS)	No changes	↑ rearing and postural instability (GS)
Tsika et al., 2014	Mouse	Human cDNA (RC)	PDGFβ	22 m	RC (1-2 x end. LRRK2)	Conditional DAT-Cre expression	No changes (SNpc neuronal morphology changes) (RC)	No changes	No changes
Dranka et al., 2014	Mouse	Whole hLRRK2 (RG or WT) (Same as Li et al, 2009)	hLRRK2	15 m	R1441G, WT (5-10 x end. LRRK2)	BAC	No changes	-	↑ latency to fall in RR and reduced olfaction (RC)
Tsika et al., 2015	Rat	Human cDNA (WT, GS)	Syn-1 Promoter	42 days post injection	WT (4 x), GS (3-4 x) compared to uninjected hemi.	Striatal injection of AV	SNpc neurodegeneration in all genotypes	-	No changes
Liu et al., 2015	Mouse	Human cDNA (WT or GS)	Pitx3	18 m	GS, WT (3-6 x end. LRRK2)	KI	Age-dependent loss of TH+ axon terminals in striatum	↓ DA release and ↓ DA protein and gene expression (GS)	No changes

Author/ year	Species	Gene	Promotor	Max. age	LRRK2 expression	Genetic Design	Pathology	DA alterations	Behaviour
Beccano-Kelly et al., 2015	Mouse	Lrrk2 KO and whole hLRRK2 (WT)	hLRRK2	3-6 m	WT (2-4 x end. LRRK2)	KO or BAC	-	Altered DA dependent short term plasticity (WT)	↓ rearing and impaired LTM (WT)
Garcia-Miralles et al., 2015	Mouse	Human cDNA (GS and WT)	Thy1.2	12-13 m	GS, WT (2 x end. LRRK2)	KI	-	-	
Yue et al., 2015	Mouse	Whole mLrrk2 (GS)	mLrrk2	12 m	GS (1 x end. LRRK2)	Site directed mutagenesis	-	↓ in total striatal DA, HVA and DOPAC and impaired DA release at 12 m (GS)	Hyperactivty (young GS) and olfactory changes (GS)
Sloan et al., 2016	Rat	Whole hLRRK2 (GS, RC, WT)	hLRRK2	18-21 m	GS (5-6 end. LRRK2), WT, RC (2-3 end. LRRK2)	BAC	No changes	↓ striatal DA release (GS, RC > WT)	L-Dopa responsive ↓ latency to fall (GS, RC)
Xiong et al., 2017	Mouse	Human cDNA (GS)	hLRRK2	22 m	GS (10-15 x end. LRRK2)	Tet. Induced	-	-	Impaired pole test (GS), ↓ OFE activity with amphetamine (GS)
Giesert et al., 2017	Mouse	Whole hLRRK2 (RC)	hLRRK2	28 month	RC (1 x end. LRRK2)	BAC	No changes	-	Impaired pole test, cat walk and olfaction (RC)
Tozzi et al., 2018	Mouse	Whole mLrrk2 (GS)	mLrrk2	6 m	GS (1 x end. LRRK2)	KI	-	-	
Xiong et al., 2018	Mouse	Human cDNA (GS)	TH	20 m	GS (3-5 x end. LRRK2)	Tet. induced	No SNpc neurodegeneration, ↑ astrogliosis in striatum and VMB (GS)	↓ striatal DA, DOPAC and HVA (GS)	L-Dopa responsive ↓ activity in OFE with AMPH, imapired pole test (GS)

In most of the *LRRK2* mutant models, no overt neurodegeneration within the SNpc has been identified in R1441C/G (Li et al., 2009; Lin et al., 2009; Tong et al., 2009; Dranka et al., 2013; Tsika et al., 2014; Sloan et al., 2016; Giesert et al., 2017), G2019S (Li et al., 2010;, Chou et al., 2014; Walker et al., 2014; Tsika et al., 2015; Garcia-Miralles et al., 2015; Yue et al., 2015; Sloan et al., 2016; Xiong et al., 2017) or I2020T (Maekawa et al., 2012) mutations, despite the ageing of models as much as 24 months. Changes in SNpc tyrosine hydroxylase positive (TH^+) neuronal morphology have been observed (Li et al., 2009; Lee et al., 2014). As well, loss of neuronal nuclei positive ($NeuN^+$) nuclei in the striatum has been observed with the expression of the G2019S mutations (Tsika et al., 2015). Furthermore, the expression of the G2019S mutation has been associated with an age dependent loss in axonal terminal density in the striatum (Liu et al., 2015). Collectively, this indicates that some of these models may be reflecting the initial phases of a neurodegenerative phenotype. Some models have reported some degree of DA neuronal loss with the expression of mutant LRRK2 (Lee et al., 2010; Ramonet et al., 2011; Dusonchet et al., 2011; Chen et al., 2012). However, such reports have utilised either heterologous promoters or utilised viral transductions, and may be a consequence of high levels of expression. Indeed, models that have used a knock-in methodology for mutant Lrrk2 expression, and retain endogenous levels of the transgene, show subtle or no phenotype (Tong et al., 2009; Li et al., 2009; Longo et al., 2014; Tsika et al., 2014; Giesert et al., 2017). A recent publication observed a significant increase in neuronal loss in the SNpc of a TH-driven, tetracycline-inducible model expressing human LRRK2-G2019S from 15 months onwards (Xiong et al., 2018). However, the same research group also observed no changes in a tetracycline-inducible LRRK2-G2019S model when the endogenous human LRRK2 promoter was

used (Xiong et al., 2017) highlighting the significance of endogenous vs. foreign promoters.

Despite a typical lack of neurodegeneration observed in LRRK2 rodent models of PD, which is indeed true of many genetic animal models of PD not just LRRK2, many of the TG models report dysfunction in DA homeostasis, as well as neuronal firing. Reduced striatal DA release have been reported in mutant LRRK2 models (Li et al., 2009; Li et al., 2010; Chou et al., 2014; Yue et al., 2015; Liu et al., 2015; Sloan et al., 2016) as well as reuptake (Zhou et al., 2011; Chen et al., 2012), with no changes seen with the overexpression of WT-LRRK2 (Beccano-Kelly et al., 2015). Although altered DA release and reuptake has been observed in rats expressing human WT LRRK2 (Sloan et al., 2016). Typically, these changes are observed in the absence of any gross changes in total striatal DA and its metabolites or proteins involved in its recycling (Tong et al., 2009; Li et al., 2010; Ramonet et al., 2011; Zhou et al., 2011; Chou et al., 2014) although some reports observe changes in total DA as well as decreases in DOPAC and HVA expression (Liu et al., 2015; Yue et al., 2015; Xiong et al., 2018). *Ex vivo* changes to SNpc neuronal firing in mutant LRRK2 tissue slices have also been observed. Patch clamp recordings have shown decreased firing rates in the SNpc neurons of 8-month old LRRK2-G2019S animals (Chou et al., 2014). As well, the expression of human LRRK2-R1441C decreases bursts and induces regular firing patterns in neurons in the SNpc (Sloan et al., 2016). Interestingly, the overexpression of human WT-LRRK2 has been observed to alter DA short term plasticity (Beccano-Kelly et al., 2015). Such changes have been attributed to alterations in impairments in D1 and D2 receptor functions (Tong et al., 2009). In support of this, changes in striatal D1 and D2 receptor densities and function in both WT and mutant LRRK2 have been

observed (Tong et al., 2009; Melrose et al., 2010; Chou et al., 2014; Beccano-Kelly et al., 2015).

Like the lack of neurodegeneration of LRRK2 TG animals, α-synuclein pathology is frequently absent from the brains of mutant animals (Tong et al., 2009; Li et al., 2010; Melrose et al., 2010; Herzig et al., 2011; Zhou et al., 2011; Dusonchet et al., 2011; Ramonet et al., 2011; Maekawa et al., 2012; Chen et al., 2012) however a non-significant increase in monomeric α-synuclein has been reported in the striatum of anterograde adenoviral (AV) injected LRRK2-G2019S expressing animals (Tsika et al., 2015). Recently, one study has been able to recapitulate α-synuclein pathology in the striatum and ventral midbrain (Xiong et al., 2018) and olfactory bulb, cortex and hippocampus (Xiong et al., 2017) of tetracycline-inducible G2019S expressing animals, with increased high molecular weight species and phosphorylated forms of α-synuclein observed. Double TG animals have been developed, which overexpress A53T mutant α-synuclein and co-express mutant LRRK2 or Lrrk2$^{-/-}$ (Lin et al., 2009; Daher et al., 2012; Herzig et al., 2012) in an attempt to examine the effects of their co-expression on pathology. It has been reported that mutant LRRK2 increased striatal pathology and this is ameliorated by the KO of endogenous Lrrk2 (Lin et al., 2009; Daher et al., 2012), however this is not always replicated (Herzig et al., 2012), most likely due to differences in transgene expression and promoters used in these studies.

Tests of motor-coordination have indicated subtle or no impairments in mutant animals (Tong et al., 2009; Lin et al., 2009; Li et al., 2010; Herzig et al., 2011; Herzig et al., 2012; Dranka et al., 2013; Walker et al., 2014; Tsika et al., 2014; Tsika et al., 2015;

Liu et al., 2015), although others have reported significant impairments in motor coordination (Li et al., 2009; Ramonet et al., 2011; Zhou et al., 2011; Chen et al., 2012; Bichler et al., 2013; Longo et al., 2014; Chou et al., 2014; Lee et al., 2014; Dranka et al., 2014; Sloan et al., 2016; Xiong et al., 2017; Giesert et al., 2017). It seems that alterations in locomotor activity is paralleled by changes in DA homeostasis (Li et al., 2009; Li et al., 2010; Chou et al., 2014; Yue et al., 2015; Sloan et al., 2016; Xiong et al., 2017). The role of DA in these motor changes is further supported by the L-DOPA responsiveness of some of these models (Chen et al., 2012; Li et al., 2009; Sloan et al., 2016; Xiong et al., 2017). Similarly, non-motor functions such as changes in cognition, anxiety or sensory deficits have not been observed (Tong et al., 2009; Maekawa et al., 2012; Herzig et al., 2012) however on report did observe changes in olfaction in the tetracycline inducible G2019S model (Xiong et al., 2018). One other study also reported alterations in gastrointestinal function in R1441C expressing animals (Bichler et al., 2013).

Lrrk2 KO rodent brains have not been reported to display signs of neurodegeneration of alterations in DA homeostasis (Andres-Mateos et al., 2009; Lin et al., 2009; Tong et al., 2010; Daher et al., 2014) and behavioural changes are also not observed. However, Lrrk2 KO animals have been reported to show dramatic α-synuclein pathology in the kidneys, as well as biphasic, age-dependent changes in autophagy proteins (Tong et al., 2010). It has however been demonstrated that the inactivation of Lrrk2 and its functional homolog Lrrk1 results in earlier mortality and age-dependent, selective neurodegeneration of DAn in the SNpc in mice (Giaime et al., 2017), highlighting the essential role of Lrrk in the survival of DAn.

1.5 Aims of this thesis

The overall aim of this thesis is to investigate the pathological mechanisms associated with LRRK2 in the autophagy pathway using primary cortical cultures from a human *LRRK2* (h*LRRK2*)-BAC TG rat model of PD which has previously been characterised with regards to pathology and behaviour previously in Sloan et al. (2016). The presence of pathogenic mutations in this animal model leads to age-dependent impairments in DA dorsal striatal release and reuptake and motor deficits. Further characterisation *in vitro* of the *LRRK2*-BAC TG rat model will elucidate the molecular mechanisms underlying the pathogenic effect of *LRRK2* mutations. This will be detailed in 3 chapters:

- Establishment of primary cortical neuronal and astrocytic cultures from P1 pups harbouring human *LRRK2*-BAC TG rats and their nTG littermate controls (Chapter 3)
- Characterising the autophagy pathway in nTG, LRRK-hWT, LRRK2-R1441C and LRRK2-G2019S cortical cultures (Chapter 3)
- Identifying molecular mechanisms associated with lysosomal deficits in mutant LRRK2 cortical cultures (Chapter 4)
- The use of probe-molecules and their derivatives known to target the lysosome to ameliorate lysosome deficits in mutant LRRK2 cortical cultures (Chapter 5)

Chapter 2: Methods and Materials

2.1 Animal husbandry

Sprague Dawley (SD) rats were maintained in accordance with UK Home Office regulations, under the Animals (scientific Procedures) Act of 1986. Animals were grouped in (55 x 40 cm) cages with bedding and had constant access to food and water. Animals were fed RM1 diet (special Diets Services). Room atmosphere was maintained at 22°C at 60-70% humidity and animals were kept in a 12 hour light/dark cycle. Schedule 1 killing was performed via rising concentrations of CO2 and confirmed via cervical dislocation. Experimental animals were matched for age and all experiments were conducted in the light cycle.

2.2 Genotyping

2.2.1 DNA extraction from tissue clip

Ear or tail clips were incubated in 450 µl lysis buffer (50 mM KCl, 1.5 mM MgCl2, 10 mM Tris, 0.45% NP40, 0.45% Tween-20 and 0.5 mg/ml proteinase K, pH 8.5) for 2 hours at 55°C and at 95°C for 20 minutes to inactivate proteinase K.

2.2.2 Polymerase chain reaction for genotyping

Polymerase chain reaction (PCR) was performed for the purposes of genotyping (see Table. 2.1 and Fig. 2.1 for genotyping PCR components and programme). Human specific primers were designed for exons 8, 20 and 38 of the LRRK2 transgene. PCR

products were separated using an agarose gel (1% agarose, 0.005% ethidium bromide in Tris/Borate/ethylenediaminetetraacetic acid (EDTA) (TBE) buffer) at 150 V. Gels were imaged using the Chemidoc™Touch Imaging System (BioRad).

Table. 2.1. *Genotyping PCR components*

Reaction components	Volume (µl)
Genomic DNA	1
10x PCR Buffer	1.5
$MgCl_2$	0.9
dNTP 10 mM stock	0.75
Primer pair (10 mM forward and reverse)	1.5
Q-solution	3
Ampli Taq-Gold DNA-polymerase	0.2
MilliQ H_2O	6.15

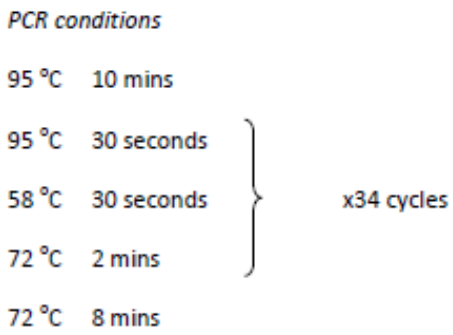


Figure. 2.1. *Genotyping PCR conditions*

Table. 2.2. *Genotyping PCR primers*

Target	Sense Oligo Sequence (5' to 3')	Anti-Sense Oligo Sequence (5' to 3')
Rat Prolactin	GCTTCTGAGCAATGACACCA	ATTCCAGGAGTGCACCAAAC
LRRK2 Exon 08	AAAGCTGTGCAGCAGTACCC	CACAGGACAGAAAAGGCATTG
LRRK2 Exon 20	GCTGTGGAAGAAGGAACAGC	CAGATGATTTAGGTCAGGTTTTTG
LRRK2 Exon 38	CTCAGATTGCCCCTGACTTG	GGCTGCTTCACTTAACTCACC

2.3 Generation of primary cortical cultures

TG male rats were bred with a pair of SD females to produce transgenic and non-transgenic littermates in the same litters. P1 rats were tail clipped and marked for genotyping. A minimum of 3 animals per genotype were pooled for each experiment. Tail clips were processed and genotyped as described with the standard genotyping protocol. Genotyped P1 pups were culled in accordance with UK Home Office regulations, under the Animals (scientific Procedures) Act of 1986. Brains were extracted and placed in fresh, ice cold Neurobasal(A) media for transportation. Meninges were removed and cortical areas were dissected and shredded into ~0.5 mm pieces in a sterile petri dish with sterile scalpels and collected in ice cold, fresh Neurobasal(A) media. Tissue was incubated at 37°C in Neurobasal(A) medium (Life Technologies) plus 0.1% trypsin and 0.5 μg/ml DNase for 20 minutes. Trypsin was inactivated with 20% foetal bovine serum (FBS) containing Neurobasal(A) and samples centrifuged at 200 x *g* at 37°C for 5 minutes. FBS containing media was then replaced with wash media and centrifuged at 200 x *g* at 37°C for 3 minutes (x 2). Wash media was removed and replaced with growth media (Neurobasal(A) media, 1 x Anti-Anti, 2 mM L-glutamine, 1x Anti-Anti, 1.75 μg Fungizone, 1X B27). Tissue was triturated using a P1000 pipette (10x) and then with a P200 pipette (~30x). Cells were

counted using trypan blue and diluted for plating (see Table. 2.3 for cell densities). Cells were kept at 37°C, 5% CO2, 95% relative humidity and 50% of medium was replaced every 2 days. All assays were completed at 14 DIV.

Table. 2.3. *Cell densities*

Plate type	Cell density	Volume
24-well	8 x 10^5 / ml	500 µl
24-well ; coverslip	1.875 x 10^6 / ml	80 µl
96-well	7.5 x 10^5 / ml	100 µl
T75	1 x 10^6 / ml	15 ml

2.4 Generation of primary astrocytic cultures

Astrocytic cultures were generated via the same method as cortical cultures described, with the exception of media composition and plating; cells were diluted in astrocytic media containing DMEM (Life Technologies), 5.5 mM glucose (Sigma), 20% FBS, 1x Anti-Anti and 1.75 µg Fungizone in T75 flasks (Corning). Once astrocytes reached confluency at 7 DIV, T75s were shaken at 200 rpm at 37°C for 3 hours followed by 150 rpm at 37°C overnight in order to remove non-astrocytic cells. Remaining cells were then trypsinised and sub-cultured in 24-well plates as before and 50% of the medium was replaced every 3 days up to 14 DIV.

2.5 Generation of primary neuronal cultures

Neuronal cultures were generated via the same method as cortical cultures as described, with the exception of AraC (Cytosine-1-β-D-arabinofuranoside (Sigma)) treatment; cells were treated with 1 µM AraC in normal growth media at 1 DIV for 24/48 hours. AraC media was replaced with fresh neuronal growth media and maintained as previously described.

Table. 2.4. *Compound treatment concentrations and times*

Compound	Supplier	Catalogue #	Working concentration	Time
Chloroquine	Sigma	C6628	20 µM	8h
Rapamycin	Tocris	1292	100 nM	24h
Trehalose	Sigma	T9531	500 µM	24h
Flubendazole	LKT labs	F4679	1 µM	3h
Nilotinib	Cayman Chemical	10010422	10 µM	24h
Clioquinol	Abcam	ab120355	1 µM	48h
Torin1	Tocris	4247	200 nM	6h
Ionomycin	Sigma	I0634	8 µM	-
GPN	Abcam	ab145914	1.5 mM	-
CPA	Sigma	C1530	40 µM	-
FCCP	Sigma	C2920	80 µM	-
ML SA1	Sigma	SML0627	1 mM	-
MLi-2	Tocris	5756	50 nM	2h
MG132	Sigma	M8699	500 nM	24h

2.6 Antibodies

Table. 2.5. *Antibodies for immunostaining*

Target	Supplier	Catalogue #	Species	Dilution
B-III Tubulin	Abcam	ab107216	Chicken	1:1000
GFAP	Abcam	ab4674	Chicken	1:1000
MAP2	Abcam	ab92434	Chicken	1:1000
MAP2	Millipore	MAB5622	Rabbit	1:1000
NeuN	Millipore	MAB5326	Mouse	1:500
LC3	Cell Signalling	2775	Rabbit	1:200
LAMP1	Santa-cruz	Sc-20011	Mouse	1:100
GFP	Invitrogen	A11122	Rabbit	1:100
LC3	Sigma	SAB1305552	Mouse	1:200
P62	Abcam	ab56416	Mouse	1:500
58k-Golgi	Abcam	Ab27043	Mouse	1:500

Table. 2.6. *Antibodies for western blotting*

Target	Supplier	Catalogue #	Species	Dilution
Actin	Abcam	ab49900	Mouse	1:50000
LC3	Sigma	L7543	Rabbit	1:3000
Lamp1	Abcam	ab24170	Rabbit	1:500
P62	Abcam	Ab109012	Rabbit	1:1000
GFP	Invitrogen	A11122	Rabbit	1:100
LRRK2	Abcam	ab133474	Rabbit	1:500
Beclin1	Abcam	ab62557	Rabbit	1/500
Lamp2a	Abcam	ab18528	Rabbit	1/1000
Phosph. mtor Ser2448	Cell Signalling	2971S	Rabbit	1/500
Mtor	Cell Signalling	4517	Mouse	1/500
Hsp70	Cell Signalling	4872	Rabbit	1/500
Ubiquitin	Dako	Z0458	Rabbit	1/1000
vATPase A1	Abcam	ab176858	Rabbit	1/500
Phosph. LRRK2 Ser935	Abcam	ab133450	Rabbit	1/500
Phosph. LRRK2 Ser1292	Abcam	ab203181	Rabbit	1/500

2.7 Fixation of cells and Immunocytochemistry

Cells were washed 3x with DPBS+/+ and fixed by incubation in methanol previously cooled to -20°C for 5 minutes and then washed 3x with DPBS +/+. Fixed cells were incubated for 60 minutes at room temperature in DPBS+/+/0.1% TritonX/10% normal goat serum/2% BSA to block non-specific binding, then incubated with primary antibodies in DPBS+/+/TritonX/1% normal goat serum/2% BSA over night at 4°C. Cells were washed 3x DPBS +/+ and incubated with secondary antibodies in DPBS+/+/TritonX/1% normal goat serum/2% BSA for 1 hour at room temperature. Cells were then washed 3x in DPBS +/+ and incubated in 1 μg/ml DAPI (Life Technologies) for 10 minutes at room temperature in PBS/0.1% TritonX100/1% normal goat serum. Coverslips were mounted onto Superfrost® plus (VWR) microscope slides using fluorosave reagent (Millipore) and stored at 4°C in the dark. Cells were imaged using an Invitrogen™ EVOS™ FL Auto cell imaging system at 60 x magnification. Unless stated, all immunostaining data was obtained from β-III Tubulin/MAP2 positive cells.

2.8 Immunohistochemistry

2.8.1 Transcardial perfusion

Rats were anaesthetised using 50 mg/ml pentobarbital and perfused with 30 ml 0.2 M phosphate buffer (PB) followed by 200 ml 4% paraformaldehyde (PFA) in 2 M PBS. Brains were removed and placed in 4% PFA at 4 °C (Transcardial perfusions were performed by Natalie Connor-Robson)

2.8.2 Tissue embedding

Fixed brains were paraffin-embedded using a Shandon Excelsior (Thermo). The following steps were taken during the embedding process under vacuum conditions: 90 minutes 70% ethanol, 90 minutes 80% ethanol, 90 minutes 90% ethanol, 3 x 90 minutes 100% ethanol, 2 x 90 minutes Histoclear (Fisher), 120 minutes Histoclear, 2 x 60 minutes paraffin wax, 120 minutes paraffin wax. Paraffin blocks were sectioned at 4 µm using a microtome and mounted on slides. (Paraffin embedding was performed by Natalie Connor-Robson, Department of Physiology, Anatomy and Genetics, Oxford).

2.8.3 Tissue rehydration and staining

Paraffin embedded tissue was rehydrated by immersion in the following: 20 minutes xylene, 20 minutes 100% ethanol, 10 minutes 95% ethanol, 10 minutes 70% ethanol, 10 minutes 50% ethanol and 5 minutes dH_2O. Antigen retrieval was then performed using pH 6.0 citrate buffer (40 µM sodium citrate dihydrate, 60 µM citric acid, H_2O) and heat-mediated antigen retrieval procedure was performed. Briefly, tissue was microwaved for 5 minutes at 50% power, followed by 2 minutes break and 2 minutes at 50% power (x2), and cooled on ice. Tissue was incubated in 10% normal goat serum in PBS/0.04% tween for 60 minutes at room temperature to block non-specific binding. Slices were incubated in primary antibody overnight in blocking solution, washed 3 x PBS and incubated in appropriate secondary antibodies in blocking solution for 1 hour at room temperature. Slides were washed 3 x PBS and incubated in 1 µg/ml DAPI (Life Technologies) for 10 minutes at room temperature in PBS/0.04% tween. Tissue was washed in 3 x PBS and mounted using fluorosave reagent (Millipore) and stored at 4°C

in the dark. Tissue was imaged using a Leica DMR light microscope and captured using a Nikon DS-Fi1 camera at 60x magnification.

2.9 Protein biochemistry

2.9.1 Cellular lysis

For in vitro cellular lysis, cells were washed 3 x DPBS +/+ and 200 µl of radio-immunoprecipitation buffer (RIPA) buffer (50 mM Tris, 150 mM NaCl, 0.1% sodium dodecyl sulphate (SDS), 0.5.% Na deoxycholate, 1% Igepal (pH 7.4)) containing protease (cOmplete EDTA-free, Roche) and phosphatase (PhosSTOP, Roche) inhibitors were added to each well and cells scraped using a pipette tip. Alternatively, cells were scraped on ice and centrifuged at 280 x *g* for 5 minutes, supernatants removed and cell pellets frozen on dry ice and stored at -80°C until needed. Lysates were centrifuged at 10,000 x *g* at 4 °C for 10 minutes. Supernatants were retained and stored at -20 °C.

2.9.2 Tissue homogenization

Following schedule 1 killing, brains were removed from animals and snap frozen on dry ice. Tissue was then homogenised on ice using a tissue tearer (Biospec Products) in RIPA buffer containing protease and phosphatase inhibitors. Tissue homogenates were then centrifuged at 10,000 x *g* at 4 °C. Both the supernatant and the pellet were separated and stored at -20 °C.

2.9.3 Protein quantification and sample preparation

Bicinchonic acid solution was combined with Copper(II) Sulfate Pentahydrate 4% Solution (50:1) to make BCA solution. 5 µl of protein sample was added to a well of a 96-well plate. 100 µl BCA solution was added to each well and incubated at 37°C for 30 minutes. Absorbance was read at 562 nm and the concentration of protein calculated from a bovine serum albumin standard curve.

2.9.4 Western Blotting

Cells were lysed in RIPA (50 mM Tris pH 8, 150 mM NaCl, 1% NP-40, 0.5% NaDeoxycholate, 0.1% SDS) with protease and phosphatase inhibitors. Lysates were diluted to 2 µg/µl and 6 x Laemmli sample buffer added (12% SDS, 30% β-mercaptoethanol, 60% Glycerol, 0.012% Bromophenol blue and 375 mM Tris pH 6.8) and samples were reduced and denatured at 95°C for 5 minutes. Samples were loaded into 4-15% Criterion Tris-HCl polyacrylamide gels (BioRad) alongside BLUeye Prestained Protein Ladder (Geneflow) and Magic Mark XP (Invitrogen) to determine target protein molecular weight. Electrophoresis was performed at 150 V for ~45 minutes and proteins transferred to a polyvinylidene difluoride (PVDF) membrane using a Trans-Blot Turbo Transfer System (BioRad) which utilises Trans-Blot Turbo Midi PVDF transfer packs (BioRad) in accordance to manufacturer's instructions. Membranes were blocked in 5% non-fat milk (Sigma) in TBS/0.1% Tween-20 (TBS-T) for 1 hour at room temperate and subsequently incubated with primary antibody in blocking solution overnight at 4°C. Membranes were washed with TBS-T (3x 5 minutes) and incubated in horseradish peroxidase (HRP)-conjugated secondary antibody (1:1000) (BioRad) in blocking solution for 1 hour. Membranes were washed

in TBS-T (3x 5 minutes) and developed using ECL solution (Millipore). Membranes were imaged using the Chemidoc™Touch Imaging System (BioRad) and quantified using ImageLab (BioRad).

2.9.5 Co-immunoprecipitation

Dynabeads™ Protein G (Invitrogen) were washed 3 x in PBS +/+ using a magnetic rack (BioRad) and, using 1.5 mg/sample, incubated with 40 µg of antibody/sample overnight at 4°C whilst rotating. Beads were washed 3 x in PBS +/+ and beads were then incubated with cell lysates (2.4 mg of protein/sample) for 3 days at 4°C whilst rotating. Flow through was removed for analysis and beads washed 3 x in PBS +/+ and boiled at 65°C in 3 x Laemmli sample Buffer and assessed via SDS-PAGE.

2.10 Lysosensor imaging and quantification of lysosome pH

Lysosomal pH was measured using the LysoSensor™ Green DND-189 (Life Technologies). Primary cortical cultures were labelled with 1 µM LysoSensor™ Green DND-189 in growth media for 2 hour and either immediately imaged or incubated for 10 minutes in pH calibrated solutions. pH calibration solutions were generated in Hanks Buffered Salt solution (GIBCO, Life Technologies) containing 20 mM MES (4-Morpholineethanesulfonic acid), 110 mM KCl and 20 mM NaCl, supplemented with 30 µM nigericin and 15 µM monensin, sterile filtered and titrated to pH values of 3, 4, 5, 6 and 7. Nuclei were stained with Hoechst 33258 for ten minutes and cells were imaged using an Invitrogen™ EVOS™ FL Auto cell imaging system at 20x magnification. pH values were calculated using a standard curve generated from the pH calibrations.

2.11 RNA extraction and QPCR

To extract RNA, 333 µl of TRIZOL (Invitrogen) per 24-well dish was added and incubated at room temperature for 15 minutes. Wells were pooled in triplicates and collected in 2 ml microcentrifuge tubes. 150 µl chloroform was added and tubes were shaken and left to incubate at room temperature for a further 2 minutes. Samples were centrifuged for 10 minutes at 4°C at 10,000 x *g*. The aqueous phase was transferred to a new microcentrifuge tube. An equal volume of 70% ethanol was added to each sample. RNase Easy mini kit (Qiagen) was used according to manufacturer's instructions. Briefly, samples were loaded into supplier columns and centrifuged at 10,000 x *g* for 30 seconds and flow through discarded. 350 µl RW1 buffer and centrifuged at 10,000 x *g* for 15 seconds and flow through discarded. 80 µl of DNase I/RDD buffer was added to column membrane and incubated at room temperature for 10 minutes. RW1 buffer was added and columns centrifuged at 10,000 x *g* for 15 seconds. RPE buffer was added to columns, centrifuged for 10,000 x *g* for 30 seconds, repeated, and 30 µl RNase free water was added and RNA eluted.

For reverse transcription, 1 µl of random primers, 1 µg RNA and 1 µl of 10 mM dNTP mix was added to 13 µl RNase free water. Samples were heated to 65°C for 5 minutes and incubated on ice for 1 minute. 4 µl 5x first-strand buffer, 1 µl 0.1 M DTT, 1 µl RNase out and 1 µl SuperScipt III were added to each sample. Samples were incubated at 25°C for 5 minutes followed by 55°C for 60 minutes and 70°C for 15 minutes.

2.12 C^{14}-valine pulse-chase protein degradation assay

C^{14}-valine (5 µl) was added to each well of cells for 48 hours at 37°C in a humidified incubator with 5 % CO2. Cells were washed 4 x with fresh media and incubated for a further 24 hours in 1 mM C^{12}-valine containing media. Short-lived protein degradation via the proteasome is measured during this 24 hours period and 200 µl aliquots of either untreated or MG132 treated media were collected from each well at selected time points and proteins precipitated by adding to 200 µL ice-cold 20% trichloroacetic acid (TCA). After 24 hours media was replaced with fresh media containing 1 mM C^{12}-valine and selected compounds (10 µM chloroquine; 1 µM clioquinol; 50 nM MLi-2). To measure protein degradation by autophagy, 200 µl aliquots of media were collected from each well at selected time points and proteins precipitated by adding to 200 µL ice-cold 20% trichloroacetic acid (TCA). Samples were centrifuged at 17,000 x g for 10 minutes to pellet the proteins and the supernatant was transferred to a scintillation vial and 3 ml scintillation fluid added. At the end of the time course the remaining media was removed and the cells lysed by the addition of 500 µl 0.1 M sodium hydroxide for 5 minutes at 37°C. The lysate was transferred to a scintillation vial and 3 ml scintillation fluid added. Counts were measured using a scintillation counter and protein degradation by autophagy calculated as: % = 100 x (total counts for supernatant/total counts for supernatant and lysate). In order to account for free valine in media that was released due to non-lysosomal/proteasomal degradation, the % calculated for chloroquine/MG132 was subtracted from untreated/MLi-2/Clioquinol treated % (See Fig. 2.2).

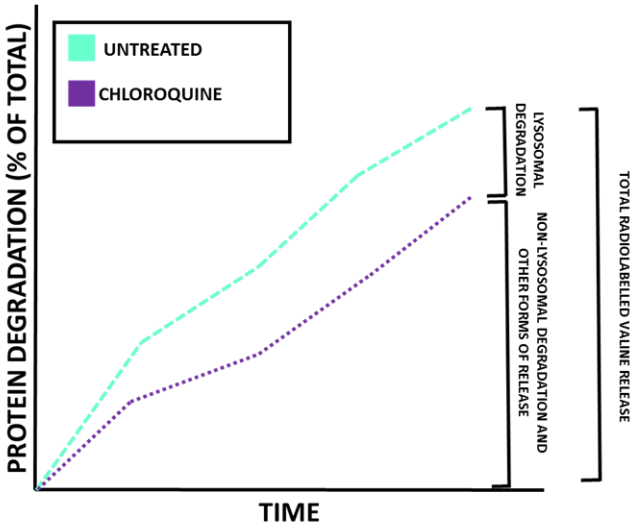


Figure. 2.2. *Schematic diagram of the pulse chase assay calculation.*

2.13 ^{3}H-Glutamate uptake assay

At 14 DIV, astrocyte cultures in 24-well plates were washed 3 x with DPBS+/+ and then incubated with 50 nM L-[3,4-^{3}H]-Glutamic Acid in 135 mM NaCl, 3.1 mM KCl, 1.2 mM CaCl2, 1.2 mM MgSO4, 0.5 mM KH2PO4, and 2.0 mM glucose, adjusted to pH 7.4, for 10 min. Sodium independent uptake was measured by incubating cells under the same conditions, substituting 135 mM choline chloride for sodium chloride. The uptake assay was stopped by the addition of 500 µM cold ^{1}H-Glutamic Acid (Sigma). Supernatant was removed, cells were washed 2 x DPBS+/+, and then lysed in 200 µl NaOH (0.1 M). 5 µl of lysate per sample was taken for protein quantification by BCA assay, and the remainder of each sample was transferred to individual scintillation vials. 3 ml Optiphase Supermix (Perkin Elmer) scintillation fluid was added to each scintillation vial, which were capped and inverted before analysis using a Tri-Carb 2800 TR liquid scintillation counter (Perkin Elmer). Data were normalised to protein content as calculated using a BCA assay.

2.14 Calcium imaging

Cortical cultures were incubated with 2.5 mM Fura2-AM (Molecular Devices) in normal growth media for 1 hour and imaged on a FlexStation 3 Multi-Mode Microplate Reader (Molecular Devices). Light excited at 340 nm and 380 nm, detected at 510 nm, were measured and the ratio of unbound:bound calcium signal calculated (ΔF/F). After establishing a baseline signal for 30 seconds, calcium compounds were injected into wells and the ratio measured for 60/120 seconds. Fold-change between baseline signal and peak amplitude was calculated to assess calcium store content.

2.15 Zinc imaging

Cortical cultures were incubated with 5 µM FluoZin-3AM (Life Technologies) and 100 nM LysoTracker Red DND-99 (Life Technologies) for 1 hour in neuronal growth medium supplemented with 0.02% pluronic acid F127 (Life Technologies). Cells were washed to remove unbound dye and incubated for 30 minutes to allow for the de-esterification of the dye. Nuclei were stained with Hoechst 33258 for ten minutes and imaged on an Invitrogen™ EVOS™ FL Auto cell imaging system at 20x magnification.

2.16 DQ™ BSA assay

Cortical cultures were incubated with 30 µg/ml DQ™ BSA (Life Technologies) in fresh media for one hour and washed 3 x in DPBS +/+ and imaged on an Opera Phenix™ spinning disc confocal microscope (Perkin Elmer) at 40x magnification.

2.17 Deglycosylation assay

PNGase F deglycosylation reagents were purchased from NEB. 2 µl of GlycoBuffer was added to 20 µg of cell lysate in 10 µl of H_2O. 3 µl of PNGase F was added to each sample and samples were incubated for 37°C for 2 hours. 6 x Laemmli sample buffer was added and deglycosylated protein observed by mobility shifts on SDS-PAGE gels.

2.18 Cell profiler image analysis

For image analysis, images were quantifyed using Cell Profiler™. Neurons were identified manually using β-III tubulin stain. Puncta (LC3/LAMP1/p62/YPet/58-k) were converted to greyscale and enhanced, suppressing background and using the Otsu method (to threshold brightness) and size exclusion, puncta were identified (reference Otsu paper here). Puncta were then overlaid onto each other to identify those co-localising (see Fig. 2.3). The same pipeline was used for lysosensor and DQ-BSA assays with the overlay step removed.

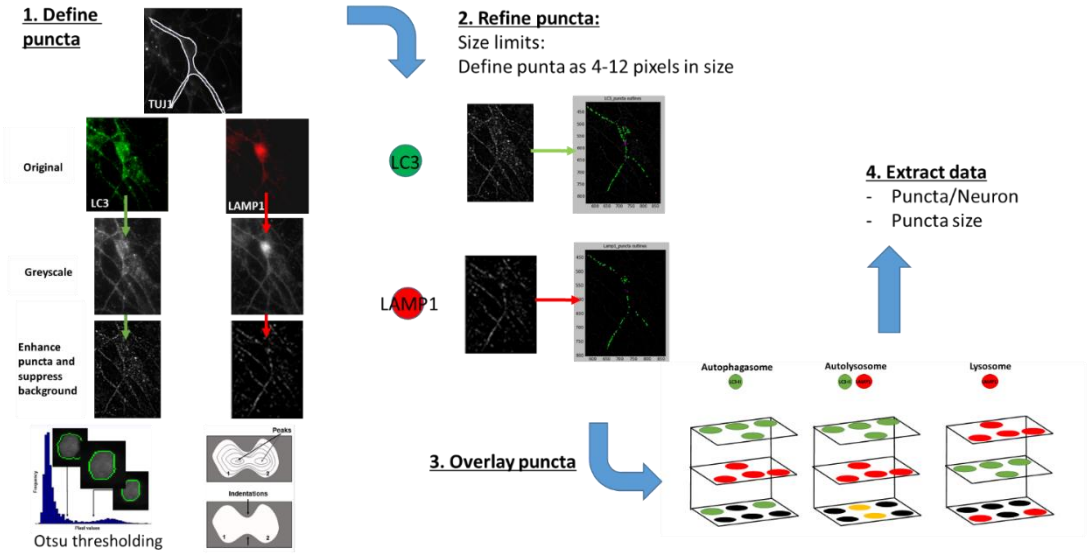


Figure. 2.3*. Schematic diagram of cellprofiler image analysis pipeline.*

Chapter 3: Exploring the involvement of LRRK2 in the autophagy pathway

3.1 Introduction and aims

As described in section 1.3.4, LRRK2 has been implicated in a wide range of cellular functions, many of which have been demonstrated to be perturbed by the G2019S and R1441C mutations, such as autophagy. As alluded to, the current evidence for the role of LRRK2 in autophagy is not well defined and often contradictory. The differential effect of endogenous LRRK2 levels and LRRK2 overexpression has not been thoroughly investigated and it is not known if the two enzymatic domains orchestrate facilitating or opposing functions. The differences in cell models used could lend an explanation to the differences reported; differences in LRRK2 splice variant expression in primary neurons, astrocytes and microglia have been reported (Giesert et al., 2013) and differences in LRRK2 activators, substrates and partners vary between cell types (Wallings et al., 2015). The majority of the current literature has described *in vitro* work in immortalised cell lines and patient fibroblasts as opposed to primary cultures (Table 3.1).

Authors	Model	LRRK2 gene	Effects on autophagy
Plowey et al., 2008	SH-SY5Y	hLRRK2 cDNA (GS)	↑ autophagic vacuoles
Alegre-Abarrategui et al., 2009	HEK293	BAC hLRRK2 (WT & RC)	↑ autophagic vacuoles
Gomez-Suaga et al., 2012	HEK293	Human LRRK2 cDNA (WT and GS)	↑ autophagic vacuoles
Sanchez-Danes et al., 2012	iPSC derived vmDA Neurons	GS and WT	↑ autophagic vacuoles and **i** autophagic flux
Bravo-San Pedro et al., 2013	Patient derived human primary fibroblasts	GS and WT	↓ autophagic vacuoles
Manzoni et al., 2013	Patient derived human primary fibroblasts	GS, RC, YC and WT	Inhibited LC3-II response to starvation
Su and Qi, 2013	HEK293	hLRRK2 cDNA (GS)	↓ LC3-II levels
Schapansky et al., 2014	RAW264.7	Endogenous	↓ membrane recruitment with autophagy stimulation
Saez-Atienzar et al., 2014	SH-SY5Y	Endogenous	↑ LC3-II and p62 with Lrrk2 kinase inhibition
Saha et al., 2014	Primary C.Elegans DA neurons	LRRK2 cDNA (GS and WT)	↑ autophagic vacuoles and accelerated age-related loss of autophagy
Su et al., 2015	Patient derived human primary fibroblasts	GS and control	↓ LC3-II levels and ↑ autophagic flux
Henry et al., 2015	Primary cortical mouse astrocytes	BAC mLRRK2 (GS, RC, YC)	↑ Lysosome size and ↓ pH
Hockey et al., 2015	Patient derived human primary fibroblasts	GS and control	↑ Lysosome size and NAADP-evoked calcium release
Manzoni et al., 2016	H4 neuroglioma cells	Endogenous	LRRK2 kinase inhibition ↑ LC3-II in a Beclin1 dependent manner
Park et al., 2016	HEK293	hLRRK2 cDNA (WT GS, RC, DA, GR)	LRRK2 binds to p62 and ↓ p62 phosphorylation
Manzoni et al., 2018	H4 neuroglioma and primary rat astrocytes	Endogenous	LRRK2 kinase inhibition ↑ ULK1 phosphorylation

Table 3.1 An overview of reports of LRRK2 and autophagy in in vitro models. *Studies reporting in immortalised cell lines and patient fibroblasts have been highlighted in blue. ↑ = increased, ↓ = decreased. Abbreviations: RC, R1441C; GS, G2019S; DA, D1994A ; GR, G2385R .*

Neurons are especially vulnerable to deficiencies in autophagy substrate clearance. This is evident from the observation that genes involved in the autophagy and converging endosomal pathway have been causatively linked to neurodegenerative diseases (described in section 1.2). Without the aid of cell division, which mitotic cells can depend upon to decrease the burden of intracellular waste, neurons are largely dependent on autophagy to prevent the accumulation of cellular protein and damaged organelles. It is therefore questionable why so much of the reported literature of LRRK2 and its involvement in autophagy rely on cell lines as their model of choice. This is further emphasised by the fact that both normal and pathological ageing are often associated with decreased autophagic potential (Rubinsztein et al., 2011); something that would compromise the nervous system but is not recapitulated *in vitro* in primary fibroblasts and immortalised cell lines. We therefore decided to investigate the role of LRRK2 and its mutations in primary neuronal cultures in order to delineate the role of LRRK2 in autophagy in a disease relevant cell type.

Furthermore, previous reports of LRRK2 in autophagy that have utilised disease relevant cell types, such as TG rodent tissue or iPSC derived midbrain DAn (Table 3.1 and 3.2), seldom report more than relatively superficial accounts of the autophagy pathway in their models. Research in mammalian autophagy has been historically plagued by two major considerations. First is the challenge of capturing a dynamic process with static measurements and the limitations associated with biological inferences from these. Secondly is separating form from function and the common pitfall of assigning function to autophagy based on its detection. For example, the accumulation of early intermediates of the pathway could be used to assume increased autophagy induction, whereas the same can be seen when later stages of the pathway

are blocked. Given these considerations it is understandable how, using static measurements alone as is the case in much LRRK2 research thus far, misconceptions can be drawn. Therefore, to elucidate whether LRRK2 resides in the initiation or clearance steps, this chapter sets out to monitor autophagy as a dynamic process and to modulate autophagy in order to probe the effects of LRRK2 on the various stages of the pathway.

Authors	Model	LRRK2 gene	Effects on autophagy
Ramonet et al., 2011	Transgenic mouse	hLRRK2 cDNA (GS, RC and WT)	enlarged and ↑ autophagic vacuoles
Hinkle et al., 2012	Lrrk2$^{-/-}$ mouse	KO	↑ p62 in kidneys
Tong et al., 2012	Lrrk2$^{-/-}$ mouse	KO	Age-dependent biphasic alterations in LC3-II levels in kidneys
Baptista et al., 2013	Lrrk2$^{-/-}$ rat	KO	↑ Increased lysosomes in kidneys
Tsika et al., 2014	Transgenic mouse	hLRRK2 cDNA (RC)	No changes
Tsika et al., 2015	AV striatal injected rat	hLRRK2 cDNA (WT and GS)	No changes
Yue et al., 2015	KI mouse	GS	↑ LC3-II levels
Fuji et al., 2015	Non-human primate	Endogenous	↓ Lysosomal dysregulation in urine after kinase inhibition
Schapansky et al., 2018	KI mouse	GS	↓ LAMP1 and LC3-I (*in vivo*) ↑ Increased LC3-II and **i** flux
Mamais et al., 2018	Human post-mortem	GS, iPD and control	↓ LAMP1 and p62 in BG

Table 3.2 An overview of reports of LRRK2 and autophagy in animal models and human post mortem. *↑ = increased, ↓ = decreased. Abbreviations: RC, R1441C; GS, G2019S; DA, D1994A; GR, G2385R; KO, knock-out; AV, anterograde adenovirus; iPD, idiopathic PD.*

Chapter aims

1. To establish and characterise primary cortical cultures from hLRRK2-BAC TG rats
2. To investigate alterations in the autophagy pathway caused by the presence of hWT-LRRK2, LRRK2-R1441C and LRRK2-G2019S

3.2 Results

3.2.1 Establishing primary cortical culture cell populations

To determine the ratio of neurons vs. non-neuronal cells in primary cultures established from P1 rat pups (nTG and those harbouring hWT, G2019S or R1441C LRRK2 protein), 14 DIV cultures were co-immunostained for a neuronal specific nuclear marker (NeuN), microtubule associated protein 2 (MAP2), glial fibrillary acidic protein (GFAP) and DAPI (Fig. 3.1a). Nuclei co-stained with both DAPI and NeuN were deemed neuronal, and DAPI-only stained cells were deemed non-neuronal. A consistent ratio of neuronal:non-neuronal cells was demonstrated in all cultures with 30-40% of cells staining positive for NeuN (Fig. 3.1b). From here on, such mixed cultures will be termed 'cortical cultures'.

Although LRRK2 is ubiquitously expressed, substantial levels of both LRRK2 protein and mRNA has been detected in blood mononuclear cells (PBMCs; Hakimi et al., 2011), primary microglia (Gillardon et al., 2012), primary macrophages (Schapansky et al., 2014) and astrocytes (Giesert et al., 2013), with relatively low endogenous expression seen in primary neurons (Schapansky et al., 2014). Furthermore, there is

increased expression of LRRK2 protein found in the striatum and cortex compared to other brain regions (Giesert et al., 2013). These differences, as well as the identification of specific functions of LRRK2 within specific systems such as the immune system (Thevenet et al., 2011; Gardet et al., 2010), lends to the hypothesis that LRRK2 could play different roles within different cell types and tissue. This could be explained by tissue specific expression of LRRK2 partners, or by differential splicing of LRRK2 in different cell types. Although little is known about LRRK2 splice variants, it has been shown that primary neurons, astrocytes and microglia of mice show differential expression of 3 splice variants of LRRK2 (Giesert et al., 2013). It was therefore deemed necessary to generate cultures of both pure astrocytes and pure neurons in addition to mixed cortical cultures in order to further delineate cell-specific functions of LRRK2.

3.2.2 Generating pure astrocytic cultures

To generate a pure astrocytic culture as a tool to assess LRRK2 function in this cell type in isolation to neurons, an alternative primary culture method was developed. Astrocytic cultures were assessed for both β-III tubulin/MAP2 and GFAP expression; no β-III tubulin expression was seen compared to cortical culture counterparts with mixed cell-types, and immunofluorescence showed no MAP2 staining (Fig. 3.1c and d). Western blots for microglia markers (ionized calcium-binding adapter molecule 1 [IBA1] and major histocompatibility complex II [MHC-II]) showed no microglia present in these astrocytic cultures (Fig. 3.1e). A 100% pure astrocytic culture has therefore been produced.

3.2.3 Generating enriched neuronal cultures

An alternative method was developed to create an enriched neuronal culture. Cultures were treated with various concentrations of AraC which interferes with DNA synthesis in mitotic cells, to kill off glial cells. Neuronal cultures were stained for NeuN, MAP2 and GFAP and neuronal cell percentage was calculated for each condition. Although no one condition resulted in a 100% pure neuronal culture, there was a significant increase from the original 30-40% to 80-90% in cultures treated with AraC at a lower concentration of 1 µM for 2 days (Fig. 3.1f). These cultures will be referred to as 'neuronal cultures'.

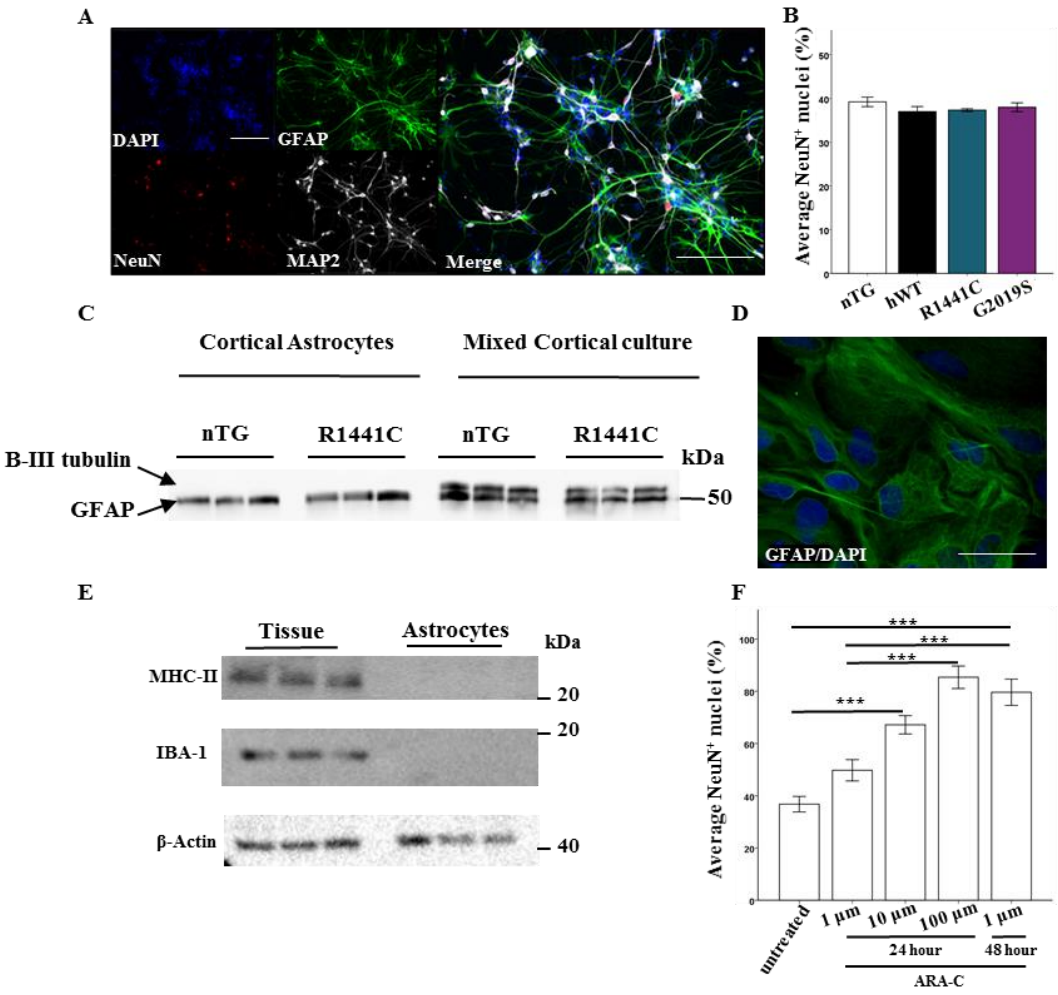


Figure 3.1. Establishing primary cortical cultures. *Primary cortical cultures from P1 pups were generated and characterised. (**A, B**) Cultures at DIV 14 were stained for MAP2, GFAP and NeuN in order to assess neuronal:non-neuronal cell ratio (Bars represent mean +/- SEM; N = 3). (**C**) Western blots for β-III tubulin and GFAP were performed to assess total protein level. (**D**) Primary astrocytic cultures were stained for MAP2 and GFAP in order to determine astrocyte purity. (**E**) Western blots for MHC-II and Iba1 were performed with astrocytic cell lysates to determine presence of microglia. (**F**) Neuronal cultures were stained for NeuN in order to assess neuronal:non-neuronal cell ratio. Bars represent mean +/- SEM. (N = 3; ***, P<0.001; One-Way ANOVA, Tukey HSD post-hoc). Scale bar = 200 μm.*

3.2.4 Assessing endogenous Lrrk2 and transgene protein expression in primary cortical cultures

Primary cortical cultures from P1 rat pups were generated and characterised for both the human LRRK2 transgene protein (utilising the transgenic N-terminal YPet protein tag of 26.8 kDa) and endogenous Lrrk2 protein expression. hWT-LRRK2 and LRRK2-R1441C neurons express similar levels of the hLRRK2 transgene, whereas LRRK2-G2019S cultures express a 2-3-fold increase in transgene levels relative to both hWT-LRRK2 and LRRK2-R1441C (Fig. 3.2a). With regards to total LRRK2 protein expression (endogenous and transgene protein), both hWT-LRRK2 and LRRK2-R1441C cortical cultures expressed 2-3 fold increased expression relative to nTG cultures and LRRK2-G2019S cortical cultures demonstrated 5-6 fold increased expression (Fig. 3.2b). Co-immunofluorescence staining for the transgene protein, the neuronal marker MAP2, and the astrocytic marker GFAP, confirmed transgene presence in neurons and astrocytes, respectively (Fig. 3.2c and d).

It has been demonstrated previously that Lrrk2 expression increases over the first two weeks postnatally (Giesert et al., 2013), therefore the levels of transgene expression over the first 21 days *in vitro* were assessed. Cultures at DIV 7, 14 and 21 were analysed by western blot for YPet expression. For LRRK2-R1441C, LRRK2-G2019S and hWT-LRRK2 cultures, transgene expression did not significantly differ at any time point (Fig. 3.2e). As a result, all data regarding transgene phenotypes were taken from 14 DIV cultures.

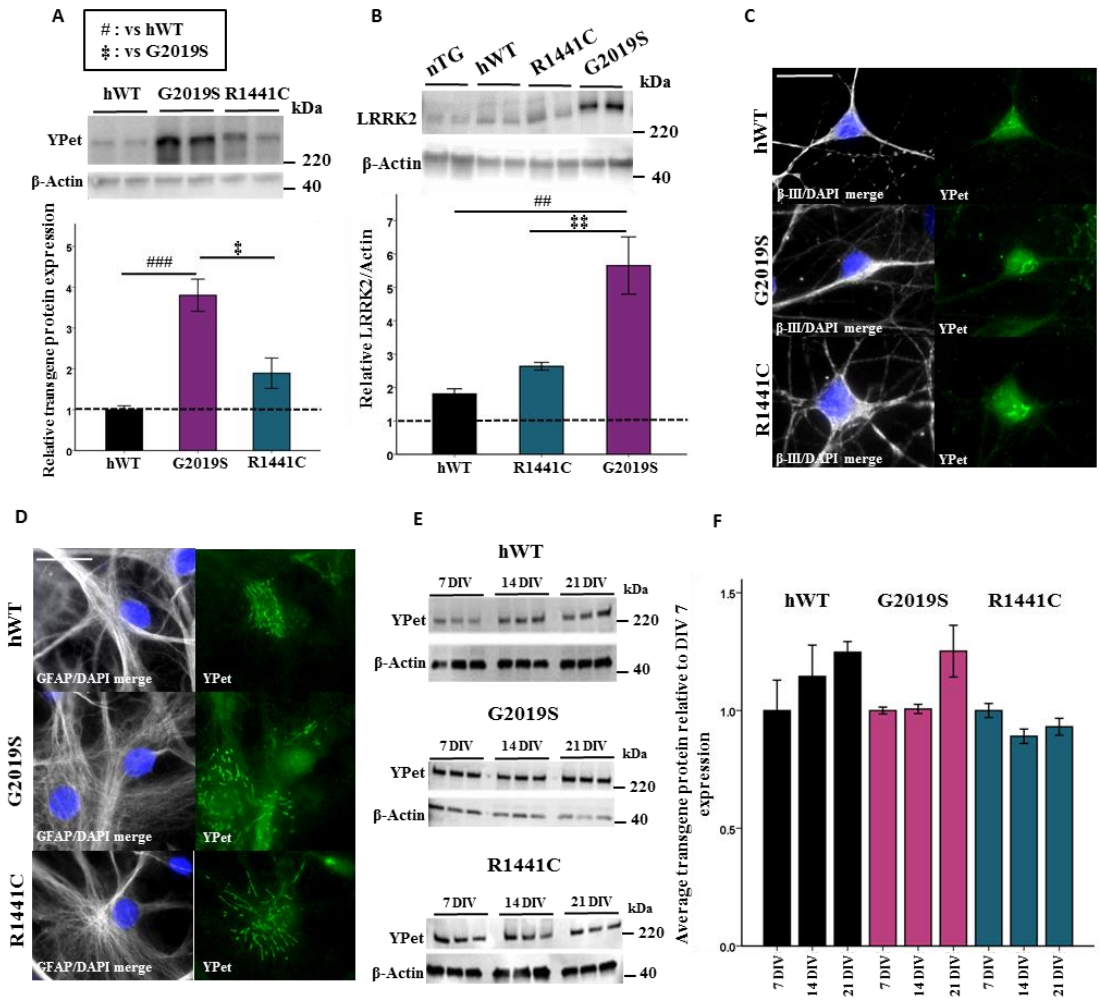


Figure 3.2. Assessing LRRK2 protein expression. *Primary cortical cultures from P1 pups were assessed for LRRK2 protein expression. (**A**) Western blots for YPet expression were quantified to assess transgene protein levels and normalised to hWT levels. (**B**) Western blots for Lrrk2 were quantified to assess total Lrrk2 protein levels and normalised to nTG littermate controls. (**C, D**) Cultures at 14 DIV were stained for MAP2/GFAP and YPet to assess transgene expression. (**E, F**) Western blots for YPet expression at 7/14/21 DIV were quantified and normalised to 7 DIV expression. Bars represent mean +/- SEM. (N = 3; *, P< 0.05; **, P<0.005; ***, P<0.001; One-Way ANOVA, Tukey HSD post-hoc). # = vs. hWT, ‡ = vs. G2019S. Scale bar = 10 µm.*

A decrease in hLRRK2 protein expression was observed in cultures with increased proportion of neurons (Fig. 3.3a) reflecting what has been reported previously in the literature. However, despite previous reports demonstrating increased expression of endogenous Lrrk2 in astrocytes compared to neurons (Giesert et al., 2013), our astrocytic cultures had decreased transgene protein expression compared to cortical cultures (Fig. 3.3b). Pro-inflammatory molecules were added to cultures in an attempt to increase LRRK2 expression as has been demonstrated in other glial cell types (Moehle et al., 2014) but is yet to be demonstrated in astrocytes. However, despite using concentrations of these compounds and time points which have been repeatedly reported to increase LRRK2 expression *in vitro*, no significant increases were observed for either compounds (Fig. 3.3b). Furthermore, when comparing the morphology of astrocytes in the different cultures, those in the cortical cultures displayed a more typical astrocytic morphology, with a typical 'star-like' appearance, whereas those in the pure astrocytic cultures lacked any elongated processes and displayed a rounder and flatter appearance (see Fig. 3.1a and Fig. 3.1d). This difference in morphology could represent the activated state of these astrocytes, where there is an increase in cellular processes as activation increases (Wihelmsson et al., 2006). STAT1 (signal transducer activators of transcription type 1) is a crucial transcription factor in astrocyte activation and was therefore assessed in these cultures. Despite being present in the cortical cultures, the phosphorylated form of the protein (indicative of astrocyte activation) and total STAT1 protein could not be detected in the pure astrocytic cultures (Fig. 3.3c).

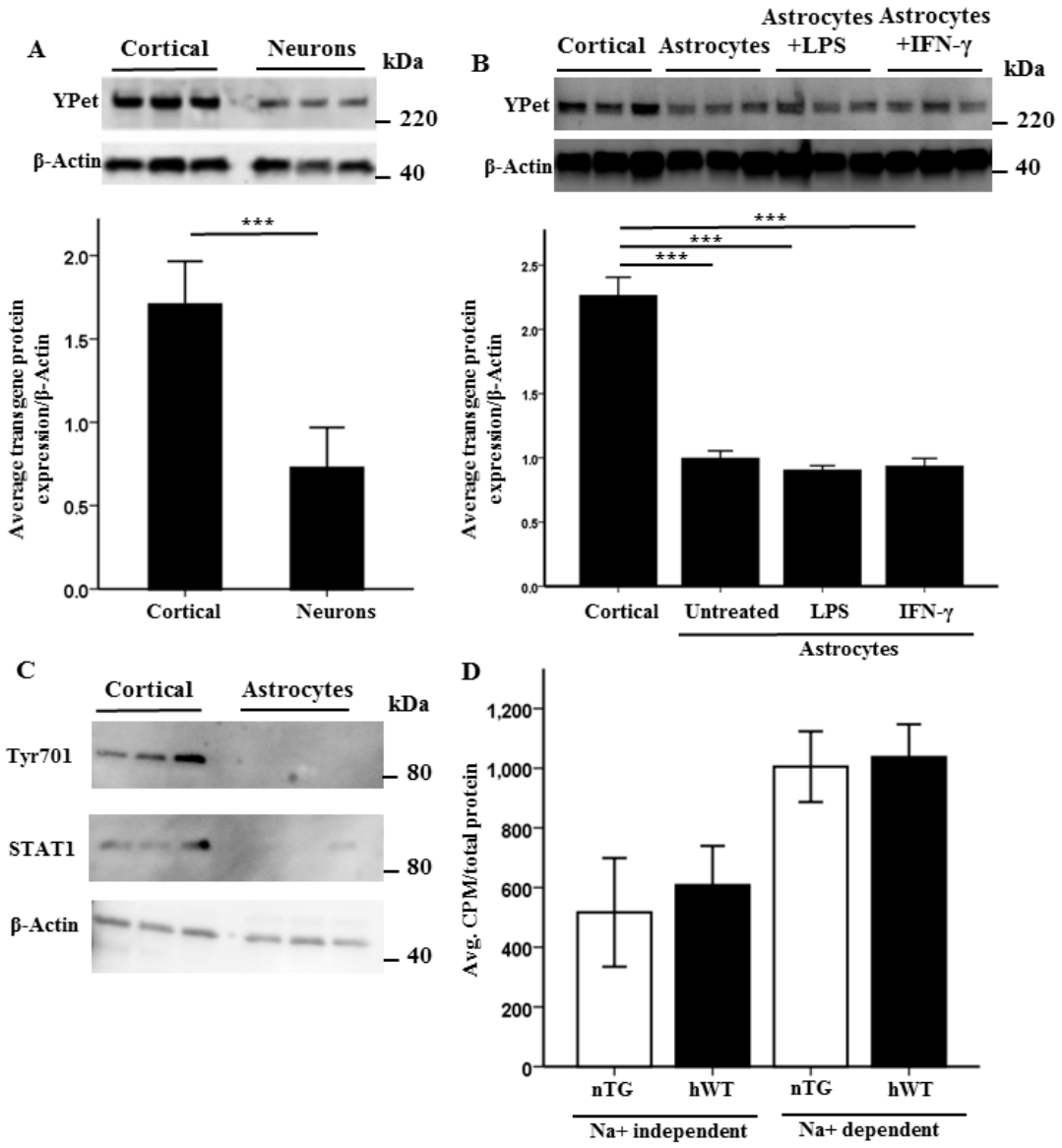


Figure 3.3. Establishing astrocyte and neuronal cultures. *Primary astrocytic and neuronal cultures from P1 nTG and hWT pups were assessed for LRRK2 protein expression and functionality. (**A**) Western blots for YPet expression were quantified in cell lysates from hWT cortical and neuronal cultures. (Bars represent mean +/- SEM; N = 3; ***, P<0.001; Independent T-test). (**B**) Western blots for YPet were quantified to assess protein levels in hWT cortical and astrocytic cultures in the presence of LPS and IFN-γ (Bars represent mean +/- SEM; N = 3; ***, P<0.001; One-Way ANOVA, Tukey HSD post-hoc). (**C**) Total STAT1 protein expression and it phosphorylated form at tyrosine 701 was assessed via western blot. (**D**) Glutamate uptake in nTG and hWT astrocytic cultures was quantified. Bars represent mean +/- SEM (N = 3; One-Way ANOVA, Tukey HSD post-hoc).*

3.2.5 Assessing astrocytic glutamate uptake

In vivo, astrocytes take up glutamate in a sodium dependent manner through their glutamate transporters (Schousboe et al. 1977). To determine whether these astrocytes were functional, glutamate uptake was assessed by incubating astrocytes with L-[3,4-3H]-Glutamic acid for 10 minutes in the presence or absence of sodium, and measuring the glutamate content of the cells. Cultured astrocytes demonstrated the specific uptake of glutamate in the presence of sodium, indicating the expression of functional glutamate transporters at the cell surface (Fig. 3.3d). However, due to decreased transgene protein expression and a lack of response to pro-inflammatory stimuli, these pure astrocytes were not considered an ideal model to characterise the role of LRRK2 in autophagy. Therefore the remainder of the data presented here is from cortical cultures.

3.2.6 Quantifying basal autophagy protein levels

LC3 is a protein involved in the formation of autophagic vesicles. In its unlipidated state (LC3-I), it is freely present in the cytoplasm. However, upon lipidation to LC3-II it is recruited to the membrane of autophagosomes where it remains until degradation following lysosomal fusion. LRRK2-R1441C cultures exhibited a significant increase in LC3-II (Fig. 3.4a), although no significant differences in LAMP1 (an essential lysosomal protein) or p62 (an LC3 binding protein degraded by the lysosome) protein levels were observed (Fig. 3.4b and c). In the cell, the amount of LC3-II usually correlates well with the number of autophagosomes. It is a common misconception that increased LC3-II levels are exclusively indicative of increased autophagosome production and therefore autophagic activity. Given that autophagosomes are an

intermediate structure in this dynamic pathway, the number of autophagosomes observed at any specific time point is a function of the balance between the rate of their generation and the rate at which they mature to autolysosomes. Therefore, it is crucial to assess the expression levels of other proteins involved in different stages of the autophagy process to begin to elucidate the reasons for increased LC3-II levels.

Beclin1 has a central role in inducing autophagy; it interacts with several cofactors to regulate the lipid kinase, VPS34, and to promote the formation of Beclin1-VPS34-VPS15 core complexes, which induce nucleation of the phagophore and subsequent autophagosome biogenesis. No significant differences were observed between genotypes in Beclin1 protein expression assessed via western blot (Fig. 3.4d). Similarly, no significant differences were observed between genotypes in protein levels of LAMP2a (an essential lysosomal protein associated with chaperone mediated autophagy) (Fig. 3.4e) or phosphorylated mTOR (a key homeostatic regulator that regulates lysosomal biogenesis and autophagic processes) (Fig. 3.4f). A significant decrease in HSP70 (a molecular chaperone involved in chaperone mediated autophagy) protein was observed in LRRK2-G2019S cortical cultures compared to LRRK2-R1441C cultures (Fig. 3.4g).

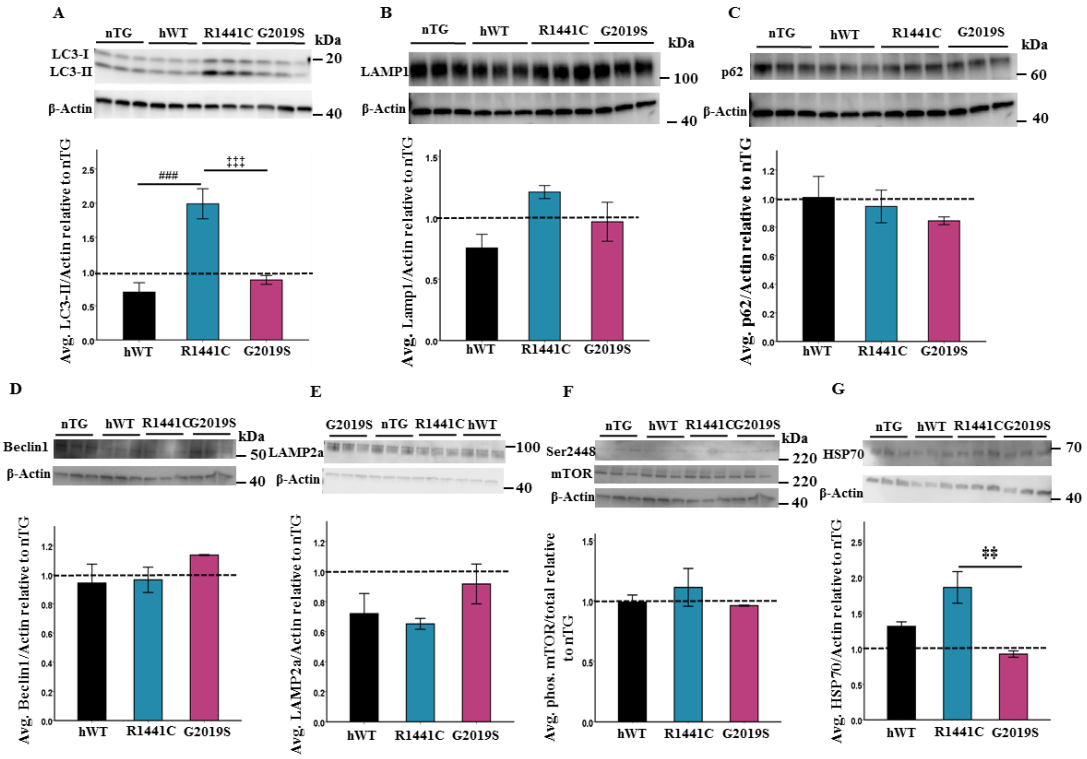


Figure 3.4. Assessing basal autophagy protein levels. *Primary cortical cultures from P1 pups were assessed for autophagy protein levels. Western blots for (**A**) LC3-II, (**B**) LAMP1, (**C**) p62, (**D**) Beclin1, (**E**) LAMP2a, (**F**) phosphorylated. mTOR at Serine 2448 and (**G**) HSP70 were quantified and normalised to nTG littermate controls. Bars represent mean +/- SEM. (N = 3; ***, P<0.001; One-Way ANOVA, Tukey HSD post-hoc). # = vs. hWT, ‡ = vs. G2019S.*

3.2.7 Autophagosome, autolysosome and lysosome quantification in neurons of primary cortical cultures

Primary cortical cultures contained a mixed population of cells, comprising 30-40% neurons. Therefore, it cannot be determined from these protein western blot data if the LC3-II phenotype observed was being driven by the neurons or another cell type present. Furthermore, changes in overall basal LC3-II levels are hard to interpret and can be indicative of increased autophagosome biogenesis as well as a decrease in autolysosome maturation, leading to an accumulation of autophagosomes and undegraded cargo. Therefore, co-immunofluorescence staining for the autophagy proteins LC3, LAMP1 and the neuronal marker β-III tubulin were used to quantify autophagosomes, autolysosomes and lysosomes specifically in neurons. LRRK2-R1441C neurons showed a significant increase in autophagosome number and a significant decrease in autolysosome number (Fig.3.5a and b). No significant differences were observed in the hWT-LRRK2 and LRRK2-G2019S neurons.

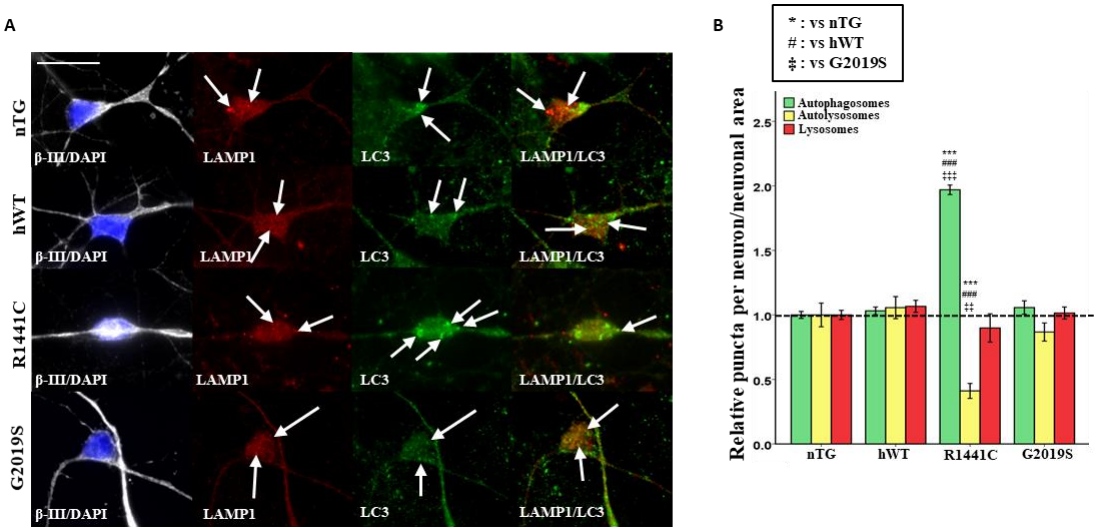


Figure 3.5. Assessing basal autophagy levels by immunofluorescence. *(**A, B**) 14 DIV primary cortical cultures were fixed and stained for β-III tubulin, LC3 and LAMP1 and autophagy puncta were quantified and normalised to nTG littermate controls. Bars represent mean +/- SEM. (N = 3; **, P<0.005; ***, P<0.001; Kruskal-Wallis non-parametric ANOVA, bonferroni post-hoc). * = vs. nTG, # = vs. hWT, ‡ = vs. G2019S. Scale bar = 10 μm.*

3.2.8 Investigating LC3 changes in cortical and midbrain tissue of aged animals

In order to observe whether this LRRK2-R1441C dependent autophagy phenotype was present in aged tissue, 22-month old rat cortical slices were stained for LC3 and puncta quantified in $MAP2^+$ cells (Fig. 3.6a). Cortical neurons from aged LRRK2-R1441C rats showed a significant increase in LC3 puncta number (Fig. 3.6b), and no changes in puncta size were seen (Fig. 6c). Midbrain slices were stained for LC3 and puncta quantified in TH^+ neurons (Fig. 3.6d). Interestingly, TH^+ neurons in the midbrain of both LRRK2-R1441C and LRRK2-G2019S animals demonstrated a significant increase in LC3 puncta (Fig. 3.6e) although no differences in LC3 puncta size was observed (Fig. 3.6f). Therefore, although the effects of the LRRK2-R1441C are present in different neuronal cell types, the effects of LRRK2-G2019S on the autophagy pathway might be cell-type dependent.

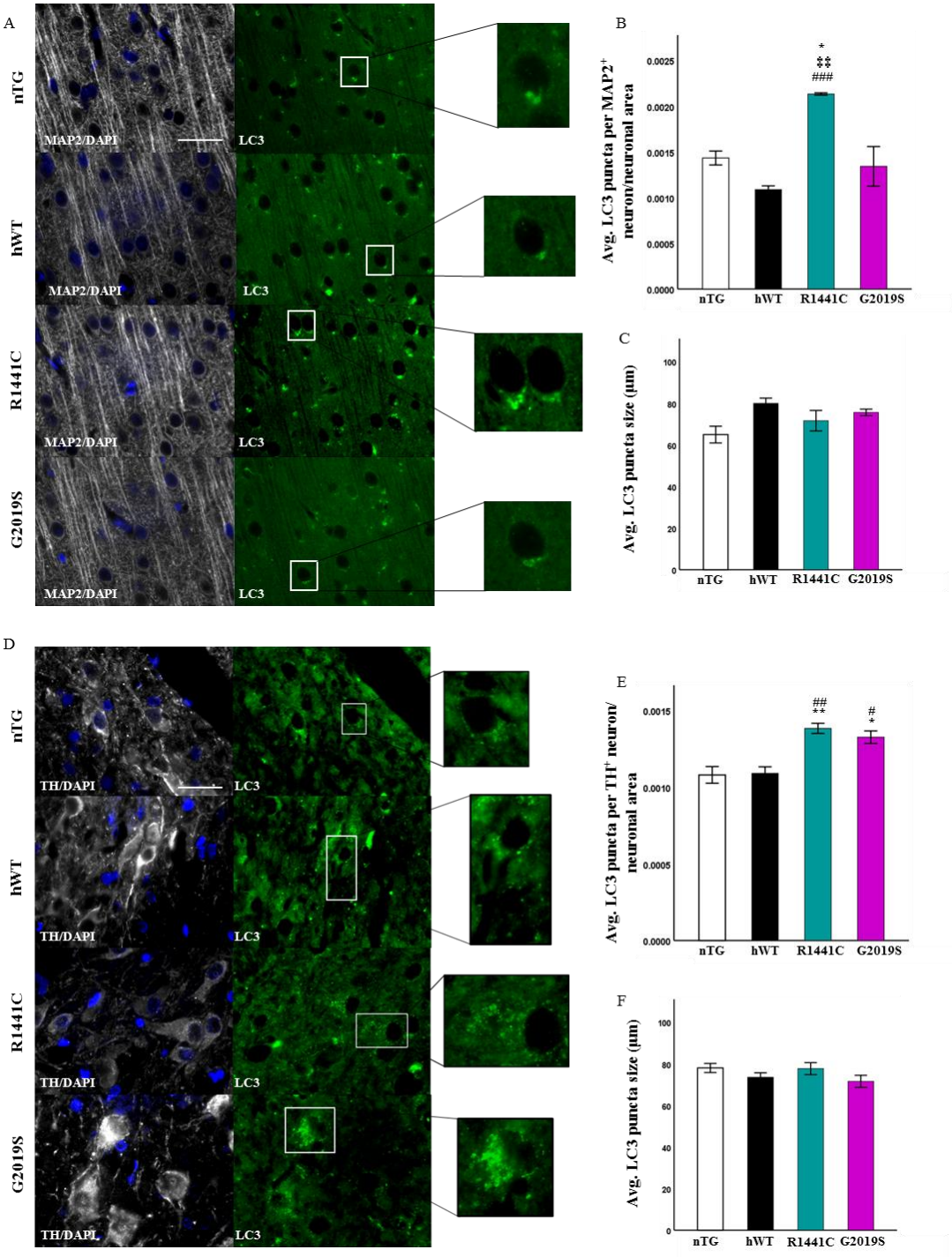


Figure 3.6. Assessing LC3 in aged tissue. *(**A**) 22-month old rat cortical slices were stained for LC3 and MAP2. (**B, C**) LC3 puncta number normalised to MAP2+ cell size and puncta size quantified. (**D**) 22-month old rat midbrain slices were stained for LC3 and TH. (**E, F**) LC3 puncta number normalised to TH+ cell size and puncta size quantified. Bars represent mean +/- SEM. (N = 3; *, P<0.05; **, P<0.005; ***, P<0.001; one-way ANOVA, Tukey HSD post-hoc). * = vs. nTG, # = vs. hWT, ‡ = vs. G2019S. Scale bar = 50 µm.*

3.2.9 Autophagy modulating compound treatments to probe autophagic flux

Steady state LC3-II protein levels and autophagy puncta counts can be difficult to interpret in terms of overall flux through the autophagy pathway as both induction of autophagy and the inhibition of autophagosome clearance can result in the increases observed. However, a decrease in autolysosome maturation indicates an inhibition of autophagosome clearance. LC3-II protein expression and autophagy puncta fold changes were assessed in the presence of modulators of the autophagy pathway to discriminate between these two possibilities. In the presence of chloroquine, which blocks lysosomal acidification and therefore autophagic flux, both LC3-II protein expression (Fig. 3.7a) and autophagosome fold-change (Fig. 3.7b and c) from basal were significantly decreased in LRRK2-R1441C cultures. Furthermore, the autolysosome count for LRRK2-R1441C did not decrease with chloroquine as observed in the other three genotypes. Taken together, these data suggest a block in autophagosome clearance and a deficit in autolysosome maturation in LRRK2-R1441C cortical cultures, as opposed to an increase in autophagy induction. Intriguingly, both hWT and LRRK2-G2019S neurons demonstrated a significant decrease in autophagosome fold-change relative to nTG with chloroquine treatment, with no differences observed in autolysosome fold-change, indicating an inhibition in autophagosome biogenesis (Fig. 3.7b and c).

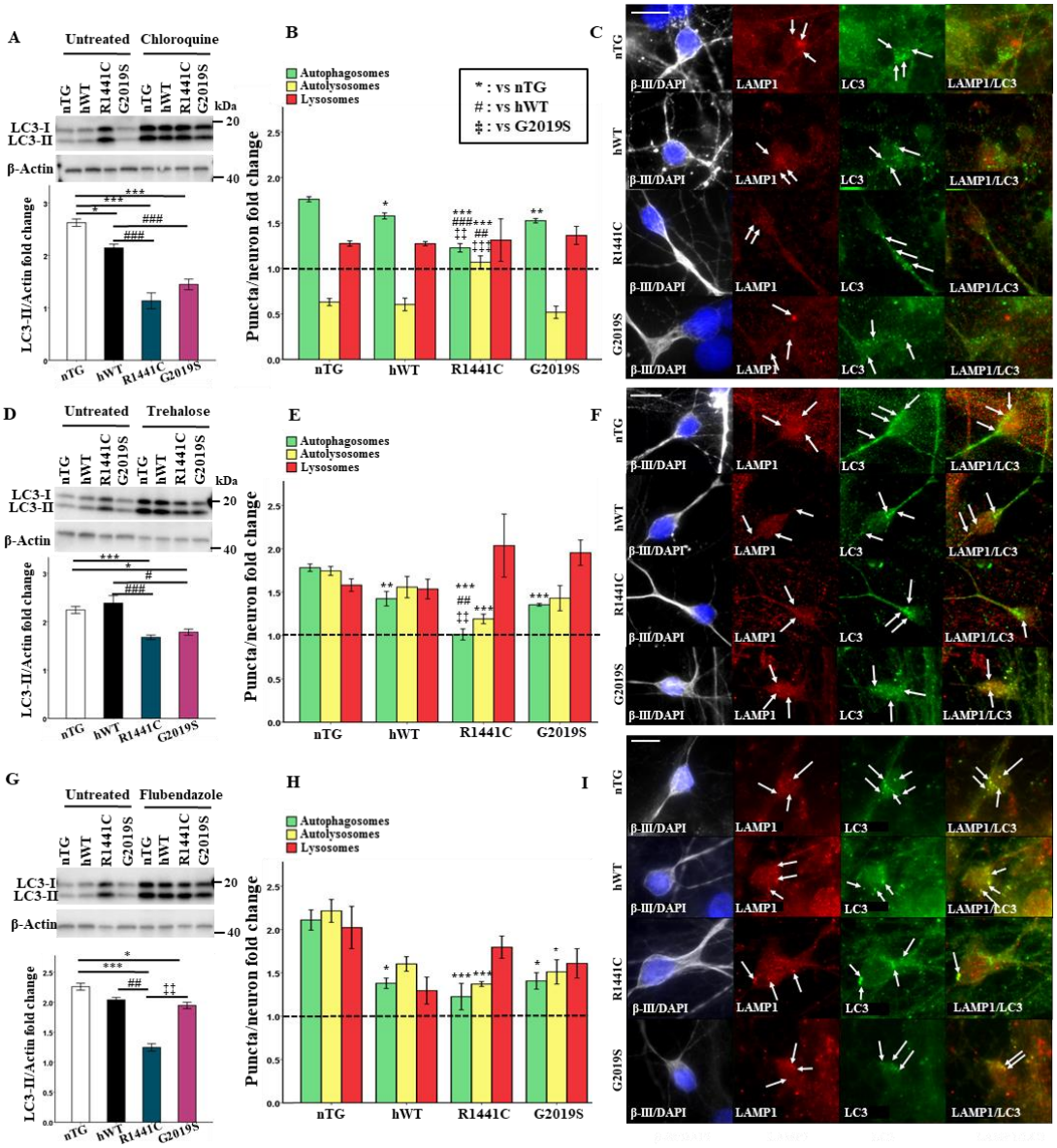


Figure 3.7. Autophagy modulating compound treatments. *(**A**) Western blots for LC3-II fold changes were quantified to assess autophagic flux in response to chloroquine. (**B, C**) 14 DIV cortical cultures were fixed and stained for β-III tubulin, LC3 and LAMP1 and puncta per neuron counts normalised to neuronal size to quantify fold changes from basal in response to chloroquine. This was repeated for (**D, E, F**) trehalose and (**G, H, I**) flubendazole. Bars represent mean +/- SEM (N = 3; *, P < 0.05; **, P<0.005; ***, P<0.001; Kruskal-Wallis non-parametric ANOVA, bonferroni post-hoc). * = vs. nTG, # = vs. hWT, ‡ = vs. G2019S. Scale bar = 10 µm.*

To assess whether the accumulation of autophagosomes in LRRK2-R1441C neurons could be rescued by increasing lysosome number, cultures were treated with trehalose, a compound known to induce lysosomal biogenesis (Sergin et al., 2017) via transcription factor EB (TFEB) nuclear translocation (Wu et al., 2015). Despite an increase in lysosomes after trehalose treatment, LRRK2-R1441C autolysosome fold-change from basal remained significantly decreased compared to nTG (Fig. 3.7e and f), suggesting an inherent autophagosome-lysosome fusion deficiency in these neurons. Furthermore, there was a significant decrease in autophagosome fold-change from basal levels in all three hLRRK2 genotypes compared to non-transgenic (nTG) neurons, suggesting an inhibitory effect of hLRRK2 expression on autophagosome production. A strikingly similar phenotype was present with Flubendazole treatment (Fig. 3.7g, h and i). Flubendazole has been shown to induce autophagy initiation and flux via the destruction of dynamic microtubules, resulting in mTOR deactivation and dissociation from lysosomes leading to TFEB nuclear translocation (Chauhan et al., 2015). Again, despite an increase in lysosomal biogenesis, the LRRK2-R1441C autolysosome phenotype was unable to be rescued, signifying a potential deficit in autolysosome maturation.

3.2.10 Lysosome size and localisation

Many factors contribute to a cells lysosomal fusion capacity including the abundance of lysosomes at the perinuclear microtubule-organizing centre (MTOC), the capacity of autophagosomes to move to the MTOC (Korolchuk et al., 2011) and the acidic intraluminal pH (Kawai et al., 2007). It has been demonstrated that there is a tight coupling between lysosomal pH and lysosomal size, with increased pH reducing both fusion and degradation capacity of lysosomes accompanied by lysosomal swelling (Busch et al., 1996). Lysosomal size and cellular localisation was therefore investigated in primary cortical cultures. After fixing and staining for LAMP1 and MAP2 (Fig. 3.8a), LRRK2-R1441C neurons exhibited increased LAMP1 size (Fig. 3.8b). When co-staining with pericentrin, a marker for MTOC, no differences in LAMP1 puncta distance from MTOC were observed (Fig. 3.8c). Therefore, although there are no discrepancies in lysosome location within the cells, LRRK2-R1441C neurons may have dysfunctional lysosomal pH as indicated by increased lysosomal swelling.

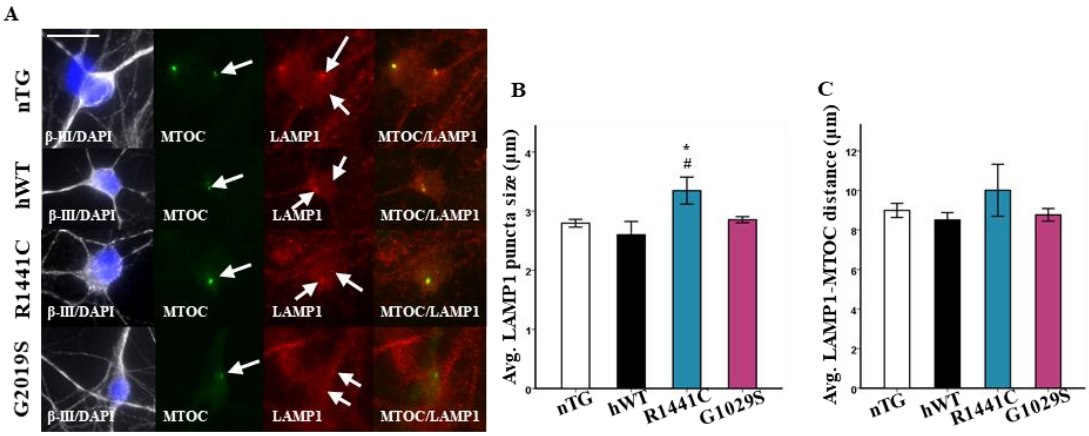


Figure 3.8. Lysosome size and localisation. *(**A**) 14 DIV cortical cultures were fixed and stained for β-III tubulin, LAMP1 and MTOC. (**B, C**) Lysosome size and distance from MTOC were quantified. Bars represent mean +/- SEM (N = 3; *, P < 0.05; Kruskal-Wallis non-parametric ANOVA, bonferroni post-hoc). * = vs. nTG, # = vs. hWT. Scale bar = 10 µm.*

3.2.11 LRRK2 localisation to autophagy-related proteins

It has been reported that hWT and mutant hLRRK2 colocalise with markers of the autophagy pathway (Alegre-Abarrategui et al., 2009). Co-immunofluorescence staining in LRRK2-R1441C primary neurons demonstrated an increase in hLRRK2 colocalisation with the autophagy markers p62 and LAMP1 compared to both hWT-LRRK2 and LRRK2-G2019S cultures (Fig. 3.9a, b, c and d). However, no significant differences were observed between genotypes in transgenic hLRRK2 colocalisation with LC3 (Fig. 3.9e and f). Interestingly, all TG neurons exhibited skein-like hLRRK2-positive structures observed using the YPet tag as previously reported in HEK293 cell lines harbouring the LRRK2-R1441C BAC construct (Alegre-Abarrategui et al., 2009). Further co-immunofluorescence demonstrated that such skein-like structures display discrete co-localisation to the trans-Golgi marker, 58k (Fig. 3.9g and h). Furthermore, LRRK2-R1441C neurons exhibited decreased colocalisation of hLRRK2 to the trans-Golgi marker compared to hWT and LRRK2-G2019S neurons. The decreased colocalisation of LRRK2-R1441C to the trans-Golgi, and its increased colocalisation to autophagic puncta, is a potential mechanism by which mutations alter hLRRK2 normal function.

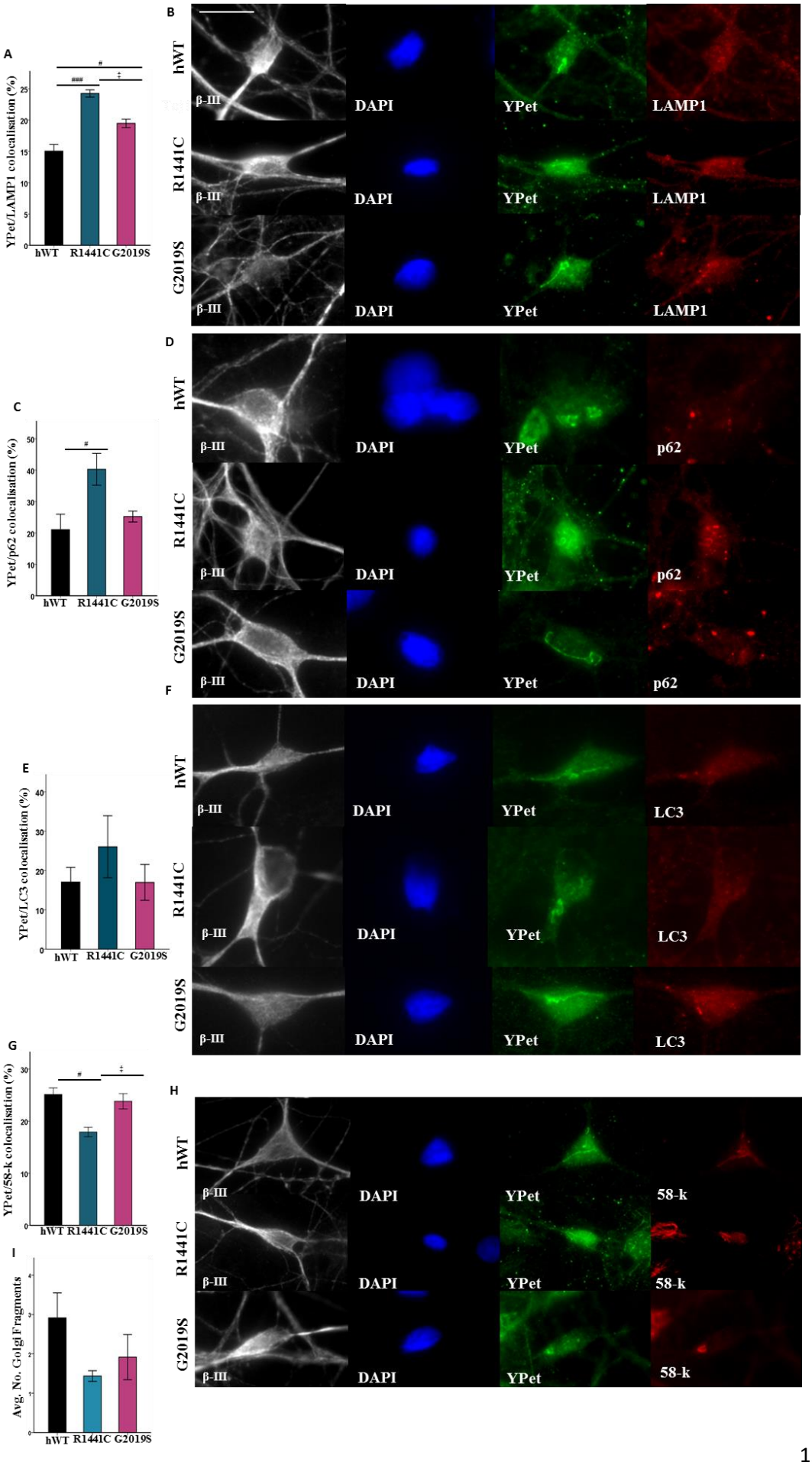

A
YPet/LAMP1 colocalisation (%)
hWT R1441C G2019S
B
hWT
R1441C
G2019S
β-III
DAPI
YPet
LAMP1
C
YPet/p62 colocalisation (%)
hWT R1441C G2019S
D
p62
E
YPet/LC3 colocalisation (%)
hWT R1441C G2019S
F
LC3
G
YPet/58-k colocalisation (%)
hWT R1441C G2019S
H
58-k
I
Avg. No. Golgi Fragments
hWT R1441C G2019S

Figure 3.9. LRRK2 localisation to autophagy proteins. *(**A, B**) 14 DIV cortical cultures were fixed and stained for YPet and LAMP1 and colocalisation quantified in β-III tubulin^{+} cells (% of YPet colocalised). This was repeated for YPet colocalisation to (**C, D**) p62 (**E, F**) LC3 and (**G, H**) 58-k. (**I**) Golgi fragmentation was quantified from 58-k staining in β-III tubulin^{+} cells. Bars represent mean +/- SEM (N = 3; *, P < 0.05; ***, P<0.001; One-way ANOVA, bonferroni post-hoc). * = vs. nTG, # = vs. hWT. Scale bar = 10 μm.*

3.2.12 Effects of human LRRK2 on trans-Golgi fragmentation

Given the genotype dependent alterations in hLRRK2 localisation to the trans-Golgi, and previous evidence implicating LRRK2 in trans-Golgi morphology (Beilina et al., 2014; Fujimito et al., 2018), fragmentation of the trans-Golgi network was quantified in neurons in primary cortical cultures. Despite changes in hLRRK2 localisation to the trans-Golgi network, no changes in particles per neuron were observed (Fig. 3.9i).

3.2.13 Analysing lysosomal protein degradation

To assess whether a decrease in autolysosome maturation was coupled with changes in lysosomal protein degradation, a pulse chase assay using C^{14} radiolabelled valine was carried out, based on the protocol developed by Gronostajski and Pardee (1984). A significant decrease in lysosomal protein degradation was observed in LRRK2-R1441C cortical cultures (Fig. 3.10a). hWT and LRRK2-G2019S cultures had decreased lysosomal protein degradation compared to nTG controls at the final time point, but were still significantly greater compared to LRRK2-R1441C cultures. These changes in protein degradation reflect the changes seen in autophagy puncta counts and autophagic flux already described. These data suggest that the presence of hWT-

LRRK2 or LRRK2-G2019S inhibits the production of autophagosomes, whereas LRRK2-R1441C is capable of decreasing autolysosome maturation.

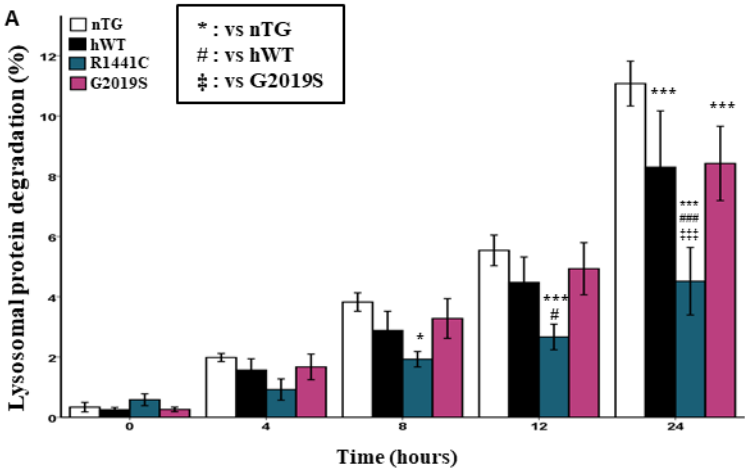


Figure 3.10. Lysosomal protein degradation. *14 DIV cortical cultures were incubated with radiolabelled valine for 48 hours and CPM was measured over 24 hours in untreated cultures or in the presence of chloroquine to calculate lysosomal protein degradation. Bars represent mean +/- SEM (N = 3; *, P < 0.05; **, P<0.005; ***, P<0.001; Two-way ANOVA, bonferroni post-hoc). * = vs. nTG, # = vs. hWT, ‡ = vs. G2019S*

3.2.14 The ubiquitin proteasome system

The need for energetic homeostasis and proteostasis requires that both degradative systems, the ubiquitin proteasome system (UPS) and autophagy, are tightly controlled and coordinated during the lifetime of a cell. These two systems were long considered to be independent from one another. However, genetic studies in mice demonstrated that inactivation of autophagy by the knockout of essential autophagic genes results in the accumulation and aggregation of ubiquitinated proteins (Hara et al., 2006). It has previously been proposed that ubiquitinated proteins could be degraded by autophagy,

and deficits in autophagy lead to a subsequent build up in these undegraded ubiquitin-labelled proteins (Korolchuk et al., 2010). However, there is evidence that impaired autophagy directly effects flux through the UPS. This decreased flux through the UPS is mediated by the accumulation of p62 as its knock-down and overexpression are able to rescue and exacerbate these effects, respectively (Korolchuk et al., 2009; Qiao & Zhang, 2009). Furthermore, several proteins, such as α-synuclein (Cuervo et al., 2004), are known to be substrates of both degradative pathways. Given this, and the observed deficits in autophagy in hLRRK2 neurons, the effects of hLRRK2 on the UPS were investigated.

3.2.15 UPS protein expression and proteasome degradation

Expression of UPS-related proteins was measured to assess basal autophagy levels in cortical cultures. Western blot analysis of ubiquitin showed no significant differences between the hLRRK2 genotypes (Fig. 3.11a and b). It has previously been demonstrated that in response to decreased UPS flux and degradation, there is an increase in the expression of proteins involved in the unfolded protein response (UPR) (Hoyer-Hansen & Jaatela, 2007). The UPR is an ER-to-nucleus signalling pathway that results in the transcriptional activation of a variety of genes, including those involved in protein folding and degradation in the ER. Binding immunoglobulin protein (BIP) is a HSP70 molecular chaperone located in the lumen of the ER that binds newly synthesised proteins as they are translocated into the ER and a target gene product of the UPR. Western blot analysis of BIP showed no significant differences between the hLRRK2 genotypes (Fig. 3.11c).

The same pulse chase assay using C^{14} radiolabelled valine that was carried out to assess lysosomal protein degradation can also be used to assess proteasomal protein degradation. The UPS is responsible for degrading short-lived, abnormal, denatured, or damaged proteins whilst the autophagy pathway, by contrast, is primarily responsible for the degradation of most long-lived proteins. Therefore the timing of sample collection in this assay can be altered to measure protein degradation in these two pathways. Collecting samples in the 24 hour period prior to when samples are collected to measure lysosomal protein degradation, and utilising the proteasome inhibitor MG132, allows for the measurement of proteasomal protein degradation. A significant decrease in proteasomal protein degradation was observed in LRRK2-R1441C cortical cultures. Additionally, a significant decrease was observed in hWT-LRRK2 and LRRK2-G2019S cultures however these were still significantly increased relative to LRRK2-R1441C cultures (Fig. 3.11d).

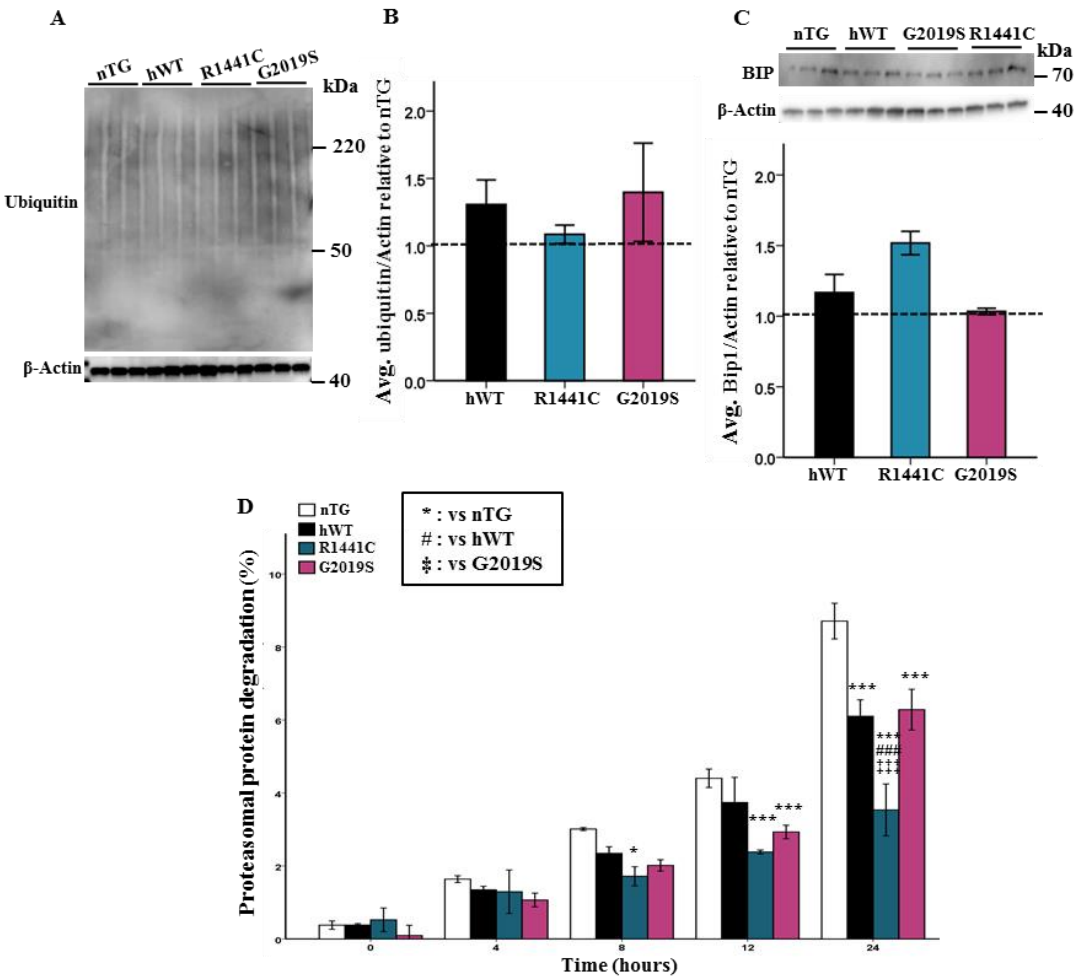


Figure 3.11. Ubiquitin proteasome system. *Western blots for (**A, B**) ubiquitin and (**C**) BIP protein levels were quantified (Bars represent mean +/- SEM, N = 3; One-Way ANOVA, Tukey HSD post-hoc). (**D**) 14 DIV cortical cultures were incubated with radiolabelled valine for 48 hours and CPM was measured over 24 hours in untreated cultures or in the presence of MG132 to calculate proteasomal protein degradation. Bars represent mean +/- SEM (N = 3; *, P < 0.05; **, P<0.005; ***, P<0.001; Two-way ANOVA, bonferroni post-hoc). * = vs. nTG, # = vs. hWT, ‡ = vs. G2019S*

3.3 Discussion

This chapter described the establishment of primary mixed cortical cultures to characterise the effect of PD-associated *LRRK2* mutations on the autophagy pathway. Despite previous reports in the literature, pure astrocytic cultures had decreased LRRK2 protein expression relative to mixed cortical cultures. In peripheral immune cells, stimulation by LPS increases LRRK2 expression (Shapansky et al., 2014) via the activation of Toll-like receptor (TLR4) and the consequential stimulation of the MyD88-dependent pathway (Dzamko et al., 2014). LPS and interferon-γ were applied to pure astrocytic cultures in an attempt to increase transgene expression, as previously demonstrated, to upregulate LRRK2 expression in monocytes (Gardet et al., 2011). However, the application of these pro-inflammatory molecules was unable to increase LRRK2 protein expression in these cultures and the lack of STAT1 expression, a crucial transcription factor in astrocyte activation (Barcia et al., 2011), is most likely responsible for this. Three possible hypotheses can be drawn from these data; pure astrocytic cultures are in a robust resting state and require more stimulation, astrocytes in these cultures are not functional, or these cultures may contain an alternative, perhaps progenitor, glial cell. It has been demonstrated that progenitor cells do not have the capacity to perform glutamate uptake like mature astrocytes (Santos et al., 2017). The pure astrocytic cultures were able to take up glutamate and therefore it would appear they are functional and are indeed astrocytes. However, due to the lack of LRRK2 protein expression, and the inability to increase LRRK2 protein expression with pro-inflammatory stimulation, it was deemed appropriate to continue all work in the primary cortical cultures with mixed cell-types.

In this chapter the effects of PD-associated *LRRK2* mutations on the autophagy pathway in primary cortical cultures were reported. Mixed primary cortical cultures demonstrated that LRRK2-R1441C and hWT-LRRK2/LRRK2-G2019S exert differential effects on the autophagy pathway. LRRK2-R1441C inhibits the maturation of autolysosomes, with LRRK2-R1441C expressing neurons displaying increased co-localisation with both p62 and LAMP1, as well as a decrease in trans-Golgi localisation compared to that of hWT-LRRK2 and G1029S-LRRK2. Furthermore, the inability to rescue the observed autolysosome maturation deficit in LRRK2-R1441C expressing neurons by increasing lysosomal biogenesis, is suggestive of an inherent deficit in lysosomal function in these cultures. This is further supported by the observation that LRRK2-R1441C expressing cultures demonstrate decreased lysosomal protein degradation relative to nTG, hWT-LRRK2 and LRRK2-G2019S expressing cultures. These observations place hLRRK2-R1441C at the lysosome, at the point of autophagosome-lysosome fusion.

With regards to hWT-LRRK2 and LRRK2-G2019S, the decrease in autophagic flux reported suggests that the expression of either hWT-LRRK2 or LRRK2-G2019S is capable of inhibiting the production of autophagosomes, a phenotype that has previously been reported in the literature (Manzoni et al., 2016, Manzoni et al., 2013, Sanchez-Danes et al., 2012). This is however the first time that the inhibitory effect of LRRK2 in this process has been described in primary neurons. It has recently been reported that LRRK2 is able to inhibit the autophagy pathway via its interaction with Beclin1-containing class II PI3-kinase (Manzoni et al., 2016) and that this Beclin1 complex colocalises with trans-Golgi markers (Kihara et al., 2001). The colocalisation of the hWT-LRRK2 and LRRK2-G2019S transgene to the trans-Golgi could therefore

underlie its inhibitory role on the autophagy pathway as observed in the results presented. Furthermore, many validated as well as potential LRRK2 targets are involved in pathways converging and diverging at the Golgi. Rab8 and Rab3 have been verified as true LRRK2 targets (Steger et al., 2016) and both of these GTPases have been implicated in biosynthetic trafficking from the Golgi to the ER and plasma membrane (Stenmark, 2009; Galea and Simpson 2015).

The definitive read-out of autophagy activity is the degradation of proteins by the lysosome. Although other assays can be employed to indirectly measure this, such as the delivery of mRFP-GFP-LC3 to the lysosome (which exploits the difference in the nature of these two fluorescent proteins), the radioactive pulse chase assay is considered the most quantitative assay. It provides a precise numerical readout that reflects the fate of all long-lived cellular proteins and avoids the pitfalls associated with measuring a single autophagic substrate such as LC3 or p62. Only two other reports have used the methods employed here to assess the effects of LRRK2 on lysosomal protein degradation, where it was reported that the *I2020T* and *G2019S* mutations lead to increased and decreased lysosomal protein degradation, respectively (Ohta et al., 2008; Henry et al., 2015). However, reports utilising alternative methods have also demonstrated changes in protein degradation in the presence of mutant LRRK2 (Gomez-Suaga et al., 2014).

Autophagy phenotypes were also replicated *in vivo,* with LRRK2-R1441C neurons in aged cortical tissue exhibiting increased LC3-positive puncta. With regards to reporting changes in autophagy protein levels *in vivo*, the current literature is varied. Unlike in the brain, alterations in LC3 and p62 protein levels have consistently been reported in

the kidneys of LRRK2-TG animals (Tong et al., 2010; Hinkle et al., 2012; Tong et al., 2012) most notably due to much higher expression levels of LRRK2 in the kidneys relative to the brain, making it crucial for kidney homeostasis (Biskup et al., 2006; Herzig et al., 2011). Conversely, such differences are not always seen in the brain of LRRK2-TG animals. Various reports have described no changes (Tsika et al., 2014; Tsika et al., 2015), whereas both increases (Yue et al., 2015; Ramonet et al., 2011) and decreases (Schapansky et al., 2018; Orenstein et al., 2013) have also been reported. There are a number of reasons for these inconsistencies. Firstly, results may vary with regards to the region of the brain being reported on. For example the data reported here demonstrated that LRRK2-G2019S had differential effects on LC3 protein expression in the cortex compared to the *SNpc*. Secondly, there are differences in the use of cDNA, the complete LRRK2 genomic DNA sequence or the use of exogenous or endogenous promotors. Models which have reported no differences in autophagy protein levels have utilised exogenous promotors such as synapsin1 (Tsika et al., 2015) or a conditional-DAT-cre system (Tsika et al., 2014) and therefore potentially fail to recapitulate the physiological spatiotemporal expression patterns of hLRRK2. In contrast, data presented here utilise a BAC model which, due to the use of the full human genetic locus and its native promotor, ensures more physiologically appropriate expression patterns.

Alterations in the UPS have previously been demonstrated in other models (Däschel et al., 2007; Tong et al., 2010; Lichtenberg et al., 2011) and the kinase activity of LRRK2 has been shown to not be critical for its impairment of the UPS (Lichtenberg et al., 2011). It is therefore not surprising that we observed that the LRRK2-G2019S mutation does not confer additional toxicity compared with hWT-LRRK2. It is feasible that a

kinase-independent toxic mechanism depends on exceeding a threshold level of activity, which may be lowered by pathogenic mutations. This kind of mechanism is supported by the finding that homo- and heterozygous carriers of *LRRK2* mutations are clinically indistinguishable (Ishihara et al., 2006).

As described, the data presented in this chapter places LRRK2-R1441C at the lysosome, at the key point of autophagosome-lysosome fusion. This phenotype of decreased autolysosome maturation in mutant LRRK2 models has previously been reported in the literature (Sanches-Danes et al., 2012). However, what is lacking in such reports that describe a build-up of autophagic vacuoles without confirming decreased autolysosome maturation (Plowey et al., 2008; Alegre-Abarrategui et al., 2009; Ramonet et al., 2011; Gomez-Suaga et al., 2012; Saha et al., 2014), is a comprehensive characterisation of the lysosomes in these models. Therefore, the exact role of LRRK2 at the lysosome is still unclear. Given this, the focus of the remainder of the data presented will focus primarily on identifying underlying deficits in LRRK2-R1441C lysosomes and their effect on the observed decrease in autolysosome maturation and lysosome protein degradation.

Chapter 4: Identifying mechanisms underlying lysosomal deficits in mutant LRRK2 cortical cultures

4.1 Introduction and aims

Lysosomes are cytoplasmic membrane-enclosed organelles containing hydrolytic enzymes that degrade macromolecules and cell components. Many factors regulate lysosomal function and subsequent protein degradation, which will be investigated in this chapter in order to identify underlying mechanisms of the previously described LRRK2-R1441C autolysosome maturation deficit.

Lysosomes depend on maintaining a highly acidic pH in their lumen to successfully perform their digestive function. It is well established that lysosomal pH is maintained by the action of vacuolar-type H^+ ATPase (vATPase), a membrane-bound proton pump that uses the free energy of ATP hydrolysis to drive protons against their electrochemical gradient into the lysosomal lumen. The vATPases are multisubunit complexes composed of a cytosolic, soluble V_1 subcomplex and a membrane-embedded V_0 subcomplex. Each subcomplex is composed of multiple protein subunits (see Fig. 4.1). In a recent meta-analysis of GWAS's the neuron specific, a1 subunit of the V_0 subcomplex, encoded by *ATP6V0A1*, was identified as a novel PD risk loci (Chang et al., 2017). With each proton pumped by the vATPase, a voltage difference across the lysosomal membrane is generated which inhibits further pumping. Therefore, the movement of a counterion accompanies proton movement in order to dissipate the transmembrane voltage. Graves et al. (2008) demonstrated that it is the

action of a separate pump, an antiporter exchanging two Cl^- ions moving into the lysosomal lumen for a single proton moving out, that facilitates this process. The ClC family of Cl^- channels and antiporters is the largest known family of Cl^- transporters and can be subdivided into those found on intracellular organelles and those found on the plasma membrane. There is broad agreement that ClC-7 is a $2Cl^-/1H^+$ antiporter localized in the lysosomal membrane and ClC-4/5 and 6 are localised to endosomes and late endosomes, respectively (Mindell, 2012).

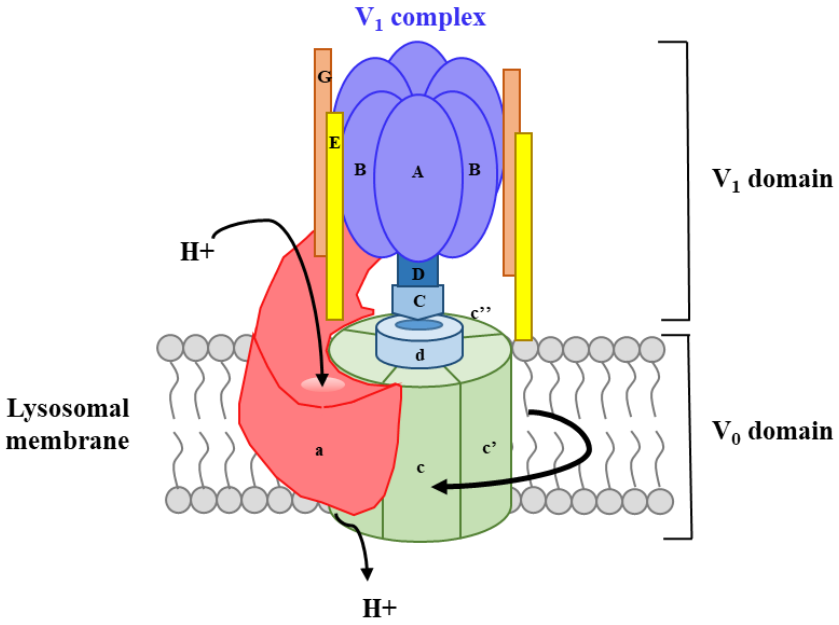


Figure 4.1. Structure of the v-type proton ATPase. *The soluble V_1 complex (purple) is made up of the ATP hydrolysing A and B subunits. The rotor, made up of the c, c' and c'' subunits (green), is embedded in the membrane and carries protons from uptake sites on the cytoplasmic side to release sites on the lysosome lumen side. The a subunit (red) contains access pathways to both sides of the membrane. The a1 isoform is specific to neurons and the ATP6V0A1 locus is associated with PD. The D and C subunit of the V_1 domain and the d subunit of the V_0 domain comprise the central stalk (blue) which connects the two domains. The E and G subunits (orange and yellow) compose the peripheral stalks*

Substantial shifts in pH, such as those induced by drugs like chloroquine, can severely disrupt degradative enzyme activity and also block fusion of autophagosomes and lysosomes (Klionsky et al., 2008). Elevations in lysosomal pH have previously been reported in cellular models of Alzheimer's disease (AD) (Coffey et al., 2014; Lee et al., 2010) and lysosome dysfunction is increasingly placed at the centre of neurodegenerative disease pathways. Increased lysosomal pH would not only decrease lysosomal fusion capacity and lysosomal enzyme activity (Lee et al., 2010), but has also been reported to have much more far-reaching consequences. Altered lysosomal degradation induces axonal transport impairment (Lee et al., 2011) and increases oxidised lipids and ROS (Yang et al., 2008), leading to lysosomal membrane permeabilisation resulting in apoptosis and necrosis (Guicciardi et al., 2004). Evidence for the role of LRRK2 in lysosomal pH modulation is contradictory, with both increases and decreases in lysosomal pH being reported in different model systems (Gomez-Suaga et al., 2012; Henry et al., 2015). As was previously discussed in chapter 3, the reason for such conflicting reports is primarily due to the use of different model systems and the methods LRRK2 expression and LRRK2 expression levels.

Ca^{2+} is one of the most common second messengers involved in a variety of intracellular signalling events, which in turn control a vast array of cellular processes, including gene expression, exocytosis, cell growth, cell motility and cell death (Clapham, 2007; Berridge, 2012). The Ca^{2+} concentration in lysosome lumen ($[Ca^{2+}]_{iy}$) is estimated to be about 500 μM (Patel & Cai, 2015). The local Ca^{2+} release from lysosomes is crucial for lysosome function; lysosome fusion capacity has been shown to be inhibited by the Ca^{2+} chelator 1,2-bis(2-aminophenoxy) ethane-N,N,N′,N′-tetraacetic acid (BAPTA) and this inhibition was reversed by adding additional Ca^{2+}

(Pryor et al., 2000). An expanding number of lysosomal ion channels, including Ca^{2+}-permeable ones, have been identified. TRPML1 (transient receptor potential cation channel 1) belongs to the mucolipin subfamily, which also includes TRPML2 and 3. These proteins are all non-selective cation channels that contain a predicted six transmembrane domain with cytosolic amino (N)- and carboxyl (C)- termini, as well as a channel pore located between transmembrane 5 and 6 that is permeable to Na^{+} and Ca^{2+} ions. Mutations in human *MCOLN1*, which encodes for TRPML1, have been associated with Mucolipidosis type IV disease (ML-IV), a lysosomal storage disorder (LSD) characterized by accumulation of various lipids in lysosomes (Feng & Yang, 2017).

The final step in the autophagy pathway is achieved by membrane fusion between the autophagosome and lysosome. At present, several groups of proteins have been implicated in the autophagosome-lysosome fusion process, including SNARE proteins. Functionally, SNAREs are classified into v-SNAREs and t-SNAREs, which are associated with vesicle and target compartments, respectively (Jahn & Scheller, 2006). SNARE proteins are crucial to the completion of membrane fusion between autophagosomes and lysosomes. Specific to the autophagy pathway, is has been suggested that syntaxin-17 (v-SNARE) interacts with the cytosolic synatosomal-associated protein 29 (SNAP29; v-SNARE) (Itakura et al., 2012) and lysosomal VAMP7 (Fader et al., 2009), and VAMP8 (Furuta et al., 2010) (t-SNAREs), for the autophagosome-lysosome fusion. LRRK2 has been implicated in SNARE protein interaction; LRRK2 has been found to interact with the endocytic SNARE complex and LRRK2-dependent phosphorylation of Snapin in hippocampal neurons of rats

decreases the number of readily releasable vesicles and the extent of exocytotic release (Yun et al., 2013).

Important evidence for a physiological role of LRRK2 in regulating autophagy has come from *Lrrk2*$^{-/-}$ animals. Age-dependent, bi-phasic alterations in LC3-II and p62 have been reported in *Lrrk2*$^{-/-}$ kidneys (Tong et al., 2012) together with the accumulation of lysosomes in peripheral organs (Baptista et al., 2013). Elevated lipofuscin has also been reported in *Lrrk2*$^{-/-}$ kidneys (Baptista et al., 2013). However, decreases in LC3 accumulation have also been reported in other cell models such as macrophages (Schapansky et al., 2014), suggesting possible cell-type specific effects of the knock-out of Lrrk2. It is therefore currently unclear if the effects of mutant LRRK2 on the autophagic system are caused by a toxic gain or loss-of-function.

Increased kinase activity has been reported in PD-associated *LRRK2* mutations, with the exception of Y1699C, as measured by phosphorylation of the autophosphorylation site Ser1292 (Sheng et al., 2012; Steger et al., 2016). Furthermore, the overexpression of the LRRK2 kinase domain, as well as inhibition of LRRK2 kinase activity, induces alterations of the autophagy-lysosomal pathway (Gomez-Suaga et al., 2012; Manzoni et al., 2013; Saez-Atienzar et al., 2014). The potential link between LRRK2 kinase activity and cellular function, coupled to dysfunction of LRRK2 in disease, has spurred the development of small molecular inhibitors targeting this enzymatic activity (Atashrazm & Dzamko, 2016). Cis-2,6-dimethyl-4-(6-(5-(1-methylcyclopropoxy)-1H-indazol-3-yl)pyrimidin-4-yl)morpholine (MLi-2), is a potent, selective, and centrally active inhibitor of LRRK2 kinase activity that has been described as suitable for

exploring the therapeutic potential and safety of LRRK2 kinase inhibition (Fell et al., 2015).

Chapter aims

1. Establish if the mutant LRRK2 autophagy deficits observed are driven by a toxic loss or gain-of-function
2. Identify the role of the LRRK2 kinase domain in the regulation of autophagy
3. Identify lysosomal dysfunction underlying the LRRK2-R1441C autophagy deficit

4.2 Results

4.2.1 Characterising the effect of Lrrk2-knock out on the autophagy pathway

Primary cortical cultures were prepared from *Lrrk2*$^{-/-}$ rats to compare the loss-of-function phenotype with mutant autophagy phenotypes likely caused by a gain-of-function. Lrrk2 expression in primary cortical cultures was first assessed to confirm KO at the protein level (Fig. 4.2a). A significant increase in LC3-II protein level was observed in *Lrrk2*$^{-/-}$ primary cortical cultures compared to WT littermates (Fig. 4.2b). No changes were observed in LAMP1 or p62 protein expression (Fig. 4. 2c and d). In order to assess whether this increase in LC3-II was caused by an increase in autophagosomes and/or autolysosomes, LC3/LAMP1 co-immunofluorescence was performed. Both autophagosome and autolysosome numbers were significantly

increased in *Lrrk2*$^{-/-}$ neurons (Fig. 4.2e and f) and a pulse chase assay demonstrated that this was associated with an increase in lysosomal protein degradation (Fig. 4.2g). Overall, these data are consistent with WT Lrrk2 having a physiological function of reducing autophagic activity.

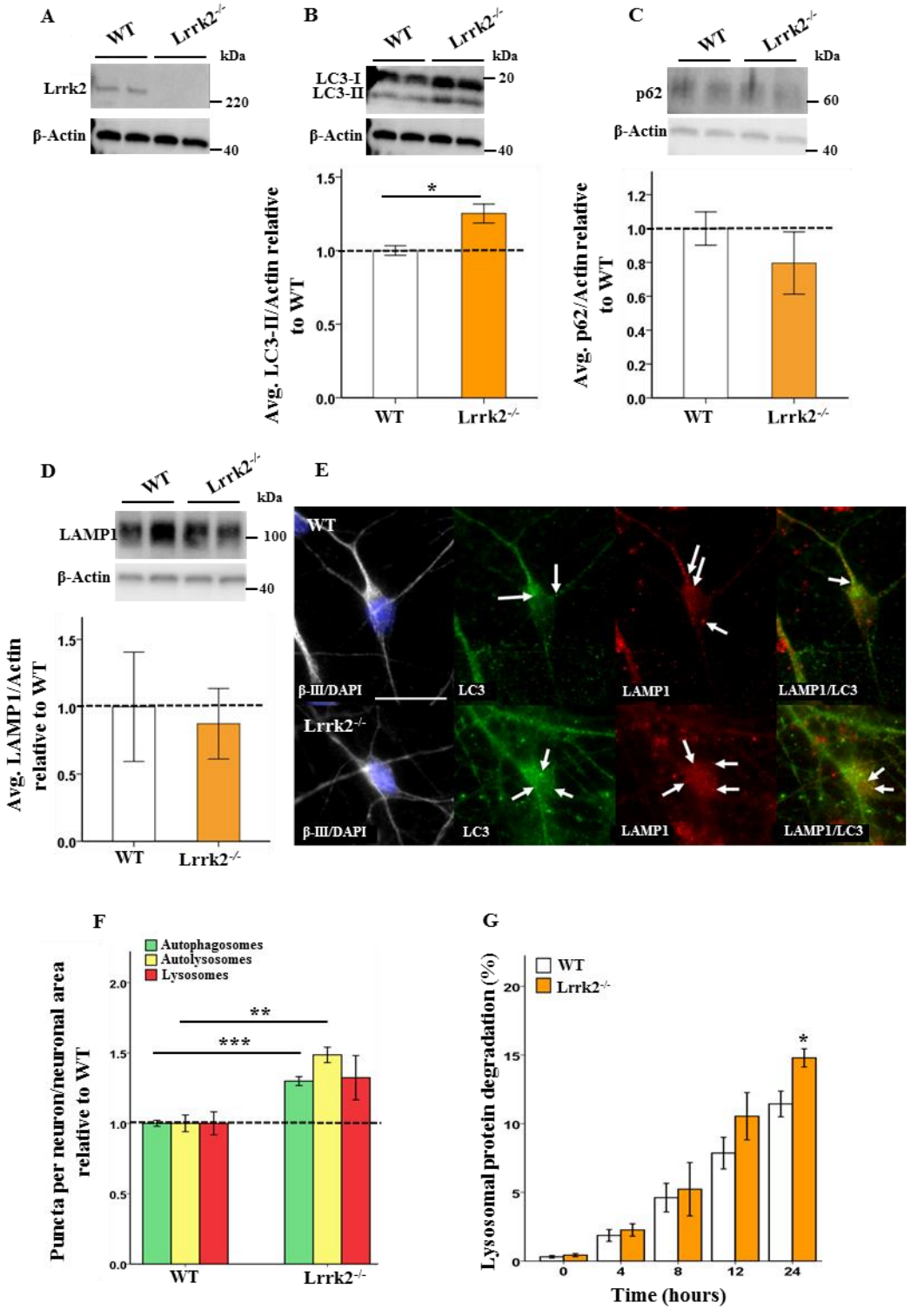


Figure 4.2. Lrrk2$^{-/-}$ neurons have increased autophagic activity *Primary cortical cultures from P1 pups were generated and characterised. (**A**) Western blots for Lrrk2 were quantified to ensure knock-out. (**B, C, D**) Western blots for LC3-II, p62 and LAMP1 were quantified and normalised to WT littermate controls in order to assess basal protein level. (**E, F**) Lrrk2$^{-/-}$ DIV 14 cultures were fixed and stained for LC3/LAMP1/MAP2 and co-immunofluorescence and puncta quantified and normalised to littermate controls (bars represent mean +/- SEM, N = 3; *, P<0.05; Independent Samples T-test). (**G**) 14 DIV neuronal cultures were incubated with radiolabelled valine for 48 hours and CPM was measured over 24 hours in untreated cultures or in the presence of chloroquine to calculate lysosomal protein degradation. Bars represent mean +/- SEM (N = 3; *, P < 0.05; Two-way ANOVA, bonferroni post-hoc). Scale bar = 10 μm.*

4.2.2 The role of LRRK2 kinase activity in autophagy

Utilising the MLi-2 compound described above, primary cortical cultures were prepared and treated with MLi-2 at 50 nM for 2 hours and LRRK2 phosphorylation levels were assessed to establish that kinase activity had been decreased (Fig. 4.3a). At basal levels, an increase in phosphorylated LRRK2 at Ser1292 was observed in LRRK2-G2019S and LRRK2-R1441C cultures relative to hWT-LRRK2, however this failed to reach significance (Fig. 4.3b). Both LRRK2-R1441C and LRRK2-G2019S cortical cultures had a significantly decreased fold-change in Ser1292 levels compared to both nTG and hWT-LRRK2 cultures (Fig. 4.3c). LC3-II protein levels were assessed by western blot to observe potential downstream effects of LRRK2 kinase inhibition on autophagy. hWT and LRRK2-G2019S both demonstrated increased LC3-II levels in response to MLi-2 treatment whilst no significant changes were seen in LRRK2-R1441C cultures (Fig. 4.3d, e, f and h). Intriguingly, MLi-2 had the opposite effect on endogenous Lrrk2 in nTG cultures, decreasing LC3-II levels. In order to confirm that

observed alterations in LC3-II levels were dependent on LRRK2 kinase inhibition as opposed to off target effects, *Lrrk2*$^{-/-}$ cultures were treated with MLi-2. No changes in LC3-II levels were observed in *Lrrk2*$^{-/-}$ cultures with MLi-2 treatment relative to WT litter mate controls (Fig. 4.3g and i). As has been discussed, alterations in LC3-II levels, whilst telling, cannot differentiate between inhibition of autophagy at the point of the lysosome and activation at the point of autophagosome biogenesis. Pulse chase assays were therefore performed in order to quantify protein degradation in response to kinase inhibition. Reflecting the alterations in LC3-II protein levels, lysosomal protein degradation was significantly increased in response to MLi-2 treatment in both hWT and LRRK2-G2019S cultures (Fig. 4.3j). LRRK2-R1441C cultures, however, showed no significant changes in protein degradation levels with kinase inhibition. As well, a significant decrease in lysosomal protein degradation was also observed in nTG cultures with MLi-2 cultures, reflecting LC3-II protein expression fold changes.

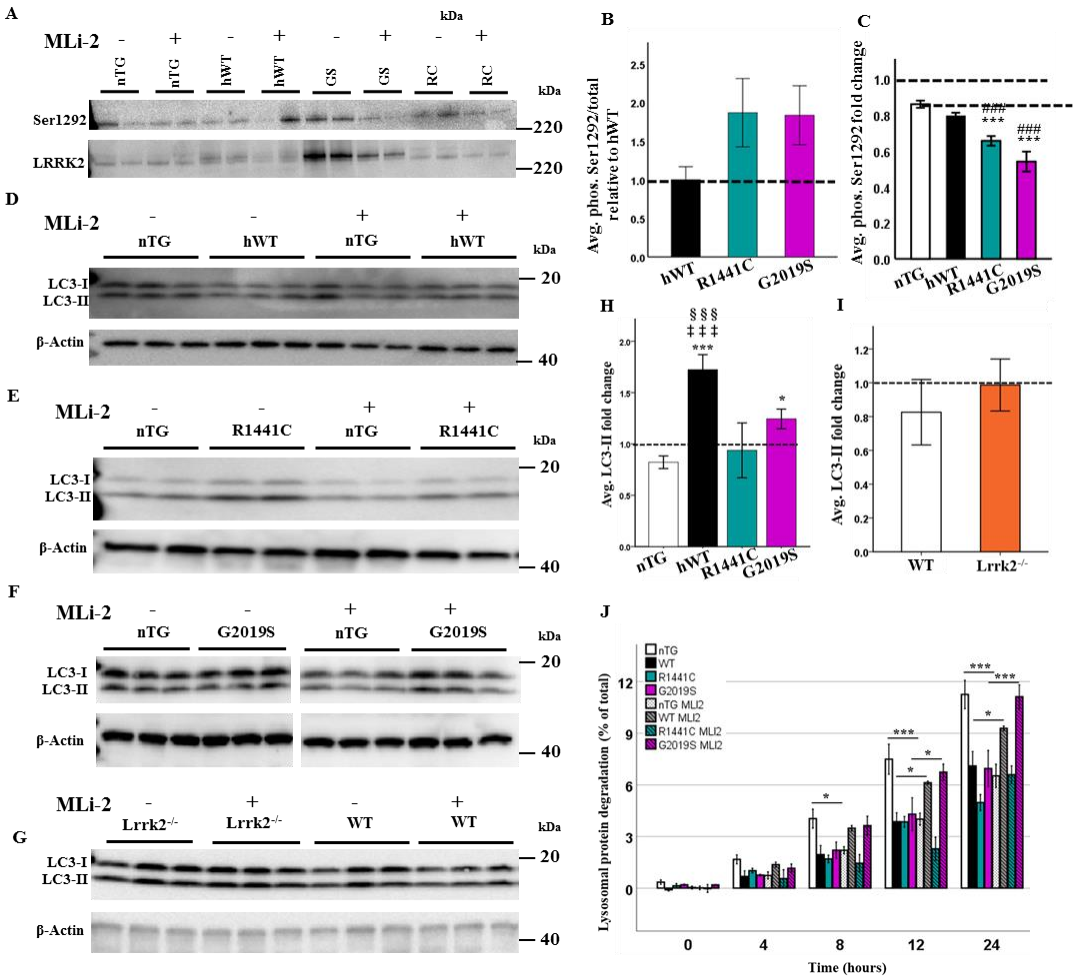


Figure 4.3. LRRK2 kinase inhibition and autophagy *(**A**) Primary cortical cultures at DIV 14 were treated with the LRRK2 kinase inhibitor MLi-2 and assessed for phosph.LRRK2 at Ser1292 expression via western blot (GS = G2019S, RC = R1441C). (**B**) Basal levels of phos.LRRK2 at Ser1292 over total LRRK2 was quantified. (**C**) Phos.LRRK2 at Ser1292 fold-change in response to MLi2 was quantified. (**D, E, F, G**) Primary cortical cultures were treated with MLi-2 and LC3-II expression was observed via western blot. (**H**) LC3-II fold changes in response to kinase inhibition were quantified (N = 3; *, P < 0.05; ***, P < 0.001; Kruskal-Wallis non-parametric ANOVA, bonferroni post-hoc) * = vs. nTG, § = vs. R1441C, ‡ = vs. G2019S. **(I)** LC3-II fold change in response to MLi-2 were quantified in Lrrk2$^{-/-}$ DIV 14 cultures and WT littermate controls (Bars represent mean +/- SEM, N = 3; Independent Samples T-test). **(J)** 14 DIV cultures were incubated with radiolabelled valine and CPM was measured over 24 hours in untreated or Mli-2 treated cultures calculate lysosomal protein degradation. Bars represent mean +/- SEM (N = 3; *, P < 0.05; ***, P < 0.001; Three-way ANOVA, bonferroni post-hoc).*

4.2.3 Quantifying lysosomal pH

Both lysosomal degradation and autophagosome-lysosome fusion are highly dependent on lysosomal pH. As defects in autolysosome maturation were evident in LRRK2-R1441C neurons, we asked if altered lysosomal pH could account for the compromised vesicle fusion. Using the pH sensitive dye LysoSensor™ Green DND-189, which exhibits increased fluorescence in increasingly acidic organelles, and using a pH/fluorescence standard curve in cells incubated in pH-calibrated solutions (Fig. 4.4a), lysosomal pH levels were quantified in cortical cultures. Measurement of average lysosomal pH across genotypes demonstrated that lysosomal pH was significantly increased in LRRK2-R1441C expressing cultures, with an average lysosomal pH of 5.5 (Fig. 4.4b and c).

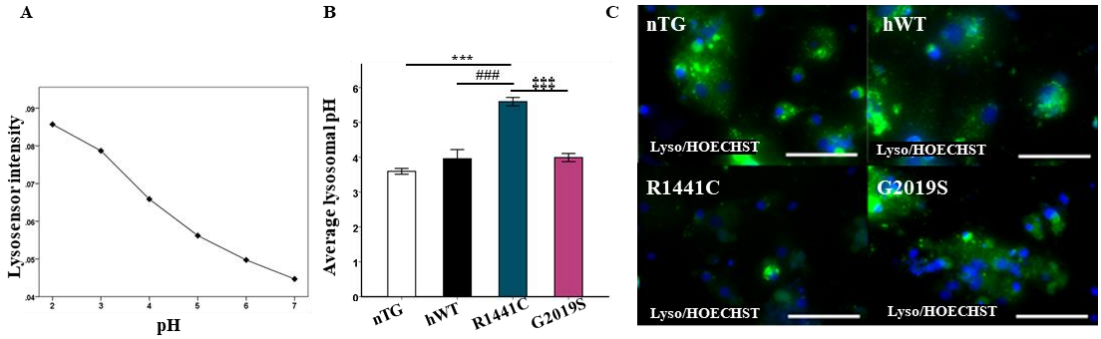


Figure 4.4. R1441C neuronal cultures exhibit increased lysosomal pH. *(**A**) Using the pH sensitive dye lysosensor, pH titrated buffers were used to create a lysosomal pH standard curve. (**B, C**) From this, lysosomal pH was quantified in primary cortical cultures from P1 pups at DIV 14. HOECHST = live cell nuclei marker. Bars represent mean +/- SEM (N = 3; ***, P<0.001; Kruskal-Wallis non-parametric ANOVA, bonferroni post-hoc). * = vs. nTG, # = vs. hWT, ‡ = vs. G2019S. Scale bar = 200 µm.*

4.2.4 Assessing lysosomal pH pump expression

As described, the primary driver of acidification of the lysosome is the vATPase proton pump. The a1 subunit of this pump situated in the transmembrane complex has been found to be a risk loci for PD and was therefore assessed in this model. Protein level quantification revealed that this subunit was down regulated in LRRK2-R1441C cultures and was also upregulated in LRRK2-G2019S cultures (Fig. 4.5a and b). mRNA expression of the a1 subunit revealed no significant differences between genotypes (Fig. 4.5c), suggesting the differences seen at protein level are not caused by changes in transcription

Counterion pathway is also crucial for maintaining lysosomal pH in order to dissipate the luminal-positive transmembrane voltage generated by proton translocation. The ClC family of chloride channels have been implicated and identified as crucial to this process. mRNA quantification of these different antiporters revealed no significant differences between genotypes in ClC-4/5/6/7 mRNA expression levels (Fig. 4.5d, e, f and g).

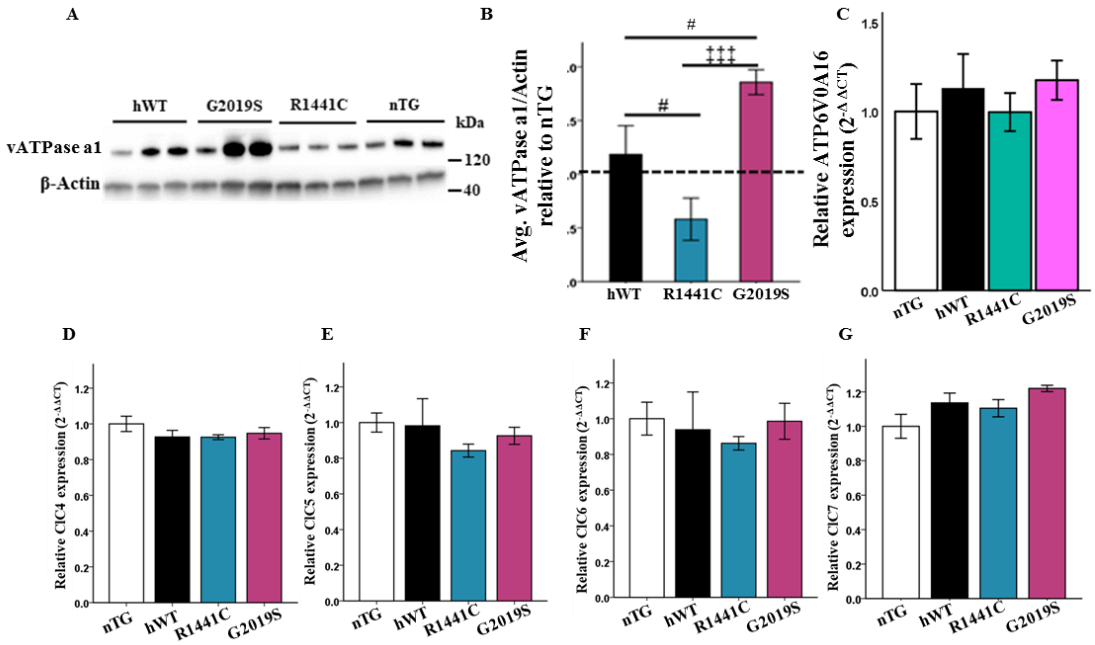


Figure 4.5. R1441C cortical cultures exhibit decreased vATPase a1 expression. *(**A, B**) vATPase a1 protein expression levels were assessed and quantified in 14 DIV primary cortical cultures from transgenic animals and normalised to nTG littermate control levels (bars represent mean +/- SEM, N = 3; *, P<0.05, One-Way ANOVA, Tukey HSD post-hoc). mRNA levels for (**C**) vATPase a1, (**D**) ClC4, (**E**) ClC5, (**F**) CLC6 and (**G**) ClC7 were measured and quantified ($2^{-\Delta\Delta CT}$) relative to nTG in DIV 14 primary cortical cultures. Bars represent mean +/- SEM (N = 3; Kruskal-Wallis non-parametric ANOVA, bonferroni post-hoc).*

4.2.5 The effects of LRRK2 on intracellular calcium stores

Local Ca^{2+} release from lysosomes is required for late endosome-lysosome fusion (Pryor et al., 2000). We therefore measured Ca^{2+} signalling from different intracellular stores in primary cultures using the ratiometric Ca^{2+} sensitive dye, Fura2-AM. We first showed a significantly increased whole cell Ca^{2+} content in LRRK2-R1441C cultures assayed by the response to ionomycin (Fig. 4.6a and b). It was also observed that LRRK2-R1441C expression induced a significantly decreased fluorescence ratio at

basal levels prior to compound administration (Fig. 4.6c). Together this suggests an increase in Ca^{2+} in intracellular stores and a decrease in cytosolic Ca^{2+} levels.

We then administered compounds to assess the Ca^{2+} content of specific organelles. Gly-Phe-β-naphthylamide (GPN) is a membrane permeant peptide which diffuses into the cells and into lysosomes, where it is cleaved by the peptidase cathepsin C (found only in lysosomes) (Berg et al., 1994). The products of GPN accumulate in lysosomes and, because these products are osmotically active, cause the organelles to swell and rupture, releasing lysosomal content (Mindell, 2012). GPN led to an increased response in LRRK2-R1441C cultures relative to the other genotypes (Fig. 4.6d and e). No significant differences between genotypes were observed in response to FCCP or CPA (Fig. 4.6f, g, h and i) which lead to Ca^{2+} release from the mitochondria and ER, respectively. The increase in whole cell Ca^{2+} content in response to ionomycin was therefore presumably caused by alterations in lysosomal Ca^{2+}.

TRPML1 is a cation channel located on lysosomal membranes and is one of the channels responsible for the local release of Ca^{2+}. We used ML SA1, a compound capable of inducing TRPML1 mediated Ca^{2+} release, to investigate release from lysosomes. We observed a significantly decreased lysosomal Ca^{2+} release in response to ML SA1 in the LRRK2-R1441C cultures relative to all other genotypes (Fig. 4.6j and k) as well as a significant decrease in ML SA1 response in LRRK2-hWT and LRRK2-G2019S relative to nTG. Such decreased local Ca^{2+} release may explain the decrease in fusion efficiency seen between the autophagosomes and lysosomes.

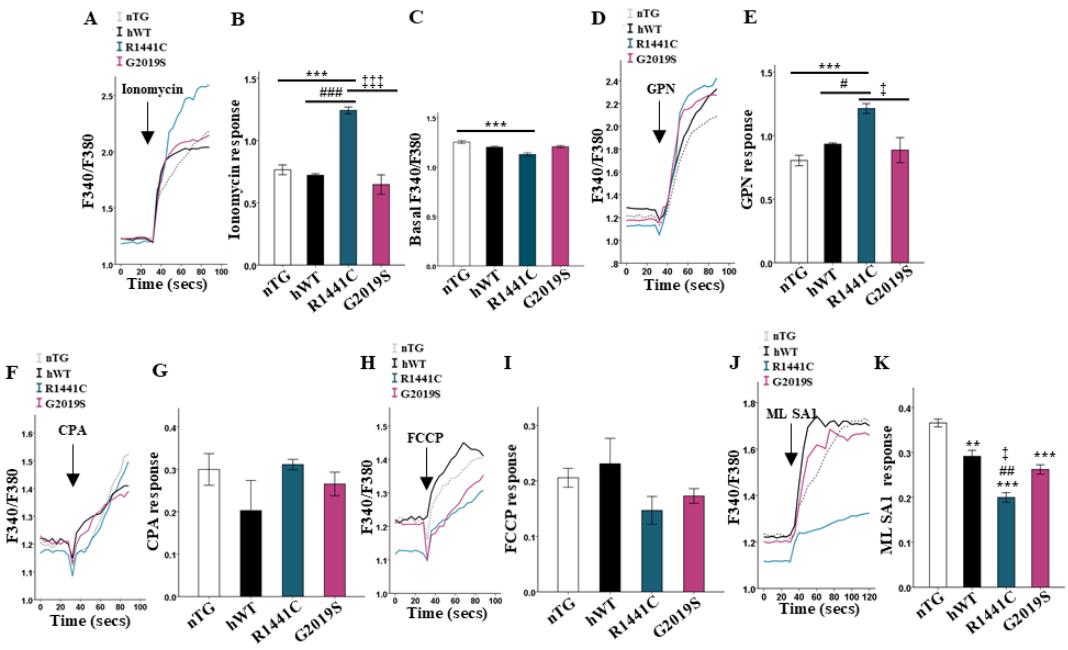


Figure 4.6. R1441C neurons have impaired lysosome Ca^{2+} ***dynamics.*** *(**A, B**) 14 DIV cortical cultures were incubated with Fura2-AM and fluorescence ratio quantified at basal and after the injection of ionomycin and delta quantified. (**C**) Baseline Fura2-AM was quantified across all lines to assess cytosolic* Ca^{2+} *content. (**D, E**) GPN was used in order to quantify lysosomal* Ca^{2+} *content. (**F, G**) CPA was used in order to quantify ER* Ca^{2+} *content. (**H, I**) FCCP was used in order to quantify mitochondira* Ca^{2+} *content. (**J, K**) ML SA1 was used in order to quantify* Ca^{2+} *release from TRPML1 channels. Bars represent mean +/- SEM (N = 3; *, P < 0.05; **, P<0.005; ***, P<0.001; Kruskal-Wallis non-parametric ANOVA, bonferroni post-*

Given these observations, mRNA expression levels were quantified for *Mcoln1*, the gene encoding for TRPML1, to determine whether a decreased response to ML SA1 in LRRK2-R1441C cultures is caused by decreased channel expression. No significant differences in *Mcoln1* mRNA expression levels between genotypes were observed (Fig. 4.7a). Although not reaching statistical significance (p=0.051), a trend was observed for decreased *Mcoln2* mRNA in LRRK2-R1441C cultures compared to LRRK2-G2019S cultures (Fig. 4.7b).

TPCs are a novel family of endolysosomal Ca^{2+} channel proteins. TPC2 is localised to lysosomes and is the receptor for NAADP. It has been demonstrated that a lysosomal NAADP receptor such as TPC2 may be a target for LRRK2, (Gómez-Suaga et al., 2012). This causes Ca^{2+} release from lysosomes, followed by Ca^{2+}-induced Ca^{2+} release from the ER and activation of a CaMKK/AMPK pathway to induce autophagy, while simultaneously alkalinizing lysosomal pH (Gómez-Suaga et al., 2012). TPC2 mRNA quantification revealed no significant differences between genotypes (Fig. 4.7c). NAADP, like other major messengers for Ca^{2+} mobilization, is passively membrane-impermeant. Therefore a cell-permeant acetoxymethyl ester derivative of NAADP (NAADP-AM) is often synthesised and utilised in order to study NAADP-mediated Ca^{2+} release. Due to logistical restraints, however, NAADP-AM could not be purchased for this study. NAADP-AM is an extremely unstable compound, and is currently not made to purchase in the UK. Suppliers are located in the USA (AAT Bioquest) and do not ship to the UK.

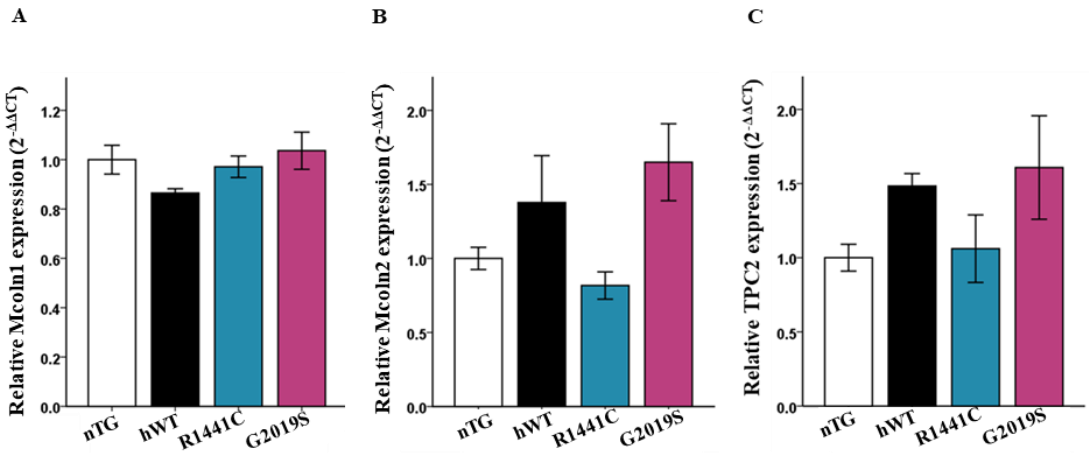


Figure 4.7. Ca2+ channel mRNA expression. *mRNA levels for (**A**) Mcoln1, (**B**) Mcoln2 and (**C**) TPC2 were measured and quantified ($2^{-\Delta\Delta CT}$) relative to nTG in DIV 14 primary cortical cultures. Bars represent mean +/- SEM (N = 3; Kruskal-Wallis non-parametric ANOVA, bonferroni post-hoc).*

4.2.6 Changes in SNARE protein and RNA levels in primary cortical cultures

It has been suggested that syntaxin-17 interacts with the cytosolic SNAP29 and lysosomal VAMP7 and VAMP8 for the autophagosome-lysosome fusion. Given the evidence of a potential autophagosome-lysosome fusion deficit in LRRK2-R1441C cultures, the protein and mRNA expression levels of these SNARE components were assessed. A significant decrease in syntaxin-17 protein expression was observed in both LRRK2-G2019S and LRRK2-R1441C cultures (Fig. 4.8a and b). No significant differences were observed in SNAP29 expression (Fig. 4.8c and c) and a decrease in VAMP7 was seen in LRRK2-R1441C cultures (Fig. 4.8e and f). Significant differences in expression were also seen at the mRNA level (Fig. 4.8g, h and i).

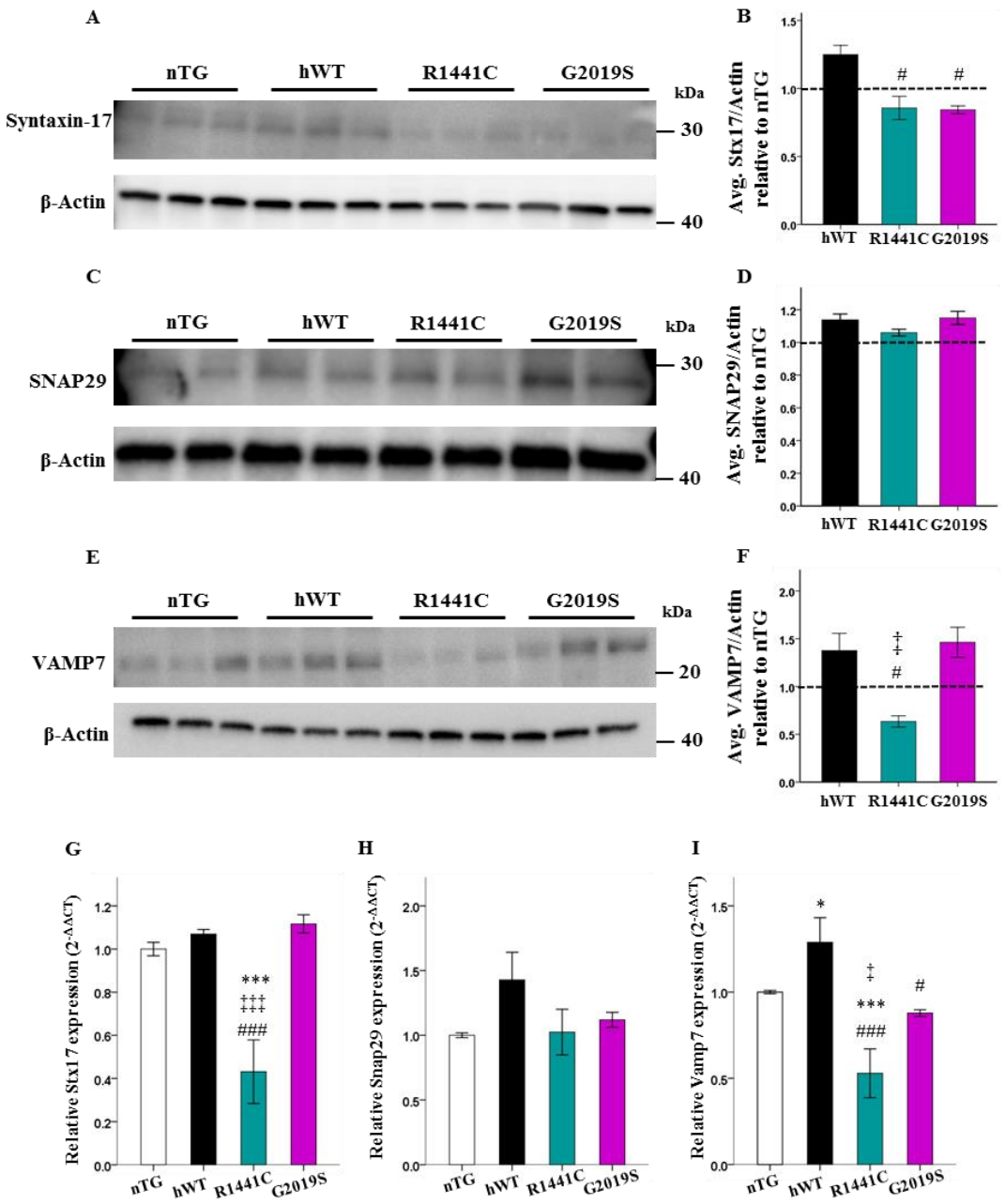


Figure 4.8. SNARE protein and mRNA levels. *Western blots for (**A, B**) Syntaxin-17, (**C, D**) SNAP29 and (**E, F**) VAMP7 protein expression levels were assessed and quantified in 14 DIV primary cortical cultures from transgenic animals and normalised to nTG littermate controls (bars represent mean +/- SEM, N = 3; *, P<0.05; One-Way ANOVA, Tukey HSD post-hoc). mRNA levels for (**G**) Syntaxin-17, (**H**) Snap29 and (**I**) Vamp7 were measured and quantified ($2^{-\Delta\Delta CT}$) relative to nTG in DIV 14 primary cortical cultures. Bars represent mean +/- SEM (N = 3; Kruskal-Wallis non-parametric ANOVA, bonferroni post-hoc). # = vs. hWT, ‡ = vs. G2019S.*

4.2.7 Characterising LRRK2-vATPase a1 binding

vATPase a1 is a subunit enriched in neurons in the transmembrane V_0 subcomplex of the vATPase proton pump which is trafficked to and from the Golgi to the lysosome. Here it is able to form the full vATPase complex with the V_1 subcomplex. I hypothesised that LRRK2 is a binding partner of the a1 subunit of vATPase and is a component of regulating its trafficking. Co-immunoprecipitation with both endogenous Lrrk2 in nTG cell lysates and YPet in hLRRK2-TG cell lysates was performed in order to assess binding to vATPase a1. I demonstrated that endogenous rodent Lrrk2 is capable of binding to vATPase a1. Furthermore, hWT and LRRK2-G2019S also bind to this subunit however, LRRK2-R1441C demonstrates a loss of this binding capacity (Fig.4.9a and b). It must be noted, however, that to ensure a true interaction/loss-of-interaction between hLRRK2 and vATPase a1, appropriate co-IPs for positive and negative controls need to be carried out. In this instance, co-IP for hLRRK2 and 14-3-3, and vATPase a1 and Lrrk1 would be appropriate positive and negative controls, respectively.

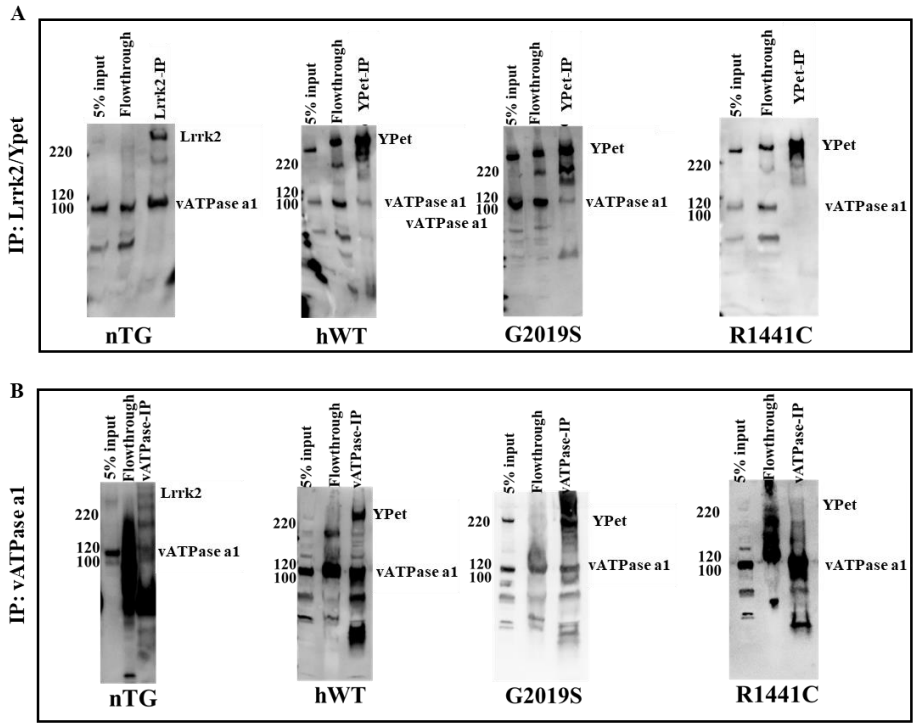


Figure 4.9. LRRK2 and vATPase a1 co-immunoprecipitation. *(**A**) Lrrk2 and YPet were immunoprecipitated from nTG and TG, respectively, cortical cultures at 14 DIV and vATPase a1 protein expression observed. (**B**) vATPase a1 was immunoprecipitated from nTG and TG cortical cultures at 14 DIV and Lrrk2/YPet protein expression observed*

4.2.8 Monitoring vATPase a1 cellular localization

In order to replicate what was observed in the co-immunoprecipitations, vATPase a1–YPet colocalisation was assessed via co-immunofluorescence. A significant decrease in vATPase a1 colocalisation to LRRK2-R1441C, relative to hWT-LRRK2, was observed (Figure 4.10a and b). The vATPase a1 subunit is localised to the lysosomal membrane and is trafficked from the Golgi to its cellular target. The correct binding of vATPase a1 to interaction partners mediates this trafficking. vATPase a1 colocalisation to the Golgi and lysosomes was therefore assessed. A significant decrease in vATPase a1-LAMP1 colocalisation was observed in LRRK2-R1441C neurons relative to both hWT-LRRK2 and LRRK2-G2019S. Furthermore, a significant increase was observed

in LRRK2-G2019S neurons, relative to hWT-LRRK2 (Figure 4.10c and d). A signficiant decrease in vATPase a1-58k colocalisation was also observed in both LRRK2-R1441C and LRRK2-G2019S neurons relative to hWT-LRRK2 (Figure 4.10e and f). It can therefore be concluded that a loss in LRRK2-R1441C binding capacity to vATPase a1 is associated with the mislocalisation of the vATPase a1 subunit. Furthermore, the increase in vATPase a1 protein expression in LRRK2-G2019S cortical cultures observed in Figure 4.5 is associated with increased vATPase a1 localisation to the lysosome in these neurons.

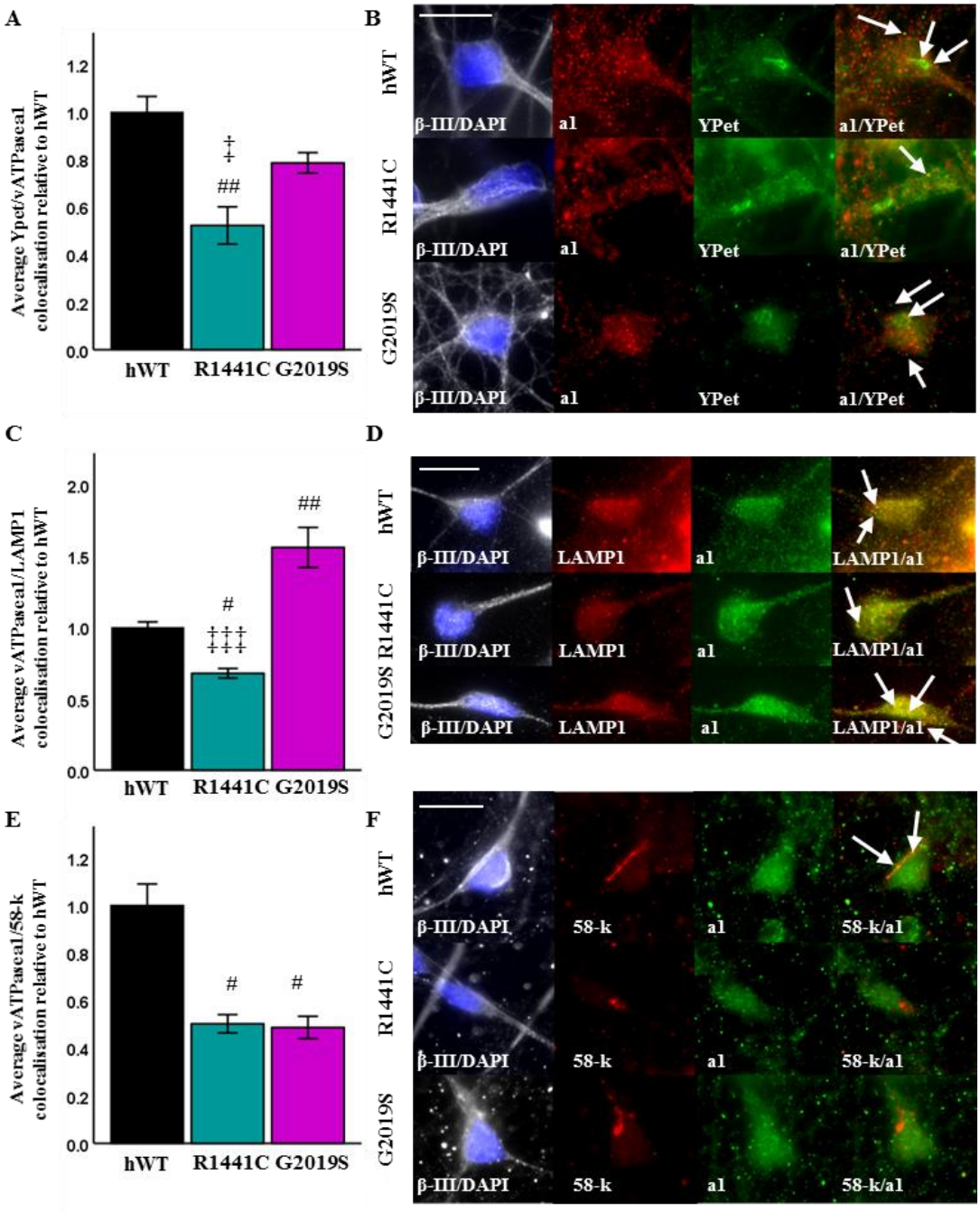


Figure 4.10 vATPase a1 cellular localisation . *(**A, B**) 14 DIV cortical cultures were fixed and stained for YPet, vATPase a1 and β-III tubulin and colocalisation quantified relative to hWT. (**C, D**) Colocalisation between vATPase a1 and LAMP1 was quantified relative to hWT in 14 DIV cortical cultures (**E, F**) Colocalisation between vATPase a1 and the Golgi marker 58-k was quantified relative to hWT in 14 DIV cortical cultures. Bars represent mean +/- SEM (N = 3; *, P < 0.05; **, P < 0.01; ***, P<0.001; Ove-way ANOVA, bonferroni post-hoc). * = vs. nTG, # = vs. hWT. Scale bar = 10 μm.*

4.2.9 Observing vATPase a1 glycosylation

vATPase a1 subunit is glycosylated in the ER and loss of this glycosylation leads to impaired delivery to the lysosome (Lee et al., 2010). Lysates from cortical cultures were treated with PNGase F, an amidase which removes N-linked oligosaccharides from glycolproteins, in order to deglycosylate the vATPase a1 subunit. This enzyme was used as opposed to Endo H, a commonly used glycosidase, as it has been demonstrated that vATPase a1 is insensitive to Endo H deglycosylation (Lee et al., 2010). PNGase F treated lysates were probed for vATPase a1 protein and compared to untreated samples. PNGase F treatment was able to degylcosylate vATPase a1 (Fig. 4.11a) and this was apparent in all genotypes. Intriguingly, a lower molecular weight band was observed in the PNGase F treated samples as well as a lower molecular weight band in the untreated LRRK2-R1441C and LRRK2-G2019S samples. It was hypothesised that these intermediate bands may represent partially deglycosylated vATPase a1. In order to determine this, the heavily glycosylated protein LAMP1 was probed for. It was observed that LAMP1 was fully deglycosylated as indicated by the presence of a lower molecular weight band at 42 kDa in PNGase F treated samples (Fig. 4.11b). It seems therefore that there are no differences in glycosylation of vATPase a1 between genotypes. However, the presence of this lower molecular weight band may be indicative of a cleaved product or potential splice variant of the subunit.

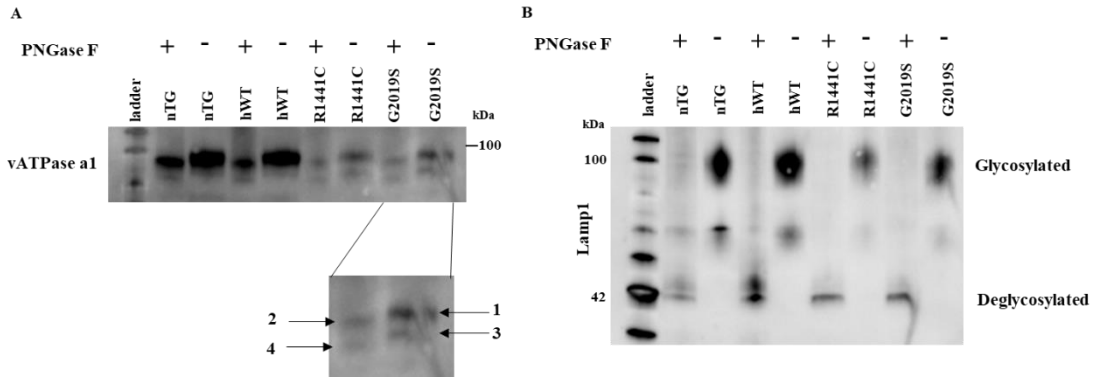


Figure 4.11. vATPase a1 glycosylation. *(**A**) Primary cortical culture lysates were probed for vATPase a1 in the presence or absence of PNGase F to observe deglycosylation. (**B**) Primary culture lysates were probed for LAMP1 in the presence or absence of PNGase F to observe deglycosylation. 1 = Glycosylated, 2 = deglycosylated 3 = Cleaved product/splice variant 4 = Cleaved product/Splice variant deglycosylated*

4.3 Discussion

In this chapter the effects of *LRRK2* mutations on lysosome regulation and function were reported. It was demonstrated that LRRK2-R1441C cortical cultures exhibit a decrease in lysosomal acidity as well as an increase in lysosome Ca^{2+} content with concomitant decreases in cytosolic Ca^{2+} levels. This increase in lysosomal Ca^{2+} was accounted for by decreased local Ca^{2+} release from the lysosomal Ca^{2+} channel, TRMPL1. Based on data from *Lrrk2*$^{-/-}$ cultures described here, this phenotype is due to a gain-of-function with the *LRRK2-R1441C* mutation. It appears that the origin of this phenotype may be alterations in vATPase a1 subunit expression levels and interaction with LRRK2-R1441C compared to the other genotypes, whereby a decrease in both protein expression level and interaction with LRRK2-R1441C were reported.

This is the first time such an increase in autophagy levels with *Lrrk2*$^{-/-}$ has been reported in neurons from primary cortical cultures. Much of the prominent autophagy related phenotypes in *Lrrk2*$^{-/-}$ models have been reported in kidney tissue (Tong et al., 2012). This has primarily been accounted for by the fact that LRRK2 has higher expression in the kidneys relative to the nervous system (Biskup et al., 2007) as well as the fact that the LRRK2 paralogue, LRRK1, is expressed in the brain and therefore may be able to compensate for a loss of LRRK2 in KO models. Other phenotypes have been described in the brains of KO models, such as alterations in dendritogenesis (Hinkle et al., 2012), impaired synaptic vesicle endocytosis and transmission in the hippocampus (Arranz et al., 2014) and a protective effect of loss of Lrrk2 from LPS exposure in the *SNpc* (Daher et al., 2014). LRRK2 has been found to be decreased in certain brain regions such as the midbrain relative to others (Sloan et al., 2016) which may elucidate to why exposure to stressors such as LPS are required to make the effects of *Lrrk2*-KO apparent. As well, it has been argued that rats show a greater level of susceptibility to PD-promoting toxin exposure and genes (Zheng et al., 2012). Therefore, similarly, an effect of *Lrrk2*-KO may be more apparent in rats than mice, which may explain why an effect of *Lrrk2*-KO on autophagy was observed in cortical neurons here.

I described here that LRRK2 kinase inhibition is able to ameliorate the inhibitory effects of hWT-LRRK2 and LRRK2-G2019S on autophagosome biogenesis, a finding previously demonstrated in the literature (Manzoni et al., 2016). However, this was not observed in LRRK2-R1441C cultures, with lysosomal protein degradation remaining decreased, indicating that kinase activity may in fact not be putative to this lysosomal phenotype. Furthermore, kinase inhibition of endogenous Lrrk2 in nTG cultures elicited the opposite effect on autophagy, decreasing lysosomal protein degradation.

One potential explanation for such discrepancy may lie in inherent differences between human LRRK2 and rodent Lrrk2. Previous reports demonstrating the inhibitory effects of LRRK2 on autophagy using kinase inhibitors have primarily depended on the use of human cell lines (Manzoni et al., 2018; Manzoni et al., 2016). Although one report did demonstrate this same phenotype in bone-derived dendritic cells from a mouse model of IBD (Takagawa et al., 2018) and another in primary cortical astrocytes (Manzoni et al., 2016) the role of the kinase domain in autophagy regulation was only demonstrated using the inhibitor, LRRK2-IN1. LRRK2-IN1 has been shown to have significant off-target effects (Luerman et al., 2014) and specifically off target effects on the autophagy pathway (Schapansky et al., 2014). Therefore the findings in Takagawa et al. (2018) and Manzoni et al. (2016) are potentially confounded by this. However, Manzoni et al. (2016) did confirm the affects of LRRK2 kinase inhibition on autophagy with the alternative inhibitor GSK2578215A, and showed no off-target affects of both inhibitors with the use of $LRRK2^{-/-}$ astrocytes. Conversely, with more selective inhibitors it has been demonstrated that Lrrk2 kinase inhibition decreases autophagy and phagocytosis in murine monocytes and microglia (Schapansky et al., 2014). Furthermore, a biomarker for lysosomal degradation, di-docosahexaenoyl (22:6) bis(monoacylglycerol) phosphate (di-22:6-BMP), was decreased in the urine of non-human primates treated with LRRK2 kinase inhibitors (Fuji et al., 2015). Collectively, together with the data presented here, it seems the role of LRRK2 kinase activity in autophagy may not be conserved between species.

I described in this chapter that the presence of LRRK2-R1441C induces decreased Ca^{2+} release from TRPML1 channels situated on the lysosome membrane. Interestingly, both the ion conductance and channel open probability of TRPML1 are regulated by

pH. Chen et al. (2014) found that, upon channel activation, channel conductance was higher at pH 4.6 than at pH 7.2. It seems, therefore, that the loss of lysosomal acidity in the LRRK2-R1441C cortical cultures presented here could be the underlying cause of the TRPML1 Ca^{2+} release deficit. However, in work that contradicts Chen et al. (2014), Raychowdhury et al. (2004) found that TRPML1 activity was in fact inhibited by acidic pH. However, the two conflicting studies can in fact be consolidated. It was shown that in Raychowdhury et al. (2004) that, although acidic pH reduced the current of the channel, it did not affect the single channel conductance. Therefore, taking the two together, it seems that TRPML1 is more likely to open as pH rises, but when it is open, ion conductance is higher at more acidic pH. It therefore could be feasible that decreased lysosomal acidity could be the culprit behind altered lysosomal Ca^{2+} dynamics described here. However, it should be noted that most of the work investigating TRMPL1 regulation has been conducted in non-physiological conditions, using constitutively active mutants (Feng et al., 2014) and receptors in the absence of ligands (Raychowhdury et al., 2004). The effect of pH on TRPML1 function therefore needs further characterisation in order to be fully elucidated.

It has also been previously suggested that the regulation of lysosomal Ca^{2+} release by lysosomal luminal pH may be bi-directional, with lysosomal Ca^{2+} able to regulate lysosomal pH. Another proposed mechanism for the dissipation of the luminal-positive transmembrane voltage, as well as anion permeability via ClC channels, is cation transportation. TRPML channels have been suggested as responsible for this and *MCOLN1* mutations in ML-IV patient fibroblasts increase lysosomal pH (Bach et al., 1999), supporting this hypothesis. However, whereas ClC channels have been well established in the counterion pathway in lysosomal pH regulation, evidence for the role

of TRMPL channels is more tentative. For example, TRPML channels have also been shown to both maintain (Pryor et al., 2006) and even decrease lysosomal pH (Soyombo et al., 2006). Therefore, the exact role of Ca^{2+} channels in lysosomal pH regulation remains to be determined.

It has also been demonstrated that increased lysosome lumen Ca^{2+} content can decrease TRPML1 function (Li et al., 2017). Luminal pore aspartate residues of the TRPML channel carry negative charges which attracts and binds extracellular/luminal Ca^{2+}, thereby blocking Ca^{2+} release and monovalent cation conduction. However, lowering the lysosomal pH to 4, which is close to the pKa of the aspartate side chain, results in protonation of the aspartates and reduces the net amount of negative charge and attenuates the Ca^{2+} block. It therefore appears that a dual role of pH and Ca^{2+} are responsible for TRPML1 regulation which could lend an explanation to the concomitant increase in luminal Ca^{2+} and decrease in TRMPL1 Ca^{2+} release observed in the data presented here.

Lysosomal pH is implicated in lysosomal Ca^{2+} loading (Christensen et al., 2002). H^+ pumps, which exhibit a decrease in function with an increase in lysosomal pH, have been speculated to be responsible (Chruchill et al., 2002). It is curious therefore that LRRK2-R1441C cortical cultures demonstrated an increase in lysosomal Ca^{2+} content, despite having more alkaline lysosomal lumen. However, it has recently been demonstrated that the inhibition of vATPase H^+ pumps does not prevent lysosomal Ca^{2+} refilling (Garritty et al., 2016). Furthermore, previous research implicating lysosomal pH in lysosomal Ca^{2+} loading has been solely carried out in sea urchin oocytes. Whether data collected from this model can be extrapolated and applied to

mammalian research and higher order systems is unclear. It is therefore possible that the physiological mechanisms regulating lysosomal Ca^{2+} loading are not as fully understood as previously thought.

As explained, TRPML1 belongs to the mucolipin subfamily, which also includes TRPML2 and 3. What differs between these proteins is their tissue-specific expression and sub-cellular localisation. TRPML1 is predominantly localised on the late endosomes and lysosomes, whilst TRPML2 and TRPML3 are expressed on the early/recycling endososmes in addition to late endosomes and lysosomes (Feng & Yang, 2017). Unlike TRMPL1, which is widely expressed in many cell types (Cuajungco & Kiselyov, 2017), TRMPL2 has a more limited expression pattern, being observed in the lung, stomach, colon and mammary glands (Flores & García-Añoveros, 2011). It has however been demonstrated that TRPML2 is expressed in astrocytes (Morelli et al., 2016) and has been observed to localise to recycling endosomes, lysosomes and the plasma membrane (Karacsonyi et al., 2007; Lev et al., 2010; Venkatachalam et al., 2006). As a decrease in *Mcoln2* RNA levels was observed in the LRRK2-R1441C cultures, it is therefore possible that a decrease in TRPML2 channel expression in LRRK2-R1441C astrocytes could lead to a lysosomal Ca^{2+} deficit. However, ML SA1 is a TRPML1-specific agonist as evident by the absence of any ML SA1-activated currents in *Mcoln1*$^{-/-}$ cells (Zhang et al., 2016). Therefore the ML SA1 associated Ca^{2+} changes observed in LRRK2-R1441C cultures here are due to TRPML1 deficits as opposed to a decrease in TRPML2 expression.

As discussed, in a recent meta-analysis of genome-wide association studies the a1 subunit of vATPase, encoded by *ATP6V0A1*, was identified as a novel PD risk loci

(Chang et al., 2017). This highlights not only the crucial role of the lysosome in PD but also the potential interaction of PD genetic risk factors. This same subunit has been shown to become destabilised in *Presenilin1*$^{-/-}$ cells, a model of AD, leading to elevated lysosomal pH (Lee et al., 2015). Furthermore, the blocking or knock-down of this subunit was capable of replicating the reported lysosomal phenotypes in *Presenilin1*$^{-/-}$ cells. Residues crucial for V_1/V_0 interaction in the a1 subunit have identified (Liberman et al., 2013). The N-terminus of the a1 subunit is essential for vATPase function because it serves to tether V_1 to the membrane and must withstand the torque generated by V_1 during motor movement (Cotter et al., 2015). In addition, this region contains the information necessary for correct targeting of vATPases to cellular destinations (Finnigan et al., 2012). It is intriguing, therefore, that it is this subunit that LRRK2 binds to and is downregulated in LRRK2-R1441C cultures. It has previously been demonstrated that modulation of vATPase a1 binding partners can negatively affect its function and lead to autolysosome maturation deficits similar to what has been described here (Namkoong et al., 2015).

There are multiple mechanisms that regulate the function of the vATPase. One of which is glycosylation. N-glycosylation is required for this subunit to be efficiently delivered to the lysosomes (Nishi & Forgac, 2002) and occurs post-translationally via the STT3B catalytic subunit of the oligosaccharyltransferase (OST) (Ruiz-Canada et al., 2009). It was demonstrated here that there were no differences in glycosylation between genotypes. It has been demonstrated that some binding partners of vATPase a1 only bind to unglycosylated forms of the a1 subunit in order to modulate its maturation (Lee et al., 2010). It would be interesting to determine if LRRK2 is bound to this immature form of the subunit and is implicated in its maturation, or if it is bound to the

glycosylated form and is implicated in its post-glycosylation trafficking to difference sub-cellular locations. LRRK2-R1441C neurons exhibited a decrease in a1 localisation to both the Golgi and the lysosome. Whilst LRRK2-G2019S neurons also exhibited a decrease in a1-Golgi colocalisation, an increase in a1 localisation to the lysosome was observed. It can therefore be hypothesised that LRRK2 is bound to the mature form of the a1 subunit and is implicated in the trafficking of this subunit.

In the deglycosylation assay, lower molecular weight bands were observed which were hypothesised to be either a cleaved form of the protein or a potential splice variant. To date, no reports have observed a cleaved product of the a1 subunit, so it is unclear if this could be a potential mechanism. Splice variants of the subunit however have been described, but in very little detail. Four splice variants of the a1 subunit have been identified based on the alternative splicing of two insertions, a 21bp insertion between exons 4 and 5, and a 18bp insertion between exon 17 and 18, which control the differential sorting of a1 variants to sub cellular locations and neuronal expression, respectively (Poëa-Guyon et al., 2006). However, since this report no further research has been carried out to observe functional differences between these splice variants. It would therefore be of interest to investigate the differential expression of these splice variants in these LRRK2 cortical cultures and how they alter vATPase a1 expression and function.

The regulation of other vATPase subunits has been shown to be dependent on their phosphorylation. For example, a number of studies have suggested that phosphorylation of the A subunit, which is situated in the V_1 complex, by cyclic-AMP-dependent kinase (PKA) may play a vital role in regulating vATPase function

(Alzamora et al., 2010). The key phosphorylation site was identified as serine 175. Whilst data show that the phosphorylation of the A subunit regulates vATPase activity, the underlying molecular mechanism remains unresolved. It is yet to be demonstrated if vATPase a1 is phosphorylated and, if so, how this may regulate its function. Interestingly, the interactome of the vATPase B1 subunit situated in the V_1 complex has recently been mapped (Merkulova et al., 2015). At a molecular level, the WD40 protein-protein interaction domain was highly enriched. It was suggested that these domains are involved in scaffolding vATPase B1 to its upstream regulators and downstream effectors. As LRRK2 contains a WD40 domain, it would be of interest to investigate if this is the binding site for the vATPase a1 subunit.

The data presented here have characterised in detail the underlying lysosomal dysfunction in LRRK2-R1441C cultures responsible for the autolysosome maturation deficit phenotype described. It appears that the origin of this lysosomal dysfunction is the dysregulation and subsequent decrease in vATPase a1 expression, leading to altered lysosomal pH. A complete loss of LRRK2-vATPase a1 binding in LRRK2-R1441C cultures is suggestive of a potential underlying mechanism. How this loss of binding leads to a1 dysregulation and decrease has not been fully elucidated but is an extremely interesting area for future research.

Chapter 5: Using tool compounds to correct lysosomal deficits in mutant LRRK2 cortical cultures

5.1 Introduction and aims

Intracellular protein folding and aggregation are a common phenomenon of many neurodegenerative diseases such as PD, AD, Huntington's Disease (HD) and spinocerebellar ataxias (SCA). Therefore, enhancing autophagy may be a promising therapeutic approach for clearing protein aggregations in these neurodegenerative diseases. For the treatment of PD in particular, several compounds have recently gained attention due to their ability to clear α-synuclein in animal and cell models. For example, curcumin, derived from the curry spice of turmeric, significantly decreases the accumulation of A53T α-synuclein in SH-SY5Y cells via the downregulation of mTOR signalling and increasing autophagy (Jiang et al., 2013).

The primary effect of such compounds is the upregulation of autophagy via increased autophagosome biogenesis through mTOR-dependent or independent mechanisms. Further compounds that have gained interest in PD literature, such as trehalose and flubendazole, elicit their effects on the autophagy pathway via lysosome biogenesis, as previously described. As was demonstrated in Chapter 4, this approach is unable to ameliorate the lysosomal deficits described here in the LRRK2-R1441C cultures. It is hypothesised that the deficits are driven by the alterations in lysosomal pH and Ca^{2+}. Therefore, if these lysosomal deficits can be rectified, autolysosome maturation can be

increased. Therefore, lysosome-targeting compounds, in particular those which may alter lysosomal ion dynamics and control, are of particular interest in this model.

A fundamental challenge that arises throughout biomedicine is the need to establish the relationship between disease, physiological processes and the action of small-molecule therapeutics. In 2006, the community resource Connectivity Map (CMAP) was first piloted (Lamb et al., 2006). CMAP holds the cellular transcriptomic response profiles recorded following exposure of cells to over 1000 compounds and allows these profiles to be matched against user-provided transcriptomic profiles to identify compounds that provoke a correlated or anti-correlated transcriptomic response. Given a disease-associated transcriptomic profile, compounds that provoke a correlated profile may provide insights into disease-relevant processes or new disease models, whilst compounds that provoke an anti-correlated response may themselves be of therapeutic value or provide a lead to identifying new therapies (Lamb, 2007). Utilising this resource, comparison of the profiles of purified iPSC-derived DAn derived from PD patients carrying the *LRRK2-G2019S* variant to healthy controls has previously identified significant functional convergence amongst differentially-expressed genes (Sandor et al., 2017). The perturbation in gene expression in LRRK2-G2019S DAn was significantly similar to that induced by the pesticide rotenone, an environmental cause of PD. One compound identified as significantly anti-correlated was the small-molecule, clioquinol. Clioquinol is a Zn^{2+}/ Cu^{2+} ionophore and anti-oxidant previously used extensively as an antibiotic and antimalarial. It has been shown to prevent dopaminergic cells death in MPTP-mice (Kaur et al., 2003) and rescue cognitive and motor function in *A53T*-TG mice (Finkelstein et al., 2016) and *MAPT*$^{-/-}$ mice (Lei et al., 2012). Furthermore, clioquinol has been shown to induce autophagy in cultured

astrocytes and neurons (Park et al., 2011). As well, it has been demonstrated to down-regulate mutant huntingtin expression and mitigate pathology in a mouse model of HD (Nguyen et al., 2005) and restore cognition and decrease amyloid-beta in AD transgenic mice (Adlard et al., 2008). Clioquinol is of particular interest in this instance due to the fact that it is a lysomotropic compound and lipophilic. Lipophilic or amphiphilic compounds with a basic moiety will become protonated and trapped within lysosomes (Villamil Giraldo., et al 2014). Furthermore, it has been demonstrated that clioquinol is able to reverse autophagy arrest in chloroquine-treated cells by correcting lysosomal pH (Seo et al., 2015). Collectively, this suggests clioquinol id able to increase autophagic flux by modulating the lysosome directly.

Nilotinib is a second generation Abl inhibitor that has been shown to be able to cross the BBB, stabilise or reduce α-synuclein protein levels and significantly improve motor deficits in PD patients (Pagan et al., 2016). C-Abl is a tyrosine kinase that is localised in both the nucleus and cytoplasm that has been shown to regulate the cell cycle and to induce, under certain conditions, cell growth arrest and apoptosis (Shaul, 2000). *Abl*$^{-/-}$ in MPTP treated mice has previously been found to be neuroprotective (Ko et al., 2010). Furthermore, Nilotinib has been demonstrated to enhance protein deposition into the lysosomes of *A53T*-TG mice and reverse loss of DAn and improve motor deficits (Hebron, Lonskaya & Moussa, 2013).

It is important to note that the use of these tool compounds in LRRK2-R1441C cultures is not to identify novel therapeutics, per se, but rather to use these tool compounds to confirm and reinforce the role of LRRK2-R1441C at the lysosome. It is hypothesised

here that the underlying cause of the lysosomal deficits originates from changes in lysosomal pH caused by altered vATPase a1 dynamics. Therefore, if a compounds mechanism of action is relatively well understood and is able to correct pH and, concomitantly, the downstream effects on Ca^{2+} and autolysosome maturation, this will support this hypothesis.

Chapter aims

1. Investigate effects of Nilotinib treatment on autophagy in primary cortical cultures
2. Investigate effects of clioquinol treatment on LRRK2-R1441C lysosomal deficits and identify mode of action
3. Investigate effects of lysomotropic drugs on LRRK2-R1441C lysosomal deficit

5.2 Results

5.2.1 Monitoring the effect of Nilotinib on autophagy

In order to assess whether Nilotinib was capable of reversing or reducing the LRRK2-R1441C autolysosome maturation deficit reported here, cell cultures were treated with 10 μM Nilotinib for 24 hours, fixed and then β-III tubulin/LC3/LAMP1 co-immunofluoresence performed. LRRK2-hWT, LRRK2-R1441C and LRRK2-G2019S neurons had an inhibited autolysosome response to Nilotinib treatment although this did not reach significance (Fig. 5.1a and b). From these data it seems that Nilotinib is unable to rescue the LRRK2-R1441C autolysosome maturation deficit caused by lysosomal dysfunction.

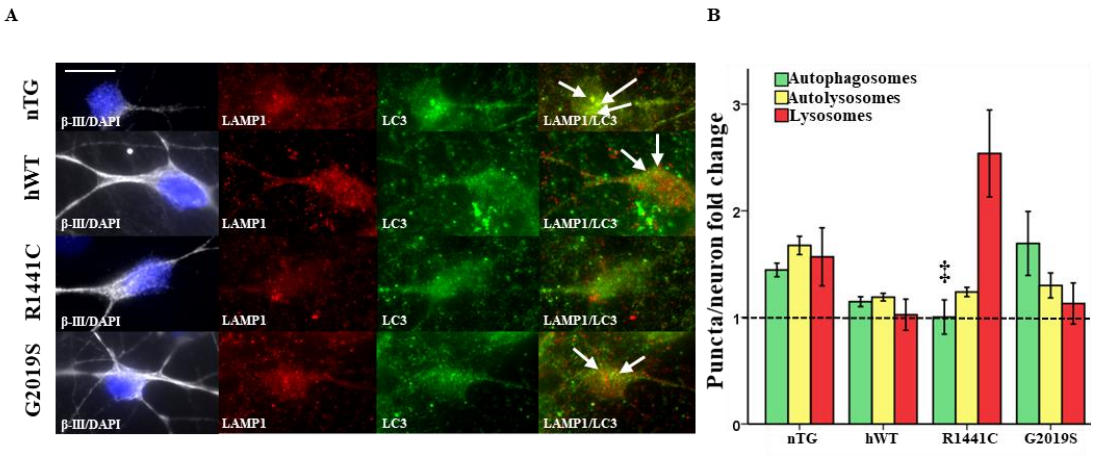


Figure 5.1. Nilotinib treatment and autophagy. *(**A, B**) DIV 14 primary cortical cultures were fixed and stained for β-II tubulin, LC3 and LAMP1 and autophagy puncta fold change in response to Nilotinib were quantified in neurons. Bars represent mean +/- SEM. (N = 3; *, P<0.05; Kruskal-Wallis non-parametric ANOVA, bonferroni post-hoc). ‡ = vs. G2019S. Scale bar = 10 µm.*

5.2.2 Assessing clioquinol treatment on autophagy in LRRK2-R1441C primary cortical cultures

Autophagy puncta counts, lysosomal pH levels and protein-degradation assays were performed in the presence of clioquinol. Treatment of primary cortical cultures with clioquinol increased LC3-II protein expression in all genotypes (Fig. 5.2a) suggesting that this compound is able to increase autophagic flux in all 4 genotypes. In order to determine if this increase in LC3-II in LRRK2-R1441C cultures reflected an increase in autolysosome maturation, co-immunofluorescence for LC3 and LAMP1 in neurons was carried out. A significant increase in autolysosome counts in LRRK2-R1441C neurons was observed in the presence of clioquinol (Fig. 5.2b and c).

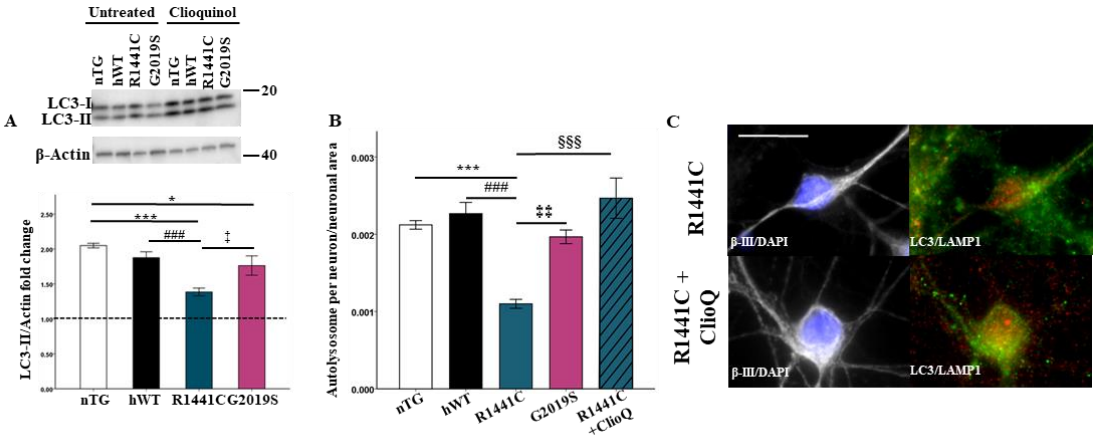


Figure 5.2. Clioquinol increases autolysosome maturation in LRRK2-R1441C neurons. *(**A**) Western blots for LC3-II were quantified to assess autophagic flux in response to clioquinol. (**B, C**) 14 DIV cortical cultures were fixed and stained for LC3 and LAMP1 in β-III tubulin^{+} cells and autolysosomes per neuron was quantified and normalised to neuronal size to assess changes in response to clioquinol. Bars represent mean +/- SEM (N = 3; *, P < 0.05; **, P<0.005; ***, P<0.001; Kruskal-Wallis non-parametric ANOVA, bonferroni post-hoc) * = vs. nTG, # = vs. hWT, ‡ = vs. G2019S, § = vs. R1441C. Scale bar = 10 µm.*

It was therefore hypothesised that, as there was an increase in autolysosome maturation in LRRK2-R1441C cultures, that clioquinol was modulating lysosomal pH levels. Using the same lysosensor assay previously described, it was demonstrated that the LRRK2-R1441C lysosomes were also significantly re-acidified from basal levels by clioquinol (Fig. 5.3a and b).

As TRPML1 Ca^{2+} release is regulated by luminal pH, the effect of clioquinol on ML-SA1 response was investigated. The presence of clioquinol increased lysosomal calcium release in LRRK2-R1441C primary cultures in response to ML SA1, indicating a correction of TRPML1 channel function (Fig. 5.3c and d) whilst total lysosomal calcium content increased (Fig. 5.3e and f). Finally, as it was demonstrated

that clioquinol was capable of ameliorating LRRK2-R1441C lysosomal deficits, the effect of the molecule on lysosomal protein degradation was investigated. Clioquinol was capable of increasing lysosomal protein degradation in LRRK2-R1441C cortical cultures as indicated by the pulse chase assay (Fig. 5.3g).

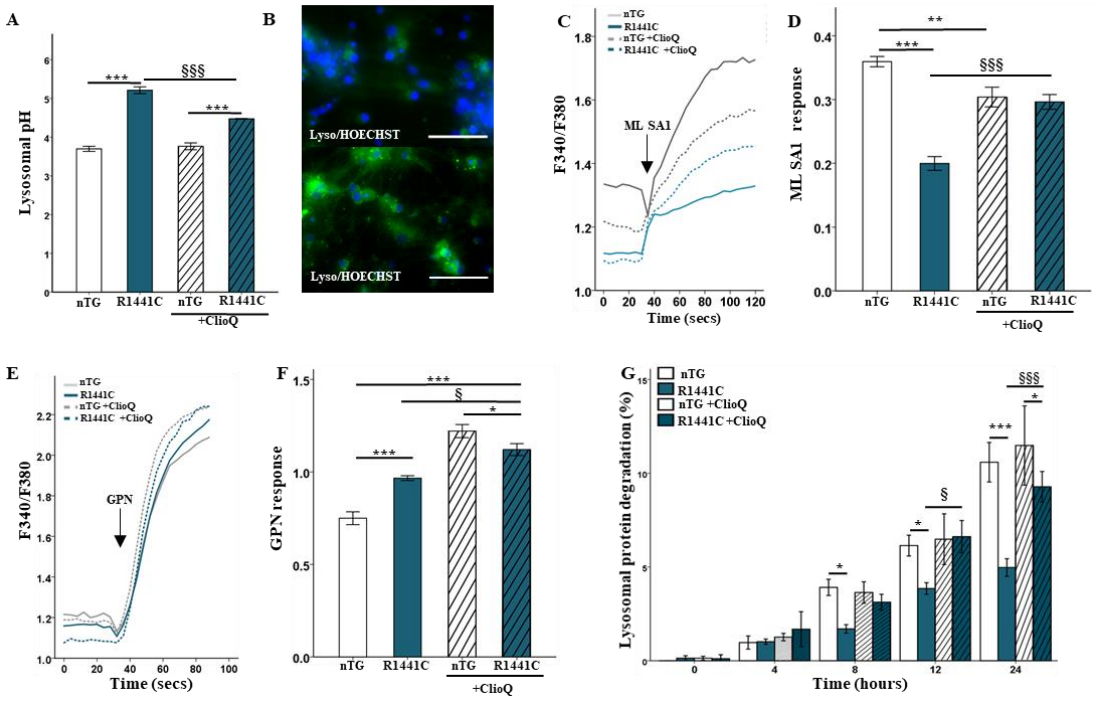


Figure 5.3. Clioquinol rescues lysosomal deficits in LRRK2-R1441C neuronal cultures. *(**A**, **B**) Lysosomal pH was quantified in response to clioquinol. (**C, D**) Cortical cultures were incubated in Fura2-AM and lysosomal calcium response to ML SA1 was measured either in the presence or absence of clioquinol. (**E**, **F**) Cortical cultures were incubated in Fura2-AM and lysosomal calcium response to GPN was measured either in the presence or absence of clioquinol. Bars represent mean +/- SEM (N = 3; *, P < 0.05; **, P < 0.01; ***, P < 0.001; Two-way ANOVA, bonferroni post-hoc). (**G**) 14 DIV cortical cultures were incubated with radiolabelled valine for 48 hours and CPM was measured over 24 hours in untreated cultures or in the presence of chloroquine or clioquinol to calculate lysosomal protein degradation. Bars represent mean +/- SEM (N = 3; *, P < 0.05; ***, P < 0.001; Three-way ANOVA, bonferroni post-hoc).* * = vs. nTG, # = vs. hWT, ‡ = vs. G2019S, § = vs. R1441C. Scale bar = 200 µm.*

5.2.3 The role of zinc in clioquinol treatment

Previous reports have suggested that clioquinol may increase lysosomal Zn^{2+} levels which then act to modulate pH (Sandor et al., 2017). Therefore, using the Zn^{2+} sensitive dye Furo-Zin3, the effect of clioquinol on lysosomal Zn^{2+} levels in LRRK2-R1441C primary cultures was assessed. It was observed that clioquinol treatment significantly increased Furo-Zin3-positive lysosomes in LRRK2-R1441C, but not nTG cultures (Fig. 5.4a and b). Lysosomal Zn^{2+} levels may functionally upregulate, or increase expression of, lysosomal proton pumps, such as vATPase and K+/H+ exchangers. Clioquinol treatment significantly upregulated protein expression of vATPase a1 in LRRK2-R1441C primary cultures (Fig. 5.4c), without changing lysosomal number (Fig. 5.4d).

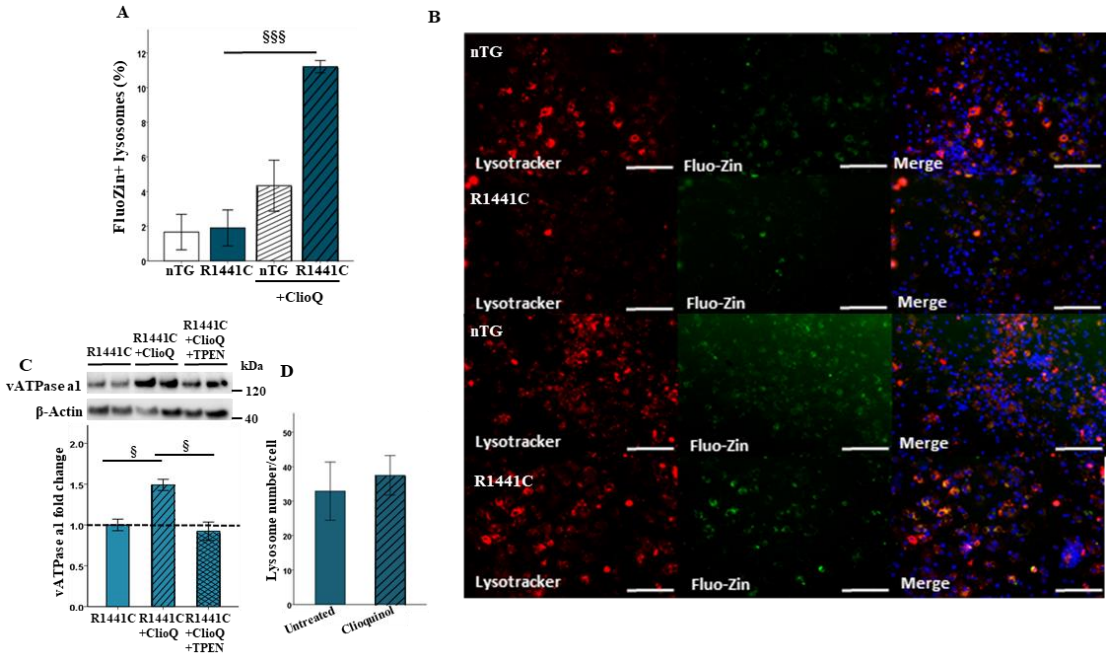


Figure 5.4. Clioquinol modulates lysosomal zinc levels and upregulates pH regulating pumps. *(**A, B**) Using the Zinc sensitive dye FluoZin-3 and the lysosome dye lysotracker, the percentage of FluoZin3^{+} lysosomes were quantified in the presence or absence of clioquinol. Bars represent mean +/- SEM (N = 3; * , P < 0.05; ***, P < 0.001; Two-way ANOVA, bonferroni post-hoc). (**C**) Western blots for vATPase a1 were quantified in LRRK2-R1441C cortical cultures in the presence or absence of clioquinol and TPEN and normalised to untreated levels. Bars represent mean +/- SEM. (N = 3; *, P<0.05, ***, P<0.001; One-Way ANOVA, Tukey HSD post-hoc). (**D**) Lysotracker puncta were quantified in LRRK2-R1441C cortical cultures in the presence or absence of clioquinol. Bars represent mean +/- SEM, N = 3, independent t-test. § = vs. R1441C. Scale bar = 200 µm.*

In order to experimentally determine whether the effects of clioquinol on the LRRK2-R1441C phenotypes were Zn^{2+} dependent, the clioquinol-rescue assays previously described were repeated in the presence of the cell-permeable, Zn^{2+} chelator N,N,N',N'-tetrakis(2-pyridylmethyl)ethane-1,2-diamine (TPEN). In the presence of TPEN, clioquinol was no longer able to significantly increase vATPase a1 expression (Fig. 5.4c), nor decrease lysosomal pH from basal levels in LRRK2-R1441C cultures (Fig. 5.5a and b). Similarly, alterations in calcium release from TRPML1 channels was no longer increased with clioquinol treatment when co-treated with TPEN (Fig. 5.5c and d). Using the pulse chase assay, in the presence of TPEN, lysosomal protein degradation decreased back to levels comparable to basal (Fig. 5.5e). Together this data provides strong evidence for the essential role of Zn^{2+} in clioquinol rescue in LRRK2-R1441C cultures.

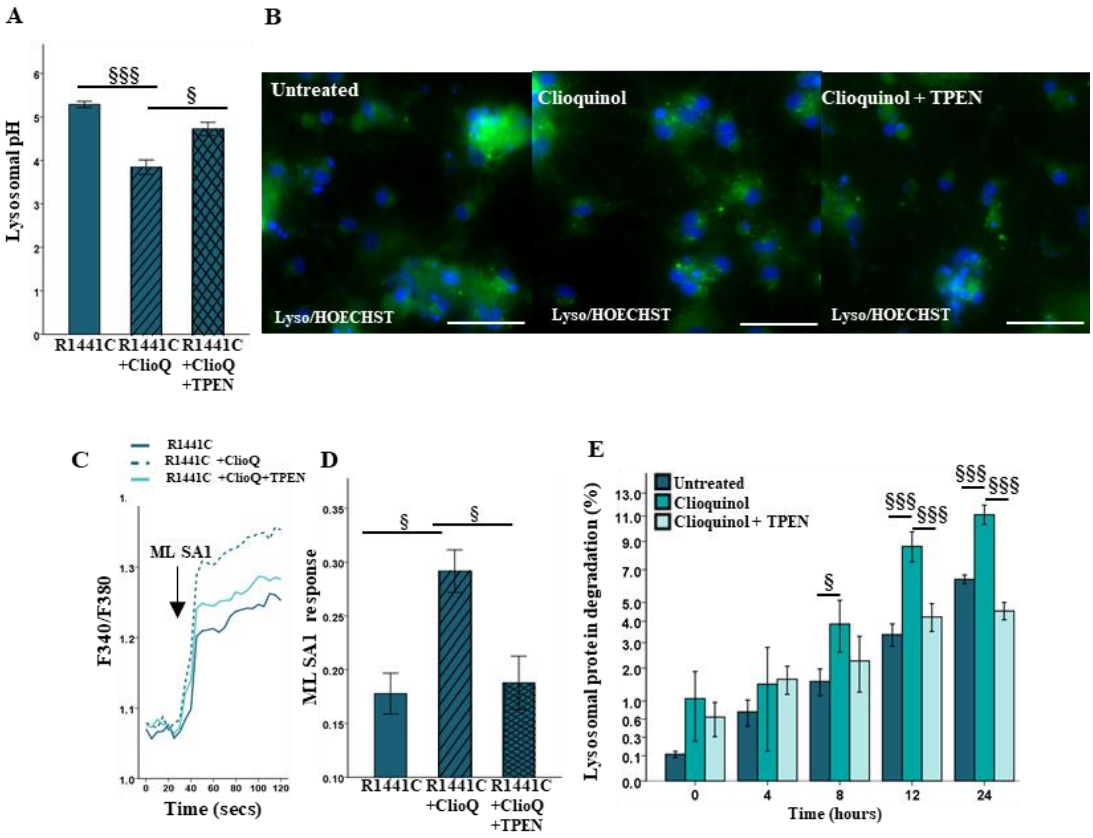


Figure 5.5. Clioquinol modulates lysosomal zinc levels corrects lysosomal pH in LRRK2-R1441C cultures. *(**A, B**) Using the pH sensitive dye lysosensor, lysosomal pH was quantified in LRRK2-R1441C clioquinol primary cortical cultures. (**C, D**) ML SA1 was used in order to quantify calcium release from TRPML1 channels. Bars represent mean +/- SEM. (N = 3; *, P<0.05, ***, P<0.001; One-Way ANOVA, Tukey HSD post-hoc). (**E**) 14 DIV LRRK2-R1441C cortical cultures were incubated with radiolabelled valine for 48 hours and CPM was measured over 24 hours in untreated cultures or in the presence of chloroquine/clioquinol/TPEN to calculate lysosomal protein degradation. Bars represent mean +/- SEM (N = 3; *, P < 0.05;*

5.2.4 The effect of primaquine and its derivatives on autolysosome maturation and protein degradation in LRRK2-R1441C cultures

Sandor et al. (2017) performed a connectivity map screen which identified clioquinol as an initial 'hit' compound for potential therapeutics. From such a data set, it is possible to extrapolate the 'hit' compounds identified and alter their chemical structures in order to increase their impact on gene signature. However, how readily achievable this is dependent on the initial chemical structure of the compound. For example, clioquinol had an enrichment score of -0.557 ($p = 0.0027$) in the connectivity map screen. As an enrichment score of -1 indicates perfect anti-correlation, clioquinol is therefore not 100% effective. However, the structure of clioquinol, due to it being an already simple molecule (Fig.5.6a), does not afford any way of modifying it without radically changing its structure, and therefore properties, and is not particularly amenable to medicinal chemistry efforts.

Another hit compound that was identified in Sandor et al. (2017) was primaquine (enrichment score of -0.394; $p = 0.03428$). Primaquine, like clioquinol, is an anti-malarial drug and is structurally similar to clioquinol; both are based on an 8-substituted quinoline scaffold. The difference is that primaquine is based off an 8-aminoquinoline structure and clioquinol off an 8-hydroxyquinoline structure. Both provide the same ionophoric motif however. (Fig. 5.6b). Furthermore, the structure of primaquine is much more complex than clioquinol, and therefore the opportunities for modification are much more diverse. Taking this all together, it was decided that primaquine would be taken and modified in order to create derivatives for screening in the LRRK2-R1441C primary cortical cultures to investigate their effects on lysosomal phenotypes

in this model. Robert Quinlan and Benoit Darlot from the medicinal chemistry group at the Target Drug Discovery Institute (TDDI), University of Oxford, made 9 primaquine derivatives to be tested in these primary cultures.

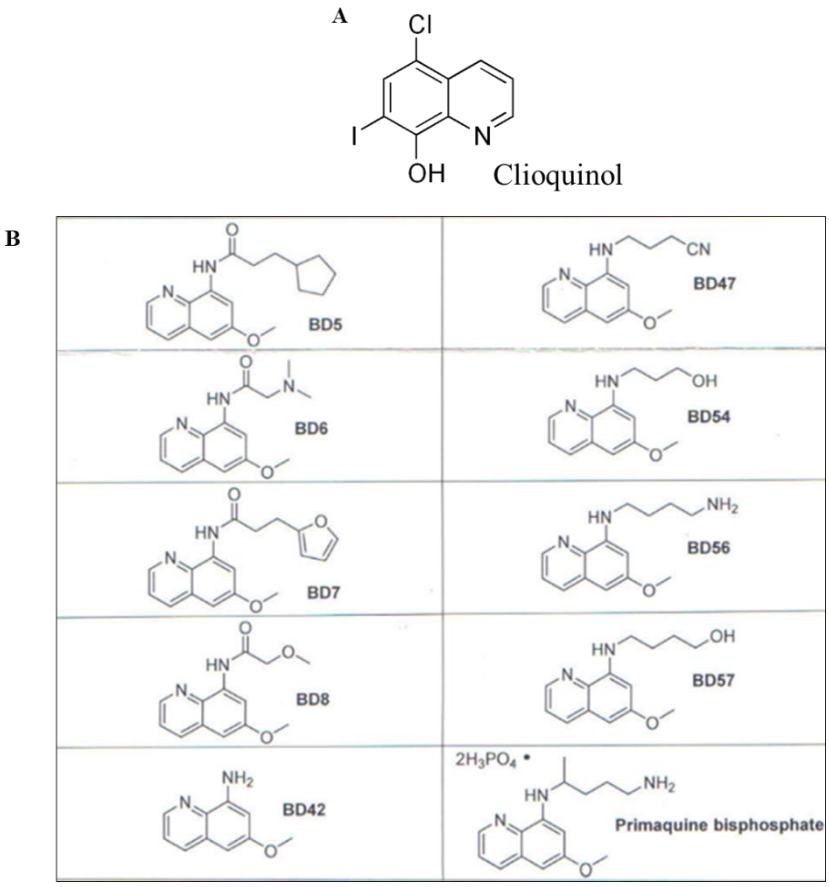


Figure 5.6. Molecular structure of (A) clioquinol and Primaquine and (B) its derivatives created by Robert Quinlan and Benoit Darlot.

Cultures were treated at two different concentrations of 1 and 10 µm for 2 hours and co-immunofluorescence for LC3 and LAMP1 was performed in neurons and autolysosomes quantified. For both concentrations, there was a significant increase from basal autolysosome count with primaquine treatment (Fig. 5.7a and b). In order to determine if there were changes in lysosomal protein degradation, an alternative assay to the pulse chase assay was performed. The DQ™-BSA assay utilises the observation that a strong quenching effect is observed when proteins are heavily labelled with bodipy dyes. Upon hydrolysis of the DQ™-BSA Red to single, dye-labelled peptides by proteases, this quenching is relieved, producing brightly fluorescent products (Fig. 5.8a). This assay requires a short incubation time of one hour, as opposed to the four days needed to perform the pulse-chase assay. Therefore, given the number of compounds being tested here, it was deemed appropriate to use the DQ-BSA as an alternative assay for logistical purposes.

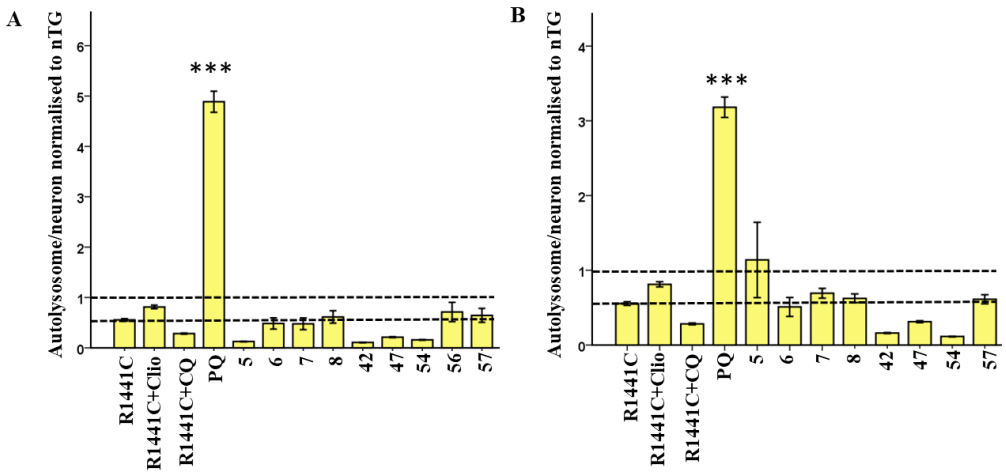


Figure 5.7. The effect of primaquine derivatives on autolysosome count in primary cortical cultures. *(**A, B**) DIV 14 primary cortical cultures were treated for 2 hours with primaquine derivatives at (**A**) 1 µm or (**B**) 10 µm, fixed and stained for β-III tubulin, LC3 and LAMP1 and autolysosome number were quantified relative to nTG controls. The two dotted lines represent nTG average (top) and LRRK2-R1441C untreated average (bottom). Bars represent mean +/- SEM. (N = 3; ***, P<0.001; Kruskal-Wallis non-parametric ANOVA, bonferroni post-hoc). * = vs. R1441C untreated*

Cells were treated with primaquine and its derivatives, as well as clioquinol for a positive control and DQ-BSA fluorescence was quantified. At the lower concentration, three of the primaquine derivatives significantly increased DQ-BSA fluorescence from basal levels (Fig. 5.8b and d). At the higher concentration, although no derivatives reached statistical significance, four increased LRRK2-R1441C levels comparable to nTG cultures (Fig. 5.8c and d). Intriguingly, primaquine did not increase lysosomal protein degradation at either concentrations despite the increase in LC3/LAMP1 colocalisation observed.

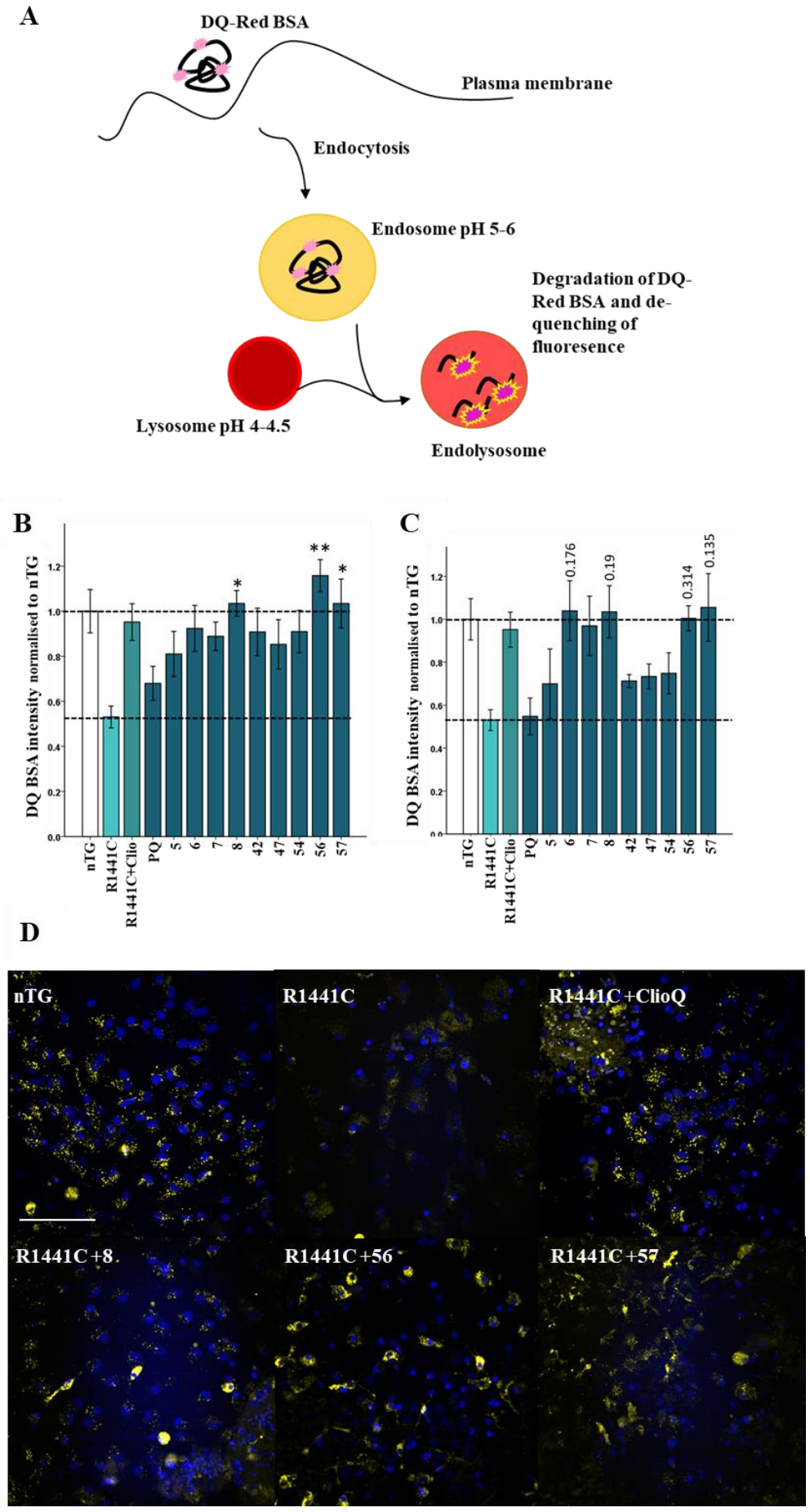

A
DQ-Red BSA
Plasma membrane
Endocytosis
Endosome pH 5-6
Degradation of DQ-Red BSA and de-quenching of fluoresence
Lysosome pH 4-4.5
Endolysosome
B
DQ BSA intensity normalised to nTG
nTG
R1441C
R1441C+Clio
PQ
5
6
7
8
42
47
54
56
57
C
DQ BSA intensity normalised to nTG
0.176
0.19
0.314
0.135
D
nTG
R1441C
R1441C +ClioQ
R1441C +8
R1441C +56
R1441C +57

Figure 5.8. The effect of primaquine derivatives on DQ^{TM}-BSA fluorescence. *(**A**) Schematic diagram of the properties of DQ^{TM}-BSA. (**B**, **C**) DIV 14 primary cortical cultures were treated for 2 hours with primaquine derivatives at (**B**) 1 µm or (**C**) 10 µm incubated with DQ^{TM}-BSA and DQ^{TM}-BSA intensity was quantified relative to nTG littermate controls. The two dotted lines represent nTG average (top) and LRRK2-R1441C untreated average (bottom). (**D**) Representative images of DQ^{TM}-BSA intensity in untreated nTG and LRRK2-R1441C cultures, LRRK2-R1441C cultures treated with Clioquinol for 48h, and LRRK2-R1441C cultures treated for 2 hours with primaquine derivatives eliciting a significant change. Bars represent mean +/- SEM. (N = 3; *, P<0.05; Kruskal-Wallis non-parametric ANOVA, bonferroni post-hoc). * = vs. R1441C untreated. Scale bar = 100 µm.*

5.3 Discussion

This chapter has demonstrated that the Zn^{2+}/ Cu^{2+} ionophore clioquinol is capable of rescuing the LRRK2-R1441C associated lysosomal phenotypes described, increasing autolysosome maturation, lysosomal protein degradation and decreasing lysosomal pH back to physiological levels. It was shown that with clioquinol treatment, the number of Zn^{2+} containing lysosomes was increased only in LRRK2-R1441C cultures and not in nTG cells. The therapeutic effect of clioquinol was shown to be Zn^{2+}-dependent, as Zn^{2+} chelation prevented any phenotypic rescue. A number of derivatives of a structurally similar compound, primaquine, were also shown to increase lysosomal protein degradation in LRRK2-R1441C cultures.

It appears that clioquinol elicits its therapeutic effects by normalising lysosomal pH, presumably due to the increase and stabilised levels of the vATPase a1 subunit. How Zn^{2+} increases lysosomal proton pump expression remains unknown and future studies

will be needed to elucidate the specific mechanism. However, based on the current literature on vATPase a1 regulation, some hypotheses can be drawn.

Effective lysosomal acidification requires proton leak from a currently unidentified leak channel (Ishida et al., 2013). Intriguingly, it has been demonstrated that this leak, or back-flux, of H^+ can be inhibited by micromolar concentrations of Zn^{2+} (Schapiro & Grinstein, 2000). As the vATPase a1 subunit is decreased in LRRK2-R1441C cultures here, it can be logically assumed that there is less proton movement into the lysosomal lumen. Therefore, the increased lysosomal zinc levels with clioquinol treatment may aid in increasing proton content in the lysosome by preventing further backflux. This in itself however does not explain how vATPase a1 subunit is subsequently increased.

It has been demonstrated that membrane-anchored a1 subunit of the vATPase undergoes S-palmitoylation on Cys-25 and has significantly decreased expression in palmitoyl-protein thioesterase 1 (Ppt1) deficient mice (Bagh et al., 2017). This palmitoylation prevents dissociation of the a1 subunit from adaptor protein complex-2 (AP-2) and interaction with adaptor protein complex-3 (AP-3), which is required for its transport to the lysosome. This can be ameliorated with the treatment of compounds that inhibit palmitoylation. Interestingly, palmitoyltransferases have been found to tightly bind to zinc (Gottlieb et al., 2015). The coordination of Zn^{2+} ions in the cysteine-rich domain of palmitoyltransferases has been shown to be required for their structural integrity (Gottlieb et al., 2015). It is therefore possible that clioquinol can increase vATPase a1 subunit expression by inhibiting palmitoyltransferases, decreasing the palmitoylation of the a1 subunit and therefore increasing a1/AP-3 interaction and

trafficking to the lysosome. Furthermore, dynamic palmitoylation (palmitoylation-depalmitoylation) facilitates the degradation of proteins that undergo palmitoylation (Bijlmakers et al., 2003). Therefore, alterations in a1 palmitoylation in LRRK2-R1441C may explain the initial decrease in expression levels, and is an interesting potential for future research. It has also been demonstrated that curcumin prevents palmitoylation of integrin β4 (Coleman et al., 2015), demonstrating potential mechanistic overlap for neurodegenerative therapeutics.

Interestingly, it has recently been demonstrated that the Zn^{2+} transporter 2 (ZnT2) interacts with vATPase and *ZnT2*-KO cells exhibit increased cytosolic Zn^{2+} lose the ability to activate vesicle acidification (Lee et al., 2017). However, it was also demonstrated that the presence of TPEN did not remediate the effect of ZnT2-attentuated cells, suggesting that the role of ZnT2 in vesicle acidification may be independent of its function in Zn^{2+} transport. It therefore seems unlikely that the increase in lysosomal Zn^{2+} levels with clioquinol treatment would mediate ZnT2-vATPase interaction.

It has also been suggested that the increase in lysosomal Zn^{2+} may serve as a driving force for a Zn^{2+}/H^{+} antiporter (Seo et al., 2015). Ten Zn Transporters (ZnTs) have been identified in humans (Fukada & Kambe, 2011; Kambe et al., 2008; Lichten & Cousins, 2009). These ZnT proteins transport zinc in a Zn^{2+}/H^{+} exchange manner (Kambe et al., 2014). No one ZnT protein has been identified to localise with the lysosome, however ZnT10 immunostaining has demonstrated localisation to early/recycling endosomes (Patrushev et al., 2012) and the Golgi apparatus (Bosomworth et al., 2012).

Interestingly, missense mutations of *ZnT10* have been shown to be linked to dystonia, a movement disorder closely related to PD and an early symptom to some patients (Quadri et al., 2012).

It is noticeable that with clioquinol treatment, R1441C cultures demonstrate a significantly higher increase in Zn^{2+} containing lysosomes compared to nTG cortical cultures. Zn^{2+} is essential for neuronal activity and also induces toxicity if the concentration is abnormally high. Patients with PD have been reported to exhibit increased levels of both Zn^{2+} and manganese in serum and cerebrospinal fluid (Fukushima et al., 2011; Hozumi et al., 2011). It has been demonstrated that increased Zn^{2+} mediated by PKA, an interactor of LRRK2 (Parisiadou et al., 2014; Greggio et al., 2017), is capable of modulating both cell death and autophagy (Hung et al., 2017). Whether this exaggerated increase in lysosomal Zn^{2+} levels is indicative of increased intracellular basal levels in LRRK2-R1441C cells remains to be determined. Nonetheless, a role of metal ions in neurodegenerative disease is becoming more apparent (Sastre et al., 2015; Ward et al., 2015).

It must be noted that clioquinol is not specific to Zn^{2+} but also binds to Cu^{2+} and, to a lesser extent, Fe^{2+} (Bareggi & Cornelli, 2010). TPEN is also capable of chelating intracellular Cu^{2+} (Hyun et al., 2001) but has been shown in multiple reports to have significantly higher affinity for Zn^{2+} (Bertuchi et al., 2014; Carraway & Dobner, 2012; Webster et al., 2003). Therefore, although it is likely that the effect of clioquinol is dependent on Zn^{2+}, it is not conclusive if there is also an effect of Cu^{2+} and/or Fe^{2+} binding in this model. Regardless, chelating of Cu^{2+} and Fe^{2+} has also been demonstrated as being beneficial for neurodegenerative disease. Curcumin has been

shown to reduce levels of amyloid and oxidized proteins via its binding to redox-active metals Cu^{2+} and Fe^{2+} and suppress inflammatory damage by preventing metal induction of NF-κβ (Baum & Ng, 2004).

It was demonstrated that primaquine was able to increase autolysosome maturation, as indicated by increased LC3/LAMP1 colocalisation, but did not increase protein degradation. Primaquine and chloroquine are both antimalarial drugs and have strikingly similar structures. Chloroquine has a hydrophobic ring structure and a weak lipophilic base where the free base passes easily through membranes (Kaufmann & Krise, 2007). It accumulates in the acidic lysosome as it becomes protonated, increasing the pH of the lysosome due to its basic amino group on the end of its carbon chain. (Ohkuma & Poole, 1978). Primaquine, however, has a similar metal binding motif to that seen in clioquinol which, based on the data presented, is crucial to its therapeutic effects. Indeed, primaquine has been shown to bind to Fe-sulfate cluster proteins (Laleve et al., 2016). Iron chelation is capable of inhibiting autophagy (Vilcassim et al., 2016) suggesting that correct iron homeostasis is required. How iron aids autophagy regulation is still not clear but may lend a clue as to how primaquine is able to increase autolysosome maturation. It can be hypothesised that, as primaquine will still be protonated and accumulate in lysosomes much like chloroquine, that despite increasing autolysosome maturation via the potential iron binding properties of primaquine, the lysosomal lumen remains alkalized and protein degradation remains decreased.

Primaquine derivatives were created and three were found to increase DQ-BSA signal in LRRK-R1441C cortical cultures. The differences between these compounds and

primaquine are all centred around the substitution on the 8-amino group which is responsible for the negative effect of primaquine on lysosomal pH. Of those that successfully ameliorated the LRRK2-R1441C phenotype, compound 8 is quite distinct from compounds 56 and 57 as it has an amide group and an ether. 56 and 57 are almost identical apart from that 56 has an amino group and 57 an hydroxyl group. It is interesting to note that primaquine and compound 56 differ only by the fact that primaquine has an extra methyl group. It can be hypothesised that this may impact the ability of compound 56 to permeabilise the lysosome, and therefore does not exhibit the concomitant increase in lysosomal pH caused by the basic amino group. As well, compound 57 may elicit effects due to the fact that its 8-amino group is acidic. It therefore can be hypothesised that compounds that retain the ionophoric motif seen in primaquine, but lack the 8-amino group that causes lysosomal alkalinisation, would be of potential therapeutic benefit in disorders associated with lysosomal deficits.

It is clear from these data that augmenting lysosomal metal ion homeostasis has potential as a future therapy. However, for future therapies a clear distinction between metal chelation and 'metal targeted strategies' needs to be made in the sense that the goal is to redistribute rather than remove metal ions. In contrast to the direct chelation approach developed for metal overload disorders, such as Juvenile hemochromatosis and Ferroportin disease, the optimum goal for neurodegenerative disease would be modulation of metal ion homeostasis aimed at restoring broken ionic balance. Febbraro et al. (2013) demonstrated that chronic intranasal deferoxamine ameliorated motor defects and pathology in an α-synuclein-PD rat model. Deferoxamine is a metal protein attenuating compound (MPAC), and it has been reported that these small molecules are useful to prevent abnormal interactions of metals in the brain with endogenous metal-

binding proteins, such as amyloid-beta and neuromelanin, which may lead to oxidative stress and MPACs show promising therapeutic effect in other neurodegenerative diseases (Bush, 2003; Sampson et al., 2014).

Such MPACs have also been utilised for the development of PET radiotracers to be used for clinical translation for neurodegenerative diseases. Krishnan et al. (2018) developed and described [^{11}C]PBT2, a second-generation 8-hydroxyquinoline analogue developed as a potential successor to clioquinol. [^{11}C]PBT2 was found to bind specifically in AD human brain tissue and with high striatal sensitivity *in vivo* in primates, providing a novel tool to assess the role of metal accumulation in striatal degeneration and other affected areas in neurodegenerative disease.

Overall, these data presented in this chapter emphasise the role of LRRK2-R1441C at the lysosome and demonstrate that modulation of lysosomal ion homeostasis provides a novel avenue for therapeutics. Some questions remain unanswered, such as the exact role of Zn^{2+} in lysosomal function and vATPase a1 subunit regulation, and these can provide the basis for future research. Finally, the demonstration that small molecules which directly target lysosome dysfunction have potential therapeutic benefits for PD fits closely with the emerging consensus on this critical area of cell biology.

Chapter 6: General discussion

6.1 Discussion

Mutations in the gene encoding LRRK2 are the most frequent cause of familial PD (Singleton et al., 2013) with pathogenic mutations leading to the development of PD which is considered clinically indistinguishable from sporadic cases (Singleton et al., 2013; Pchelina et al., 2011; Cilia et al., 2014). A pathological role of LRRK2 in disrupting the autophagy pathway in PD has previously been described, however, due to conflicting reports in the literature, it is still unclear whether LRRK2 possesses a positive or negative regulatory role in the control of autophagy and if the role of LRRK2 is at the initiation or clearance steps of the pathway. This thesis set out to investigate the effects of PD related *LRRK2-G2019S* and *LRRK2-R1441C* mutations on the autophagy pathway, and underlying molecular mechanisms, in primary cortical cultures from a *LRRK2*-BAC transgenic rat model of PD.

In Chapter 3, the autophagy pathway was characterised in each of the different genotypes. It was demonstrated that LRRK2-R1441C inhibits the maturation of autolysosomes, decreases lysosomal protein degradation and exhibits increased interaction with lysosomal proteins. LRRK2-hWT and LRRK2-G2019S cortical cultures were shown to decrease autophagosome biogenesis and be enriched at the Golgi of neurons. The lysosomal deficits underlying the decreased autolysosome maturation phenotype in LRRK2-R1441C cultures was investigated and characterised in Chapter 4. LRRK2-R1441C cultures exhibited a decrease in lysosomal acidity caused by decreased expression and mislocalisation of the crucial vATPase a1 subunit. LRRK2-R1441C also demonstrated a loss of binding to this subunit which may

underlie the alterations in vATPase a1 expression and mislocalisation observed. Furthermore, it was demonstrated in Chapter 4 that inhibition of the LRRK2 kinase domain could not ameliorate decreased lysosomal protein degradation in LRRK2-R1441C cultures, indicating that increased kinase activity is not the primary culprit in this phenotype. It does appear that the effects of hLRRK2 on the autophagy pathway are driven by a gain of function as Lrrk2$^{-/-}$ cortical cultures exhibit the opposite phenotype, with increased autophagosome biogenesis and increased lysosomal protein degradation. In Chapter 5 it was demonstrated that the Zn^{2+}/Cu^{2+} ionophore clioquinol is effective at ameliorating the lysosomal deficits observed in LRRK2-R1441C primary cortical cultures by upregulating vATPase a1 expression and subsequently reacidifying lysosomes in a Zn^{2+} dependent manner (see Fig. 6.1).

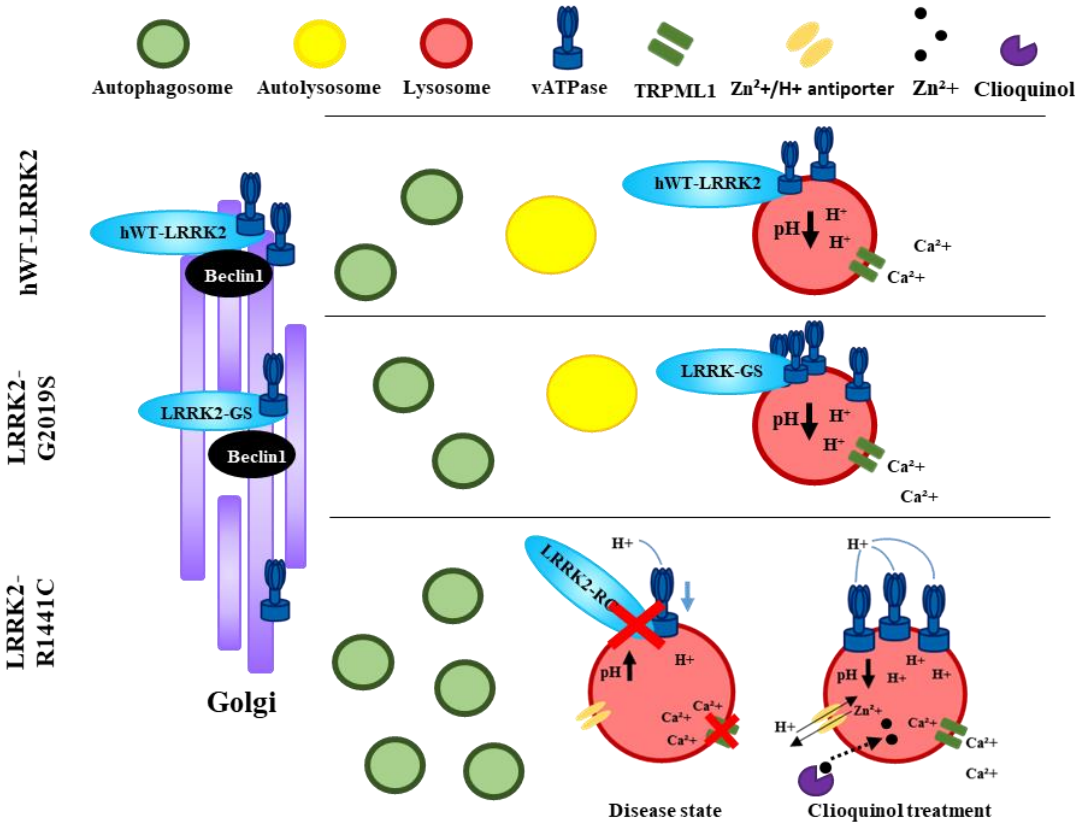


Figure 6.1 Schematic diagram of the effect of LRRK2 pathogenic mutations on the autophagy pathway. Top panel: *In the presence of hWT-LRRK2 there is a decrease in autophagosome biogenesis and protein degradation relative to nTG, possibly due to effects on Beclin1 activity by LRRK2 at the Golgi. hWT binds to vATPase a1 and is situated mainly at the Golgi.* ***Middle panel:*** *In the presence of LRRK2-G2019S the same decrease in autophagosome biogenesis as hWT-LRRK2 is observed. LRRK2-G2019S binds to vATPase a1 and exhibits increased vATPase a1 expression at the lysosome.* ***Bottom panel:*** *In the presence of LRRK2-R1441C there is a decrease in autolysosome maturation caused by dysfunctional lysosomal pH and calcium release. It is proposed that a loss of LRRK2-R1441C binding to the vATPase proton pump is the underlying mechanism for this phenotype. The modulation of lysosomal zinc content with clioquinol corrects this lysosomal deficit.*

Together, the results of this thesis provide key insights into the role of LRRK2 and its different pathogenic mutations on the autophagy pathway and regulation of lysosomal function. One of the more surprising findings in this thesis was the divergence in autophagy phenotypes between the LRRK2-R1441C and LRRK2-G2019S mutations. However, there have been other reports demonstrating divergent effects of these two different *LRRK2* mutations. For example, when assessing the effects of mutant *LRRK2* on Rab phosphorylation in HEK293 cells, it was demonstrated that unlike LRRK2-R1441C and LRRK2-Y1669C, LRRK2-G2019S was unable to increase Rab10 phosphorylation (Liu et al., 2018). In primary hippocampal neurons from knock-in *LRRK2* mice, it has also been shown that the *R1441C* mutation impairs the interaction of LRRK2 with PKARIIβ, which was not observed with the *G2019S* mutation (Parisiadou et al., 2014). What we currently understand about the interaction of the different enzymatic cores of LRRK2 may elucidate potential explanations for such divergences. As has already been described in section 1.3.3, the relationship between the GTPase domain and the kinase domain may not be bidirectional. Although the *G2019S* mutation consistently increases kinase activity (Covy et al., 2009; Luzon-Toro et al., 2007; West et al., 2005; Anand et al., 2009; Smith et al., 2006), the effect of other mutations residing in the kinase domain and those in the GTPase domain have reported inconsistent effects on LRRK2-kinase activity (West et al., 2007; Jaleel et al., 2007; Covy et al., 2009; Smith et al 2006; West et al., 2007; Anand et al., 2009; West et al., 2005; Lewis et al., 2007). Furthermore, mutants with hyperactive GTPase (R1298L) or inactive GTPase (R1398L/T1343V) cannot mimic G2019S phenotypes (Biosa et al., 2013). Whilst mutations in the GTPase domain have been reported to decrease GTP hydrolysis (Ito et al., 2007; Li et al., 2007; Daniels et al., 2011; Liao et al., 2014), the G2019S mutation has no discernible effects on GTPase activity (Xiong et al., 2010). Together it seems that mutations residing in different enzymatic domains exert differential effects on the enzymatic activity of LRRK2, which consequentially may impact cellular function differentially. The exact role of the different enzymatic cores of LRRK2 in cellular functions is not clear however, which may explain why little is understood about these divergences between mutations.

Understandably, a large percentage of the research aiming to understand LRRK2 enzymatic function has focused on its kinase activity. Kinases are appealing drug targets for pharmaceutical companies due to the fact that these enzymes are considered highly druggable and can be targeted by small-molecule chemistry. Because of this, many LRRK2 kinase inhibitors have been developed over the years to understand the role of this enzymatic domain in disease. However, this also means that there is still uncertainty about the contribution of GTPase activity to cellular toxicity. Although a number of model organisms with interesting phenotypes have been developed based upon familial mutations in the GTPase domain of LRRK2, mechanistic insight into the contribution of GTPase activity is so far lacking (Daniel & Moore, 2015). It can be hypothesised from these data presented in this thesis that the differential effects of LRRK2-G2019S and LRRK2-R1441C on lysosomal dysfunction may reside in differences in GTPase activity in these two mutations, and that the GTPase domain may be more instrumental in the role of LRRK2 at the lysosome. Understanding how GTPase activity contributes to such phenotypes will be challenging and may rely in the future upon genetic or pharmacological manipulation of the GTPase domain.

The 'date-hub' hypothesis was coined by Han et al., (2004). They described two types of 'hubs' in protein interaction networks; 'party hubs', which interact with most of their partners simultaneously at the same time and space, and 'date hubs', which bind their different partners at different times or locations. The potential for LRRK2 behaving as a 'date hub' has been discussed in the literature (Manzoni, 2017) and may explain the divergence in phenotypes between mutations described here, as well as the various discrepancies in the literature between cell and animal models of *LRRK2*-PD. For example, LRRK2-G2019S expression has been shown to increase lysosomal size and reduce lysosomal pH (Henry et al., 2015), which was not observed in the data presented in this thesis. However, Henry et al., (2015) were reporting on primary cortical astrocytes as opposed to primary neurons as reported on here. Under the

perspective of the 'date-hub' hypothesis, LRRK2 may be capable of interacting with different proteins and therefore control different cellular pathways (or modulate the same pathway differentially) based on the expression of LRRK2 activators and partners and the complexes formed in a cell-type specific manner.

Furthermore, the idea that the presence of mutations in the *LRRK2* sequence may cause a gain of novel functions implicates LRRK2 in pathological pathways that may not be relevant under physiological conditions (Wallings et al., 2015). This may lend an explanation for the divergence of phenotypes described here between the *LRRK2-R1441C* and *LRRK2-G2019S* mutations. Autophagy assays were carried out in Lrrk2-KO cortical cultures in order to discern whether pathogenic mutations led to a toxic-gain or loss of function (see Section 4.1) and it was concluded that mutations cause a toxic-gain of function. However, these data cannot separate between a potential toxic-gain of function and a toxic-gain of novel function in the LRRK2-R1441C cultures, and is an intriguing question to be answered by future research.

As touched upon in Chapter 5, the data presented in this thesis highlights the importance of lysosomes in PD and the potential therapeutic benefit of targeting these organelles. Other PD-associated mutations and genetic risk factors have also shown to cause lysosomal dysfunction. Lysosomal enzymes (e.g. GBA) and transporters (e.g ATP13A2) have been linked to both lysosomal storage disorders (LSDs) and neurodegenerative diseases (Sidransky et al., 2009; Aharon-Peretz et al., 2004; Ramirez et al., 2006; Bras et al., 2012). Mutations in *ATP13A2* lead to increased lysosomal pH and decreased lysosomal degradation in PD patient-derived fibroblasts (Dehay et al., 2012). As well, the *N370S* mutation in the *GBA* gene has been observed to reduce lysosomal Ca^{2+} in PD patient-derived fibroblasts (Kilpatrick et al., 2016). VPS35 deficiency has been reported to perturb the maturation of cathepsin D and cause α-synuclein accumulation in lysosomes of *Drosophila* (Miura et al., 2014). *A53T* mutation in the

SCNA gene also reduce lysosomal protein turn over by decreasing acidification of lysosomes (Stefanis et al., 2001; Cuervo et al., 2004). As well, a number of lysosomal proteins and enzymes have been identified as risk factors for PD, including LIMP2 (Do et al., 2011), TMEM175 (Nalls et al., 2014), ATP6V0A1, Cathepsin B and galactosylceramidase (Chang et al., 2017). Taking all of these reports together with the data described here in this thesis, it is evident that the lysosome plays a critical role in PD pathology. Furthermore, lysosomal functions decreases with age, with a rise in lysosomal pH (Cuervo & Dice, 2000). Lysosomal dysfunction has been shown to lead to the accumulation of α-synuclein (Miura et al., 2014); given that the pathological hallmark of PD is the presence of α-synuclein containing LBs reinforces the vital role of lysosomes in PD. Neurons are especially vulnerable to deficiencies in autophagy substrate clearance. Without the aid of cell division, which mitotic cells can depend upon to decrease the burden of intracellular waste, neurons are largely dependent on autophagy to prevent the accumulation of cellular protein and damaged organelles. This is further emphasised by the fact that both normal and pathological ageing are often associated with decreased autophagic potential (Rubinsztein et al., 2011). It has recently been demonstrated that idiopathic PD brains have an accumulation of ULK1, LAMP1 and p62 in the BG at post-mortem (Mamais et al., 2018), suggesting that lysosomal dysfunction may play a role in idiopathic and sporadic PD and not just familial cases. Collectively, it is evident that targeting the lysosome with small molecules, such as clioquinol and other MPACs, should be considered for future novel therapeutics.

6.2 Future directions

The work presented in this thesis has provided new evidence for mechanisms underlying the role of LRRK2 in lysosomal function and the importance of targeting this organelle in future novel therapeutics, as well as further evidence for the role of LRRK2 in autophagy. These data focused on a small number of compounds that were able to target the lysosome, however a more high-throughput approach will allow for the identification of multiple potential therapeutic drugs. The DQ™-BSA assay would be an ideal assay to take forward for such drug screening. Compared to the pulse chase assay, the DQ™-BSA is logistically suited for large screening libraries as it contains minimal steps and short incubation times. As well, it provides a read-out of the end-goal of autophagy, protein degradation, as opposed to steps further upstream the autophagy pathway such as LC3-II accumulation.

The exact role of the LRRK2 kinase and GTPase domain in the autolysosome maturation deficit associated with LRRK2-R1441C should be characterised. Kinase and GTPase activity assays should be carried out to quantify any changes in the level of these enzymatic activities with the expression of mutant *LRRK2*. The results described in this thesis may suggest that the role of LRRK2-R1441C at the lysosome is kinase independent, as kinase inhibition was unable to ameliorate the autolysosome maturation deficit. Furthermore, potential GPTase effectors of LRRK2 should be investigated as this remains to be elucidated. Recently, a whole raft of new Rab effector proteins have been identified (Gillingham et al., 2014). In *Drosophila*, 23 Rab GTPase proteins that are also found in humans were activated and attached to sepharose beads and binding partners were assessed. By combining this approach with the expression of both GTPase hyperactive and inactive *LRRK2* mutants (R1298L and R1398L/T1343V, respectively), as well as pathogenic *LRRK2* mutants, new effectors could be identified and the effect of pathogenic mutations on binding can be investigated. Interestingly, Gillingham et al., (2014) identified LRRK2 as a novel GTPase effector of Rab18 in drosophila. Rab18 has been

shown to regulate lipid droplet (LD) homeostasis, mediating the apposition of the LD phospholipid monolayer and the ER membrane (Ozeki et al., 2005). Furthermore Rab18 misregulation results in defective lipolysis and aberrantly large lipid droplets (Li et al., 2017). LRRK2 has recently been implicated in lipid droplet homeostasis, with increased Rab8 phosphorylation by LRRK2-Y1699C causing increased lipid droplet size (Yu et al., 2018).

Previously in the Wade-Martins group a dual omics study and phosphoproteomics analysis in iPSC derived DAn pointed to key roles for LRRK2 in endocytosis and endosomal vesicle trafficking. Furthermore, *in vivo* data from aged tissue from these LRRK2-BAC TG rats has demonstrated similar endocytic phenotypes and alterations in synaptic vesicle dispersion in dopaminergic terminals of the dorsal striatum of LRRK2-R1441C aged animals. As well, biochemical analysis of striatal tissue from 22-month old animals has revealed decreases in synapsin 1a/b phosphorylation, total endophilin protein levels, and increases in Rab7 and Rab10 protein expression in both LRRK2-R1441C and LRRK2-G2019S animals. It appears that these perturbations are specific to the endocytic pathway, as proteins involved in exocytosis remained unchanged. These pathways are intrinsically linked to one another, and are integral for many other cellular functions. The endosome is involved in synaptic vesicle recycling (Cousins, 2015), and converges with autophagy at the lysosome. As discussed in section 1.3.4 (iv), there is mounting evidence for the role of LRRK2 in the regulation of Rab GTPases which are instrumental in membrane trafficking. Utilising unbiased omics approaches will allow the identification of LRRK2 substrates and observe global dysregulation of these converging pathways. The potential control of the synergy of membrane dynamics by LRRK2 is an intriguing hypothesis and may explain why one definitive pathological role of LRRK2 is yet to be identified.

Overall this work has demonstrated extensive autophagy and lysosomal phenotypes in *LRRK2* mutant primary cortical cultures. Previous work has suggested such a role of LRRK2 in autophagy but reports were often contradictory and were limited by the use of immortalised cells lines and patient fibroblasts and the reporting of relatively superficial accounts of the autophagy pathway. The data presented here have been performed in disease relevant cells and have overcome the two main challenges in the autophagy literature. The first is the challenge of capturing a dynamic process with static measurements and the second is separating form from function and the common pitfall of assigning function to autophagy based on its detection. These were overcome by measuring autophagy as a dynamic process and modulating the system to probe different steps with the use of protein degradation readouts and autophagy modulating compounds such as chloroquine and trehalose. A new LRRK2 interacting partner, vATPase a1, has been identified in these data, revealing a new underlying mechanism for the role of LRRK2 in autophagy and lysosomal function. These data have demonstrated the importance of LRRK2 in lysosomal biology, as well as the critical role of the lysosome in PD and the potential of lysosome-targeting compounds as a novel therapeutic for the disease.

References

Aasly, J. O., et al. (2010) Novel pathogenic LRRK2 p.Asn1437His substitution in familial Parkinson's disease. *Movement disorders, 25*, 2156-63.

Abdelmotilib, H., et al. (2017) Alpha-synuclein fibril-induced inclusion spread in rats and mice correlates with dopaminergic neurodegeneration. *Neurobiol Dis, 105*, 84–98.

Abou- Sleiman, P. M., et al (2003). The role of pathogenic DJ- 1 mutations in Parkinson's disease. *Ann Neurol, 54*, 283–286.

Adlard, P, A., et al. (2008) Rapid restoration of cognition in Alzheimer's transgenic mice with 8-hydroxy quinoline analogs is associated with decreased interstitial Abeta. *Neuron, 59*, 43–55.

Aharon-Peretz, J., et al. (2004). Mutations in the glucocerebrosidase gene and Parkinson's disease in Ashkenazi Jews. *N Engl J Med, 351*(19), 1972–1977.

Ahlskog, J. E., & Muenter, M. D. (2001). Frequency of levodopa-related dyskinesias and motor fluctuations as estimated from the cumulative literature. *Mov Disord, 16*(3), 448–458.

Albin, R. L., Young, A. B., & Penney, J. B. (1989). The functional anatomy of basal ganglia disorders. *Trends in Neuroscience, 12*(10), 366-375.

Alegre-Abarrategui, J., et al. (2009) LRRK2 regulates autophagic activity and localizes to specific membrane microdomains in a novel human genomic reporter cellular model. *Human Molecular Genetics, 18*, 4022-4034.

Alonso-Canovas, A., et al. (2014). Dopaminergic agonists in Parkinson's disease. *Neurologica, 29*(4), 230-241.

Alzamora, R. F., et al. (2010). PKA regulates vacuolar H+-ATPase localization and activity via direct phosphorylation of the A subunit in kidney cells. *The Journal of Biological Chemistry. 285*(32), 24676–24685.

Anand, V. S., et al. (2009). LRRK2 in Parkinson's disease: biochemical functions. *FEBS J, 276*(22): 6428–6435.

Andres-Mateos, E., et al. (2009) Unexpected lack of hypersensitivity in LRRK2 knock-out mice to MPTP (1-methyl-4-phenyl-1,2,3,6tetrahydropyridine). *The Journal of neuroscience, 29,* 15846-15850.

Appel- Cresswell, S., et al. (2013). Alpha- synuclein p. H50Q, a novel pathogenic mutation for Parkinson's disease. *Mov Disord, 28,* 811–813.

Arranz, A. M., et al. (2015). LRRK2 functions in synaptic vesicle endocytosis through a kinase-dependent mechanism. *J Cell Sci 128*(3), 541-552.

Atashrazm, F., & Dzamko, N. (2016). LRRK2 inhibitors and their potential in the treatment of Parkinson's disease: current perspectives. *Clinical Pharmacology : Advances and Applications, 8,* 177–189.

Axe, E. L., et al. (2008). Autophagosome formation from membrane compartments enriched in phosphatidylinositol 3-phosphate and dynamically connected to the endoplasmic reticulum. *The Journal of Cell Biology, 182*(4), 685–701.

Bach, G., Chen, C. S., & Pagano, R. E. (1999) Elevated lysosomal pH in Mucolipidosis type IV cells. *Clin Chim Acta 280,* 173–179

Bagh, M. B., et al. (2017). Misrouting of v-ATPase subunit V0a1 dysregulates lysosomal acidification in a neurodegenerative lysosomal storage disease model. *Nature Communications, 8,* 14612.

Baptista, M. A., et al. (2013) Loss of leucine-rich repeat kinase 2 (LRRK2) in rats leads to progressive abnormal phenotypes in peripheral organs, *PloS one. 8*, e80705.

Barcia, C., et al. (2011). IFN-γ signaling, with the synergistic contribution of TNF-α, mediates cell specific microglial and astroglial activation in experimental models of Parkinson's disease. *Cell Death & Disease, 2*(4), e142–.

Bareggi, S. R., & Cornelli, U. (2012). Clioquinol: review of its mechanisms of action and clinical uses in neurodegenerative disorders. *CNS Neurosci Ther. 18(*1), 41-46.

Barker, R. A., et al. (2013). Fetal dopaminergic transplantation trials and the future of neural grafting in Parkinson's disease. *Lancet Neurol, 12*, 84-91.

Bartolomeo, S., et al. (2010). The dynamic interaction of AMBRA1 with the dynein motor complex regulates mammalian autophagy. *The Journal of Cell Biology*, *191*(1), 155-168.

Baum, L., & Ng, A. (2004). Curcumin interaction with copper and iron suggests one possible mechanism of action in Alzheimer's disease animal models. *J Alzheimers Dis, 6*(4), 367-77.

Beccano-Kelly, D. A., et al. (2014). Synaptic function is modulated by LRRK2 and glutamate release is increased in cortical neurons of G2019S LRRK2 knock-in mice. *Front Cell Neurosci 8,* 301

Beccano-Kelly, D., et al. (2015). LRRK2 overexpression alters glutamatergic presynaptic plasticity, striatal dopamine tone, postsynaptic signal transduction, motor activity and memory. *Hum Mol Genet, 24*(5): 1336–1349.

Beilina, A., et al. (2014). Unbiased screen for interactors of leucine-rich repeat kinase 2 supports a common pathway for sporadic and familial Parkinson disease. *Proc Natl Acad Sci U S A 111*(7), 2626-2631.

Bengoa-Vergniory, N., et al. (2017). Alpha-synuclein oligomers: a new hope. *Acta Neuropathologica*, *134*(6), 819–838.

Berg D, et al., (2012). MDS research criteria for prodromal Parkinson's Disease. *Movement Disorders*. *30*(12). 1600-11.

Berg, K., & Moan, J. (1994). Lysosomes as photochemical targets. *Int J Cancer*. *59*(6), 814-822.

Berger Z, et al. (2010). Membrane localization of LRRK2 is associated with increased formation of the highly active LRRK2 dimer and changes in its phosphorylation. *Biochemistry*, *49*(26), 5511–5523.

Berridge, M. J. (2012). Calcium signalling remodelling and disease. *Biochem Soc Trans. 40*(2), 297-309.

Bertuchi F. R., et al. (2014). General chelating action of copper, zinc and iron in mammalian cells. *Analytical Methods*, *6*(21):8488–8493.

Betarbet R, et al. (2000). Chronic systemic pesticide exposure reproduces features of Parkinson's disease. *Nat Neurosci 3*, 1301–1306

Bichler, Z., et al. (2013). Non-motor and motor features in LRRK2 transgenic mice. *PloS one, 8*, e70249.

Bijlmakers, M. J., & Marsh, M. (2003) The on-off story of protein palmitoylation. *Trends Cell Biol. 13*, 32–42.

Biosa A, et al. (2013). GTPase activity regulates kinase activity and cellular phenotypes of Parkinson's disease-associated LRRK2. *Hum Mol Genet, 22*(6), 1140–1156.

Biskup, S., et al. (2006) Localization of LRRK2 to membranous and vesicular structures in mammalian brain. *Ann Neurol. 60*, 557-69.

Bjorklund, L. M., et al. (2002). Embryonic stem cells develop into functional dopaminergic neurons after transplantation in a Parkinson rat model. *Proc Natl Acad Sci 99*, 2344–2349

Bosomworth, H. J., et al. (2013). Altered Expression of ZnT10 in Alzheimer's Disease Brain. *PLoS ONE, 8(*5), e65475.

Bove, J., & Perrier, C. (2012). Neurotoxin-based models of Parkinson's disease. *Neuroscience.* 51-76

Braak, H., et al. (2003). 'Staging of brain pathology related to sporadic Parkinson's disease',

Brain Pathol. 17(2): 139–145.

Branchi, I., et al. (2008). Nonmotor symptoms in Parkinson's disease: investigating early-phase onset of behavioral dysfunction in the 6-hydroxydopamine-lesioned rat model. *J Neurosci Res. 86*(9): 2050–2061.

Bras, J., et al. (2012). Use of next-generation sequencing and other whole-genome strategies to dissect neurological disease. *Nat Rev Neurosci. 13*(7), 453-464.

Bravo-San Pedro, J. M., et al. (2013) The LRRK2 G2019S mutant exacerbates basal autophagy through activation of the MEK/ERK pathway. *Cell Mol Life Sci. 70*, 121-36.

Breit, S., et al. (2004). Deep brain stimulation. *Cell Tissue Res. 318*(1), 275–288.

Burré, J., Sharma, M. & Sudhof, T. C. (2014). α-Synuclein assembles into higher-order multimers upon membrane binding to promote SNARE complex formation. *Proc. Natl Acad. Sci. USA 111,* E4274–E4283.

Bush, A. I. (2003). The metallobiology of Alzheimer's disease. *Trends Neuroscience, 26*, 207- 14.

Cannon, J. R., et al. (2009). A highly reproducible rotenone model of Parkinson's disease. *Neurobiol Dis 34*, 279–290

Cannon, J.R., et al. (2013). Expression of human E46K-mutated alpha-synuclein in BAC-transgenic rats replicates earlystage Parkinson's disease features and enhances vulnerability to mitochondrial impairment. *Experimental neurology, 240*, 44-56.

Carraway, R. E., & Dobner, P. R. (2012). Zinc pyrithione induces ERK- and PKC-dependent necrosis distinct from TPEN-induced apoptosis in prostate cancer cells. *Biochimica et Biophysica Acta-Molecular Cell Research, 1823*(2), 544–557.

Chang, D., et al. (2017). A meta-analysis of genome-wide association studies identifies 17 new Parkinson's disease risk loci. *Nature Genetics, 49,* 1511-1516.

Chaturvedi, R. K., & Beal, M. F. (2008). Mitochondrial approaches for neuroprotection. *Annals of the New York Academy of Sciences, 1147,* 395–412.

Chauhan, S., et al. (2015). Pharmaceutical screen identifies novel target processes for activation of autophagy with a broad translational potential. *Nature Communications, 6*, 8260.

Chen, C. C., et al. (2014). A small molecule restores function to TRPML1 mutant isoforms responsible for mucolipidosis type IV. *Nat Commun, 14*(5), 4681.

Chen, C.Y., et al. (2012). (G2019S) LRRK2 activates MKK4-JNK pathway and causes degeneration of SN dopaminergic neurons in a transgenic mouse model of PD. *Cell death and differentiation, 19,* 1623-1633.

Cherra, S. J., et al. (2013). Mutant LRRK2 elicits calcium imbalance and depletion of dendritic mitochondria in neurons. *Am J Pathol 182*(2), 474-484.

Chou, J.S., et al. (2014). (G2019S) LRRK2 causes early-phase dysfunction of SNpc dopaminergic neurons and impairment of corticostriatal long-term depression in the PD transgenic mouse. *Neurobiology of disease, 68,* 190-199

Christensen, K. A., Myers, J. T., & Swanson, J. A. (2002). pH-dependent regulation of lysosomal calcium in macrophages. *Journal of Cell Science. 115,* 599-607.

Chung, C. Y. et al. (2013). Identification and rescue of α-synuclein toxicity in Parkinson patient-derived neurons. *Science 342*, 983–987.

Churchill, G., et al. (2002). NAADP mobilizes Ca(2+) from reserve granules, lysosome-related organelles, in sea urchin eggs. *Cell. 111*(5): 703-708.

Cicchetti, F., et al. (2005). Systemic exposure to paraquat and maneb models early Parkinson's disease in young adult rats. *Neurobiol Dis 20*, 360–371

Cilia, R., et al. (2014). LRRK2 mutations in Parkinson's disease: Confirmation of a gender effect in the Italian population. *Parkinsonism & Related Disorders, 20*(8), 911–914.

Clapham, D. E. (2007). Calcium signalling. *Cell. 131*(6), 1047-1058

Cocheme, H. M., & Murphy, M. P. (2008). Complex I is the major site of mitochondrial superoxide production by paraquat. *J Biol Chem 283,* 1786–1798

Coffey, E. E., et al. (2014). Lysosomal alkalization and dysfunction in human fibroblasts with the Alzheimer's disease-linked presenilin 1 A246E mutation can be reversed with cAMP. *Neuroscience, 263,* 111-124.

Coleman, D. T., et al. (2015). Curcumin Prevents Palmitoylation of Integrin β4 in Breast Cancer Cells. *PLoS ONE, 10*(5), e0125399.

Colosimo, C., et al. (2003). Lewy body cortical involvement may not always predict dementia in Parkinson's disease. *Journal of Neurology, Neurosurgery, and Psychiatry, 74*(7), 852–856.

Cookson, M. R., et al. (2011). Insight into the mode of action of the LRRK2 Y1699C pathogenic mutant. *J Neurochem. 116*(2), 304–315.

Cooper, A. A., et al. (2006). α-Synuclein blocks ER–Golgi traffic and Rab1 rescues neuron loss in Parkinson's models. *Science 313,* 324–328.

Corasaniti, M. T., et al. (1991). Evidence that paraquat is able to cross the blood-brain barrier to a different extent in rats of various age. *Funct Neurol 6,* 385–391

Costa, G., et al. (2012). Paraoxonase 1 (PON1) as a genetic determinant of susceptibility to organophosphate toxicity. *Toxicology*

Cotter, K., et al. (2015). Recent Insights into the Structure, Regulation and Function of the V-ATPases. *Trends in Biochemical Sciences, 40*(10), 611–622.

Cousin, M. A. (2015). Synaptic Vesicle Endocytosis and Endosomal Recycling in Central Nerve Terminals: Discrete Trafficking Routes? *Neuroscientist. 21*(4):413-23.

Covy, J. P., & Giasson, B. I. (2009). Identification of compounds that inhibit the kinase activity of leucine-rich repeat kinase 2. *Biochem. Biophys. Res. Commun, 378*, 473–477.

Cuajungco, M. P., & Kiselyov, K. (2017). The Mucolipin-1 (TRPML1) Ion Channel, Transmembrane-163 (TMEM163) Protein, and Lysosomal Zinc Handling. *Frontiers in Bioscience (Landmark Edition), 22,* 1330–1343.

Cuervo, A. M., & Dice, J. F. (2000). Age-related decline in chaperone-mediated autophagy. *J Biol Chem, 275*(40): 31505–31513

Cuervo, A. M., et al. (2004). Impaired degradation of mutant alpha-synuclein by chaperone-mediated autophagy. *Science. 305*(5688), 1292–1295.

Dachsel, J.C., et al. (2010). A comparative study of Lrrk2 function in primary neuronal cultures. *Parkinsonism & related disorders, 16*, 650-655

Daher, J.P., et al. (2012). Neurodegenerative phenotypes in an A53T alpha-synuclein transgenic mouse model are independent of LRRK2. *Human molecular genetics, 21*, 2420-2431.

Daher, J.P., et al. (2014). Abrogation of alpha-synuclein-mediated dopaminergic neurodegeneration in LRRK2-deficient rats. *Proceedings of the National Academy of Sciences of the United States of America, 111*, 9289-9294.

Daniel, G., & Moore, D. J. (2015). Modeling LRRK2 Pathobiology in Parkinson's Disease: From Yeast to Rodents. *Curr Top Behav Neurosci*, *22*, 331-68.

Daniëls, V., et al. (2011). Insight into the mode of action of the Lrrk2 Y1699C pathogenic mutant. *Journal of Neurochemistry, 116*(2), 304–315.

Dardiotis, E., et al. (2013). The interplay between environmental and genetic factors in Parkinson's disease susceptibility: the evidence for pesticides. *Toxicology, 307*, 17–23.

Davis, G, C,. et al. (1979). Chronic Parkinsonism secondary to intravenous injection of meperidine analogues. *Psychiatry Res, 1*, 249–254.

Dawson, T. M., Ko, H. S., & Dawson, V. L. (2010). Genetic Animal Models of Parkinson's Disease. *Neuron, 66*(5), 646–661.

Dehay, B., et al. (2012) Loss of P-type ATPase ATP13A2/PARK9 function induces general lysosomal deficiency and leads to Parkinson disease neurodegeneration. *Proceedings of the National Academy of Sciences of the United States of America, 109,* 9611-9616.

Deng, H., et al. (2006). Genetic analysis of LRRK2 mutations in patients with Parkinson disease. *J Neurol Sci. 251(*1-2): 102–106.

Deng, X., et al. (2011). Characterization of a selective inhibitor of the Parkinson's disease kinase LRRK2, *Nat Chem Biol. 7*, 203-5.

Derivery, E., & Gautreau, A. (2010). Evolutionary conservation of the WASH complex, an actin polymerization machine involved in endosomal fission. *Communicative & Integrative Biology, 3*(3), 227–230.

Deyaert, E., et al. (2017). A homologue of the Parkinson's disease-associated protein LRRK2 undergoes a monomer-dimer transition during GTP turnover. *Nat Commun. 8*(1), 1008.

Di Fonzo, A., et al. (2006). Comprehensive analysis of the LRRK2 gene in sixty families with Parkinson's disease. *Eur J Hum Genet, 14*(3), 322–331.

Di Maio, R., et al. (2018). LRRK2 activation in idiopathic Parkinson's disease. *Sci Transl Med. 10*(451). pii: eaar5429

Dickson, D. W., et al. (2009). Neuropathology of non-motor features of Parkinson disease. *Parkinsonism Relat Disord. 15 Suppl 3:*S1-5.

Do, C. B., et al. (2011). Web-Based Genome-Wide Association Study Identifies Two Novel Loci and a Substantial Genetic Component for Parkinson's Disease. *PLoS Genetics, 7*(6), e1002141.

Doherty, K. M., & Hardy, J. (2013). Parkin Disease and the Lewy Body Conundrum. *Movement Disorders, 28*(6), 702–704.

Dranka, B.P., et al. (2013). Diapocynin prevents early Parkinson's disease symptoms in the leucine-rich repeat kinase 2 (LRRK2R(1)(4)(4)(1)G) transgenic mouse. *Neuroscience letters, 549*, 57-62

Drolet RE, et al. (2009). Chronic rotenone exposure reproduces Parkinson's disease gastrointestinal neuropathology. *Neurobiol Dis 36*, 96–102

Dultheil, F., et al. (2010). Interaction between ABCB1 and professional exposure to organochlorine insecticides in Parkinson disease Arch. *Neurol., 67,* 739-745.

Dusonchet, J., et al. (2011). A rat model of progressive nigral neurodegeneration induced by the Parkinson's disease-associated G2019S mutation in LRRK2. *The*

Journal of neuroscience : the official journal of the Society for Neuroscience, 31, 907-912.

Dzamko N, et al. (2014). Inflammation is genetically implicated in Parkinson's disease. *Neuroscience.*

Dzamko, N., et al. (2010) Inhibition of LRRK2 kinase activity leads to dephosphorylation of Ser(910)/Ser(935), disruption of 143-3 binding and altered cytoplasmic localization. *The Biochemical journal, 430*, 405-13.

Edmondson, D. E., Binda, C., & Mattevi, A. (2007). Structural insights into the mechanism of amine oxidation by monoamine oxidases a and b. *Archives of Biochemistry and Biophysics*, *464*(2), 269–276.

Edvardson, S., et al. (2012). A Deleterious Mutation in DNAJC6 Encoding the Neuronal-Specific Clathrin-Uncoating Co-Chaperone Auxilin, Is Associated with Juvenile Parkinsonism. *PLoS ONE, 7(*5), e36458.

Ehringer, H., & Hornykiewicz, O. (1960). Distribution of noradrenaline and dopamine (3-hydroxytyramine) in the human brain and their behavior in diseases of the extrapyramidal system. *Klin Wochenschr, 38*, 1236-9.

Elbaz. A., et al. (2004). CYP2D6 polymorphism, pesticide exposure, and Parkinson's disease *Ann. Neurol, 55*, 430-434

Ellis, J., & Fell, M. J. (2017).Current approaches to the treatment of Parkinson's Disease. *Bioorg Med Chem Lett.*

Estrada, A., et al. (2014). Discovery of highly potent, selective, and brain-penetrant aminopyrazole leucine-rich repeat kinase 2 (LRRK2) small molecule inhibitors. *J Med Chem, 57*(3), 921–936.

Fader, C. M., et al. (2009). TI-VAMP/VAMP7 and VAMP3/cellubrevin: two v-SNARE proteins involved in specific steps of the autophagy/multivesicular body pathways. *Biochim. Biophys. Acta, 1793,* 1901-1916

Febbraro, F., et al. (2013). Chronic intranasal deferoxamine ameliorates motor defects and pathology in the α-synuclein rAAV Parkinson's model. *Exp Neurol, 247,* 45-58.

Fell, M., et al. (2015). MLi-2, a Potent, Selective, and Centrally Active Compound for Exploring the Therapeutic Potential and Safety of LRRK2 Kinase Inhibition. *J Pharmacol Exp Ther, 355*(3): 397–409

Feng, X., & Yang, J. (2016). Lysosomal calcium in neurodegeneration. *Messenger 5*:56–65

Feng, X., et al. (2014). Differential mechanisms of action of the mucolipin synthetic agonist, ML-SA1, on insect TRPML and mammalian TRPML1. *Cell Calcium, 56*(6), 446–456.

Fernagut, P. O., et al. (2007). Behavioral and histopathological consequences of paraquat intoxication in mice: Effects of alpha-synuclein over-expression. *Synapse 61,* 991–1001.

Fernandez, H., & Chen, J. (2007). Monamine oxidase inhibitors: current and emerging agents for Parkinson disease. *Clin Neuropharmacol. 30*(3): 150–168.

Ferreira, F., & Mannos, J. (2017). An updated review of Parkinson's disease genetics and clinicopathological correlations. *Acta Neurol Scand, 135*(3), 273-284.

Finkelstein, D. I., et al. (2016). Clioquinol Improves Cognitive, Motor Function, and Microanatomy of the Alpha-Synuclein hA53T Transgenic Mice. *ACS Chem Neurosci. 7*(1), 119-29.

Finnigan, G. C., et al. (2012). Sorting of the Yeast Vacuolar-type, Proton-translocating ATPase Enzyme Complex (V-ATPase): identification of a necessary and sufficient golgi/endosomal retention signal in stv1p. *J Biol Chem*. *287*, 19487–19500.

Fleming, S. M., et al. (2004). Behavioral and immunohistochemical effects of chronic intravenous and subcutaneous infusions of varying doses of rotenone. *Exp Neurol 187*, 418–429

Flores, E. N, & García-Anoveros. (2011). TRPML2 and the evolution of mucolipins. *Adv Exp Med Biol, 704*, 221-8.

Fornai, F., et al. (2005). Parkinson-like syndrome induced by continuous MPTP infusion: convergent roles of the ubiquitin-proteasome system and alpha-synuclein. *Proc Natl Acad Sci U S A, 102,* 3413-3418.

Forno, L. S. (1987). The Lewy body in Parkinson's disease. *Advances in Neurology, 45*, 35-43.

Fuji, R., et al. (2015). Effect of selective LRRK2 kinase inhibition on nonhuman primate lung. *Sci Transl Med, 7*(273), 273ra15.

Fujimito, T., et al. (2018). Parkinson's disease-associated mutant LRRK2 phosphorylates Rab7L1 and modifies trans-Golgi morphology. *Biochem Biophys Res Commun.*

Fukada T., & Kambe, T. (2011). Molecular and genetic features of zinc transporters in physiology and pathogenesis. *Metallomics, 3,* 662–674.

Fukushima, T., Tan, X., & Kanda, H. (2011). Serum vitamins and heavy metals in blood and urine, and the correlations among them in Parkinson's disease patients in China, *Neuroepidemiology*. *36*(4), 240-244.

Funayama, M., K., et al. (2005). An LRRK2 mutation as a cause for the parkinsonism in the original PARK8 family. *Ann Neurol 57*(6), 918-921.

Furuta, N., et al. (2010). Combinational soluble N-ethylmaleimide-sensitive factor attachment protein receptor proteins VAMP8 and Vti1b mediate fusion of antimicrobial and canonical autophagosomes with lysosomes *Mol. Biol. Cell, 21*, 1001-1010.

G. Rozas, E., et al. (1998). The overall rod performance test in the MPTP-treated-mouse model of Parkinsonism. *J Neurosci Methods, 83*, 165-175.

Gaig, C., et al. (2007). G2019S LRRK2 mutation causing Parkinson's disease without Lewy bodies. *Journal of Neurology, Neurosurgery, and Psychiatry, 78*(6), 626–628.

Galea, G., & Simpson, J. C. (2015). High-content analysis of Rab protein function at the ER-Golgi interface. *Bioarchitecture, 5*(3-4), 44–53.

Gao, F., et al. (2017). Mitophagy in Parkinson's Disease: Pathogenic and Therapeutic Implications. *Frontiers in Neurology, 8,* 527.

Garcia-Miralles, M., J. et al. (2015). No dopamine cell loss or changes in cytoskeleton function in transgenic mice expressing physiological levels of wild type or G2019S mutant LRRK2 and in human fibroblasts. *PLoS One 10(*4), e0118947.

Gardet, A., et al. (2010) LRRK2 is involved in the IFN-gamma response and host response to pathogens. *J Immunol, 185*, 5577-85.

Garrity, A. G., et al. (2016). The endoplasmic reticulum, not the pH gradient, drives calcium refilling of lysosomes. *Elife. 5*, e15887.

Giaime, E., et al. (2017). Age-Dependent Dopaminergic Neurodegeneration and Impairment of the Autophagy-Lysosomal Pathway in LRRK-Deficient Mice. *Neuron, 96*(4), 796-807.

Giesert, F., et al. (2013). Expression analysis of Lrrk1, Lrrk2 and Lrrk2 splice variants in mice. *PloS one, 8*, e63778.

Giesert, F., et al. (2017). The pathogenic LRRK2 R1441C mutation induces specific deficits modeling the prodromal phase of Parkinson's disease in the mouse. *Neurobiol Dis, 105*, 179-193.

Gillardon, F., Schmid, R. & Draheim, H. (2012) Parkinson's disease-linked leucine-rich repeat kinase 2(R1441G) mutation increases proinflammatory cytokine release from activated primary microglial cells and resultant neurotoxicity, *Neuroscience, 208*, 41-8.

Gillingham, A. K., et al. (2014). Toward a Comprehensive Map of the Effectors of Rab GTPases. *Developmental Cell, 31*(3), 358–373.

Goldwurm, S., et al. (2011). Kin-cohort analysis of LRRK2-G2019S penetrance in Parkinson's disease. *Mov Disord 26*(11), 2144-2145.

Gomez-Suaga, P., et al. (2012). Leucine-rich repeat kinase 2 regulates autophagy through a calcium-dependent pathway involving NAADP. *Human molecular genetics, 21*, 511-25.

Gomez-Suaga, P., et al. (2014). LRRK2 delays degradative receptor trafficking by impeding late endosomal budding through decreasing Rab7 activity. *Hum Mol Genet, 23*(25), 6779-6796.

Gottlieb, C. D., Zhang, S., & Linder, M. E. (2015). The Cysteine-rich Domain of the DHHC3 Palmitoyltransferase Is Palmitoylated and Contains Tightly Bound Zinc. *The Journal of Biological Chemistry, 290*(49), 29259–29269.

Graves, A., et al. (2008). The Cl-/H+ antiporter ClC-7 is the primary chloride permeation pathway in lysosomes. *Nature, 453*(7196), 788–792.

Greggio, E., Bubacco, L., & Russo. I. (2017). Cross-talk between LRRK2 and PKA: implication for Parkinson's disease? *Biochemical Society Transactions, 45*(1), 261-267.

Grenier, K., et al. (2013). Parkin- and PINK1-dependent mitophagy in neurons: will the real pathway please stand up? *Front Neurol*

Gronostajski, R. M., & Pardee, A. B. (1984). Protein degradation in 3T3 cells and tumorigenic transformed 3T3 cells. *J Cell Physiol 119*(1), 127-132.

Grunewald, A., B. et al. (2014). Does uncoupling protein 2 expression qualify as marker of disease status in LRRK2associated Parkinson's disease? *Antioxid Redox Signal 20*(13), 1955-1960.

Guicciardi, M. E., Marcel, L., & Gregory, G. (2004). Lysosomes in cell death. *Oncogene, 23*, 2881-90.

Gumber, A., et al. (2017). Economic, Social and Financial Cost of Parkinson's on Individuals, Carers and their Families in the UK: Final Report. Sheffield Hallam University, UK.

Hakimi, M., et al. (2011). Parkinson's disease-linked LRRK2 is expressed in circulating and tissue immune cells and upregulated following recognition of microbial structures. *Journal of neural transmission, 118,* 795-808

Han, J. D., et al. (2004). Evidence for dynamically organized modularity in the yeast protein-protein interaction network. *Nature, 430*(6995), 88-93.

Hara, T., et al. (2006). Suppression of basal autophagy in neural cells causes neurodegenerative disease in mice. *Nature, 441*(15), 885-889.

Hauser, R., et al. (2007). Ten-year follow-up of Parkinson's disease patients randomized to initial therapy with ropinirole or levodopa. *Mov Disord. 22*(16), 2409–2417.

Healy, D. G., et al. (2008). Phenotype, genotype, and worldwide genetic penetrance of LRRK2-associated Parkinson's disease: a case-control study, *Lancet Neurol, 7*, 583-90.

Hebron, M. L., Lonskaya, I., & Moussa, C. E.-H. (2013). Nilotinib reverses loss of dopamine neurons and improves motor behavior via autophagic degradation of α-synuclein in Parkinson's disease models. *Human Molecular Genetics, 22*(16), 3315–3328.

Hedrich, K., et al. (2004). Distribution, type, and origin of Parkin mutations: review and case studies. *Mov Disord, 19*(10), 1146–1157.

Helwig, M., et al. (2016). Brain propagation of transduced α-synuclein involves non-fibrillar protein species and is enhanced in α-synuclein null mice. *Brain, 139*(Pt 3), 856–870.

Hely, M. A., et al. (2008). The Sydney multicenter study of Parkinson's disease: the inevitability of dementia at 20 years. *Movement Disorders, 23*(6), 837-844.

Henry, A. G., et al. (2015). Pathogenic LRRK2 mutations, through increased kinase activity, produce enlarged lysosomes with reduced degradative capacity and increase ATP13A2 expression. *Human Molecular Genetics, 24*(21): 6013-6028.

Hernandez, D. G., et al. (2005). Clinical and positron emission tomography of Parkinson's disease caused by LRRK2. *Ann Neurol 57*(3), 453-456.

Herzig, M. C., et al. (2011). LRRK2 protein levels are determined by kinase function and are crucial for kidney and lung homeostasis in mice. *Hum Mol Genet 20*(21), 42094223.

Herzig, M. C., et al. (2012). High LRRK2 levels fail to induce or exacerbate neuronal alpha synucleinopathy in mouse brain. *PloS one, 7,* e36581

Hinkle, K.M., et al. (2012) LRRK2 knockout mice have an intact dopaminergic system but display alterations in exploratory and motor co-ordination behaviors. *Molecular neurodegeneration, 7,* 25

Hockey, L. N., et al. (2015). Dysregulation of lysosomal morphology by pathogenic LRRK2 is corrected by TPC2 inhibition. *J Cell Sci 128*(2), 232-238.

Hoglinger, G. U., (2003). Chronic systemic complex I inhibition induces a hypokinetic multisystem degeneration in rats. *J Neurochem, 84,* 491–502

Houlden, H., & Singleton, A. B. (2012). The genetics and neuropathology of Parkinson's disease. *Acta Neuropathol, 124,* 32.

Hoyer-Hansen, M., & Jaattela, M. (2007). Connecting endoplasmic reticulum stress to autophagy by unfolded protein response and calcium *Cell Death Differ, 14,* 1576-1582

Hozumi, I., et al. (2011). Patterns of levels of biological metals in CSF differ among neurodegenerative diseases. *Journal of Neurological Sciences, 303*(1-2), 95-99.

Hsieh, C. H., et al. (2016). Functional Impairment in Miro Degradation and Mitophagy Is a Shared Feature in Familial and Sporadic Parkinson's Disease. *Cell Stem Cell 19*(6), 709-724.

Hsieh, C.-H., et al. (2016). Functional Impairment in Miro Degradation and Mitophagy Is a Shared Feature in Familial and Sporadic Parkinson's Disease. *Cell Stem Cell, 19*(6), 709–724.

Hudkins, R. L., et al. (2008) Mixedlineage kinase 1 and mixed-lineage kinase 3 subtype-selective dihydronaphthyl[3,4-a]pyrrolo[3,4c]carbazole-5-ones: optimization, mixed-lineage kinase 1 crystallography, and oral in vivo activity in 1-methyl-4-phenyltetrahydropyridine models, *Journal of medicinal chemistry, 51*, 5680-9.

Hung, H. H., et al. (2017). Dopamine elevates intracellular zinc concentration in cultured rat embryonic cortical neurons through the cAMP-nitric oxide signaling cascade. *Molecular and Cellular Neurosciences, 82*, 35-45.

Hyun, H. J., et al. (2001). Depletion of intracellular zinc and copper with TPEN results in apoptosis of cultured human retinal pigment epithelial cells. *Invest Ophthalmol Vis Sci*, *42*(2), 460-5.

Iranzo, A., et al. (2014). Neuropathology of prodromal Lewy body disease. *Movement Disorder, 29*, 410-415.

Ishida, Y., Nayak, S., Mindell, J. A., & Grabe, M. (2013). A model of lysosomal pH regulation. The *Journal of General Physiology, 141*(6), 705–720.

Ishihara, L., et al. (2006). Clinical features of Parkinson disease patients with homozygous leucine-rich repeat kinase 2 G2019S mutations. *Arch Neurol, 63*(9), 1250–1254.

Ishizawa, T., et al. (2003). Colocalization of tau and alpha-synuclein epitopes in Lewy bodies. *J Neuropathol Exp Neurol, 62*(4), 389–397.

Islam, M. S., et al. (2016). Human R1441C LRRK2 regulates the synaptic vesicle proteome and phosphoproteome in a Drosophila model of Parkinson's disease. *Human Molecular Genetics, 25*(24), 5365–5382.

Itakato, E., et al. (2012). The hairpin-type tail-anchored SNARE syntaxin 17 targets to autophagosomes for fusion with endosomes/lysosomes. *Cell, 151*(6), 1256-69.

Ito G, et al. (2007). GTP binding is essential to the protein kinase activity of LRRK2, a causative gene product for familial Parkinson's disease. *Biochemistry, 46*(5), 1380–1388.

Jahn, R., & Scheller, R. H. (2006). SNAREs--engines for membrane fusion. *Nat Rev Mol Cell Biol*, 7(9):631-43.

Jaleel, M., et al. (2007). LRRK2 phosphorylates moesin at threonine-558: characterization of how Parkinson's disease mutants affect kinase activity. *Biochemical Journal, 405*(Pt 2), 307–317.

Janezic, S., et al. (2013). Deficits in dopaminergic transmission precede neuron loss and dysfunction in a new Parkinson model. *Proceedings of the National Academy of Sciences of the United States of America, 110*, E4016-4025

Jenner, P. (2008). Functional models of Parkinson's disease: a valuable tool in the development of novel therapies. *Ann Neurol, 64*(Suppl 2), S16-29.

Jeon, B. S., Jackson-Lewis, V., & Burke, R. E. (1995). 6-hydroxydopamine lesion of the rat substantia nigra: time course and morphology of cell death. *Neurodegeneration 4*, 131–137.

Jeong, G. R., et al. (2018). Dysregulated phosphorylation of Rab GTPases by LRRK2 induces neurodegeneration. *Molecular Neurodegeneration, 13,* 8.

Jiang, Z., de Messieres, M., & Lee, J. C. (2013). Membrane Remodeling by α-Synuclein and Effects on Amyloid Formation. *Journal of the American Chemical Society, 135*(43), 10.1021/ja405993r.

Jinn, S., et al. (2017). TMEM175 deficiency impairs lysosomal and mitochondrial function and increases α-synuclein aggregation. *Proceedings of the National Academy of Sciences of the United States of America, 114*(9), 2389–2394.

Johnson, D. E., et al. (2016). The position of lysosomes within the cell determines their luminal pH. *The Journal of Cell Biology, 212*(6), 677–692.

Jura, N., et al. (2011) Catalytic control in the EGF receptor and its connection to general kinase regulatory mechanisms, *Molecular cell, 42*, 9-22.

Justus C. Dächsel, J. C., & Farrer, M. J. (2010). LRRK2 and Parkinson disease. *Arch Neuro, 67*(5), 542–547.

Kabeya, Y., et al. (2009). Characterization of the Atg17-Atg29-Atg31 complex specifically required for starvation-induced autophagy in Saccharomyces cerevisiae. *Biochem Biophys Res Commun, 389*(4), 612–615.

Kachergus, J., et al. (2005). Identification of a novel LRRK2 mutation linked to autosomal dominant parkinsonism: evidence of a common founder across European populations. *Am J Hum Genet 76*(4), 672-680.

Kalia, L. V., & Lang, A. E. (2015). Parkinson's Disease. *Lancet, 386*(9996), 896-912.

Kalia, L. V., et al. (2014). Clinical Correlations With Lewy Body Pathology in LRRK2-Related Parkinson Disease, *JAMA neurology.*

Kambe, T., Hashimoto, A., & Fujimoto, S. (2014). Current understanding of ZIP and ZnT zinc transporters in human health and diseases. *Cell. Mol. Life Sci, 71,* 3281–3295.

Kambe, T., Weaver, B.P., & Andrews, G.K. (2008). The genetics of essential metal homeostasis during development. *Genesis, 46,* 214–228.

Karacsonyi, C., Miguel, A. S., & Puertollano, R. (2007). Mucolipidin-2 localizes to the Arf-6-associated pathway and regulates recycling of GPI-APs. *Traffic, 8,* 1404–1414.

Kaufmann, A. M., & Krise, J. P. (2007). Lysosomal sequestration of amine-containing drugs: Analysis and therapeutic implications. *J Pharm Sci, 96,* 729–746.

Kaur, D., et al. (2003). Genetic or pharmacological iron chelation prevents MPTP-induced neurotoxicity in vivo: a novel therapy for Parkinson's disease. *Neuron, 37(*6), 899-909.

Kawamato, Y., et al. (2002). 14-3-3 proteins in Lewy bodies in Parkinson disease and diffuse Lewy body disease brains. *J Neuropathol Exp Neurol, 61*(3), 245–253.

Kett, L. R., & Dauer, W. T. (2016). Endolysosomal Dysfunction in Parkinson Disease: Recent Developments and Future Challenges. *Movement Disorders : Official Journal of the Movement Disorder Society*, *31*(10), 1433–1443.

Khoo, T. K., et al., (2013). The spectrum of nonmotor symptoms in early Parkinson disease, *Neurology, 80,* 276-281.

Kihara, A., et al. (2001). Beclin-phosphatidylinositol 3-kinase complex functions at the trans-Golgi network. *EMBO Reports, 2*(4), 330-335

Kilpatrick, B. S., et al. (2016). Endoplasmic reticulum and lysosomal Ca2+ stores are remodelled in GBA1-linked Parkinson disease patient fibroblasts. *Cell Calcium, 59*(1), 12–20.

Kirik, D., et al. (2002). Parkinson-like neurodegeneration induced by targeted overexpression of alpha-synuclein in the nigrostriatal system. *J Neurosci, 22*(7), 2780–2791.

Kirkeby, A., et al. (2012). Generation of regionally specified neural progenitors and functional neurons from human embryonic stem cells under defined conditions, *Cell reports, 1*, 703-14.

Kitada T, et al. (1998). Mutations in the parkin gene cause autosomal recessive juvenile parkinsonism. *Nature, 392*, 605–608

Klein, R., et al. (2002). Dopaminergic cell loss induced by human A30P alpha-synuclein gene transfer to the rat substantia nigra. *Hum Gene Ther, 3*(5), 605–612.

Klionsky, D. J,. et al. (2008). Does bafilomycin A1 block the fusion of autophagosomes with lysosomes? *Autophagy, 4,* 849–950.

Kluss, J. H., et al. (2018). Detection of endogenous S1292 LRRK2 autophosphorylation in mouse tissue as a readout for kinase activity. *Parkinson's Disease, 4*(13).

Ko, H. S., et al. (2010). Phosphorylation by the c-Abl protein tyrosine kinase inhibits parkin's ubiquitination and protective function. *Proceedings of the National Academy of Sciences of the United States of America, 107*(38), 16691–16696.

Koentjoro, B., et al. (2012). Phenotypic variability of parkin mutations in single kindred. *Mov Disord. 27*(10), 1299–1303.

Koentjoro, B., Park, J.-S., & Sue, C. M. (2017). Nix restores mitophagy and mitochondrial function to protect against PINK1/Parkin-related Parkinson's disease. *Scientific Reports, 7*, 44373.

Kordower, J. H., et al. (2013). Disease duration and the integrity of the nigrostriatal system in Parkinson's disease. *Brain. 136*(8), 2419-2431.

Kordower, J., et al. (2008). Lewy body-like pathology in long-term embryonic nigral transplants in Parkinson's disease. *Nat Med, 14*(5), 504-6

Korolchuk, V. I., et al. (2009). Autophagy inhibition compromises degradation of ubiquitin-proteasome pathway substrates. *Mol. Cell, 33*, 517-527.

Korolchuk, V., et al (2010). Mechanisms of cross-talk between the ubiquitin-proteasome and autophagy-lysosome systems. *FEBS Lett. 584*(7), 1393-1398.

Krack, P., et al. (2017). Current applications and limitations of surgical treatments for movement disorders. *Mov Disord. 32*(1), 36–52.

Krishnan, H. S., et al. (2018). Metal Protein-Attenuating Compound for PET Neuroimaging: Synthesis and Preclinical Evaluation of [11C]PBT2. *Mol Pharm, 15*(2), 695-702.

Kumar, K. R., Djarmati-Westenberger, A., & Grunewald, A. (2011). Genetics of Parkinson's disease. *Semin Neurol 31*(5), 433-440.

Kumar, S. M., et al. (2012). Acquired cancer stem cell phenotypes through Oct4-mediated dedifferentiation. *Oncogene, 31*(47), 4898–4911.

Kumazawa, R., et al. (2008). Mutation analysis of the PINK1 gene in 391 patients with Parkinson disease. *Arch Neurol, 65*:, 802–808.

Lalève, A., et al. (2016). The antimalarial drug primaquine targets Fe–S cluster proteins and yeast respiratory growth. *Redox Biology, 7*, 21–29.

Lamb, J. (2007) The Connectivity Map: a new tool for biomedical research. *Nat. Rev. Cancer, 7,* 54–60.

Lamb, J., et al. (2006). The Connectivity Map: using gene-expression signatures to connect small molecules, genes, and disease. *Science. 313*(5795):1929-35.

Langston, J.W., Ballard, P., Tetrud, J.W. & Irwin, I. (1983). Chronic Parkinsonism in humans due to a product of meperidine-analog synthesis. *Science, 219,* 979-980.

Langston, J.W., et al. (1999). Evidence of active nerve cell degeneration in the substantia nigra of humans years after 1-methyl-4-phenyl1,2,3,6-tetrahydropyridine exposure. *Annals of neurology, 46,* 598-605.

Lapointe N, et al. (2004). Rotenone induces non-specific central nervous system and systemic toxicity. *FASEB J, 18*, 717–719.

Lee, A. J., et al. (2017). Penetrance estimate of LRRK2 p.G2019S Mutation in Individuals of Non-Ashkenazi Jewish Ancestry. *Mov Disord, 32*(10), 1432–1438.

Lee, B.D., et al. (2010). Inhibitors of leucine-rich repeat kinase-2 protect against models of Parkinson's disease. *Nature medicine, 16,* 9981000.

Lee, J., et al. (2010). Lysosomal Proteolysis and Autophagy Require Presenilin 1 and Are Disrupted by Alzheimer-Related PS1 Mutations. *Cell. 141*(7), 1146-1158.

Lee, J.-H., et al. (2015). Presenilin 1 maintains lysosomal Ca2+ homeostasis by regulating vATPase-mediated lysosome acidification. *Cell Reports, 12*(9), 1430–1444.

Lee, J.W., et al. (2014). Behavioral, neurochemical, and pathologic alterations in bacterial artificial chromosome transgenic G2019S leucine-rich repeated kinase 2 rats. *Neurobiology of aging.*

Lee, S., et al. (2017). Zinc transporter 2 interacts with vacuolar ATPase and is required for polarization, vesicle acidification, and secretion in mammary epithelial cells. *J Biol Chem, 292*(52), 21598-21613.

Lee, S., Sato, Y., & Nixon, R. A. (2011). Lysosomal proteolysis inhibition selectively disrupts axonal transport of degradative organelles and causes an alzheimer's-like axonal dystrophy, *Journal of Neuroscience. 31*(21), 7817-7830.

Lees, A. J., Hardy, J., & Revesz ,T. (2009). Parkinson's disease. *Lancet 373*, 2055–2066.

Lei, P., et al. (2015). Clioquinol rescues Parkinsonism and dementia phenotypes of the tau knockout mouse. *Neurobiol Dis. 81*,168-75.

Lesage, S., et al. (2013). G51D α- synuclein mutation causes a novel Parkinsonian-pyramidal syndrome. *Ann Neurol 73*, 459–471.

Lev, S., et al (2010). Constitutive activity of the human TRPML-2 Channel induces Cell Degeneration. *JBC, 285*, 2771–2782.

Leverenz. J., et al. (2007). Proteomic identification of novel proteins in cortical lewy bodies. *Brain Pathol, 17*(2), 139-45.

Lewis, P. A., et al. (2007). The R1441C mutation of LRRK2 disrupts GTP hydrolysis. Biochem *Biophys Res Commun. 357*(3), 668–671.

Li X, et al. (2007). Leucine-rich repeat kinase 2 (LRRK2)/ PARK8 possesses GTPase activity that is altered in familial Parkinson's disease R1441C/G mutants. *J Neurochem, 103*(1), 238–247.

Li, C., et al. (2017). COPI–TRAPPII activates Rab18 and regulates its lipid droplet association. *The EMBO Journal, 36*(4), 441–457.

Li, J. Y., et al. (2008). Lewy bodies in grafted neurons in subjects with Parkinson's disease suggest host-to-graft disease propagation. *Nat Med 14*(5), 501–503.

Li, M., et al. (2017). Structural basis of dual Ca2+/pH regulation of the endolysosomal TRPML1 channel. *Nature Structural & Molecular Biology. 24*, 205-213.

Li, X., et al. (2007). Leucine-rich repeat kinase 2 (LRRK2)/PARK8 possesses GTPase activity that is altered in familial Parkinson's disease R1441C/G mutants. *Journal of Neurochemistry, 103*(1), 238–247.

Li, X., et al. (2010). Enhanced striatal dopamine transmission and motor performance with LRRK2 overexpression in mice is eliminated by familial Parkinson's disease mutation G2019S. *The Journal of neuroscience : the official journal of the Society for Neuroscience, 30*, 1788-1797.

Li, Y., et al. (2009) Mutant LRRK2(R1441G) BAC transgenic mice recapitulate cardinal features of Parkinson's disease. *Nature neuroscience, 12*, 826-828.

Li, Y., et al. (2009) Mutant LRRK2(R1441G) BAC transgenic mice recapitulate cardinal features of Parkinson's disease. *Nature neuroscience, 12*, 826-828

Liao, J., et al. (2014). Parkinson disease-associated mutation R1441H in LRRK2 prolongs the "active state" of its GTPase domain. *Proc Natl Acad Sci U S A, 111*(11), 4055–4060.

Liberman, R., et al. (2013). Structural Analysis of the N-terminal Domain of Subunit a of the Yeast Vacuolar ATPase (V-ATPase) Using Accessibility of Single Cysteine Substitutions to Chemical Modification. *The Journal of Biological Chemistry, 288*(31), 22798–22808.

Lichten, L.A., & Cousins, R. J. (2009). Mammalian zinc transporters: Nutritional and physiologic regulation. *Annu. Rev. Nutr, 29,* 153–176.

Lichtenberg, M., et al. (2011). The Parkinson's disease protein LRRK2 impairs proteasome substrate clearance without affecting proteasome catalytic activity. *Cell Death & Disease, 2*(8), e196–.

Lin, X., et al. (2009) Leucine-rich repeat kinase 2 regulates the progression of neuropathology induced by Parkinson's-disease-related mutant alpha-synuclein. *Neuron, 64*, 807-827.

Lin, X., et al. (2012). Conditional Expression of Parkinson disease-related Mutant α-synuclein in the Midbrain Dopaminergic Neurons causes Progressive Neurodegeneration and Degradation of Transcription Factor Nuclear Receptor Related 1. *The Journal of Neuroscience : The Official Journal of the Society for Neuroscience, 32*(27), 9248–9264

Lindvall, O., H. et al (1992). Transplantation of fetal dopamine neurons in Parkinson's disease: one-year clinical and neurophysiological observations in two patients with putaminal implants, *Ann Neurol, 31*, 155-65.

Lindvall, O., S. et al. (1989). Human fetal dopamine neurons grafted into the striatum in two patients with severe Parkinson's disease. A detailed account of methodology and a 6-month follow-up. *Arch Neurol, 46*(6), 615-31.

Ling, L.-U., e al. (2011). The role of reactive oxygen species and autophagy in safingol-induced cell death. *Cell Death & Disease, 2*(3), e129–.

Linhart, R., et al. (2014). Vacuolar protein sorting 35 (Vps35) rescues locomotor deficits and shortened lifespan in Drosophila expressing a Parkinson's disease mutant of Leucine-Rich Repeat Kinase 2 (LRRK2), *Molecular neurodegeneration. 9*, 23.

Liu, B., & Dluzen, E. (2007). Oestrogen and nigrostriatal dopaminergic neurodegeneration: animal models and clinical reports of Parkinson's disease. *Clin Exp Pharmacol Physiol. 34*(7), 555–565.

Liu, Z., et al. (2018). LRRK2 phosphorylates membrane-bound Rabs and is activated by GTP-bound Rab7L1 to promote recruitment to the trans-Golgi network. *Hum Mol Genet*. *27*(2), 385–395.

Longo, F., et al. (2014). Genetic and pharmacological evidence that G2019S LRRK2 confers a hyperkinetic phenotype, resistant to motor decline associated with aging. *Neurobiology of disease.*

Luerman, G. C., et al. (2014) Phosphoproteomic evaluation of pharmacological inhibition of leucine-rich repeat kinase 2 reveals significant off-target effects of LRRK-2-IN-1, *Journal of neurochemistry. 128,* 561-76.

Luk, K. C., et al. (2012). Intracerebral inoculation of pathological alpha-synuclein initiates a rapidly progressive neurodegenerative alpha-synucleinopathy in mice. *J Exp Med 209,* 975–986.

Luk, K., et al. (2009). Exogenous alphasynuclein fibrils seed the formation of Lewy body-like intracellular inclusions in cultured cells, *Proceedings of the National Academy of Sciences of the United States of America, 106*, 20051-56.

Luthman, J., et al. (1989) Selective lesion of central dopamine or noradrenaline neuron systems in the neonatal rat: motor behavior and monoamine alterations at adult stage. *Behav Brain Res 33*, 267–277.

Luzon-Toro, B., et al. (2007). Mechanistic insight into the dominant mode of the Parkinson's disease-associated G2019S LRRK2 mutation. *Hum Mol Genet. 16*(17), 2031-2039.

Luzón-Toro, B., et al. (2007). Mechanistic insight into the dominant mode of the Parkinson's disease-associated G2019S LRRK2 mutation. *Hum Mol Genet. 16*(17), 2031–2039.

Maas, J. W. J., Yang, J., & Edwards, R. H. (2017). Endogenous Leucine-Rich Repeat Kinase 2 Slows Synaptic Vesicle Recycling in Striatal Neurons. *Frontiers in Synaptic Neuroscience, 9*, 5.

MacLeod, D. A., et al. (2013). RAB7L1 interacts with LRRK2 to modify intraneuronal protein sorting and Parkinson's disease risk, *Neuron. 77*, 425-39

Maekawa, T., et al. (2012) The I2020T Leucine-rich repeat kinase 2 transgenic mouse exhibits impaired locomotive ability accompanied by dopaminergic neuron abnormalities. *Molecular neurodegeneration, 7,* 15.

Mak, S. K., et al. (2010). Lysosomal degradation of alpha-synuclein in vivo. *J Biol Chem 285,* 13621–13629

Mamais, A., et al. (2014). Arsenite Stress Down-regulates Phosphorylation and 14-3-3 Binding of Leucine-rich Repeat Kinase 2 (LRRK2), *Promoting Self-association and Cellular Redistribution. The Journal of Biological Chemistry, 289*(31), 21386–21400.

Mamais, A., et al. (2018). Analysis of macroautophagy related proteins in G2019S LRRK2 Parkinson's disease brains with Lewy Body pathology. *Brain res. pii: S0006-8993*(18), 30407-4.

Mandemakers, W., et al. (2012). LRRK2 expression is enriched in the striosomal compartment of mouse striatum. *Neurobiol Dis, 48*(3), 582–593.

Manzoni, C. (2017). The LRRK2–macroautophagy axis and its relevance to Parkinson's disease. *Biochemical Society Transactions, 45*(1), 155–162.

Manzoni, C., et al. (2013) Inhibition of LRRK2 kinase activity stimulates macroautophagy, *Biochimica et biophysica acta. 1833*, 2900-10.

Manzoni, C., et al. (2016). mTOR independent regulation of macroautophagy by Leucine Rich Repeat Kinase 2 via Beclin-1. *Scientific Reports. 6*, 35106.

Manzoni, C., et al. (2018). mTOR independent alteration in ULK1 Ser758 phosphorylation following chronic LRRK2 kinase inhibition. *Bioscience Reports, 38*(2), BSR20171669.

Marras, C., & Lang, A. (2013). Parkinson's disease subtypes: lost in translation? Journal of Neurology, *Neurosurgery and Psychiatry, 84*, 409-415.

Markesbery, W. R., et al. (2009). Lewy Body Pathology in Normal Elderly Subjects. *Journal of Neuropathology and Experimental Neurology, 68*(7), 816–822.

Masuda, M., et al. (2013). Prion-like spreading of pathological α-synuclein in brain, *Brain, 136,* 1128-38.

Mazzulli, J. R. et al. (2011). Gaucher disease glucocerebrosidase and α-synuclein form a bidirectional pathogenic loop in synucleinopathies. *Cell 146*, 37–52.

McCormack, A. L., et al. (2002). Environmental risk factors and Parkinson's disease: Selective degeneration of nigral dopaminergic neurons caused by the herbicide paraquat. *Neurobiol Dis 10*, 119–127.

McGough, I. J. et al. (2014). Retromer binding to FAM21 and the WASH complex is perturbed by the Parkinson disease-linked VPS35 (D620N) mutation. *Curr. Biol. 24*, 1670–1676.

McWilliams, T. G., et al. (2018). Basal Mitophagy Occurs Independently of PINK1 in Mouse Tissues of High Metabolic Demand. *Cell Metabolism, 27*(2), 439–449.e5.

Melrose, et al. (2010). Impaired dopaminergic neurotransmission and microtubule-associated protein tau alterations in human LRRK2 transgenic mice. *Neurobiol Dis 40*(3), 503-517

Mendivil-Perez, M., et al. (2016). Neuroprotective effect of the lrrk2 kinase inhibitor pf-06447475 in human nerve-like differentiated cells exposed to oxidative stress stimuli: implications for parkinson's disease. *Neurochem Re, 41*(10), 2675-2692.

Merkulova, M., et al. (2015). Mapping the H+ (V)-ATPase interactome: identification of proteins involved in trafficking, folding, assembly and phosphorylation. *Scientific Reports, 5*, 14827.

Miller, I. N., & Cronin-Golomb, A. (2010). Gender differences in parkinson's disease: clinical characteristics and cognition. *Movement Disorders, 25*(16), 2695–2703.

Mindell, J. A. (2012). Lysosomal acidification mechanisms. *Annu Rev Physiol. 74*, 69-86.

Minton, K. (2013). Membrane dynamics: How lysosomes SNARE autophagosomes. *Nat Review Mol Biol. 14*, 65

Miura, E. et al. (2014). VPS35 dysfunction impairs lysosomal degradation of α-synuclein and exacerbates neurotoxicity in a Drosophila model of Parkinson's disease. *Neurobiol. Dis. 71,* 1–13.

Moehle, M. S., et al. (2014). LRRK2 Inhibition Attenuates Microglial Inflammatory Responses. *Journal of Neuroscience, 32*(5), 1602-16011.

Morelli, M. B., et al. (2016). Overexpression of transient receptor potential mucolipin-2 ion channels in gliomas: role in tumor growth and progression. *Oncotarget, 7(*28), 43654–43668.

Mortiboys, H., et al. (2010). Mitochondrial impairment in patients with Parkinson disease with the G2019S mutation in LRRK2. *Neurology 75*(22), 2017-2020.

Muda, K., et al. (2014). PKA mediates interaction of LRRK2 with 14-3-3. Proceedings of the *National Academy of Sciences*, *111*(1) E34-E43.

Nalls, M. A., et al. (2011). Imputation of sequence variants for identification of genetic risks for Parkinson's disease: a meta- analysis of genome- wide association studies. *Lancet. 377,* 641–649

Nalls, M. A., et al. (2014). Large-scale meta-analysis of genome-wide association data identifies six new risk loci for Parkinson's disease. *Nat Genet 46*(9), 989-993.

Namkoong, S., et al. (2015). The integral membrane protein ITM2A, a transcriptional target of PKA-CREB, regulates autophagic flux via interaction with the vacuolar ATPase. *Autophagy, 11*(5), 756–768.

Nässträm, T., et al. (2011). The lipid peroxidation products 4-oxo-2-nonenal and 4-hydroxy2-nonenal promote the formation of alpha-synuclein oligomers with distinct

biochemical, morphological, and functional properties. *Free Radic. Biol. Med. 50,* 428–437.

Nguyen, A. P. T., & Moore, D. J. (2017). Understanding the GTPase Activity of LRRK2: Regulation, Function, and Neurotoxicity. *Advances in Neurobiology, 14*, 71–88.

Nguyen, H. N., et al. (2011). LRRK2 mutant iPSCderived DA neurons demonstrate increased susceptibility to oxidative stress. *Cell Stem Cell 8*(3), 267-280.

Nguyen, M., & Krainc, D. (2018). LRRK2 phosphorylation of auxilin mediates synaptic defects in dopaminergic neurons from patients with Parkinson's disease. *Proceedings of the National Academy of Sciences.*

Nguyen, T., et al. (2005). Clioquinol down-regulates mutant huntingtin expression in vitro and mitigates pathology in a Huntington's disease mouse model. *Proceedings of the National Academy of Sciences, 102*(33), 11840-11850.

Nicklas, W. J., Vyas, I., & Heikkila, R. E. (1985). Inhibition of NADH-linked oxidation in brain mitochondria by MPP+, a metabolite of the neurotoxin MPTP. *Life Sci 36,* 2503–250.

Nishi, T., & Forgac, M. (2002). The vacuolar (H+)-ATPases--nature's most versatile proton pumps. *Nat Rev Mol Cell Biol, 3*(2), 94–103.

Nishioka, K., et al. (2006). Clinical heterogeneity of α- synuclein gene duplication in Parkinson's disease. *Ann Neurol. 59,* 298–309.

Niu, J., et al. (2012). Leucine-rich repeat kinase 2 disturbs mitochondrial dynamics via Dynamin-like protein. *J Neurochem 122*(3), 650-658.

Nixon, R. (2013). The role of autophagy in neurodegenerative disease. *Nat Med. 19*(8), 983-997.

Novak I. et al. (2010). Nix is a selective autophagy receptor for mitochondrial clearance. *EMBO Rep 11,* 45–51.

Noyce, A. J., et al. (2012). Meta-Analysis of Early Nonmotor Features and Risk Factors for Parkinson Disease. *Annals of Neurology, 72*(6), 893–901.

Ohkuma, S., & Poole, B. (1978). Fluorescence probe measurement of the intralysosomal pH in living cells and the perturbation of pH by various agents. *Proceedings of the National Academy of Sciences of the United States of America, 75*(7), 3327–3331.

Ohta, E., et al. (2015). I2020T mutant LRRK2 iPSC-derived neurons in the Sagamihara family exhibit increased Tau phosphorylation through the AKT/GSK-3β signaling pathway. Hum *Mol Genet, 24(*17), 4879–4900.

Oligati, S., et al. (2014). PARK20 caused by SYNJ1 homozygous Arg258Gln mutation in a new Italian family. *Neurogenetics, 15*(3), 183–188.

Oligati, S., et al. (2016). DNAJC6 Mutations Associated With Early-Onset Parkinson's Disease. *Ann Neurol, 79(*2), 244–256

Oliveras-Salvá, M., et al. (2013). rAAV2/7 vector-mediated overexpression of alpha-synuclein in mouse substantia nigra induces protein aggregation and progressive dose-dependent neurodegeneration. *Molecular Neurodegeneration, 8,* 44.

Orenstein, S. J., et al. (2013). Interplay of LRRK2 with chaperone-mediated autophagy. *Nat Neurosci 16*(4), 394-406.

Outeiro, T. F. & Lindquist, S. (2003). Yeast cells provide insight into α-synuclein biology and pathobiology. *Science 302,* 1772–1775.

Ozeki, S., et al. (2005). Rab18 localizes to lipid droplets and induces their close apposition to the endoplasmic reticulum-derived membrane. *J cell Sci. 118*(Pt 12), 2601-2611.

Pagan, F. L, et al. (2016). Nilotinib Effects in Parkinson's disease and Dementia with Lewy bodies. *Journal of Parkinson's Disease. 6*(3), 503-517.

Paisan-Ruiz, C., et al. (2004) Cloning of the gene containing mutations that cause PARK8-linked Parkinson's disease, *Neuron. 44,* 595-600.

Pankratz, N., et al. (2009). Genomewide association study for susceptibility genes contributing to familial Parkinson disease. *Hum Genet 124, 5*93–605.

Parisiadou, L., et al. (2009). Phosphorylation of ezrin/radixin/moesin proteins by LRRK2 promotes the rearrangement of actin cytoskeleton in neuronal morphogenesis. *J Neurosci 29*(44), 13971-13980.

Parisiadou, L., et al. (2014). LRRK2 regulates synaptogenesis and dopamine receptor activation through modulation of PKA activity. *Nat Neurosci 17*(3), 367-376

Park, M. H., et al. (2011). Clioquinol induces autophagy in cultured astrocytes and neurons by acting as a zinc ionophore. *Neurobiology Disease. 42*, 242 – 251.

Park, S., et al. (2016). Interplay between Leucine-Rich Repeat Kinase 2 (LRRK2) and p62/SQSTM-1 in Selective Autophagy. *PLoS ONE, 11*(9), e0163029.

Parkinson, J. (1817). Essay of the Shaking Palsy: Wiley-Blackwell.

Parkkinen, L., et al. (2008). Alpha-synuclein pathology does not predict extrapyramidal symptoms or dementia. *Ann Neurol. 57*(1), 82–91.

Parkkinen, L., Pirttilä, T., & Alafuzoff, I. (2008). Applicability of current staging/categorization of α-synuclein pathology and their clinical relevance. *Acta Neuropathologica, 115*(4), 399–407.

Patel, S., & Cai, X. (2015). Evolution of acidic Ca^{2+} stores and their resident Ca^{2+} -permeable channels. *Cell Calcium. 57*(3), 222-230.

Patrushev, N., Seidel-Rogol, B., & Salazar, G. (2012). Angiotensin II Requires Zinc and Downregulation of the Zinc Transporters ZnT3 and ZnT10 to Induce Senescence of Vascular Smooth Muscle Cells. *PLoS ONE, 7*(3), e33211.

Pchelina, S. N., et al. (2011). Clinical features of LRRK2-associated Parkinson's disease. *Zh Nevrol Psikhiatr Im S S Korsakova. 111*(12), 56-62.

Pen, A., & Jensen, U. (2016). Current status of treating neurodegenerative disease with induced pluripotent stem cells. *Acta Neurol Scand. 135*(1), 57-72.

Perez Carrion, M., et al. (2018). The LRRK22 variant e193k prevents mitochondrial fission upon mpp+ treatment by altering LRRK22 binding to drp1. *Frontiers in Molecular Neuroscience, 11,* 64.

Perrett, R., Alexopoulou M. Z., & Tofaris, G. K. (2015). The endosomal pathway in Parkinson's disease. *Mol Cell Neurosci 66*(Pt A), 21-28.

Pfeffer, S. R. (2005). Structural clues to Rab GTPase functional diversity. *J Biol Chem 280*(16), 15485-15488.

Piccoli, G., et al. (2011). LRRK2 controls synaptic vesicle storage and mobilization within the recycling pool. *J Neurosci 31*(6), 2225-223.

Pissadaki E. K., & Bolam, P. (2013). The energy cost of action potential propagation in dopamine neurons: clues to susceptibility in Parkinson's disease. *Frontiers in Computational Neuroscience. 7(*13).

Plowey, E. D., et al. (2014). Mutant LRRK2 enhances glutamatergic synapse activity and evokes excitotoxic dendrite degeneration. *Biochim Biophys Acta 1842*(9), 1596-1603.

Plowey, E.D., et al. (2008). Role of autophagy in G2019S-LRRK2associated neurite shortening in differentiated SH-SY5Y cells. *Journal of neurochemistry, 105*, 1048-1056

Poëa-Guyon, S., et al. (2013). The V-ATPase membrane domain is a sensor of granular pH that controls the exocytotic machinery. *The Journal of Cell Biology, 203*(2), 283–298.

Polinski, N. K., et al. (2018). Best Practices for Generating and Using Alpha-Synuclein Pre-Formed Fibrils to Model Parkinson's Disease in Rodents. *Journal of Parkinson's Disease, 8*(2), 303–322.

Polymeropoulos, M. H., et al. (1997). Mutation in the alpha-synuclein gene identified in families with Parkinson's disease, *Science, 276,* 2045-47.

Postuma, R. B., et al. (2012). Identifying prodromal Parkinson's disease: pre-motor disorders in Parkinson's disease. *Movement Disorders, 27*, 617-626.

Pringsheim, T., et al. (2014). The prevalence of Parkinson's disease: a systematic review and meta-analysis. *Movement Disorders*, *29* (13), 1583-1590.

Proukakis, C., et al. (2013). A novel α- synuclein missense mutation in Parkinson disease. *Neurology, 80*, 1062–1064.

Pryor, P. R., et al. (2000). The role of intraorganellar Ca(2+) in late endosome-lysosome heterotypic fusion and in the reformation of lysosomes from hybrid organelles. *Journal Cell Biology. 149(*5), 1053-1062.

Pryor, P. R., et al. (2006). Mucolipin-1 is a lysosomal membrane protein required for intracellular lactosylceramide traffic. *Traffic. 7*(10), 1388-1398.

Przedborski, S., et al. (1995). Dose-dependent lesions of the dopaminergic nigrostriatal pathway induced by intrastriatal injection of 6-hydroxydopamine. *Neuroscience 67,* 631– 647.

Pungaliya, P., et al. (2010). Identification and characterization of a leucine-rich repeat kinase 2 (LRRK2) consensus phosphorylation motif. *PloS One. 27*(5), e13672.

Pylypenko, O., et al. (2003). Structure of Rab escort protein-1 in complex with Rab geranylgeranyltransferase. *Mol Cell 11*(2), 483-494.

Qiao, L., & Zhang, J. (2009). Inhibition of lysosomal functions reduces proteasomal activity *Neurosci. Lett, 456*, 15-19.

Quadri, M., et al. (2012). Mutations in SLC30A10 cause parkinsonism and dystonia with hypermanganesemia, polycythemia, and chronic liver disease. *Am J Hum Genet, 90*, 467–477.

Rakovic, A., et al. (2011). Mutations in PINK1 and Parkin Impair Ubiquitination of Mitofusins in Human Fibroblasts. *PLoS ONE, 6*(3), e16746.

Ramirez, A., et al. (2006). Hereditary parkinsonism with dementia is caused by mutations in ATP13A2, encoding a lysosomal type 5 P-type ATPase. *Nat Genet, 38,* 1184–1191.

Ramonet, D., et al. (2011) Dopaminergic neuronal loss, reduced neurite complexity and autophagic abnormalities in transgenic mice expressing G2019S mutant LRRK2, *PloS one. 6*, e18568.

Ramsden, N., et al. (2011) Chemoproteomics-based design of potent LRRK2-selective lead compounds that attenuate Parkinson's disease-related toxicity in human neurons, *ACS Chem Biol. 6*, 1021-8.

Rappold, P. M., & Tieu, K. (2010). Astrocytes and therapeutics for Parkinson's disease. *Neurotherapeutics 7*, 413–423.

Raychowdhury, M. K., (2004). Molecular pathophysiology of mucolipidosis type IV: pH dysregulation of the mucolipin-1 cation channel. *HumMolGenet, 13*, 617–62.

Reith, A. D., et al. (2012). GSK2578215A; A potent and highly selective 2-arylmethyloxy-5-substitutent-N-arylbenzamide LRRK2 kinase inhibitor. *Bioorganic & Medicinal Chemistry Letters, 22(*17), 5625–5629.

Reuter, S., et al. (2015). Life-threatening DBS withdrawal syndrome in Parkinson's disease can be treated with early reimplantation. *Parkinsonism Related Disorders. S1* 353-8020(18).

Reuter, S., et al. (2015). Uncoupling of dopaminergic and subthalamic stimulation: Life-threatening DBS withdrawal syndrome. *Mov Disord. 30*(10), 1407-1413.

Riachi, J. C., et al. (1989). Entry of 1-methyl-4-phenyl-1,2,3,6-tetrahydropyridine into the rat brain J *Pharmacol Exp Ther, 249*, 744-748.

Richardson, J. R., et al. (2005). Paraquat neurotoxicity is distinct from that of MPTP and rotenone. *Toxicol Sci 88*, 193–201.

Ritz, B., et al. (2009). Dopamine transporter genetic variants and pesticides in Parkinson's disease. *Environ. Health Perspect., 117*, 964-969.

Robak, L. A., et al. (2017). Excessive burden of lysosomal storage disorder gene variants in Parkinson's disease. *Brain, 140*(12), 3191-3203.

Roberts, R. F., Wade-Martins, R., & Alegre-Abarrategui, J. (2015). Direct visualization of alpha-synuclein oligomers reveals previously undetected pathology in Parkinson's disease brain. *Brain, 138*, 1642-57.

Rocca, W. A., et al. (2008). Increased risk of parkinsonism in women who underwent oophorectomy before menopause. *Neurology. 15*, *70*(3), 200–209.

Roosen, D. A., & Cookson, M. R. (2016). LRRK2 at the interface of autophagosomes, endosomes and lysosomes. *Molecular Neurodegeneration, 11*, 73.

Ross, O. A., et al. (2008). Analysis of Lrrk2 R1628P as a risk factor for Parkinson's disease. *Ann Neurol 64*(1), 88-92.

Rothaug, M., et al. (2014). LIMP-2 expression is critical for beta-glucocerebrosidase activity and alpha-synuclein clearance. *Proceedings of the National Academy of Sciences of the United States of America. 111*(43), 15573–15578.

Rubinsztein, D. C., et al. (2011). Autophagy and aging. *Cell*, *146*(5): 682–695.

Rudenko, I. N., et al. (2012) The G2385R variant of leucine-rich repeat kinase 2 associated with Parkinson's disease is a partial loss-of-function mutation, *The Biochemical journal. 446*, 99-111.

Ruiz-Canada, C., et al. (2009). Cotranslational and Posttranslational N-Glycosylation of Polypeptides by Distinct Mammalian OST Isoforms. *Cell, 136*, 272–283.

Saez-Atienzar, S., et al. (2014) The LRRK2 inhibitor GSK2578215A induces protective autophagy in SH-SY5Y cells: involvement of Drp-1-mediated mitochondrial fission and mitochondrial-derived ROS signaling, *Cell death & disease. 5*, e1368.

Saha, S., Liu-Yesucevitz, L., & Wolozin, B. (2014). Regulation of autophagy by LRRK2 in Caenorhabditis elegans. *Neurodegener Dis 13*(2-3), 110-113.

Samaranch, L., et al. (2010). PINK1- linked parkinsonism is associated with Lewy body pathology. *Brain, 133,* 1128–1142.

Samii, A., et al. (2009). NSAID use and the risk of Parkinson's disease: systematic review and meta-analysis of observational studies. *Drugs Aging, 26*(9), 769–779.

Sampson, E. L., (2014). Metal protein attenuating compounds for the treatment of Alzheimer's dementia. *Cochrane Database of Systematic Reviews, Issue 2. Art. No.: CD005380.*

Sanchez-Danes, A., et al. (2012). Disease-specific phenotypes in dopamine neurons from human iPS-based models of genetic and sporadic Parkinson's disease, *EMBO molecular medicine. 4*, 380-95

Sandor, C., et al. (2017). Transcriptomic profiling of purified patient-derived dopamine neurons identifies convergent perturbations and therapeutics for Parkinson's disease. *Human Molecular Genetics, 26*(3), 552–566.

Santos, A. B. D., Barreto, G. E., & Kohlmeier, K. A. (2014). Treatment of sleeping disorders should be considered in clinical management of Parkinson's disease. *Frontiers in Ageing Neuroscience. 6*(273).

Santos, R., et al. (2017). Differentiation of Inflammation-Responsive Astrocytes from Glial Progenitors Generated from Human Induced Pluripotent Stem Cells. *Stem Cell Reports, 8*(6), 1757–1769.

Sastre, M., Ritchie, C. W., & Nabil, H. (2015). Metal ions in Alzheimer's Disease Brain. *JSM Alzheimer's Disease and Related Dementia. 2*(1), 1014.

Satake, W., et al. (2009). Genome- wide association study identifies common variants at four loci as genetic risk factors for Parkinson's disease. *Nat Genet, 41*, 1303–1307.

Schapansky, J., et al. (2018). Familial knockin mutation of LRRK2 causes lysosomal dysfunction and accumulation of endogenous insoluble α-synuclein in neurons. *Neurobiol Dis, 111*, 26-35.

Schapansky, J., Nardozzi, J. D., & LaVoie, M. J. (2015). The Complex Relationships between Microglia, Alpha-Synuclein, and LRRK2 in Parkinson's Disease. *Neuroscience, 302,* 74–88.

Schapansky, J., Nardozzi, J. D., Felizia, F. & LaVoie, M. J. (2014) Membrane recruitment of endogenous LRRK2 precedes its potent regulation of autophagy, *Human molecular genetics. 23*, 4201-14.

Schapiro, F. B., & Grinstein, S. (2000). Determinants of the pH of the Golgi complex. *J Biol Chem. 275(*28), 21025-21032.

Schousboe, A., et al. (2014). Glutamate Metabolism in the Brain Focusing on Astrocytes. *Advances in Neurobiology, 11,* 13–30.

Schuepbach, W., et al. (2013). Neurostimulation for Parkinson's disease with early motor complication. *New England Journal of Medicine. 368*(7), 610-622.

Senoh, S., & Witkop, C. R. (1959). 6,4,5-trihydroxyphenethylamine, a new metabolite of 3,4-dihydroxyphenethylamine. *Journal of the American Chemical Society, 81*(7), 1768-1769.

Seo, B. R., et al. (2015). The zinc ionophore clioquinol reverses autophagy arrest in chloroquine-treated ARPE-19 cells and in APP/mutant presenilin-1-transfected Chinese hamster ovary cells. *Neurobiology of Ageing. 36*(12), 3228-3238.

Sergin, I., et al. (2017). Exploiting macrophage autophagy-lysosomal biogenesis as a therapy for atherosclerosis. *Nature Communications, 8,* 15750.

Shaul, Y. (2000). c-Abl: activation and nuclear targets. *Cell Death Differ, 7*(1), 10-6.

Sheerin, U. M., Houlden, H., & Wood, N. W. (2014). Advances in the genetics of Parkinson's disease: a guide for the clinician. *Mov Disord Clin Pract, 1*, 3–13.

Shen, L., & Ji, H.-F. (2013). Low uric acid levels in patients with Parkinson's disease: evidence from meta-analysis. *BMJ Open, 3*(11).

Sheng Z, et al. (2012). Ser1292 autophosphorylation is an indicator of LRRK2 kinase activity and contributes to the cellular effects of PD mutations. *Sci Trans Med. 4*(164), 164ra161.d

Shulman, J., et al. (2011). Parkinson's disease: genetics and pathogenesis. *Annu Rev Pathol. 6*, 193–222.

Sidransky, E., et al. (2009). Multicenter analysis of glucocerebrosidase mutations in Parkinson's disease. *N Engl J Med, 361,* 1651–1661.

Simon- Sanchez, J., Schulte, C., & Bras, J. (2009). Genome- wide association study reveals genetic risk underlying Parkinson's disease. *Nat Genet, 41,* 1308–1312.

Singleton, A. B., et al. (2003). alpha- Synuclein locus triplication causes Parkinson's disease. *Science. 302,* 841.

Singleton, A. B., Farrer, M. J., & Bonifati, V. (2013). The genetics of Parkinson's disease: progress and therapeutic implications, *Movement disorders : official journal of the Movement Disorder Society. 28,* 14-23.

Sloan, M., et al. (2016). LRRK2 BAC transgenic rats develop progressive, L-DOPA-responsive motor impairment, and deficits in dopamine circuit function. *Human Molecular Genetics. 25*(5), 951-963.

Smith, G. A., et al. (2016). Fibroblast Biomarkers of Sporadic Parkinson's Disease and LRRK2 Kinase Inhibition. *Molecular Neurobiology*, *53*(8), 5161–5177.

Smith, G. A., et al. (2016). Fibroblast Biomarkers of Sporadic Parkinson's Disease and LRRK2 Kinase Inhibition. *Molecular Neurobiology*, *53*(8), 5161–5177.

Smith, W. W., et al. (2006). Kinase activity of mutant LRRK2 mediates neuronal toxicity. *Nat. Neurosci, 9*, 1231–1233.

Soyombo, A. A., et al. (2006). TRP-ML1 regulates lysosomal pH and acidic lysosomal lipid hydrolytic activity. *J Biol Chem, 281*(11), 7294-301.

Spillantini, M. G., et al. (1997). Alpha-synuclein in Lewy bodies, *Nature, 388*, 839-40.

Spillantini, M. G., et al. (1998). AlphaSynuclein in filamentous inclusions of Lewy bodies from Parkinson's disease and dementia with lewy bodies, *Proceedings of the National Academy of Sciences of the United States of America, 95*, 6469-73.

Stefanis, L., et al. (2001). Expression of A53T mutant but not wild-type alpha-synuclein in PC12 cells induces alterations of the ubiquitin-dependent degradation

system, loss of dopamine release, and autophagic cell death. *J Neurosci, 21*(24), 9549–9560.

Steger, M., et al. (2016). Phosphoproteomics reveals that Parkinson's disease kinase LRRK2 regulates a subset of Rab GTPases. *Elife 5*

Stenmark, H. (2009). Rab GTPases as coordinators of vesicle traffic. *Nat Rev Mol Cell Biol, 10*(8), 513–525.

Stowe, R., et al. (2010). Evaluation of the efficacy and safety of adjuvant treatment to levodopa therapy in Parkinson s disease patients with motor complications. *Cochrane Database System Review, 7*(7), CD007166.

Su, Y. C., & Qi, X. (2013). Inhibition of excessive mitochondrial fission reduced aberrant autophagy and neuronal damage caused by LRRK2 G2019S mutation. *Hum Mol Genet 22*(22), 4545-4561.

Su, Y. C., et al. (2015). Threonine 56 phosphorylation of Bcl-2 is required for LRRK2 G2019S-induced mitochondrial depolarization and autophagy. *Biochim Biophys Acta, 1852*(1), 12-21.

Sulzer, D., & Surmeier, D. J. (2013). Neuronal vulnerability, pathogenesis, and Parkinson's disease. *Movement Disorders. 28(*1), 41-50.

Sundberg, M., et al (2013). Improved cell therapy protocols for Parkinson's disease based on differentiation efficiency and safety of hESC-, hiPSC-, and non-human primate iPSC-derived dopaminergic neurons, *Stem cells, 31,* 1548-62.

Surmeier, D. J., Guzman, J. N., & Sanchez-Padilla, J. (2010). Calcium, cellular aging, and selective neuronal vulnerability in Parkinson's disease. *Cell Calcium. 47*(2), 175-182.

Suzuki, K., et al. (2007). Hierarchy of Atg proteins in pre-autophagosomal structure organization. *Genes Cells. 12(*2), 209–218.

Takagawa, T., et al. (2018). An increase in LRRK2 suppresses autophagy and enhances Dectin-1-induced immunity in a mouse model of colitis. *Sci Transl Med. 10*(444). pii: eaan8162.

Takashi, K., & Yamanaka, S. (2006). Induction of pluripotent stem cells from mouse embryonic and adult fibroblast cultures by defined factors. Cell, *126*(4), 663–676.

Tan, E.-K., et al. (2010). Analysis of GWAS-linked loci in Parkinson disease reaffirms PARK16 as a susceptibility locus. *Neurology, 75*(6), 508–512.

Tang, F. L. et al. (2015). VPS35 in dopamine neurons is required for endosome-to-Golgi retrieval of Lamp2a, a receptor of chaperone-mediated autophagy that is critical for α-synuclein degradation and prevention of pathogenesis of Parkinson's disease. *J. Neurosci. 35*, 10613–10628.

Tanner, C. M. (2010). Advances in encironmental epidemiology. *Movement Disorders. 25(*1), 58-62.

Thevenet, J., et al. (2011). Regulation of LRRK2 expression points to a functional role in human monocyte maturation, *PloS one. 6*, e21519

Thirstrup, K., et al. (2017). Selective LRRK2 kinase inhibition reduces phosphorylation of endogenous Rab10 and Rab12 in human peripheral mononuclear blood cells. *Scientific Reports, 7*, 10300.

Thiruchelvam, M., et al. (2000). Potentiated and preferential effects of combined paraquat and maneb on nigrostriatal dopamine systems: Environmental risk factors for Parkinson’s disease? *Brain Res 873*, 225–234.

Thiruchelvam, M., et al. (2003). Age-related irreversible progressive nigrostriatal dopaminergic neurotoxicity in the paraquat and maneb model of the Parkinson's disease phenotype. *Eur J Neurosci 18*, 589–600.

Tieu, K. (2011). A Guide to Neurotoxic Animal Models of Parkinson's Disease. *Cold Spring Harbor Perspectives in Medicine, 1(*1), a009316.

Tofaris, G., et al. (2003). Ubiquitination of alpha-synuclein in Lewy bodies is a pathological event not associated with impairment of proteasome function. *J Biol Chem, 278*(45), 44405–44411.

Tong, Y., et al. (2009). R1441C mutation in LRRK2 impairs dopaminergic neurotransmission in mice. *Proceedings of the National Academy of Sciences of the United States of America, 106,* 14622-14627.

Tong, Y., et al. (2010) Loss of leucine-rich repeat kinase 2 causes impairment of protein degradation pathways, accumulation of alpha-synuclein, and apoptotic cell death in aged mice. *Proceedings of the National Academy of Sciences of the United States of America, 107,* 9879-9884.

Tong, Y., et al. (2012). Loss of leucine-rich repeat kinase 2 causes age-dependent bi-phasic alterations of the autophagy pathway. *Molecular neurodegeneration, 7*, 2.

Tsika, E., et al. (2014). Conditional Expression of Parkinson's Disease-Related R1441C LRRK2 in Midbrain Dopaminergic Neurons of Mice Causes Nuclear Abnormalities without Neurodegeneration. *Neurobiology of disease.*

Tsika, E., et al. (2015). Adenoviral-mediated expression of G2019S LRRK2 induces striatal pathology in a kinase-dependent manner in a rat model of Parkinson's disease. *Neurobiol Dis, 77*, 49–61.

Venkatachalam, K., Hofmann, T., & Montell, C. (2006). Lysosomal localization of TRPML3 depends on TRPML2 and the mucolipidosis-associated protein TRPML1. *J Biol Chem*, *28*1, 17517–17527.

Vergne, I., et al. (2009). Control of autophagy initiation by phosphoinositide 3-phosphatase jumpy. *The EMBO Journal*, *28*(15), 2244–2258.

Vilcassim, F. S., et al. (2016). The Impact of Autophagy on the Progression of the Myelodysplastic Syndromes. *Autophagy*. *128*(22), 3168.

Villamil Giraldo, A. M., et al. (2014). Lysosomotropic agents: impact on lysosomal membrane permeabilization and cell death. *Biochem Soc Trans*, *42(*5), 1460-4.

Vives-Bauza, C., et al. (2010). PINK1-dependent recruitment of Parkin to mitochondria in mitophagy. *Proc Natl Acad Sci U S A*, *107*, 378–83.

Volpicelli-Daley, L. A., Luk, K. C., & Lee, V. M-Y. (2014). Addition of exogenous alpha-synuclein pre-formed fibrils to primary neuronal cultures to seed recruitment of endogenous alpha-synuclein to Lewy body and Lewy neurite-like aggregates. *Nat Protoc 9*, 2135–2146

Walker, M. D., et al. (2014). Behavioral Deficits and Striatal DA Signaling in LRRK2 p.G2019S Transgenic Rats: A Multimodal Investigation Including PET Neuroimaging. *Journal of Parkinson's disease*

Wallings, R., Manzoni, C., & Bandopadhyay, R. (2015). Cellular processes associated with LRRK2 function and dysfunction. *The Febs Journal*, *282*(15), 2806–2826.

Wang, X., et al. (2012). LRRK2 regulates mitochondrial dynamics and function through direct interaction with DLP1. *Hum Mol Genet 21(*9), 1931-1944.

Ward, R. J., Dexter, D. T., & Crichton, R. R. (2015). Neurodegenerative diseases and therapeutic strategies using iron chelators. *Journal of Trace Elements in Medical and Biology. 31*, 267-273.

Webber, P. J., et al. (2011). Autophosphorylation in the leucine-rich repeat kinase 2 (LRRK2) GTPase domain modifies kinase and GTP-binding activities. *J Mol Biol. 412*(1), 94–110.

Webster J. M., Bentley M. T., & Wojcikiewicz, R. (2003). N,N,N′,N′-tetrakis(2-pyridylmethyl)ethylenediamine inhibits ligand binding to certain G protein-coupled receptors. *European Journal of Pharmacology, 474*(1), 1–5.

West, A. B., et al. (2005). Parkinson's disease-associated mutations in leucine-rich repeat kinase 2 augment kinase activity. *Proc Natl Acad Sci U S A.102*(46), 16842–16847.

West, A. B., et al. (2007). Parkinson's disease-associated mutations in LRRK2 link enhanced GTP-binding and kinase activities to neuronal toxicity. *Hum Mol Genet, 16*(2), 223–232.

Wilhelmsson, U., et al. (2006). Redefining the concept of reactive astrocytes as cells that remain within their unique domains upon reaction to injury. *Proceedings of the National Academy of Sciences of the United States of America, 103*(46), 17513–17518.

Wilson, C. A., et al. (2004). Degradative organelles containing mislocalized alpha-and beta-synuclein proliferate in presenilin-1 null neurons. *J Cell Biol, 165*(3), 335–346.

Winner, B., et al. (2011). In vivo demonstration that alpha-synuclein oligomers are toxic. *Proc. Natl. Acad. Sci. U.S.A. 108,* 4194–4199.

Wong, Y., et al. (2018). Mitochondria-lysosome contacts regulate mitochondrial fission via RAB7 GTP hydrolysis. *Nature.*

Wooten, G., et al. (2004). Are men at greater risk for Parkinson's disease than women? *Journal of Neurology, Neurosurgery, and Psychiatry, 75*(4), 637–639.

Wu, F., et al. (2015). Rotenone impairs autophagic flux and lysosomal functions in Parkinson's disease. *Neuroscience. 284*, 900 – 911

Xiong Y, et al. (2010) GTPase activity plays a key role in the pathobiology of LRRK2. *PLoS Genet, 6*(4), e1000902.

Xiong, Y., et al. (2017). Overexpression of Parkinson's Disease-Associated Mutation LRRK2 G2019S in Mouse Forebrain Induces Behavioral Deficits and α-Synuclein Pathology. *eNeuro, 4*(2), 4-17.

Xiong, Y., et al. (2018). Robust kinase- and age-dependent dopaminergic and norepinephrine neurodegeneration in LRRK2 G2019S transgenic mice. *Proceedings of the National Academy of Sciences of the United States of America, 115*(7), 1635–1640.

Yamada, M., et al. (2004). Overexpression of alpha-synuclein in rat substantia nigra results in loss of dopaminergic neurons, phosphorylation of alpha-synuclein and activation of caspase-9: resemblance to pathogenetic changes in Parkinson's disease. *J Neurochem, 91*(2), 451–461.

Yang, J., et al. (2008). Reactive oxygen species and nitric oxide regulate mitochondria-dependent apoptosis and autophagy in evodiamine-treated human cervix carcinoma HeLa cells, *Free Radical Research. 42*(5), 492-504.

Yu, M., et al. (2018). LRRK2 mediated Rab8a phosphorylation promotes lipid storage. *Lipids in Health and Disease, 17,* 34.

Yue, M., K., et al. (2015). Progressive dopaminergic alterations and mitochondrial abnormalities in LRRK2 G2019S knock-in mice. *Neurobiol Dis 78*, 172-195.

Yue, Z., & Yang, W. (2013). Dangerous duet: LRRK2 and α-synuclein jam at CMA. *Nat Neurosci, 16*(4), 375–377.

Yun, H. J., et al. (2013). LRRK2 phosphorylates Snapin and inhibits interaction of Snapin with SNAP-25. *Experimental & Molecular Medicine, 45*(8), e36–.

Zabetian, C. P., et al. (2005). A clinic-based study of the LRRK2 gene in Parkinson disease yields new mutations. *Neurology 65*(5), 741-744.

Zarranz, J. J., et al. (2004). The new mutation, E46K, of α- synuclein causes Parkinson and Lewy body dementia. *Ann Neurol, 55*, 164–173.

Zavodszky, E., et al. (2014). Mutation in VPS35 associated with Parkinson's disease impairs WASH complex association and inhibits autophagy. *Nature Communications, 5*, 3828.

Zhang, X., et al. (2016). MCOLN1 is a ROS sensor in lysosomes that regulates autophagy. *Nature Communications, 7*, 12109.

Zheng, Y., et al. (2012). The Effects of Bilateral Vestibular Loss on Hippocampal Volume, Neuronal Number, and Cell Proliferation in Rats. *Frontiers in Neurology, 3*, 20.

Zhou, H., et al. (2011). Temporal expression of mutant LRRK2 in adult rats impairs dopamine reuptake. *International journal of biological sciences, 7*, 753-761.

Zhu, C.,et al. (2004). Variable effects of chronic subcutaneous administration of rotenone on striatal histology. *J Comp Neurol 478*, 418–426.

Zhu, Y., C. et al. (2013). ULK1 and JNK are involved in mitophagy incurred by LRRK2 G2019S expression. *Protein Cell 4*(9), 711-721.

Zimprich, A., et al. (2004) Mutations in LRRK2 cause autosomal-dominant parkinsonism with pleomorphic pathology*, Neuron. 44,* 601-7.

Zimprich, A., et al. (2011) A mutation in VPS35, encoding a subunit of the retromer complex, causes late-onset Parkinson disease, *American journal of human genetics. 89,* 168-75.

Ziviani, E., Tao, R. N., & Whitworth, A. J. (2010). Drosophila Parkin requires PINK1 for mitochondrial translocation and ubiquitinates mitofusin. *Proc Natl Acad Sci USA.*